

PRESSURE LEACHING OF ÇALDAĞ LATERITIC NICKEL ORE

A THESIS SUBMITTED TO
THE GRADUATE SCHOOL OF APPLIED AND NATURAL SCIENCES
OF
MIDDLE EAST TECHNICAL UNIVERSITY

BY

MEHMET ALİ RECAİ ÖNAL

IN PARTIAL FULFILLMENT OF THE REQUIREMENTS
FOR
THE DEGREE OF MASTER OF SCIENCE
IN
METALLURGICAL AND MATERIALS ENGINEERING

FEBRUARY 2013

Approval of the thesis:

PRESSURE LEACHING OF ÇALDAĞ LATERITIC NICKEL ORE

submitted by **MEHMET ALİ RECAİ ÖNAL** in partial fulfillment of the requirements for the degree of **Master of Science in Metallurgical and Materials Engineering Department, Middle East Technical University** by,

Prof. Dr. Canan Özgen
Dean, Graduate School of **Natural and Applied Sciences** _____

Prof. Dr. Hakan C. GÜR
Head of Department, **Metallurgical and Materials Engineering** _____

Prof. Dr. Yavuz A. TOPKAYA
Supervisor, **Metallurgical and Materials Engineering Dept., METU** _____

Examining Committee Members:

Prof. Dr. Ahmet Geveci
Metallurgical and Materials Engineering Dept., METU _____

Prof. Dr. Yavuz A. Topkaya
Metallurgical and Materials Engineering Dept., METU _____

Prof. Dr. İshak Karakaya
Metallurgical and Materials Engineering Dept., METU _____

Prof. Dr. Abdullah Öztürk
Metallurgical and Materials Engineering Dept., METU _____

Prof. Dr. Ali İhsan Arol
Mining Engineering Dept., METU _____

Date: 01.02.2013

I hereby declare that all information in this document has been obtained and presented in accordance with academic rules and ethical conduct. I also declare that, as required by these rules and conduct, I have fully cited and referenced all material and results that are not original to this work.

Name, Last name: Mehmet Ali Recai ÖNAL

Signature :

ABSTRACT

PRESSURE LEACHING OF ÇALDAĞ LATERITIC NICKEL ORE

Önal, Mehmet Ali Recai
M.Sc., Department of Metallurgical and Materials Engineering
Supervisor: Prof. Dr. Yavuz A. Topkaya

February 2013, 160 pages

The purpose of this study was to investigate the process optimization of combined high pressure acid leaching (HPAL) and mixed hydroxide precipitation (MHP) route for the extraction of nickel and cobalt from Çaldağ lateritic nickel ore.

In order to extract nickel and cobalt values into pregnant leach solution (PLS), several process parameters of HPAL including acid load, temperature, leaching duration and particle size were investigated in comparative manner at constant solid concentration and agitation speed.

After HPAL trials, it has been found that more than one combination of parameters offered higher than 90% extraction efficiencies for both nickel and cobalt. Among them, 0.325 kg/kg acid load, 250°C, 1 hour duration and 100% -1 mm particle size was selected as the optimum conditions with 94.1% Ni and 94.0% Co extractions. A stock of PLS was prepared under the stated conditions that was treated by downstream operations in order to obtain MHP.

Initially by two-stage iron removal of downstream operations major impurities iron, chromium and aluminum were nearly completely removed with acceptable nickel and cobalt losses from PLS. Then, the nickel and cobalt were precipitated by two-stage mixed hydroxide precipitation.

In the first step of MHP, the optimum conditions were chosen as pH=7.10, 60°C and 1 hour duration. The intermediate product obtained at these conditions contained 44.3% Ni, 3.01% Co with 3.06% Mn contamination.

In summary, it was found that Çaldağ nickel laterite ore was readily leachable under HPAL conditions and PLS obtained was easily treatable in order to produce saleable MHP.

Keywords: Hydrometallurgy, Çaldağ, high pressure acid leaching, mixed nickel-cobalt hydroxide precipitation.

ÖZ

ÇALDAĞ LATERİTİK NİKEL CEVHERİNİN BASINÇ ALTINDA LIÇ EDİLMESİ

Önal, Mehmet Ali Recai
Y. Lisans, Metalürji ve Malzeme Mühendisliği Bölümü
Tez Yöneticisi: Prof. Dr. Yavuz A. Topkaya

Şubat 2013, 160 sayfa

Bu tez çalışmasının amacı, Çaldağ lateritik nikel cevherinin nikel ve kobalt değerlerinin kazanılması için birleştirilmiş basınç altında asit liçi ve hidroksit karışımı çöktürme prosesinin optimizasyonunu araştırmaktır.

Nikel ve kobalt değerleri metal yüklü çözeltiye kazanılırken, basınç altında asit liçi yönteminin çeşitli proses parametrelerinden asit miktarı, sıcaklık, liç süresi ve tane boyutu karşılaştırmalı olarak ve sabit tutulan katı oranı ve karıştırma hızıyla çalışılmıştır.

Birçok test sonucunda, birden fazla parametre kombinasyonunun %90'nın üzerinde nikel ve kobalt kazanımı sağladığı görülmüştür. Bu kombinasyonlar arasından, %94,1 nikel ve %94,0 kobalt kazanımı sağlayan 0,325 kg/kg asit cevher oranı, 250°C ve 1 saat süre ile %100 -1 mm tane boyutu optimum şartlar olarak seçilmiştir. Gerçek bir metal yüklü solüsyon stoğu bahsi geçen şartlarda hazırlanarak MHP yöntemine tabi tutularak işlenmiştir.

İlk olarak iki aşamalı demir çöktürme basamaklarından sonra, başlıca empüritelere olan demir, krom ve alüminyum neredeyse tamamen çözeltiden ayrıştırılırken nikel ve kobalt kayıpları kabul edilebilir miktarda tutulmuştur. Sonrasında, nikel ve kobalt iki aşamalı nikel-kobalt hidroksit çöktürme basamaklarında çöktürülmüştür.

Bu aşamaların ilkinde, optimum şartlar olarak pH=7,10'da 60°C ve 1 saat süre belirlenmiştir. Bu şartlar altında elde edilen ara ürün çökeltinin %44,3 Ni, %3,01 Co miktarıyla beraber %3,06 Mn kontaminasyonu içerdiği görülmüştür.

Sonuç olarak, Çaldağ lateritik nikel cevherinin büyük ölçüde basınç altında liç edilebilir olduğunun yanısıra çıkan metal yüklü solüsyonun nikel-kobalt hidroksit çöktürme yöntemiyle kolaylıkla proses edilebilir olduğu ve bu iki işlemin ardından satılabilir kalitede ara ürün sağladığı görülmüştür.

Anahtar Kelimeler: Hidrometalurji, Çaldağ, yüksek basınç altında asit liçi, nikel-kobalt hidroksit çöktürme.

To My Dear Family
&
In memory of Vehbi Dark

ACKNOWLEDGEMENTS

I would like to express my sincere appreciation and gratitude to my supervisor Prof. Dr. Yavuz A. Topkaya for patiently sharing his extensive wisdom, his kind and endless support, continuous guidance and motivation throughout this thesis study.

I cannot even get close to adequately express my gratitude and thankfulness to my dear family members Sabire, Abdurrahman, İslami, İlhami, Bünyamin, Maksud and Müdrike for their love, support, patience and being there for me throughout my whole life. I would also like to thank Birgül Cengiz for being a special relative and a wise advisor when I needed. I shall not forget Mahmut Camalan to whom I must thank in the same manner for being the closest friend I would gladly have as a brother.

I must express my special thanks to my co-workers and friends Aydın Rüßen, Şerif Kaya, Derya Kapusuz, Saeid Pournaderi, Şükrü Kılık, Gökhan Erian, Amir Fadaei, Erman Kondu, Kıvanç Korkmaz, Onur Saka for their suggestions, helps and guidance.

Kerime Güney and META Nickel and Cobalt Company are gratefully acknowledged for their extremely important support during the chemical analyses of the experimental samples.

TABLE OF CONTENTS

ABSTRACT	V
ÖZ	vii
ACKNOWLEDGEMENTS	X
TABLE OF CONTENTS	Xi
TABLE OF FIGURES	Xiv
LIST OF TABLES	Xvii
CHAPTERS	
1. INTRODUCTION	1
2. LITERATURE REVIEW	3
2.1. NICKEL AND NICKEL ORE TYPES	3
2.1.1. SULFIDE TYPE NICKEL ORES	6
2.1.2. OXIDE TYPE NICKEL ORES	6
2.2. PRODUCTION METHODS OF NICKEL FROM LATERITE ORES	10
2.2.1. PYROMETALLURGICAL ROUTES	10
2.2.2. CARON PROCESS	11
2.2.3. HYDROMETALLURGICAL ROUTES	12
2.2.3.1. ATMOSPHERIC LEACHING (AL)	12
2.2.3.2. HIGH PRESSURE ACID LEACHING (HPAL)	15
2.2.3.3. OTHER ROUTES AND FUTURE DEVELOPMENTS	19
2.2.3.3.1. AMAX AND EPAL PROCESSES	19
2.2.3.3.2. DIRECT NICKEL PROCESS (DNI)	19
2.2.3.3.3. BY-PRODUCT SCANDIUM RECOVERY	20
2.3. EFFECT OF PROCESS PARAMETERS ON HPAL PROCESS	21
2.3.1. EFFECT OF ACID LOAD	21
2.3.2. EFFECT OF PULP DENSITY AND AGITATION SPEED	22
2.3.3. EFFECT OF TEMPERATURE	22
2.4. CHEMISTRY OF HIGH PRESSURE ACID LEACHING	23
2.4.1. SULFURIC ACID CHEMISTRY	23
2.4.2. IRON CHEMISTRY	24
2.4.3. ALUMINUM CHEMISTRY	27
2.4.4. MAGNESIUM CHEMISTRY	28
2.4.5. MANGANESE-NICKEL-COBALT CHEMISTRY	30
2.4.6. LEACH RESIDUE CHARACTERISTICS	31
2.5. DOWNSTREAM PROCESSES ON PREGNANT LEACH SOLUTIONS	35
2.5.1. MIXED SULFIDE PRECIPITATION (MSP)	36
2.5.2. DIRECT SOLVENT EXTRACTION (DSX)	37
2.5.3. MIXED HYDROXIDE PRECIPITATION (MHP)	38
2.5.3.1. RECYCLE LEACH	42

2.5.3.2.	FIRST IRON REMOVAL STAGE (FER1)	42
2.5.3.3.	SECOND IRON REMOVAL STAGE (FER2)	43
2.5.3.4.	FIRST MIXED HYDROXIDE STAGE (MHP1)	44
2.5.3.5.	SECOND MIXED HYDROXIDE STAGE (MHP2)	46
2.5.3.6.	MANGANESE REMOVAL STAGE	46
2.6.	PREVIOUS STUDIES ON ÇALDAĞ ORE DEPOSIT	46
2.6.1.	GEOLOGICAL AND MINERALOGICAL CHARACTERIZATION STUDIES	47
2.6.2.	ATMOSPHERIC HEAP/ COLUMN LEACH STUDIES	51
3.	SAMPLE CHARACTERIZATION, EXPERIMENTAL SET-UP AND PROCEDURE	53
3.1.	SAMPLE DESCRIPTION	53
3.1.1.	SAMPLE PREPARATION AND PHYSICAL CHARACTERIZATION OF ORE SAMPLE	53
3.2.	CHEMICAL CHARACTERIZATION OF ORE SAMPLE	59
3.3.	MINERALOGICAL CHARACTERIZATION OF ORE SAMPLE.....	60
3.3.1.	XRD EXAMINATIONS	62
3.3.2.	DTA-TGA EXAMINATIONS	64
3.3.3.	SEM EXAMINATIONS.....	65
3.3.3.1.	SEM EXAMINATIONS ON PARTICLES OF FIRST SAMPLE HOLDER.....	68
3.3.3.2.	SEM EXAMINATIONS ON PARTICLES OF SECOND SAMPLE HOLDER.....	74
3.3.4.	CONCLUSIONS OF THE CHARACTERIZATION OF RUN-OF-MINE SAMPLES	77
3.4.	EXPERIMENTAL PROCEDURES	78
3.4.1.	PROCEDURE FOR HIGH PRESSURE ACID LEACHING (HPAL) EXPERIMENTS	78
3.4.2.	PROCEDURE FOR DOWNSTREAM EXPERIMENTS.....	81
3.4.2.1.	FIRST IRON REMOVAL AND NEUTRALIZATION STEP (FER 1).....	81
3.4.2.2.	SECOND IRON REMOVAL STEP (FER 2).....	84
3.4.2.3.	FIRST MIXED HYDROXIDE PRECIPITATION (MHP 1)	85
3.4.2.4.	SECOND MIXED HYDROXIDE PRECIPITATION (MHP 2)	86
4.	RESULTS AND DISCUSSION	89
4.1.	HIGH PRESSURE ACID LEACHING EXPERIMENTS	89
4.1.1.	EFFECT OF ACID TO ORE RATIO ON METAL EXTRACTIONS.....	90
4.1.2.	EFFECT OF TEMPERATURE AT TWO A/O RATIOS.....	94
4.1.3.	EFFECT OF LEACHING DURATION AT TWO A/O RATIOS.....	99
4.1.4.	EFFECT OF PARTICLE SIZE AT TWO DIFFERENT TEMPERATURES	104
4.1.5.	OPTIMUM CONDITIONS FOR HPAL EXPERIMENTS	106
4.1.6.	LEACH RESIDUE CHARACTERIZATION	107
4.1.6.1.	XRD EXAMINATION OF LEACH RESIDUE	108
4.1.6.2.	SEM EXAMINATION OF LEACH RESIDUE	111
4.2.	DOWNSTREAM EXPERIMENTS	114
4.2.1.	FIRST IRON REMOVAL EXPERIMENTS	114
4.2.1.1.	CHARACTERIZATION OF PRECIPITATES OF FIRST IRON REMOVAL.....	118
4.2.2.	SECOND IRON REMOVAL EXPERIMENTS	122
4.2.2.1.	CHARACTERIZATION OF PRECIPITATES OF SECOND IRON REMOVAL.....	125
4.2.3.	FIRST MIXED HYDROXIDE PRECIPITATION EXPERIMENTS	130
4.2.3.1.	CHARACTERIZATION OF PRECIPITATES OF FIRST MIXED HYDROXIDE PRECIPITATION	133
4.2.4.	SECOND MIXED HYDROXIDE PRECIPITATION EXPERIMENTS.....	136
4.2.4.1.	CHARACTERIZATION OF PRECIPITATES OF SECOND MIXED HYDROXIDE PRECIPITATION	138

5. CONCLUSIONS	141
REFERENCES	143
APPENDICES	151
A. EXAMPLE OF METAL EXTRACTION OR PRECIPITATION CALCULATIONS	151
B. POURBAIX DIAGRAMS OF NICKEL AND COBALT	153
C. EDX RESULTS OF PARTICLES OF FIRST SAMPLE HOLDER	155
D. EDX RESULTS OF PARTICLES OF SECOND SAMPLE HOLDER	158

LIST OF FIGURES

FIGURES

FIGURE 1 WORLD NICKEL PRODUCTION (LEFT) AND NICKEL RESERVE (RIGHT) BY 2011 WITH RESPECT TO COUNTRIES.	3
FIGURE 2 IONIC RADII OF SOME IMPORTANT ELEMENTS [10].....	5
FIGURE 3 MOST IMPORTANT NICKEL LATERITE AND SULFIDE DEPOSITS OF THE WORLD.....	5
FIGURE 4 TYPICAL ORE PROFILE INCLUDING ALL POSSIBLE LAYERS [15].....	7
FIGURE 5 TYPICAL PROFILE LAYERS OF A LATERITIC ORE WITH CHARACTERISTIC NICKEL BEARING MINERALS.	9
FIGURE 6 TYPICAL LATERITE PROFILES WITH VARYING CLIMATE AND WEATHERING CONDITIONS AND RESPECTIVE PROCESSING OPTIONS [8].....	10
FIGURE 7 PYROMETALLURGICAL (LEFT) AND CARON PROCESS (RIGHT) FLOWSHEETS FOR LATERITIC NICKEL DEPOSITS.	11
FIGURE 8 FLOWSHEET OF HEAP LEACHING (A) AND SCHEMATIC VIEW TAKEN FROM ÇALDAĞ HEAP LEACH PROJECT (B) [19]	14
FIGURE 9 SIMPLIFIED HIGH PRESSURE ACID LEACHING FLOWSHEET.....	15
FIGURE 10 SCHEMATIC VIEW OF HIGH PRESSURE ACID LEACHING FLOWSHEET FOLLOWED BY MHP DOWNSTREAM CHOICE.	17
FIGURE 11 COUNTER-CURRENT-DECANTATION CIRCUIT.....	18
FIGURE 12 OVERALL ENERGY REQUIREMENTS AND NICKEL RECOVERIES OF HYDROMETALLURGICAL PROCESS ROUTES (ADOPTED FIGURE FROM [31]).	19
FIGURE 13 INNOVATIVE ATMOSPHERIC CHLORIDE LEACHING PROCESS WITH SCANDIUM RECOVERY STAGE (NEOMET PROCESS) [36].	20
FIGURE 14 TEM IMAGES OF DIFFERENT STRUCTURES BEFORE AND AFTER PRESSURE LEACHING [41,63].	33
FIGURE 15 SEM IMAGES OF AMORPHOUS SILICA AND BASIC IRON SULFATE [54]; AMORPHOUS SILICA WITH HIGHER MAGNIFICATION [17], LARGE ALUNITE/JAROSITE PARTICLES AFTER HYPERSALINE WATER HPAL, FINE HEMATITE-SILICA PARTICLES AFTER TAP WATER HPAL [51].....	33
FIGURE 16 ALL POSSIBLE IONIC REPLACEMENTS WITHIN THE ALUNITE STRUCTURE [39].....	35
FIGURE 17 TYPICAL MIXED SULFIDE PRECIPITATION FLOWSHEET.....	36
FIGURE 18 DSX FLOWSHEET FROM BULONG OPERATION [71].....	38
FIGURE 19 SCHEMATIC VIEW OF COMPLETE HPAL + MHP PROCESS TRAIN [74].....	40
FIGURE 20 STABILITY CURVES FOR SEVERAL IONS WITH RESPECT TO MOLARITY AND pH AT AMBIENT CONDITIONS (25°C AND 1 ATM) [70].....	41
FIGURE 21 SUPERIMPOSED HORIZONS OF THE ÇALDAĞ LATERITE: SILICA CAP, LIMONITE ZONE AND FRESH SERPENTINITE [86].....	47
FIGURE 22 LATERITIC PROFILE OF ÇALDAĞ NICKEL-COBALT ORE WITH NICKEL, COBALT, IRON AND MANGANESE DISTRIBUTIONS [84].....	48
FIGURE 23 IN-SITU IMAGES OF HEMATITE, NORTH AND SOUTH PITS OF ÇALDAĞ ORE (LEFT) AND LOCATION OF THE PITS ON A MAP (RIGHT) [87].....	49
FIGURE 24 PROFILE VARIATIONS OF THREE PITS IN ÇALDAĞ NICKEL DEPOSIT [87].....	50
FIGURE 25 MINERAL CONTENTS (WT. %) (RIGHT) AND THEIR DISTRIBUTIONS (LEFT) IN SAMPLES TAKEN FROM ÇALDAĞ ORE BY USE OF QEMSCAN METHOD (5000 COUNTS) [15].	51

FIGURE 26 CRUSHING, GRINDING AND SAMPLING PROCESSES OF ÇALDAĞ LATERITIC NICKEL ORE.....	55
FIGURE 27 PARTICLE SIZE DISTRIBUTION OF -1 MM ÇALDAĞ ORE SAMPLE (LOGARITHMIC SCALE).	57
FIGURE 28 PARTICLE SIZE DISTRIBUTION OF -0.5 MM ÇALDAĞ ORE SAMPLE (LOGARITHMIC SCALE). ...	58
FIGURE 29 PARTICLE SIZE DISTRIBUTION OF -1.4 MM ÇALDAĞ ORE SAMPLE (LOGARITHMIC SCALE). ...	59
FIGURE 30 XRD RESULTS OF ÇALDAĞ RUN OF MINE SAMPLE.	63
FIGURE 31 DTA-TGA ANALYSIS RESULT FOR ÇALDAĞ LATERITIC SAMPLE.	65
FIGURE 32 IMAGES OF SAMPLE HOLDERS PRIOR TO GOLD COATING.	67
FIGURE 33 TWO INTERCALATED PHASES IN PARTICLE L: PRIOR TO GOLD COATING (C), SEM IMAGE (B) AND EDX RESULT TAKEN AT THE JUNCTION REGION (A).	67
FIGURE 34 SEM VIEWS AND CLASSIFICATIONS OF PARTICLES IN A QUARTER OF FIRST SAMPLE HOLDER.	69
FIGURE 35 EDX RESULT OF GENERAL VIEW OF GROUP 1 FOR MAPPING OF EXISTING ELEMENTS.	69
FIGURE 36 MAPPING RESULTS OF GROUP 1 FOR DETECTED ELEMENTS.	70
FIGURE 37 EDX RESULTS OF PARTICLE I (CALCIUM SULFATE) AND PARTICLE J (CALCITE).	70
FIGURE 38 EDX RESULT OF GENERAL VIEW OF GROUP 2 FOR MAPPING OF EXISTING ELEMENTS.	72
FIGURE 39 MAPPING RESULTS OF GROUP 2 FOR DETECTED ELEMENTS.	73
FIGURE 40 IMAGE OF SECOND SAMPLE HOLDER WITH PARTICLES PRIOR TO GOLD COATING.	74
FIGURE 41 SEM IMAGE AND ELEMENTAL MAPPING OF LOWERMOST QUARTER HAVING FULL OF SERPENTINE PARTICLES.	75
FIGURE 42 SEM IMAGE AND ELEMENTAL MAPPING OF MANGANESE-RICH QUARTER WITHOUT PARTICLES U AND V.	76
FIGURE 43 TITANIUM AUTOCLAVE USED IN HPAL EXPERIMENTS.....	78
FIGURE 44 HEATING CURVE OF LOADED AUTOCLAVE TO THE HIGHEST TEMPERATURE (260°C) STUDIED.	80
FIGURE 45 EXPERIMENTAL SET-UP FOR DOWNSTREAM EXPERIMENTS (CaCO ₃ SLURRY IS REPLACEABLE FOR UPCOMING STEPS).....	84
FIGURE 46 EFFECT OF ACID TO ORE RATIO ON NICKEL, COBALT AND IRON EXTRACTIONS.	91
FIGURE 47 TERMINAL FREE ACID CHANGES WITH ACID LOAD.	93
FIGURE 48 EFFECT OF ACID TO ORE RATIO ON OTHER IMPURITY METAL EXTRACTIONS.....	94
FIGURE 49 EFFECT OF TEMPERATURE ON NICKEL, COBALT AND IRON EXTRACTIONS AT 0.325 KG/KG (A) AND 0.275 KG/KG (B) A/O RATIOS.	96
FIGURE 50 EFFECT OF TEMPERATURE ON OTHER IMPURITY METAL EXTRACTIONS AT 0.325 KG/KG (A) AND 0.275 KG/KG (B) A/O RATIOS.	97
FIGURE 51 TERMINAL FREE ACID CHANGE OF SOLUTION WITH TEMPERATURE OBTAINED AT DIFFERENT A/O RATIOS.	98
FIGURE 52 EFFECT OF LEACHING DURATION ON NICKEL, COBALT AND IRON EXTRACTIONS AT 0.275 KG/KG (A) AND 0.325 KG/KG (B) A/O RATIOS.	100
FIGURE 53 EFFECT OF LEACHING DURATION ON OTHER IMPURITY METAL EXTRACTIONS AT 0.275 KG/KG (A) AND 0.325 KG/KG (B) A/O RATIOS.	101
FIGURE 54 TERMINAL FREE ACID CHANGE WITH RESPECT TO LEACHING DURATION AT TWO DIFFERENT ACID LOADS.....	102
FIGURE 55 OXIDATION-REDUCTION POTENTIAL OF SOLUTION WITH RESPECT TO LEACHING DURATION AT TWO DIFFERENT A/O RATIOS.	103
FIGURE 56 EXTRACTION EFFICIENCIES OF NICKEL, COBALT AND IRON WITH RESPECT TO PARTICLE SIZE AT 245°C (A) AND 250°C (B).....	104
FIGURE 57 EXTRACTION EFFICIENCIES OF OTHER IMPURITY METALS WITH RESPECT TO PARTICLE SIZE AT 245°C (A) AND 250°C (B).....	105

FIGURE 58 XRD RESULTS OF LEACH RESIDUE OBTAINED AT THE OPTIMUM HPAL CONDITIONS AND OF ORIGINAL ORE SAMPLE.	110
FIGURE 59 SEVERAL SEM VIEWS OF LEACH RESIDUE OBTAINED AT THE OPTIMUM CONDITIONS OF HPAL.	112
FIGURE 60 PRIMARY AND SECONDARY HEMATITE (B, C) AND ALUNITE (A, D) PARTICLES.	113
FIGURE 61 PRECIPITATION OF IMPORTANT METALS WITH pH INCREASE AT THE FIXED CONDITIONS OF 90°C AND 120 MINUTES IN FER 1.	115
FIGURE 62 pH VARIATION WITH CONSTANT RATE OF 1000 µL PER 5 MINUTES CaCO ₃ ADDITION AT 90 °C IN FER 1.	118
FIGURE 63 pH VS. TEMPERATURE STABILITY DIAGRAM FOR IRON-WATER SYSTEM IN 0.5 M Fe ₂ (SO ₄) ₃ SOLUTION [123].	119
FIGURE 64 XRD RESULT OF THE PRECIPITATE SAMPLE OBTAINED AT THE OPTIMUM CONDITIONS OF FER 1 STEP.	120
FIGURE 65 SEM IMAGES OF SEVERAL PHASES IN THE PRECIPITATE SAMPLE OF FER 1 STEP AT THE OPTIMUM CONDITIONS.	121
FIGURE 66 EFFECT OF pH ON PRECIPITATION OF SEVERAL METALS IN FER 2 STEP.	123
FIGURE 67 EFFECT OF PRECIPITATION DURATION ON NICKEL, COBALT AND IRON PRECIPITATIONS IN FER 2 STEP.	124
FIGURE 68 XRD RESULT OF PRECIPITATES OBTAINED AT THE OPTIMUM CONDITIONS OF FER 2.	127
FIGURE 69 SEM IMAGES OF BASSANITE PARTICLES AND AGGLOMERATES OF PHASE MIXTURE IN FER 2.	128
FIGURE 70 SEM IMAGES AND EDX RESULTS OF TWO DIFFERENT AGGLOMERATES OF FER 2.	129
FIGURE 71 EFFECT OF pH ON PRECIPITATION OF SEVERAL METALS IN MHP 1 STEP.	131
FIGURE 72 XRD RESULT OF THE PRECIPITATE OBTAINED AT THE OPTIMUM CONDITIONS OF MHP 1.	134
FIGURE 73 SEM IMAGES OF MHP 1 AGGLOMERATE.	135
FIGURE 74 TWO AGGLOMERATES OF MHP 1 WITH RESPECTIVE EDX RESULTS.	136
FIGURE 75 pH EFFECT ON SEVERAL IMPORTANT METAL PRECIPITATIONS DURING MHP 2 STEP.	137
FIGURE 76 XRD RESULT OF MHP 2 PRECIPITATE OBTAINED AT THE OPTIMUM CONDITIONS.	139
FIGURE 77 POURBAIX DIAGRAM FOR NICKEL-WATER SYSTEM AT 25°C, 10 ⁻⁶ MOLAR.	153
FIGURE 78 POURBAIX DIAGRAM FOR COBALT-WATER SYSTEM AT 25°C, 10 ⁻⁶ MOLAR.	154
FIGURE 79 EDX RESULT OF PARTICLE A (QUARTZ WITH IRON AND CALCIUM INCLUSIONS).	155
FIGURE 80 EDX RESULT OF PARTICLE B (FERRUGINOUS SERPENTINE).	155
FIGURE 81 EDX RESULT OF PARTICLE C (Mn-IRON OXIDE).	156
FIGURE 82 EDX RESULT OF PARTICLE G (Cr-HEMATITE).	156
FIGURE 83 EDX RESULT OF PARTICLE H (Mn-IRON OXIDE WITH FERRUGINOUS Ca-SMECTITE (SHINY REGIONS)).	156
FIGURE 84 EDX RESULTS FROM TWO SECTIONS OF PARTICLE E.	157
FIGURE 85 EDX RESULT OF PARTICLE D (FERRUGINOUS SMECTITE)	157
FIGURE 86 EDX RESULT FOR TWO DISINTEGRATED PARTICLES F AND F1.	157
FIGURE 87 EDX RESULTS OF PARTICLES M, N AND P.	158
FIGURE 88 EDX RESULTS OF PARTICLES Q, R AND U.	159
FIGURE 89 EDX RESULTS OF PARTICLES S AND T.	159
FIGURE 90 EDX RESULTS FOR PARTICLES Y, Z AND W.	160

LIST OF TABLES

TABLES

TABLE 1 NICKEL MINERALS AND NICKEL-BEARING MINERALS [9].	4
TABLE 2 ATOMIC OR IONIC RADII OF IMPORTANT ELEMENTS WITH THEIR COORDINATION STATE (ADOPTED FROM [10]).	5
TABLE 3 FREQUENCY OF LATERITIC ORE TYPES BASED ON DOMINANT NICKEL BEARING LAYER TYPES WITH THEIR AVERAGE GRADES (ADOPTED FROM [14]).	9
TABLE 4 ORE TYPES WITH EXTRACTION METHODS AND RECORDS FOR PROCESSING (INCLUDING DEVELOPING PROJECTS) (ADOPTED FROM [14]).	12
TABLE 5 COMPARISON OF HPAL AND AL WITH RESPECT TO SEVERAL ISSUES [20,31].	18
TABLE 6 TYPICAL MIXED SULFIDE PRECIPITATE COMPOSITION [67].	37
TABLE 7 TYPICAL MHP COMPOSITION [67].	45
TABLE 8 NICKEL RESERVES OF TURKEY [5].	47
TABLE 9 MINIMUM WEIGHT OF SAMPLE FOR ORDINARY ORES WITH RESPECT TO PARTICLE SIZE.	54
TABLE 10 MOISTURE AMOUNT OF ROM SAMPLE.	56
TABLE 11 BULK DENSITY AND SPECIFIC GRAVITY OF ROM SAMPLES.	56
TABLE 12 PARTICLE SIZE DISTRIBUTION OF -1 MM ÇALDAĞ ORE SAMPLE.	57
TABLE 13 PARTICLE SIZE DISTRIBUTION OF -0.5 MM ÇALDAĞ ORE SAMPLE.	58
TABLE 14 PARTICLE SIZE DISTRIBUTION OF -1.4 MM ÇALDAĞ ORE SAMPLE.	59
TABLE 15 CHEMICAL COMPOSITION OF ÇALDAĞ LATERITIC ORE SAMPLE.	60
TABLE 16 XRF AND ICP ANALYSIS RESULTS OF SCANDIUM.	60
TABLE 17 FREQUENCIES OF DETECTED NICKEL-BEARING MINERALS BY THEIR COUNTS AND PERCENTAGE OF DEPOSITS CONTAINING MINERALS AMONG ALL 117 LATERITE DEPOSITS (ADOPTED FROM [14]).	61
TABLE 18 A TYPICAL COMPOSITION OF INPUT FOR HPAL EXPERIMENTS.	79
TABLE 19 SOME PROPERTIES AND RESPECTIVE MEASUREMENTS OF PREGNANT LEACH SOLUTION STOCK.	82
TABLE 20 PROPERTIES OF PREGNANT LEACH SOLUTION AFTER THE FIRST IRON REMOVAL WITH NEUTRALIZATION STEP.	84
TABLE 21 PROPERTIES OF NEW PREGNANT LEACH SOLUTION AFTER THE SECOND IRON REMOVAL STAGE.	85
TABLE 22 PROPERTIES OF NEW PREGNANT LEACH SOLUTION AFTER THE FIRST MIXED HYDROXIDE PRECIPITATION STAGE.	86
TABLE 23 CHEMICAL ANALYSIS OF DEIONIZED WATER SOURCE UTILIZED BOTH IN HPAL AND MHP EXPERIMENTS.	87
TABLE 24 THEORETICAL SULFURIC ACID CONSUMPTION PER TON OF DRY ÇALDAĞ ORE SAMPLE.	90
TABLE 25 EXPERIMENTAL PARAMETERS OF THE FIRST SET OF EXPERIMENTS FOR THE OPTIMIZATION OF ACID LOAD.	91
TABLE 26 EXPERIMENTAL CONDITIONS OF EFFECT OF TEMPERATURE SERIES.	95
TABLE 27 THREE MOST HIGHLIGHTED CHOICES WITH OPERATIONAL CONDITIONS AND RESPECTIVE EXTRACTION EFFICIENCIES AFTER TEMPERATURE AND A/O RATIO EXPERIMENTS.	99
TABLE 28 EXPERIMENTAL CONDITIONS OF LEACHING DURATION EXPERIMENT SERIES.	99

TABLE 29 FOUR MOST HIGHLIGHTED CHOICES AFTER THREE SETS OF HPAL EXPERIMENTS.	103
TABLE 30 EXPERIMENTAL CONDITIONS FOR PARTICLE SIZE EXPERIMENTS.	104
TABLE 31 FOUR MOST HIGHLIGHTED CHOICES FOR THE OPTIMUM OPERATION CONDITIONS OF HPAL.	106
TABLE 32 EXTRACTION EFFICIENCIES AT THE OPTIMUM CONDITIONS, LEACH RESIDUE AND PREGNANT LEACH SOLUTION COMPOSITIONS OBTAINED AT THESE CONDITIONS.	107
TABLE 33 EXPERIMENTAL CONDITIONS AND RESPECTIVE EXTRACTION EFFICIENCIES OF THE ULTIMATE TEST.	108
TABLE 34 EFFECT OF ADDITIONAL 1 HOUR RESIDENCE TIME ON NICKEL AND IRON PRECIPITATIONS IN FER 1.	116
TABLE 35 THE OPTIMUM CONDITIONS, PRECIPITATION EFFICIENCIES AND COMPOSITIONAL CHANGES OF FER 1 STEP.	117
TABLE 36 REPRODUCIBILITY OF THE OPTIMUM CONDITION EXPERIMENTS OF FER 1 STEP (WT.%).....	118
TABLE 37 CHEMICAL COMPOSITION OF PRECIPITATE OBTAINED AT THE OPTIMUM CONDITIONS OF FER 1 STEP.	119
TABLE 38 THE OPTIMUM CONDITIONS, PRECIPITATION EFFICIENCIES AND COMPOSITIONAL CHANGES FOR FER 2 STEP.	125
TABLE 39 CHEMICAL ANALYSIS OF PRECIPITATE OBTAINED AT THE OPTIMUM CONDITIONS OF FER 2 STEP.	125
TABLE 40 CHEMICAL COMPOSITIONS OF MHP 1 PRECIPITATES (DRY) OBTAINED AT DIFFERENT pH VALUES.	132
TABLE 41 THE OPTIMUM CONDITIONS, PRECIPITATION EFFICIENCIES AND COMPOSITIONAL CHANGES FOR MHP 1 STEP.	132
TABLE 42 CHEMICAL COMPOSITION OF THE SOLID PRODUCT OBTAINED AFTER MHP 1 STEP.....	133
TABLE 43 COMPOSITIONAL CHANGES BEFORE AND AFTER MHP 2 STEP.	138
TABLE 44 CHEMICAL COMPOSITION OF MHP 2 PRECIPITATE OBTAINED AT THE OPTIMUM CONDITIONS.	138
TABLE 45 EXPERIMENTAL DATA FOR THE OPTIMUM HPAL CONDITIONS FOR SOLID BASED EXTRACTION CALCULATIONS.	151
TABLE 46 EXPERIMENTAL DATA AT THE OPTIMUM HPAL CONDITIONS FOR LIQUID BASED EXTRACTION CALCULATIONS.	152
TABLE 47 EXPERIMENTAL DATA OBTAINED AT THE OPTIMUM MHP 1 CONDITIONS FOR NICKEL PRECIPITATION %.	152

CHAPTER 1

INTRODUCTION

Nickel is a critical metal for a wide range of area from industrial process to daily life basis. More specifically, utilization of nickel is more important on ferrous and nonferrous alloy production, aerospace and military applications, battery and coinage production, coating and petro-chemical applications and so on. Due to its superior properties that results in such a wide range of utilization, nickel demand is continuously increasing with development of technology that creates more branches for nickel consumption [1].

In 2011, the world total nickel production was approximately 1589 million Mt while the total nickel consumption was 1572 million Mt and this is expected to increase to 1670 million MT by the end of 2012. The increase in nickel demand is mainly from China (44% of the total nickel consumption in 2011) and also from developing countries. The cash nickel price varies between 17000 and 22000 US Dollar/Mt tonne [2].

Until a half-century ago, the vast majority of nickel production was met from sulfide type nickel deposits with 90% of the total production. However, this trend has been increasingly changed in favor of the lateritic nickel deposits which are the competitive of the former. That is because of the depletion of old sulfide reserves and lack of new explorations. On the other hand, lateritic ores have been spotted, classified and studied extensively in very short time and now there exists 117 lateritic nickel reserves that have been reported worldwide. The increasing capacity and less effort requirements on mining highlight the laterites over the world.

However, the pace of their utilization for nickel production could not reach the level of their exploration. Today, there are three major routes for nickel production from laterites. Pyrometallurgical, Caron and hydrometallurgical methods have been designed, tested and utilized for nickel extraction depending on the ore types. Yet there is no absolute winner among these choices especially when the complexity of laterite mineralogy is considered. Despite theoretically applicable to all, these choices are rather specialized for consumption of specific portion of laterites. Although energy-intensive pyrometallurgical and Caron processes have offered several benefits especially for saprolitic and/or nontronitic type laterite ores, the best choice for a limonitic ore is widely accepted to be hydrometallurgical processes [3].

It is well known that the high pressure acid leaching (HPAL) process is one of the two most common hydrometallurgical routes that are utilized for the extraction of nickel and cobalt in industrial applications. Despite atmospheric acid leaching process (AL) suggests some advantages by means of lower capital cost, simpler process equipment, rapid ramp-up period and easier maintenance with high on-stream availability over HPAL, it also suffers from several weaknesses. The most important superiority offered by HPAL is that it enables a remarkably higher nickel and cobalt extractions for any ore type provided that it is suitable for hydrometallurgical route (i.e. low magnesium content). Another critical benefit comes out of HPAL option is the faster reaction kinetics at higher operation temperatures (230° to 270°C versus 90°C) that reduces the residence time from about 12 hours to 0.5 to 1.5 hours. As long as the environmental concerns are the only important parameter, the winner of

the competition would definitely be HPAL as the resultant iron phase in solid waste is mostly jarosite (a chemically unstable hydrated potassium-iron sulfate compound) for AL. Additionally; in open system option of AL (Heap Leaching) acid rains over heaps could be environmentally hazardous especially for surrounding agricultural fields if the necessary precautions are not taken carefully. Due to these factors, recently a HPAL plant is being built by META Nickel Cobalt Inc. for Gördes lateritic nickel ore neighboring Çaldağ ore deposit.

Being the first atmospheric acid heap leaching project, Çaldağ lateritic nickel deposit has owned a worldwide fame and was known with its previous owner European Nickel PLC but recently it has handed over its operating rights to a young company called VTG Holding. Additionally, having the highest amount of proven reserve according to the State Planning Organization (DPT) which is stated to be 33.3 million tons, this lateritic deposit is still one of the most important nickel reserves of Turkey with a reasonable grade [4,5].

Within this study, the priority was given to the high pressure acid leaching of Çaldağ lateritic nickel ore since the operation cost, quality of leach liquor, impurity control and resultant quality and solubility of intermediate product (mixed hydroxide precipitate-MHP or mixed sulfide precipitate-MSP) are greatly dependent on the performance of this method. The optimum process parameters that were found to have the most potential impacts on HPAL in the literature were studied. These parameters are temperature, acid to ore ratio, leaching duration and particle size. Among the several combinations, the most efficient combination was determined by means of nickel and cobalt extractions with consideration of possible future industrial concerns. Within these concerns, one of the most precious rare earth elements, scandium, that was found to exist in Çaldağ ore was also investigated as it might be a by-product of the process. After the determination of the optimum parameters, a stock of nickel and cobalt bearing pregnant leach solution (PLS) was prepared at these conditions for downstream processes where this highly contaminated solution was cleaned by precipitation from most of these impurities (i.e. Fe, As, Cr, Al, Cu, Zn) to very low levels (<10 ppm) and used for the production of a saleable product called MHP containing minimum 30-35% nickel and 3-5% cobalt with < 5% manganese in dry state.

In industrial projects, once again, there are two competing, well-developed options for the downstream processes (i) mixed hydroxide precipitation (MHP) and (ii) mixed sulfide precipitation (MSP) while there are other less-attractive and still-in-search options such as resin-in-pulp (RIP), direct solvent extraction (DSX), etc. Within this study, it was decided to utilize the MHP process which is more simple and applicable downstream process to investigate the impurity removal control and production of an intermediate product especially from PLS solutions containing [Ni]: [Mn] ratio more than 3:1 [6].

Impurity removal from PLS is correlated with precipitation behavior of impurity metals to their respective hydroxide with respect to the pH variation and molarity. Pregnant leach solutions are highly acidic (generally less than pH 1) due to the residual free acid (30-50 g/L) which is necessary for the prevention of reverse reaction of cationic nickel and cobalt in PLS resulting in the precipitation of nickel and cobalt sulfates. The fundamental logic beneath the MHP process is the step-by-step increment of solution pH from highly acidic (<1) to slightly basic (8-8.5) by the aid of reagent additions. The reason for not directly increasing the solution pH to approximately 7 where nickel and cobalt precipitates is that both nickel and cobalt precipitations can emerge at lower pH values due to super-saturation of metals and also adsorption of nickel and cobalt by other metal hydroxides during precipitation. Therefore, it is crucial to minimize the nickel and cobalt losses until the pH reaches the value where nickel and cobalt hydroxides are produced (i.e. MHP 1).

In summary, in this study it is aimed to primarily investigate the leachability of Çaldağ lateritic nickel ore which is a potential candidate for nickel and cobalt supply of Turkey under high pressure and high temperature conditions and also to determine the optimum parameters throughout the steps of mixed hydroxide precipitation method that will be ended up with a saleable, intermediate product of nickel and cobalt hydroxides.

CHAPTER 2

LITERATURE REVIEW

2.1. Nickel and Nickel Ore Types

According to the British Geological Survey (2008) report the abundance of nickel in the Earth's crust is average of 80 ppm listing it at the 24th most abundant element whereas for the core, nickel is the fifth common element [7]. Today, with respect to another survey of the same institute, the supply risk of nickel is not critical being 6.2 over 10 (the highest risk). This is mainly because of the fact that new nickel ores are being discovered while new nickel-cobalt projects are being initiated or already-in-operation projects are being enlarged. Additionally, nickel is readily recyclable from scrap materials; however, the technology still needs to be upgraded and requires further interest due to environmental concerns caused by the technology and economic cost it dictates to suppliers which in turn keeps the recycling option at negligibly low levels. On the contrary, mining option is the dominant nickel source especially for being the lowest cost supply option. Hence available nickel resource is dependent on a balance between declining operating ore grades and increasing ore site number (more realistically increase in the proportion of lateritic nickel deposits) [8]. According to a recent report, the leading world nickel producer countries are Russia, Indonesia, Philippines, Canada, Australia, and New Caledonia followed by other countries. On the other hand the sequence for total nickel reserves of countries is a little shifted by leading of Australia as can be seen in Figure 1.

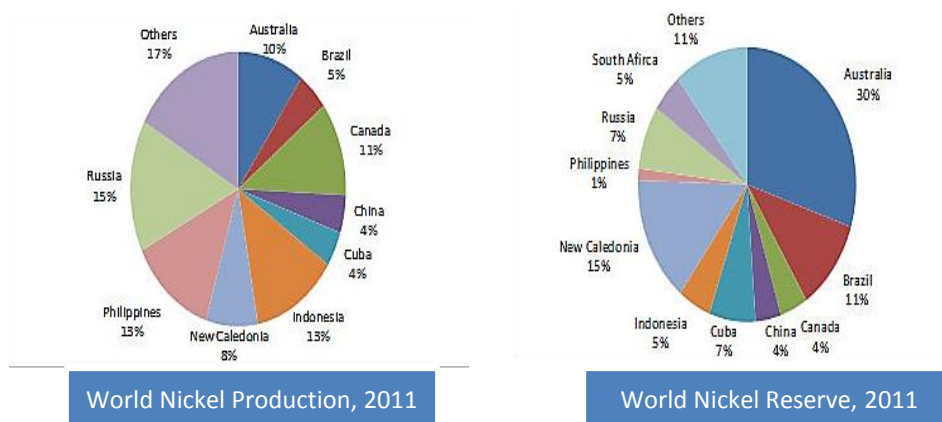


Figure 1 World nickel production (left) and nickel reserve (right) by 2011 with respect to countries.

The occurrence of nickel in nature is not as elemental form but rather as either discrete nickel minerals such as sulfide and arsenide or more commonly as limited replacement for cations of other minerals such as iron oxides or manganese oxyhydroxides. Nickel associated minerals are summarized in Table 1 with their theoretical formula and nickel content. Due to similar oxidation state (which is (+2) for nickel) and similar ionic radius with several transition metals (iron, cobalt, etc.), nickel is generally found in dispersion of several types of minerals such as iron oxide or hydroxide and manganese oxyhydroxide or iron sulfide. Apart from these transition metals, nickel can replace some magnesium in several magnesium silicate minerals such as serpentine or garnierite. Most commonly seen cation replacements and their relative ionic/atomic radii are given in Figure 2. Other important cations or anions have been included in Table 2 for comparison. As can be seen substitutions between Ni/Mg/Fe^{2+/3+}/Co and between Al³⁺/Si are possible due to close radii without causing a significant distortion in original mineral structure as they are being replaced. Additionally, this results in a side benefit. Coexistence of some valuable metals such as cobalt and scandium with nickel deposits enables the winning of more than one valuable element in one process train. Nowadays, it has been found that scandium is also associated with nickel ores which is another transition element that is even more valuable however rarer than nickel and cobalt (generally less than 200 ppm). As a result of this partial solid solubility of nickel in several minerals, it can be seen that nickel was enriched as economically valuable ore deposits under certain conditions throughout the world map in Figure 3. The major portion of these deposits (especially laterites) is generally cumulated on tropical to sub-tropical climate zones with some exceptions of humid regions in Eastern Europe or arid regions like central Western Australia. The classical divisions of nickel ore deposits are (1) lateritic type and (2) sulfide type depending on the state of nickel. These sub-types of ore deposits are further divided with respect to the host mineral state that will be discussed below.

Table 1 Nickel minerals and nickel-bearing minerals [9].

Mineral Type	Ideal Formula	%Ni	Color
Sulfides			
Pentlandite	(Ni,Fe) ₉ S ₈	34.22	Bronze-Yellow
Millerite	NiS	64.67	Brass-Yellow
Heazlewoodite	Ni ₃ S ₂	73.30	Bronze-Yellow
Polydymite	Ni ₃ S ₄	57.86	Steel-Gray
Violarite	Ni ₂ FeS ₄	38.94	Violet-Gray
Siegenite	(Co,Ni) ₃ S ₄	28.89	Steel-Gray
Arsenides			
Niccolite or nickeline	NiAs	43.92	Copper-Red
Maucherite	Ni ₁₁ As ₈	51.85	Platinum-Gray
Rammelsbergite	NiAs ₂	28.15	Tin-White
Gersdorffite	NiAsS	35.42	Steel-Gray
Antimonides			
Breithauptite	NiSb	32.53	
Arsenates			
Annabergite	Ni ₃ As ₂ O ₈ .8H ₂ O	29.40	Apple-Green
Silicates and Oxides			
Garnierite	(Ni,Mg) ₆ Si ₄ O ₁₀ (OH) ₈	≤47%	Green-Gray
Nickeliferous limonite	(Fe,Ni)O(OH).nH ₂ O	0.8-1.5%	Yellow-Brown

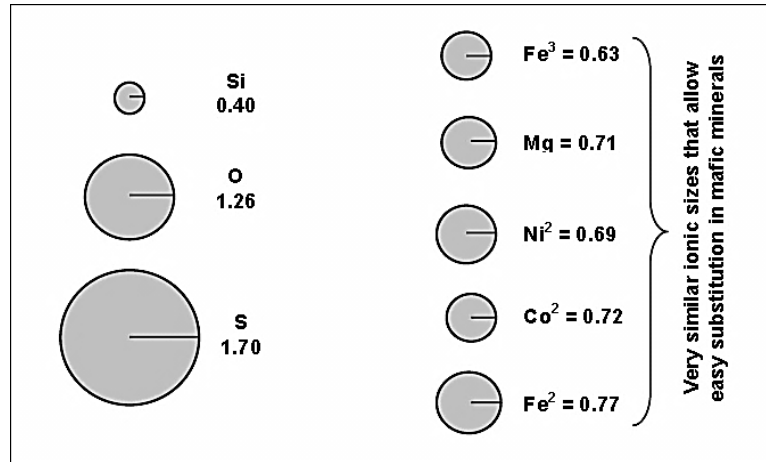


Figure 2 Ionic radii of some important elements [10].

Table 2 Atomic or ionic radii of important elements with their coordination state (Adopted from [10]).

Atom/Ion	Radius (Angstrom)	Atom/Ion	Radius (Angstrom)
Si	0.40 (IV)	Cr ³⁺	0.76 (VI)
Al ³⁺	0.53 (IV)	Fe ²⁺	0.77 (IV)
Cr ⁶⁺	0.58 (VI)	Sc ³⁺	0.75 (III)
Fe ³⁺	0.63 (IV)	Mn ²⁺	0.80 (IV)
Ti	0.65 (VI)	Na	1.13 (IV)
Mn ⁴⁺	0.67 (IV)	Ca	1.14 (VI)
Co ³⁺	0.69 (VI)	O	1.26 (VI)
Ni ²⁺	0.69 (IV)	K	1.52 (VI)
Mg	0.71 (IV)	Cl	1.67 (VI)
Co ²⁺	0.72 (IV)	S ²⁻	1.70 (VI)

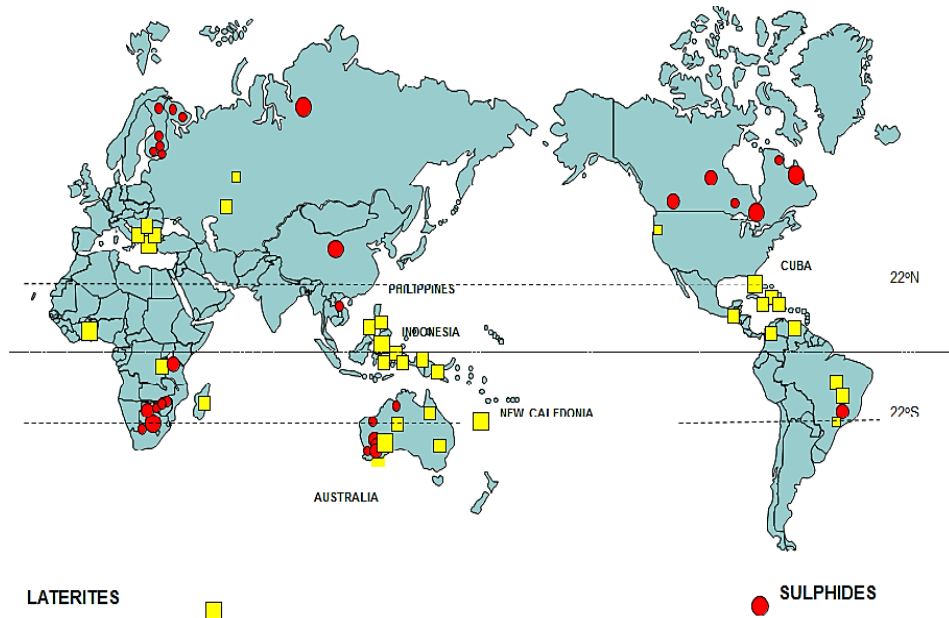


Figure 3 Most important nickel laterite and sulfide deposits of the World.

2.1.1. Sulfide Type Nickel Ores

Sulfide type nickel ores are the resultant product of volcanic or hydrothermal processes that include cobalt and/or copper with more frequently precious metals like platinum and rhodium apart from nickel. General mechanism is the supersaturation of uprising magma by sulfur producing immiscible nickel and other mentioned metal sulfide phases on cooling. However, being the oldest ores, the chemical alteration of deposits by hydrothermal activities and interaction of the base rock with the thermally active fluids generally varies the ore grade by re-activation of nickel and sulfur in their mineral forms. Generally, this type of ores contain an average of 0.4-2.0% nickel, 0.2-2.0% copper, 10-30% iron, 5-20% sulfur with other minerals like silica, magnesia, alumina, and calcium oxide. Characteristic mineral phases are Fe-Ni-Cu sulfide such as pyrrhotite (Fe_{1-n}S), millerite (NiS), pentlandite ($\text{Fe,Ni}_9\text{S}_8$) and chalcopyrite (CuFeS_2) together with other minerals like pyrite (FeS_2), magnetite (Fe_3O_4) and ilmenite (FeTiO_3). Among them the highest individual nickel load comes from pentlandite with 34.22% of nickel content. Unlike lateritic ores, sulfide types have high nickel grades and may extent both vertically and horizontally on a large area and can be found as distinct sulfide body or groups of deposits allowing cheaper and simpler mining methods. On the other hand, currently there is a decline in operability of magmatic sulfide ores due to depletion of already existing ores after several years of extraction and absence of sufficient new ore explorations. The depletion of sulfide type ores creates the necessity for mining at lower sections of ore deposit which increases the capital and operation costs of the operation. These requirements highlight its competitive ore type with lower grade but higher world capacity. The three most famous sulfide ore types that are still in use are located at Norilsk (Russia), Sudbury and Voisey's Bay (Canada) [7,11,12].

General route for nickel extraction from sulfide type ores can be summarized as follows: Underground or open-cut mining of reserve is followed by concentration of ore feed by flotation. After enrichment, ore is fed to the smelters in order to produce nickel-copper matte which is further treated in refineries to obtain final pure metal product. With respect to this simple and standardized processing condition, sulfides are overshadowing more sophisticated laterites that cause laterites to be more expensive sources.

2.1.2. Oxide Type Nickel Ores

Oxide type nickel ores or more commonly laterites also have long commercialization past going back to 1875 in New Caledonia after 10 years they had been discovered for the first time. However, these sources were overshadowed by Sudbury ore site production which started in 1905 and totally dominated the world nickel production for the next 70 years. The trend on sulfide type nickel ores has continued up to now and today the highest portion of nickel production is still driven from these ore deposits. The interesting point here is that laterites are estimated to have 84 million metric tons nickel capacity worldwide which corresponds to roughly 70% of the world total nickel reserve. On the contrary, laterite ore deposits are responsible for only 40% of the total nickel production rest being covered by sulfide type ores [8,13].

Oxide type nickel ores are of great interest since the problematic issues in sulfide type ores confine the nickel supplier companies on exploration of new ore resources and hence new technological developments in order to meet continuously growing future nickel demand. Being more complex in mineralogy and having lower grades with respect to sulfide ore type have not decreased the attraction on laterites. Instead within a very short time, the number of lateritic nickel ore deposits has reached to 117 and most of them have been classified with respect to their mineralogical profile [14]. However, the project developments could not have reached the same pace due to operational problems mainly caused by wide variations in mineralogy of these ores and absence of the absolute winner of the most beneficial extraction process on these ore types. Furthermore, refinement issues to obtain the final product are still in development. Despite some well-developed flowsheets offered, they came up with sensitive balance between pros and cons. In order to understand these pros and cons of nickel extraction procedures from these ores, the nature of laterites are to be known in detail.

Nickel laterites are the product of chemical and mechanical weathering of ultramafic rocks called laterization. On average, an ultramafic rock can contain 0.3% nickel and 0.06% cobalt [15]. Laterization involves dissolution of original minerals more commonly olivine, movement of dissolved

elements in solutions and precipitation of these mobilized elements in another location. This mechanism results in a nickel and/or cobalt deposit only if these base rocks contain a protolith lithology that is essentially enriched in nickel. Weathering of these rocks occurs in two distinct stages. In the first stage severe weathering of protolith occur after which it may transform into serpentinite (olivine dominated parent rock) with a concentration of up to 5% nickel and 0.06% cobalt. During this initial stage, sweeping of more mobile elements (Mg, Si, Ca, Na) occur through lower sections while less mobile (Si) or immobile elements (Fe, Al, Cr, Ti, Mn) remain and concentrate in upper sections. Further weathering on the resultant serpentinite creates the actual laterite profile and more prone to include several factors during its weathering than protolith does which results in a complicated profile. These so-called factors include climate, geomorphology, chemistry and rate of chemical weathering (including Eh and pH of circulating water), drainage and tectonics apart from mineralogy of peridotite itself [16]. On the other hand, mechanical weathering during laterization can also influence the process by creating fractures and faults which expend the surface area of the parent host material that is being exposed to chemical weathering. Additionally, removal of sections by fault zones enables the interactions between the host materials with nearby ultramafic rocks such as carbonates. As described, interchange positions between metallic and/or non-metallic ions within the precipitated minerals more complicate the scenario. All these factors interplay and change the mineralogy of whole laterite during a very long time period and create complicated ore profiles to deal with. When nickel concentrations are considered, these factors are more crucial for the reason nickel not being concentrated in a distinctive level but rather distribute all through the profile in varying portions.

Researchers have classified the laterites with respect to their weathering profile and also by their mineralogical characteristics. Apart from that some researchers divide the lateritic ore types by their main nickel-bearing mineral type as iron-oxide (limonite), clay silicate (nontronite) and magnesium hydrous silicate (saprolite) as can be seen in Figure 4. Typical resultant ore profile that idealized to include all possible layers can be seen in this figure. However, the natural profiles are more complex and unique. They either do not follow the exact sequence that will be described as follows or generally miss one or more layers or contain all the layers within the exact sequence [15]. Besides, there are external forces to be considered that can mix up the layers in limited portions such as erosion, landslip, earthquakes, faults and fractures, etc. As a result each ore deposit should be studied by a careful in situ mineralogical examination for the exact geomorphology. Within that manner geological and mineralogical studies carried out so far will be discussed in another section for Çaldağ laterite deposit.

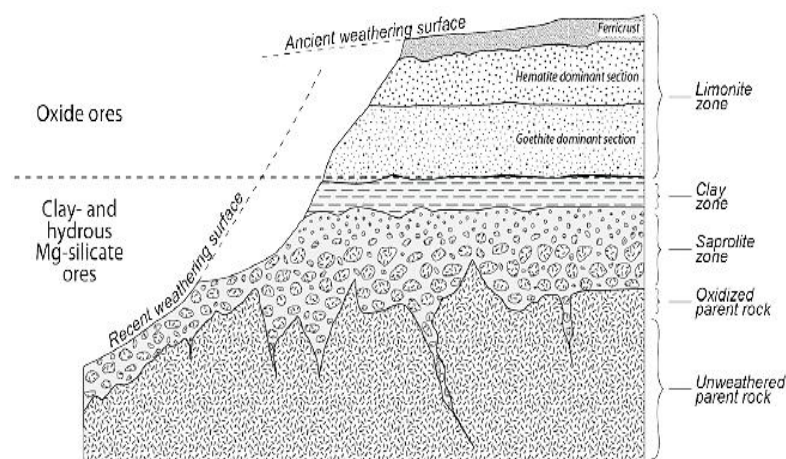


Figure 4 Typical ore profile including all possible layers [15].

In the general scenario there exists a limonite zone covered with economically invaluable ferricrust both of which are mainly iron dominated as iron is insoluble and readily oxidizes in solution during laterization. Limonite zone is divided into two types of sub-zones. Red limonite is very alike of

ferricrust and dominated with hematite (Fe_2O_3) with some goethite (FeOOH) containing <0.8% Ni, <0.1% Co and >50% Fe. On the other hand, the lower zone, yellow limonite, is mainly goethite with some hematite or other iron oxides containing <1.5% Ni, <0.2% Co and <50% Fe. Overall of this zone is an average composition of 1.4% Ni, >40% Fe and 0.15% Co with low silica and magnesia. The nickel associated minerals are generally iron oxides commonly as goethite with less commonly other iron oxides such as hematite ($\alpha\text{-Fe}_2\text{O}_3$), maghemite ($\gamma\text{-Fe}_2\text{O}_3$), and magnetite (Fe_3O_4) [3,17]. Many laterites include a common feature of a thin but hard layer of manganese and cobalt rich layer usually right below of the limonite layer or sometimes intermixed with it. As can be seen in the Figure 5 minerals correlated to this thin layer are types of manganese oxyhydroxide such as lithiophorite and asbolane (or asbolan). These manganese phases can exist in coarse grains and generally are problematic by means of cobalt extractions since cobalt is found to highly associate with these minerals [13]. Apart from these minerals some non-nickeliferous minerals such as gibbsite can exist in lower amounts.

Below limonite layer a silicate dominated region starts since most of the iron is entrapped in the limonite zone and now the major players are magnesium and partly aluminum as silicates. Hence, nickel association is unavoidably with these silicates as can be seen in Figure 5. The clay zone or smectite-quartz zone or nontronite zone is composed of soft smectitic minerals (nontronite, montmorillonite and beidellite) with hard quartz. It is also known as transition zone between iron oxide/hydroxide dominated limonite and magnesium silicate dominated saprolite zones. Generally it does not exist for most of the laterite ores but those suffer from insufficient water circulation in arid regions (i.e. central Western Australia) were found to contain this layer. The reason for their existence is the restricted mobilization of elements due to lack of sufficient solvent (water) media. Most commonly observed mineral is nontronite (iron rich smectite) $\text{Na}_{0.3}\text{Fe}_2(\text{Si},\text{Al})_4\text{O}_{10}(\text{OH})_2 \cdot n(\text{H}_2\text{O})$ that gives its name to the zone. Nontronite is the main nickel bearing mineral with 2% individual nickel capacity together with some goethite and manganese oxyhydroxide contributions. Along with nontronite other smectites such as montmorillonite $(\text{Mg},\text{Ca})\text{O} \cdot \text{Al}_2\text{O}_3 \cdot 5\text{SiO}_2 \cdot 6\text{H}_2\text{O}$ (magnesium rich smectite) and beidellite $\text{Na}_{0.5}\text{Al}_2(\text{Si}_{3.5}\text{Al}_{0.5})\text{O}_{10}(\text{OH})_2 \cdot n(\text{H}_2\text{O})$ (aluminum rich smectite) can also contribute to the ore grade.

Below this transition zone there is saprolite zone or serpentine zone. Basically, this zone is the altered parent rock (generally olivine) with some remnant of it in fresh state. Mineralogy is generally dependent on the nature of the parent rock and degree of its serpentinization and hence the degree of water drainage. An average composition of the saprolite zone can be given as 2.4% Ni, 0.05% Co and less than 15% of iron with high amount of magnesia and silica. Saprolite layer is less humid with respect to upper layers due to lowered water inclusion. The major phases are expectedly hydrous magnesium silicates such as serpentines $\text{Mg}_3\text{Si}_2\text{O}_5(\text{OH})_4$. However, nickel substitution for magnesium creates a new mineral called garnierite. On the other hand, most of the authors do not accept garnierite as a mineral but rather termed as a general name for Ni-Mg silicates which usually occur as a mixture of two or more of serpentine, talc, smectite, sepionite and chlorite $(\text{Ni},\text{Fe},\text{Mg})_5\text{Al}(\text{AlSi}_3)\text{O}_{10}(\text{OH})_8$. Other observable minerals in this zone are goethite, magnetite, maghemite, chromite (FeCr_2O_4). The bottom section is unaltered bed rock or source rock that is responsible for the laterite profile. The major constituent of the rock is olivine blended with varying amounts of pyroxene. However, fissures of serpentine and chlorite from upper section can also be observed. Generally this bed rock is left in situ without any operation on it.

Ore type	Zone	Section	Alternative nomenclature	Nickel-bearing minerals
Oxide	Limonite	Fisolithic	nodular ironstone; ferricrete layer; durmicrust; iron pan; iron cap; canga; cuirasse	Goethite Hematite Asbolan Lithophorite Heterogenite
		hematite dominant	fine-grained saprolite; Red Laterite	
		goethite dominant	<i>in-situ</i> limonite zone; Yellow Laterite	
Silicate	Clay		intermediate zone; smectite-quartz- zone; quartz goethite zone, nontronite zone; mottle clay zone;	Nontronite Beidellite Montmorillonite Saponite
		Hydrous Mg-Silicate	Saprolite; serpentine ore; soft serpentine, soft saprolite; saprolitic serpentine; coarse grained saprolite	
	Oxidized parent rock	hard saprolite; saprolitic peridotite; saprock		

Figure 5 Typical profile layers of a lateritic ore with characteristic nickel bearing minerals.

As mentioned previously, another division type for lateritic nickel deposits are made with respect to the state of dominant nickel bearing minerals. Actually, these sub-types can be interchangeably used for laterite layers with the sequence of Fe-oxide being limonite layer, clay silicate being nontronite layer and Mg-silicate being saprolite layer. The frequency of these ore types and respective nickel and cobalt grades are listed in Table 3 based on several technical information data. As can be seen while nickel grade is the highest for Mg-silicates due to Mg-Ni interchanges in serpentines, it is Fe-oxides for cobalt due to correlation of manganese oxyhydroxide minerals with cobalt. However, the general tendency of nickel is that nickel content increases with the increase in the depth of the layer while cobalt is majorly affected by the mobility and existence of manganese. But it is quite clear that cobalt content is the highest for limonite type ores due to manganese association.

Table 3 Frequency of lateritic ore types based on dominant nickel bearing layer types with their average grades (Adopted from [14]).

Sub-type of laterite deposit	Number of Deposits	Average nickel grade %	Average cobalt grade %
Iron oxide	61	1.14	0.09
Clay silicate	12	1.27	0.06
Hydrous magnesium silicates	44	1.44	0.06
Total/Average	117	1.30	0.08

2.2. Production Methods of Nickel from Laterite Ores

Due to complex and diverse mineralogy of laterites, varying nickel and operation-related metal contents between the ore deposits and within the layers of each deposit, different processes are in commercial use for nickel and cobalt extractions within specified layers. The only common step for all methods is that they generally excavate the ore by open-cut mining due to extensive surface area but shallow depth of laterites. The open-cut mining is followed by simple upgrading methods like discarding of gangue minerals since flotation is not available due to scattered nickel distribution in several nickel-bearing minerals.

Today, there are three well-developed and commercially utilized production options of nickel from laterite deposits namely pyrometallurgical (ferronickel or matte smelting) routes, hydrometallurgical (atmospheric or high pressure acid leaching) routes or Caron process route. Despite the fact that all can be theoretically applied to whole laterite profile, the economic concerns restricted the processes by ore-type. Each process is almost specialized for utmost capability for distinctive layers that can be seen in Figure 6. Limonite layer is the most suitable for hydrometallurgical processes while saprolite layer is more suitable for rotary-kiln electric furnace (RKEF) representing pyrometallurgical route. The reasoning for this diversion will be discussed as follows.

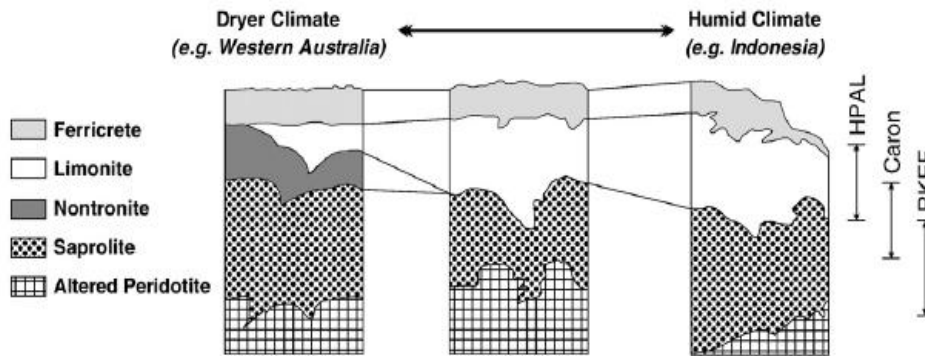


Figure 6 Typical laterite profiles with varying climate and weathering conditions and respective processing options [8].

2.2.1. Pyrometallurgical Routes

Pyrometallurgical routes are constituted by two sub-options which are smelting to either ferronickel product or iron-nickel sulfide matte. The choice whether the product from smelters will be transformed into ferronickel or matte is mainly dependent of magnesia-to-silica ratio of ore feed or basicity of slag formed in the furnace. Most laterite projects around the world that utilizes the pyrometallurgical routes prefer RKEF plants with resultant product being commonly ferronickel. A general flowsheet of pyrometallurgical process can be seen in Figure 7. Chiefly preferred ore type is saprolite dominated one that include low moisture and iron content but high amount of magnesia and silica together with higher nickel grade with respect to other types. Low moisture and high quality slag forming elements make the saprolite the most suitable ore feed to this route.

In the ferronickel production option, the ore feed is first subjected to blending and drying followed by calcination and pre-reduction at 850°C to 1000°C. RKEF plant is where the ore feed is dried, calcined and reduced after which the resultant product is fed into smelters at temperature reaching 1600°C where the slag is discarded. The rest of the flow is forwarded to refining unit in order to produce final ferronickel product with 20% to 50% nickel content. In sulfide matte production a similar route is

followed that is applied for nickel-copper matte production from sulfide type nickel ores. Here again the affinity for nickel to sulfur is basically utilized principle. In order to achieve that goal the feed is sulfurized prior to smelting by a sulfur-containing reagent such as gypsum ($\text{CaSO}_4 \cdot 2\text{H}_2\text{O}$). Resultant product coming from converters contains 78% nickel within the sulfide matte. Despite RKEF uses much cheaper heat source than shaft reduction furnaces (coal versus oil) these processes are still high energy demanding processes with critical environmental problems due to SO_2 emission [18]. Furthermore, inability to obtain cobalt as by-product and losses of valuable nickel in discarded slag decrease the benefits of the process. As a result of that, high ore grade is required for process to be beneficial which restricts the process applicability on most of the laterite deposits. Today some Chinese stainless steel producers have developed a process for blending limonite ores with conventional iron ore to achieve an input for stainless steel. However, the limonite ore should have uneconomic grades to be treated with other options with trace cobalt contents and up to 60% iron. Such a highly iron dominated limonitic ore is in Acoje, Philippines.

2.2.2. Caron Process

One of the oldest nickel extraction method dated back to 1940 is Caron process that combines the parts of the flowsheet of hydro- and pyrometallurgical methods together. Unfortunately, this process is somehow being abandoned during the race between other process routes. Actually, only 5 plants have ever been constructed but 4 (i.e. Yabulu, Australia and Berong, Philippines) of them are still in operation which proves its reliability [13]. Still this reliability is worth for 5 more laterite deposits to be considered for Caron process as can be seen in Table 4. General flowsheet for Caron process can be seen in Figure 7 and begins with drying and grinding followed by calcination and reduction of ore feed just like in pyrometallurgical routes. The aim of these pre-treatments at 750°C is to selectively reduce nickel and also cobalt in their elemental state under a reducing media leaving unreduced gangue portion of the ore feed as discharge. After that step, resultant product is let to leach at temperatures close to ambient temperature and under atmospheric pressure in ammonia-ammonium carbonate solution. By doing so, a solution is gained that contains ammine complexes of nickel and cobalt. This solution is forwarded to ammonia removal stage where nickel and cobalt precipitate as carbonates. After that step either calcination is applied to transform these carbonates into their respective oxides or it can be refined by solvent extraction and electro-refining. The resultant final products are generally with composition of 75-85% nickel and 45-55% cobalt [9].

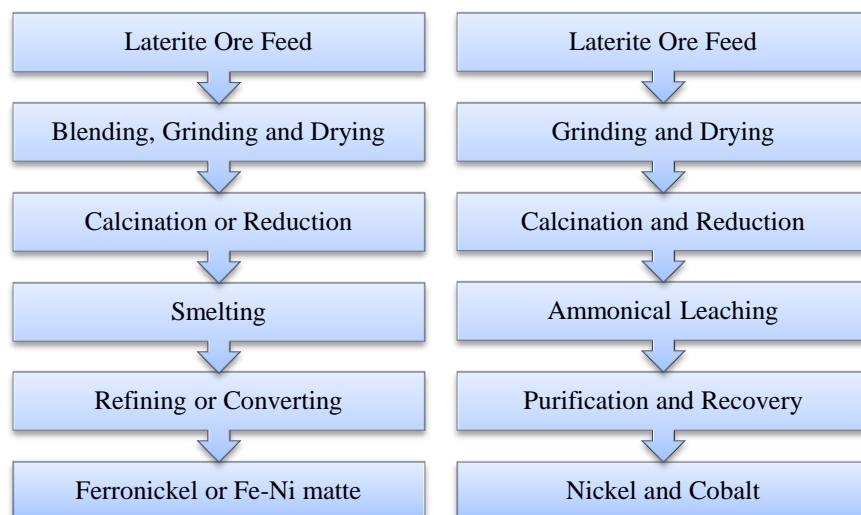


Figure 7 Pyrometallurgical (left) and Caron process (right) flowsheets for lateritic nickel deposits.

2.2.3. Hydrometallurgical Routes

From the date 1959 when the first high pressure acid leaching plant was constructed in Moa Bay, Cuba hydrometallurgical routes started to function as an alternative route for the two old-fashioned models proposed in previous sections. As can be seen in Figure 6 and Table 3 the nickel content is increasing as the depth of the ore increases down to saprolite. RKEF and Caron processes are suitable as far as nickel grade is high enough to meet the process costs and preferentially ore feed is not so humid to be severely dried and calcined by means of high heat energy source requirements. However, there should have been a new approach especially for limonite type laterites that are more commonly discovered but relatively low in grade and with a moisture content from 25% to 40% (or for some even more than 40% depending on the geological conditions) (See Tables 3 and 4). At that point, researchers defined new, acid-centered flowsheets to extract nickel from ores that are low in grade and containing low concentrations of acid consuming elements (i.e. Mg). Within these flowsheets the utmost temperature required is 270°C which is well below the other two process options. The general temperature ranges of the flowsheets are between ambient temperatures to 250°C depending on the sub-routes which decreases the operational outcome by means of heat energy costs. This new approach also eliminates most of the environmental concerns due to high amount of waste and toxic gases (such as SO₂) released during heating the ore feed in calcination stage. As a side benefit, other precious metals (such as scandium) that might exist within the ore feed together with nickel and cobalt can be extracted within the acid media giving the chance of their recovery and utilization. Under this subject two well-developed flowsheets and other developing options will be discussed as follows.

Table 4 Ore types with extraction methods and records for processing (including developing projects) (Adopted from [14]).

Subtype of laterite deposits	Number of deposits	Number of records for processing	Nickel extraction methods			
			Ni-Fe smelting	HPAL	AL	Caron
Clay silicate	12	8	5	1	2	-
Hydrous Mg-silicate	44	35	26	7	2	-
Iron oxide	61	47	9	21	7	10
Total	117	90	40	29	11	10

2.2.3.1. Atmospheric Leaching (AL)

Atmospheric leaching is a simple, cheap and less heat-intense process and covers several modifications of actual one which is heap leaching process. These variations are agitation, vat, column and in-situ leaching. Column leaching is not an industrial application but rather a laboratory scale modification of heap leaching. Temperature of these processes range from 25°C to 105°C depending on the process condition but the pressure is kept constant at 1 atm for all variations. The solvent is either organic or inorganic acid. Among the others, heap and agitation leaching are the most important ones for industrial applications. Hence these two processes will be detailed.

Heap leaching experience was triggered by European Nickel PLC (laterally named as Sardes Nickel, a subsidiary company) in Çaldağ lateritic ore deposit in Western Turkey. The process is quite simple and has proven itself to be successful as it will be discussed further in another section provided for Çaldağ. The route starts with the formation of ore feed in the shape of high heaps (4-5 meters in height) on special membranes after ore preparation steps such as grinding, crushing etc. with simple coarse ore rejection route is completed. Once the heaps are compiled and set ready for leaching, the irrigation of the ore feed by sulfuric acid is initiated atop of the heaps. As the acid flows through the heaps and percolates in the fine ore particles, it derives the nickel and cobalt out of the host minerals

with the reactions during acid attack. The resultant solution which is called as pregnant leach solution or PLS due to nickel and cobalt load with several contaminants is directed to and collected in special ponds nearby. A schematic view taken from Çaldağ heap leaching project and process flowsheet can be seen in Figure 8.

Reactions are just same as those occur in sulfuric acid HPAL process that will be discussed in further sections. The exceptions are the reactions regenerating acid related to precipitation reactions of specific elements (iron and aluminum) that are characteristic for HPAL conditions. Despite the reactions are about the same, due to lower operational temperatures and the only driving force being gravitational, reaction kinetics is quite slow. As a result, extensive residence times are required for a heap to be sufficiently depleted from nickel and cobalt or in other words high extraction goals can be achieved. The extraction efficiencies are less than 85% for nickel with very long leaching durations as long as 1.5 years or even more requiring large land supply for each heap formation. Besides, high acid consumption of process is another drawback resulting from this low selectivity. In addition to that, lack of earlier precipitation reactions of specific elements create a problematic product solution (PLS) to be purified in downstream processes and a waste solid product to nature as disposal. Precipitation of iron in the form of chemically unstable jarosite can cause environmental problems in long time periods as this complex compound dissolve in time and release unwanted ions on turning into hematite.

The selectivity of heap leaching is poor for nickel and cobalt over other metals such as iron and aluminum that are generally very high in concentration in limonite ore feed with respect to approximately 1% nickel and <1% cobalt. Hence with their extraction, one should deal with a highly contaminated solution to purify in order to obtain an intermediate or final product. Another operational problem is the decline in permeability of heap as the percolation and reactions of acid destroy the agglomerates in time. Agglomeration is helpful such that it uplifts the permeability of heap. Additionally, ore feeds that are relatively rich in clay minerals and goethite are also difficult to treat since the clay minerals are known to deteriorate the permeability of the heaps and goethite creates a high mass loss which can be detrimental for heap structure. According to Willis (2012) the major advantage proposed for favoring the heap leaching which is the low capital cost is contradictable. Despite heap leach option removes the requirements of expensive autoclaves and CCD tanks (as collected solution is solid free) it actually leaves the other necessary operational services and utilities just the same. It is estimated that the capital cost saving by the choice of heap leach rather than HPAL plant at the same conditions is by 15% to 20%. On the other hand, revenue of valuable metal extractions decreases by 15% to 20% with the less metal recovery by heap leaching exactly in the same percentage ranges [6]. Hence the major highlight of heap leaching is somehow doubtful at that point.

Due to its low metal extraction values and high acid consuming behavior with respect to HPAL option, researchers agree on the fact that heap leaching is best suitable for low grade laterites or low capacity ore deposits that could not meet the capital costs of HPAL or any other atmospheric leaching options (i.e. agitation leaching). Additionally, low clay including, hematite rich ore feed is the most preferred option. This restriction is related to the permeability effects of so-called minerals in heaps as hematite causes less mass loss unlike goethite. Additionally, saprolitic ore feed are also suitable for their high silica content which is reluctant to dissolve and does not create detrimental mass loss in heap during acid percolation.

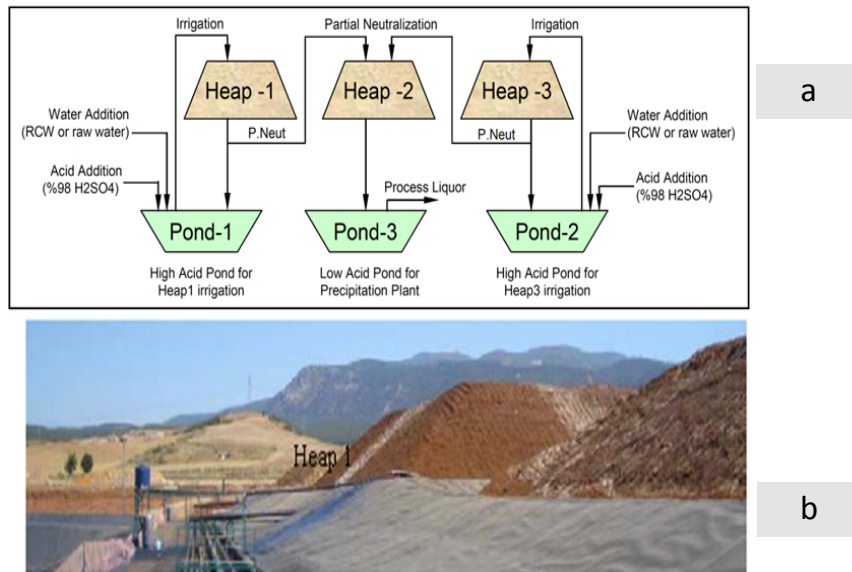


Figure 8 Flowsheet of heap leaching (a) and schematic view taken from Çaldağ heap leach project (b) [19].

Another process option that is utilized by industry under atmospheric conditions is agitation leaching. Today many atmospheric leaching projects are tank or more commonly known as agitation leaching processes and actually the only heap leaching project ever tried in Turkey is that in Çaldağ. Agitation leaching route is a more accelerated form of heap leaching with utilization of carbon steel reaction tanks rather than heap formation. The acceleration of reaction kinetics are due to higher operational temperature which is about 95°C (but can be up to 105°C) and treatment of slurry with mechanical or aerial stirring within the tanks that increases the effective acid-ore feed interaction and fastens reaction rates. Generally the feed size ranges between 0.5 to 1.0 mm for sufficient extraction process and solid concentrations between 25% and 30% are suited most while the nickel and cobalt extractions are at least 80% and within down to 10 hours of residence time [6,20]. After leaching is conducted in several tanks in series, colloidal mixture is forwarded to counter-current-decantation tanks where solid and liquid parts are separated from each other. While overflow PLS is directed to neutralization unit for metal recoveries the underflows are discharged as solid wastes.

Despite its beneficial points such as shorter durations with higher extraction efficiencies than heap leaching and simpler process equipment with low maintenance with respect to HPAL, many problems associated with sulfuric acid heap leaching are still valid for agitation option. High acid consumption due to lack of iron and aluminum re-precipitation reactions (see HPAL section) is once again the most important problem both for high operational cost and also instable and problematic resultant waste solid (i.e. jarosite) [21]. Hence low iron containing saprolitic ore feeds are most suitable for this process. Typically, the acid consumption of atmospheric leaching is 0.8 to 1.0 kg/kg of dry ore depending on the concentration of acid consumer elements. For a saprolitic ore feed containing constant high nickel grade will require almost the same amount of acid input for either HPAL or AL option in case of which HPAL will be less attractive due to higher capital cost of HPAL plant.

In last decades, there have been many efforts for improvement of AL flowsheet. Several different acid types were studied in order to observe their efficiencies. Chander (1982) reported the sequence of increase in nickel extractions with increase in acid strength such as perchloric, nitric, sulfuric, hydrochloric and oxalic acid while Valix et al. (2001) studied the efficiency of bioleaching in comparison to chemical leaching and it was stated that at the same acid concentrations latter one was less effective due to dual effect of fungus and bacterium and acid by means of ore dissociation and process participation [22,23]. Other studies including chemical variations (reagent additions, two stage atmospheric leaching, redox-controlled AL options and so on) can be found as brief summaries in

worthful studies elsewhere [24,25]. Today there are three new AL projects that are being proposed for Weda Bay (Indonesia), Dutwa (Tanzania) and Zambales (Philippines) ore deposits.

2.2.3.2. High Pressure Acid Leaching (HPAL)

As stated before, the history of high pressure acid leaching (alternative nomenclatures: HPAL/PAL/HiPAL) is back to first generation plant, Moa Bay in Cuba that started to operate in 1959. However, the interest in HPAL technology was seriously interrupted for almost four decades after that initiation due to several engineering problems mainly caused by severe operational conditions that overcome the unqualified engineering materials. With development of engineering technology which led to more trustworthy reaction-bearing autoclaves, three new projects were initiated in late 1990s in Western Australia, namely Murrin Murrin, Cawse and Bulong. Among them only Murrin Murrin could have survived up to now while others had suffered different operational problems and unavoidably closed [21]. Despite this discouraging situation, a great knowledge was gained and a third generation of HPAL continued the trend with Goro (New Caledonia) and Rio Tuba (Philippines) projects in 2004. After that third generation the process has been of interest with considerable offers that can highlight its applicability mainly on limonitic laterites that exist most frequently. Several HPAL plants have been developed or in development stage such as Ravensthorpe, Kalgoorlie, Gladstone Pacific, Mount Margaret in Australia; Coral Bay, Mindoro in Philippines; Vermelho in Brazil; Goro and Prony in New Caledonia; Weda Bay and Gag Island in Indonesia; Ramu in Papua New Guinea; Sechol in Guatemala; Ambatovy in Madagascar and so on [3,26]. The situation in Turkey is also promising due to the efforts by META Nickel and Cobalt Company. According to recent news, this company is constructing a HPAL plant on nickel reserves in Gördes, Manisa. As it is a limonitic type laterite ore, it is believed that Çaldağ nickel ore will be also suitable to be considered as an ore feed for HPAL plant. Within this study this alternative situation was tried to be investigated in laboratory scale. A simple flowsheet can be seen in Figure 9 including further steps after high pressure acid leaching.

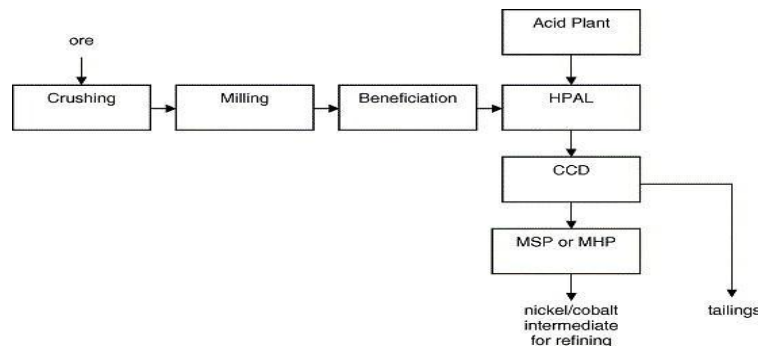


Figure 9 Simplified high pressure acid leaching flowsheet.

High pressure acid leaching by definition operates at pressure range between 35 to 55 atm, temperature range between 240° to 270°C and residence time between 0.5 hour to 1.5 hours [27]. The expected minimum extraction percentages of nickel and cobalt should be at least 95% but rarely can be as low as 90% for each. Ore preparation steps are similar to that for any other process except that the optimum particle size range for HPAL is generally in 250 to 500 microns but this is not a strict limitation. As the main nickel bearing mineral is goethite which naturally occur in fine grain sizes gangue mineral rejection is applied to concentrate nickel in ore feed. Ore feed is then slurred with a pre-determined solid concentration and thickened prior to injection into pre-heaters that can range between 25% and 45%. Degree of thickening is mainly dependent on the rheology of slurry which is mainly dependent on the ore mineralogy of ore feed. Hydrophilic minerals such as expendable phyllosilicates may restrict the solid concentration below the range 25% to 30% [1]. Water supply can

be from hypersaline (sea water) to tap or fresh water sources depending on the supply abilities of plant. Both the solid concentration and the water source type have important influences on the process train. Logically, the higher the solid concentration fed into autoclaves the higher the capacity of process and the higher the operation benefits but there are some limitations. According to David (2008) slurries containing higher than 42% solid will create an excessive viscosity that could not be pumped even with currently used positive displacement pumps [28]. On the other hand water supply characteristics are of concern for especially the scale formation problem (the most detrimental problem suffered in Moa Bay plant) and also leach residue character. These issues will be detailed in following sections. In preheaters, the slurry temperature is raised step by step up to 200°C by low pressure steam injection. Additionally, the heat within the discharge from autoclave is partially used. After that stage, slurry is fed into first compartment of the autoclave while sulfuric acid injection is also applied in the meantime.

The autoclave design has changed greatly in last 4 decades to optimize the efficiency especially against acid corrosion. The first generation autoclave used in Moa Bay was 4 separate, vertical, acid-brick and lead-lined compartments in series with agitation of steam power. As can be seen from Figure 10, HPAL autoclaves are now horizontal, titanium-lined carbon steels with up-to-7 compartments in series in one vessel. Agitation is now gained by titanium blade agitators in each compartment and acid injection applied in tantalum dip-tubes [6]. Usage of titanium as major material is especially important for the presence of chloride coming from hypersaline water sources in any section of autoclave as titanium is not only resistant to sulfuric acid but also chloride. After the entrance of slurry in first compartment, the determined amount of concentrated sulfuric acid (98.5% w/w) in accordance with pre-determined acid to ore ratio and high pressure steam at temperatures between 265°C to 275°C are released from pipelines into the autoclave to maintain leaching conditions described above. Another reason for steam inlet to the autoclave environment is the prevention of vaporization of inputs. The amount of acid insertion is majorly related to ore mineralogy of feed and any ore blend options that have been chosen. Typically a limonitic ore feed would require an acid load between 200 kg to 400 kg per ton of dry ore depending on the ore response to acid dissolution while it is 1000 kg per ton of dry ore for average atmospheric acid leaching process [6]. Besides, some portion of this acid load remains within the resultant leach solution. The resultant leach solution from HPAL contains typically 30-50 g/L free sulfuric acid that is essentially required for some reasons that will be mentioned in the following sections. If the ore feed mineralogy is depicted to have high concentrations of magnesium and/or the extent of iron and aluminum re-precipitation reactions are insufficient the demand in acid load will increase due to the fact that the acid loss in magnesium sulfate and the extent of acid bond to basic sulfate forms of iron and aluminum will increase. As limonitic laterites are lower in nickel grade, an approach to blend this ore feed with higher nickel grade saprolitic ore was proposed. However, this higher revenue of nickel would definitely require higher acid consumption as saprolitic ore feed is rich in net acid consumers. In that case a limit for a bearable acid cost can be gained by a blend containing magnesium in strict range of 4.5% to 5.5%. Resultant acid demand for such a limonite-saprolite blend can rise up to 550 kg per ton of dry ore [1,6].

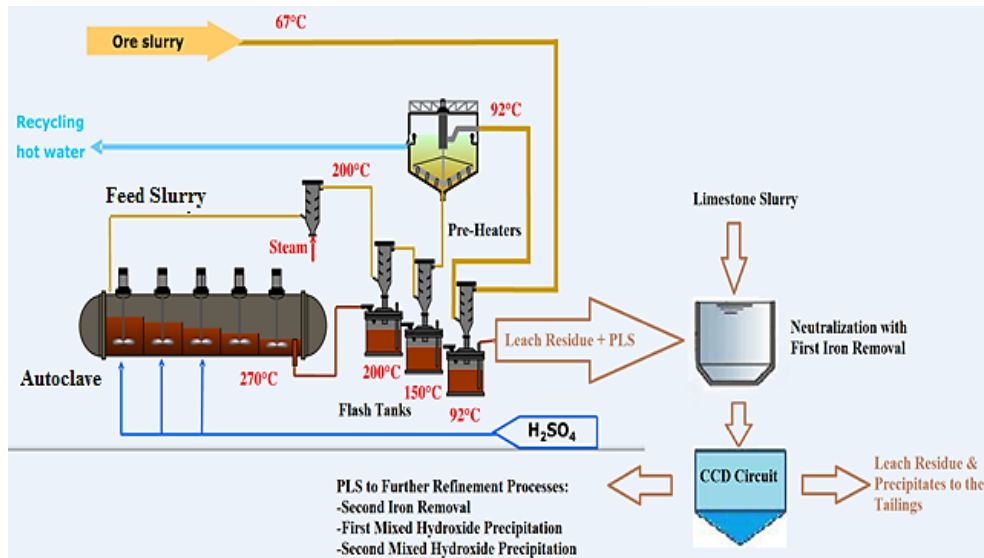


Figure 10 Schematic view of high pressure acid leaching flowsheet followed by MHP downstream choice.

After the acid leaching is performed, thereby complete dissolution of nickel and/or cobalt bearing minerals are achieved, the heterogeneous mixture is forwarded to counter-current-decantation tanks after pressure letdown of the sludge. The sludge contains several metal loaded liquid pregnant leach solution (PLS) and hematite dominated solid leach residue. Counter-current-decantation or CCD tanks are utilized in all HPAL plants in order to separate these solid and liquid parts of sludge obtained after pressure acid leaching. Commercial HPAL plants generally contain 6-7 CCD tanks in series with varying capacities [29]. The wash water is generally the barren solution directed from downstream applications. By washing action any interrupted leach solution can be disintegrated from solid part and the further loss is highly prevented. It is quite important to adjust the pH level of this barren solution so as not to cause any afterward precipitation of any metal as respective hydroxides (pH relation with so-called metal hydroxides will be discussed in downstream application). The aim is generally towards to lower the pH of the solution as it also helps better settling behaviors of the solid wastes. Here it can be seen that depending on the downstream application a slight change may occur in HPAL circuit. For mixed hydroxide precipitation route, prior to CCD tanks the colloidal sludge is subjected to limestone slurry addition in order to neutralize and precipitate most of the iron (First Iron Removal). A schematic view of three CCD tanks in series can be seen in Figure 11 with explanation of working principles which is a simple one. While solids are settled at the bottom of the tanks and forwarded to the tailings as underflow, the liquid section is directed to second iron removal unit as overflow [27]. Prior to the release to the nature, solid wastes are neutralized by lime addition in order to remove their environmental hazards.

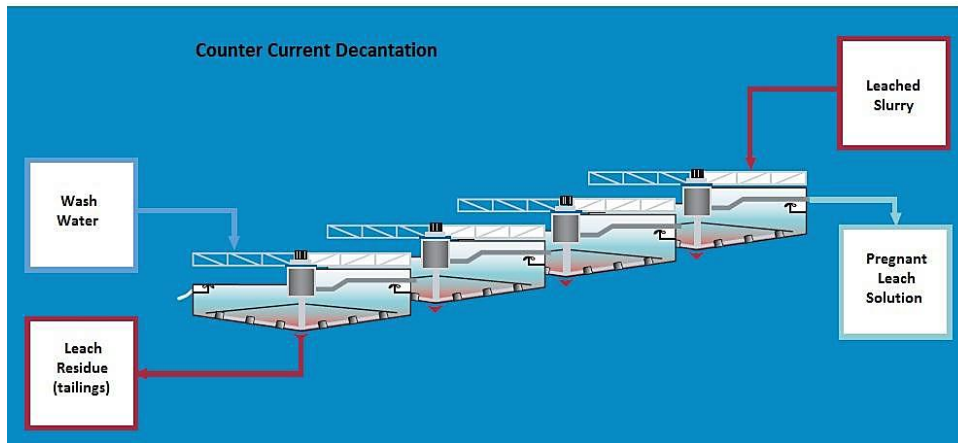


Figure 11 Counter-current-decantation circuit.

The comparison between HPAL and AL (overall) processes is made in Table 5 and Figure 12 for several important issues. The expensive autoclaves with care-requiring setup; sensitive designing and on-stream issues forced by harsher operational conditions and the higher energy requirement for especially heating purposes are major drawbacks for HPAL process. On the other hand, higher extraction efficiencies are warranted by HPAL in shorter residence time with lower acid consumption. All these together bring out higher output and capacity of process train in the same time limit and ore grade. Additionally, resultant leach liquor can also be problematic for some AL solutions creating low quality intermediates to be sold with less profit. This is mainly due to high iron dissolution and mostly iron being in divalent form that is hard to remove from the solution prior to gain an intermediate nickel product. According to Chou et al. (1977) a drastic increase in Ni:(Fe+Al) ratio occurs before and after the HPAL operation which is not possible for AL. This ratio is usually about 0.03 to 0.04 in the ore feed whereas in leach liquor it approximately transforms into 3 to 4 with 100 to 150-fold increase [30]. Hence, the liquor is more easily treatable and costs fewer reagents for its less impurity amount. In the same manner, solid waste is another issue to deal with. In AL process the leach residue is mainly goethite or more commonly jarosite (if fresh water is not used) both of which are in greater volume with respect to hematite of the HPAL process. As a result larger capacity CCD tanks and storage land is required for these residue types due to their chemical nature. Goethite is hydroxide transform of hematite with water expansion. Jarosite on the other hand is a complex compound that incorporates several other elements than iron and oxygen. Consequently, HPAL option is seemingly more attractive especially when limonitic ore feed such as Çaldağ lateritic ore is concerned.

Table 5 Comparison of HPAL and AL with respect to several issues [20,31].

Issue	High Pressure Acid Leaching	Atmospheric Acid Leaching
Capital cost	High	Low
Maintenance	High	Low
Acid consumption	Low	High
Residence time	Short	Moderate to Long
Downstream Applications	Predictable	Some difficult solutions
Extraction efficiency	High (at least 90%)	Variable (75%-90%)
Energy Requirement	Moderate	Low
CO ₂ Emission	About the same	About the same
Solid Disposal Risk	Low	High
Settling Characteristics	Less Problematic	More Problematic

Process	Embodied energy (CJ/t Ni)	CHC emissions (t CO ₂ e/t Ni)		Overall nickel recovery (%)
		With acid plant	Without acid plant	
<i>Hydrometallurgical</i>				
High pressure acid leach	272	22.7	27.3	92
Atmospheric acid leach	167	14.6	25.1	80
Enhanced pressure acid leach	249	17.8	23.2	85
Heap leach	211	17.6	28.0	73

Figure 12 Overall energy requirements and nickel recoveries of hydrometallurgical process routes (Adopted figure from [31]).

2.2.3.3. Other Routes and Future Developments

2.2.3.3.1. AMAX and EPAL Processes

As there is varying applicability of processes on varying ore feed types described so far and unfortunately laterite ores are generally not perfectly classified with respect to these choices, there have been several studies to develop flowsheets to treat whole deposits in one process train without any restrictions. For that purpose the first attempt was made in 1970 for New Caledonian laterites that include both limonitic and saprolitic ore layers in one deposit. There has been a process called AMAX that proposed the utilization from these layers in one setup. This process offered the same route as conventional HPAL pattern with utilization of free acid coming with leach liquor and contacting this free acid with inletting saprolitic ore feed as neutralizing agent. Coarse grained saprolitic ore is first calcined and then atmospherically leached with the leach liquor forwarded from CCD tanks of HPAL unit. Despite a considerable extraction is performed on saprolitic feed the residue from this second leaching is sent back to the pressure leaching unit while the liquid is forwarded to mixed sulfide precipitation section. By doing so magnesium depleted residue creates a magnesium diluted feed concentration in original pressure leaching unit. Since magnesium is not so crucial for treatment of PLS by MSP route this process is beneficial for its offerings. After the re-birth of HPAL by late 1990s some of the HPAL plants have applied test works of this process such as Mindoro, Agata and Berong in Philippines, Weda Bay and Sulawesi in Indonesia.

Another process that tried to utilize the free acid of leach solution with additional acid input is called as enhanced pressure acid leaching or shortly EPAL process. It is offered by BHP Billiton and patented with the same company. It is a combination of HPAL and AL process in one route and constructed in Ravensthorpe ore deposit in 2005. Once again the HPAL circuit is initiated with limonitic ore feed. Saprolitic ore section is leached by HPAL discharge and with additional acid input under atmospheric conditions to obtain secondary leach slurry. This second leach slurry is treated with pH increment for iron precipitation (just like in first iron removal of MHP process) while released free acid dissolves saprolite input. The details of this process can be seen elsewhere [32]. However, plant in Ravensthorpe has never reached the goals and suffered a premature closure due to profitability concerns [31]. Still, it is being reactivated by its new owner now.

2.2.3.3.2. Direct Nickel Process (DNi)

In recent years, Direct Nickel Limited developed a new atmospheric leaching route in collaboration with Parker Research Center that has the ability to treat the whole body offering several promising benefits suffered by previously mentioned routes. The process has the capability to extract 95% Ni and 85% Co with only 20 to 30 kg nitric acid per ton of ore in 1 to 4 hours of residence time from any ore deposit types. The company prediction is to be capable of 20000 tons nickel production by the end of 2016 on Mambare laterite in Papua New Guinea. By the success of this process, uneconomic and low grade lateritic nickel ores can also be extracted by profitable operations and hence the role of lateritic nickel ores will further increase. The process is basically atmospheric nitric acid leaching in stainless steel tanks at temperatures close to 100°C which is followed by MHP route for intermediate

production. The most interesting property of the process is the almost full recovery of all reagents within the process train which includes fresh nitric acid regeneration and MgO recovery as powder form that is used in MHP stage [33].

2.2.3.3.3. By-Product Scandium Recovery

Scandium is a widely dispersed rare earth element in several ore sites of different minerals. However, due its lack of affinity, it hardly forms ore mineral with common ore forming anions such as sulfur and it rather prefers to be in solid solution with over 100 minerals. As a result scandium generally occurs in 5 to 100 ppm as a trace constituent especially in ferromagnesian mineral deposits such as pyroxene and biotite and rare-earth mineral deposits. This is the reason for scandium to be a by-product material of several mining activities of different ore deposits or alternatively being recovered from previously processed tailings or residues of different ores. This type of production is currently occurring in China, Kazakhstan, Russia, and Ukraine without any technical data of mine producers. Today there are a few industrial applications of scandium basically for metal halide light lamps to simulate natural sunlight. Future developments are towards its utilization in fuel cells and as aluminum alloys by aerospace and specialty market offering as strongest and lightest alloys as possible. Scandium co-existence with nickel laterites are of knowledge for a few decades such as those in Youngstown and Syerston in Australia. It was estimated to exist from 10 to 30 ppm in Australian laterites [34,35]. In that manner, the treatment of a great deal of nickel laterites can include new stages in order to recover precious scandium element during HPAL process. Preliminary testworks have indicated that solvent extraction or ion exchange techniques are operable for scandium recovery after the PLS obtained [26]. Willis (2012) mentioned a new process called Neomet by Neomet Technologies Inc. which is based on chloride acid leaching in an “atmospheric autoclave” system. The flowsheet of the process can be seen as in Figure 13. Here it is important to mention the placement of additional Sc-Recovery stage after CCD separation of liquid and solid sections and prior to impurity removal stages for iron, aluminum and chromium [6]. This point will be referred back in Chapter 3 due to a shift in experimental setup of conventional MHP route.

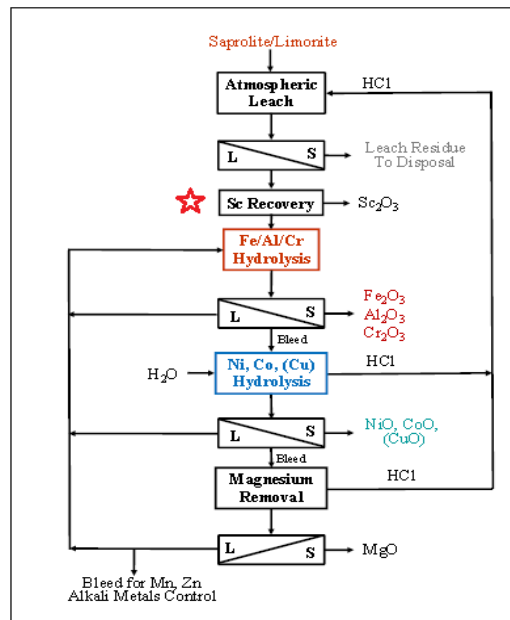


Figure 13 Innovative atmospheric chloride leaching process with scandium recovery stage (Neomet process) [36].

In summary, a great interest is rising for scandium revenue that might be applicable in near future to HPAL plants. According to a report, Metallica Resource NL Company has reached the feasibility stage on extraction of scandium together with nickel and cobalt at five different ore sites nearby Mount Garnet, Australia covered by Nornico project. The scandium grade of these five neighboring deposits ranges between 34 ppm and 169 ppm and it is estimated that company will be one of the leading scandium producers by 40000 kg scandium per year [37]. The situation of scandium existence in Çaldağ lateritic ore deposit is greatly important for that manner. According to a report by USGS scandium prices are variable based on its compound or elemental state, purity level and supply format as ingot or dendritic metal. While scandium oxide with 99.0% purity costs for 900 US Dollar/kg it goes up to 3260 US Dollar/gr for 99.9995% purity [34]. In comparison with nickel or cobalt prices such a by-product will definitely create an important cost relief of HPAL process.

2.3. Effect of Process Parameters on HPAL Process

Despite the use of pressure acid leaching autoclaves are quite in a narrow range and many HPAL plants operate at relatively close values of parameters, the extraction performances for several elements in output differ greatly. This is simply due to the varying, complex and unique compositions of laterite ores and their unpredictable response to acid attack even at the same operational parameters. This reason by itself is the major answer to why each HPAL plant needs to conduct testworks by means of laboratory; pilot and ramp-up studies prior to “grand opening”. In this section, however, the effects of several parameters on the performance of HPAL process will be discussed on the basis of previously conducted studies.

2.3.1. Effect of Acid Load

The most important parameter of HPAL is acid load or acid to ore ratio or shortly a/o ratio. It is both rate-determining and rate-determined parameter as acid is the medium for the complete pressure acid leaching kinetics. Moreover, acid consumption is the most important operational parameter for economic concerns. As previously stated, generally the HPAL plants inlet an a/o ratio between 0.2 to 0.4 kg/kg for limonitic ores whereas it may increase to 0.55-0.6 kg/kg depending on the magnesium containing mineral content of the ore feed. As stated, major HPAL plants such as those as second generation Cawse, Murrin and Bulong and later generations Coral Bay and Ramu chose or have chosen an a/o ratio between 0.2 to 0.6 kg/kg [3]. On determination of this parameter, there are several parameters that should lead the possible maximum nickel and cobalt extractions with the lowest amount of acid loss. Above all, the ore mineralogy has the greatest effect on the acid load requirement. Whittington and Muir stated that iron, aluminum, magnesium and silicon are the major acid consumers [3]. However, most of the silicon existence occurs in acid-resisting minerals such as quartz, talc, and kaolinite whereas it may also exist in other silicates such as smectites, serpentines and much less commonly with iron minerals. The occurrences of other elements will be discussed in Chapter 3. The comparison between the second generation HPAL plants can show the situation which is magnesium and aluminum dictated. Low magnesium content of Cawse required an a/o ratio of 0.375 kg/kg whereas it is or was 0.40 and 0.52 kg/kg for moderate Murrin and high-magnesium Bulong, respectively [29]. On the other hand, in Ramu project reports it is stated to be 0.27 kg/kg which is well below the previous three values. This situation depicts the optimum necessary acid amount can be variable fundamentally on the basis of ore mineralogy.

In another point of view, there is free acid. A minimal residual free sulfuric acid amount between 30-50 g/L is required for prevention of nickel and cobalt losses as precipitates of reverse reactions that will be discussed in chemistry section. On the other hand, the limitation at the uppermost amount for remnant free acid comes from two basic problems. The first one is that dissolution-precipitation reactions of iron and aluminum are inversely affected due to excessive acidic media which hinders the hydrolysis reactions [38]. The second problem is related to downstream applications especially for hydroxide precipitation. The higher the resultant free acid in PLS, the higher amount it will consume the reagent for neutralization and the higher the operational costs will be. Acid load is also related to after-operation issues such as scale formations and CCD performance. Scale formation will be discussed later but it is reported that high acid concentrations was found helpful in scale formation problem. CCD performance by means of solid liquid separation efficiency could suffer from silica chemistry in relation with free acid. During discharge from autoclaves to CCD tanks, the sludge

experiences a reduction in its remnant acid concentration which may trigger the hydrolysis reaction of dissolved silicic acid that transforms into colloidal amorphous silica [39]. Amorphous silica is an undesired product that can be responsible for afterward nickel losses and scale formation. Moreover, its problematic gel behavior causes solid liquid separation to be difficult. Hence the remnant free acid should tolerate such a decrease –if occurs- in order not to cause any amorphous silica formation. On the other hand, utilization of lower acid concentrations will cause lower extraction values for nickel and cobalt. This can be either due to undissolved nickel and/or cobalt bearing ore particles or insufficient free acid in solution or slower initial rates of reactions that would require longer durations than normal situation.

2.3.2. Effect of Pulp Density and Agitation Speed

Pulp density or solid concentration in autoclave slurry is briefly mentioned in operation sequence of high pressure acid leaching. Now it is desired to express the effects of variation in solid concentration on reaction kinetics. Krause et al. (1998) stated that there were no remarkable effect of pulp density on extraction efficiencies as far as it was ranged between 25% and 40% [38]. Further increase in solid concentration was found to increase the impurity contamination amount of pregnant leach solution and also could cause highly viscous slurry to effectively stir during autoclave operation. The inefficient stirring would definitely decrease the process performance as the agitation is required at some degree to provide effective acid-ore interactions and also fluent heat turbulence to supply homogenous heat amount in all sections of autoclave. According to Stopic and Friedrich (2004), agitation speed had a positive effect on nickel extraction [40]. They also summarized the results obtained by Sobol which showed that higher rate by more rapid stirring shortened the residence time of the pressure leaching. On the contrary, Georgiou and Papangelakis (1998) reported that agitation speed in the range between 450 rpm to 650 rpm had negligible effect on extraction values [41]. Additionally, Chou et al. (1976) stated that extraction performance is completely independent after a short initial mixing, while Tindall and Muir (1997) also agreed with the conclusion derived by Chou et al. in the range between 130 rpm to 410 rpm [42][30]. However, it is worth to mention that there were some attempts for reduction of scaling problem in Moa Bay by vigorous stirring. As a result an agitation speed that can create sufficient turbulence within the autoclave will be adequate without any further investigation to be done for improvement in extraction percentages. With this reasoning, it can be stated that during this thesis work, the effects of agitation and pulp density variations were not researched during experimental examination of ore feed for the determination of the optimum conditions. It was rather preferred to keep these variables constant as 30% solid concentration and 400 rpm agitation rate based on the previous thesis studies.

2.3.3. Effect of Temperature

As mentioned previously, HPAL autoclaves are generally operated between 240°C to 270°C which is quite adequate for satisfactory extractions. Temperatures below 230°C were stated by several authors as being incapable to provide sufficient driving force for the reaction kinetics and could result in longer residence time for efficient extraction values [3,38,40]. On the other hand, in excess temperatures of 270°C, insoluble and nickel incorporated magnesium sulfate formations become favorable due to reduction in solubility of magnesium and this results in unnecessary nickel losses that would end up in the tailings with no chance of recovery [43]. Additionally, any increase in temperature would come at the expense of more durable autoclave and acid injection system requirements since pressure is temperature dependent and can demand more qualified titanium grades with higher costs. For example shifting the autoclave operation temperature from 250°C to 260°C means an exponential increase in pressure from about 39 atm to about 46 atm. Such a drastic increase in pressure with only ten degree raise of temperature displays the critical decision-making process for as low as temperature option by maximum possible nickel and cobalt extractions. In addition to that, serious operational problems may occur due to engineering faults that may end up with health threatening situations. In literature, the operation temperatures of second generation HPAL plants were reported as 255°C for Murrin, 250°C for both Bulong and Cawse and the upper limit which is 270°C has been reported for only Goro HPAL operations while the rest being around 250°C [3,29].

2.4. Chemistry of High Pressure Acid Leaching

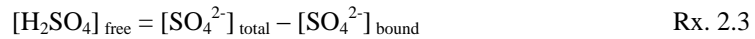
In summary of the effects of several operational parameters, the most important parameters are acid load, temperature and residence time. So long as the mineralogy allows, it is possible to attain high nickel and cobalt extractions by a temperature close to 250°C, acid to ore ratio between 0.2 to 0.6 kg/kg varying with ore composition and sufficient leaching durations. Pulp density and agitation speed have negligible effects on extractions. In this section, the kinetics and chemistry background of the pressure leaching will be discussed.

2.4.1. Sulfuric Acid Chemistry

As mentioned before, one of the key roles in pressure acid leaching is played by sulfuric acid which is readily ionized at ambient temperatures with simple reaction Rx. 2.1 and it experiences a secondary dissociation due to its polyprotic nature by subsequent Rx. 2.2 as follows:



At temperatures above 150°C, secondary dissociation by former reaction suppresses the latter one and sulfuric acid behaves as proton supply to the media [38]. Actually, the basic logic for utilization of sulfuric acid in pressure leaching lies in the transformation of polyprotic sulfuric acid into monoprotic form and supplementary behavior for sufficient hydronium ion activity. This ion activity triggers several modes of acid attacks in order to disintegrate responsive minerals and/or ion exchange some weakly bond cations/anions from loosely bond layered structures such as phyllosilicates. However, sufficient amount of excessive acid must be present in order to maintain the expected ion activity from full dissociation of acid which actually does not occur due to loss in ion activity with increasing temperature. Additionally, the free acid concept was defined by Krause et al. (1998) with a simple mass balance as follows:



where the first term represents the free acid concentration, the second and third terms are the total terminal sulfate amount in solution and the sulfate amount that was bond to the metal sulfates within the solution, respectively [38]. The free acid that is desired to be maintained will increase with increasing concentrations of metal sulfates. This is because of the fact that laterally formed metal sulfates act as proton sinks which reduces hydronium ion activity. For instance, when primarily formed magnesium sulfate as kieserite ($\text{MgSO}_4 \cdot \text{H}_2\text{O}$) dissolves by general reaction of metal oxides with sulfuric acid (Rx's 2.4 and 2.5), it subsequently dissociates to its ionic components and anionic section bonds with hydronium ions to form HSO_4^- :

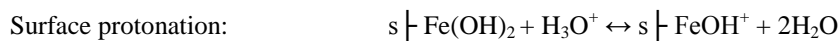


where M is replaceable with Ni, Co, Fe (ferrous form), Mg, Cu, Zn.

This behavior of magnesium was described in literature that will be discussed in following parts. However, within that manner, it is noteworthy to mention that the terminal free acid of pregnant leach solutions at room temperature is not truly representative of the real free acid concentration in autoclave conditions at the exact reaction temperature. This phenomenon was studied by Baghalha and Papangelakis (1998) and Rubisov et al. (2000) where they narrowed down the members in polymetallic leach solution into ternary system including sulfates of iron, aluminum and pseudo-magnesium as the three pits. The rest divalent metallic sulfates were classified in that for pseudo-magnesium tip due to their similar behavior with magnesium sulfate. Aluminum sulfate is steady against dissociation once it is formed in solution as complex sulfate and latterly transforms into its respective solid phase (alunite). Pseudo-magnesium class was found to have major impact (especially

magnesium) on hydrogen ion activity. Majority of magnesium remains dissolved in solution (as divalent magnesium) releasing SO_4^{2-} which creates the case described above [44,45]. That is the main reason for high acid consumption of magnesium rich ore feeds in HPAL operations. In order to suppress the negative effect of magnesium on activity, additional acid must be injected to enhance the proton concentration and thus its activity. However, at that point there is another limitation for acid load. Despite increased acid concentration or proton molarity favors the reaction rates (hence shortened duration) and improve settling characteristics of leach residue (favored hematite production-will be discussed later) there exists a critical acid concentration beyond which excessively dissolved and supersaturated iron, chromium, magnesium and other metallic ions start to precipitate as respective basic sulfates and cause acid losses into leach residue [38,46]. This formation creates basic sulfates that are not desired for that reason.

The mechanisms resulting in dissolution of metal oxides in acidic media were modeled as four different types of modes, namely surface hydroxylation, surface protonation, anion adsorption and desorption. The ability of metal oxide to adsorb water and protons is critical for its dissolution [47]. Goethite surface is expected to provide an anion adsorption surface under acidic conditions that would be subsequently attracted and be expectedly invaded by free protons. The rate of Rx. 2.6 of hematite formation will be dependent on desorption of neutral and ion-paired species FeOHX and subsequent nucleation of hematite. Desorption must be a reduction process or induced by further acid attack on the $\text{s}-\text{Fe}$ bond:



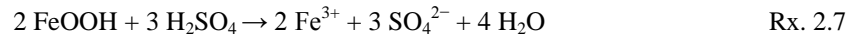
2.4.2. Iron Chemistry

Limonitic ores naturally have high iron concentrations. As a result, the pressure leaching kinetics is highly sensitive to iron behavior. In most of these laterites iron generally occurs as its respective mineral forms most commonly as goethite and hematite but less commonly as maghemite and magnetite. Since goethite is the highest nickel and/or cobalt bearing mineral on cumulative, its complete dissolution and following nickel desorption is greatly important.

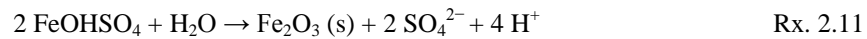
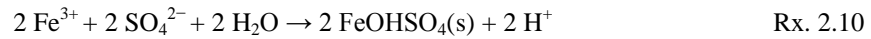
Since iron is in trivalent form in all these mineral forms (except for magnetite), the dissolution of the minerals increase the trivalent iron (ferric) concentration in pregnant leach solutions which is followed by precipitation reactions. When literature is considered, the main reactive for iron oxides was given as goethite since the rest of them both display the same mechanisms and some generally remain untouched even prolonged leaching durations (i.e. maghemite). Here again, goethite dissolution will be discussed. Goethite with chemical formula FeOOH undergoes the net reaction as follows:



As can be seen the transformation of goethite into hematite is simply a thermal transformation accelerated by acid catalyzer. This is actually valid for temperatures higher than 150°C in which range the free energy of the reaction is negative so that goethite is unstable. However, the detailed studies on goethite to hematite transformation in acidic media showed that this is actually not that simple. In many papers, this transformation is referred as dissolution-precipitation process due to simultaneous dissolution of goethite which is followed by rapid precipitation of hematite. On the other hand, two types of reaction series have been proposed for this process so far. In the first mechanism, it was thought that goethite directly and rapidly transforms into hematite after goethite dissolution and ferric iron formation is completed in the way that is listed as in reactions 2.7 to 2.9 where the last reaction is the overall reaction [3]. Georgiou and Papangelakis (1998, 2004) also showed that there were no evidences of existence of ferrous phase other than hematite in their XRD and TEM studies on leach residue [41,48] suggesting that the direct hematite formation can be condition-dependent.



The second offered mechanism mentions an intermediate phase formation prior to hematite production. The reaction mechanism includes formation of basic ferric sulfate which later transforms into hematite with sulfate release. The reaction series in that case are as follows (after goethite dissolution by Rx. 2.7) with the overall reaction Rx. 2.9.



In both mechanisms, the resultant net acid consumption is zero if only hematite is the only resultant product. This is actually regeneration of initially consumed acid by iron and does not mean any acid addition into the solution. However, the production of only basic iron sulfate creates 2 mole acid per 2 moles of goethite (Rx. 2.10) whereas dissolution of 2 moles goethite consumes 3 moles acid (Rx. 2.7) leaving total of 1 moles of acid loss. Several authors claimed that the reaction product is initially basic iron sulfate and it gradually transforms into hematite under certain conditions by Rx. 2.11. This means that there should be a sudden drop in acid concentration which gradually recovers itself with iron dissolution and hematite precipitation. On the other hand, Papangelakis et al. (1996) suggested that in very first time period just after acid attack, iron concentration soars to very high levels such that solution becomes extremely supersaturated by iron. This supersaturation is subsequently balanced by rapid hematite precipitation with ex situ homogenous nucleation. In the meantime, nickel and cobalt concentrates within dissolving iron minerals (goethite and hematite) released from disintegrated structure and pass to the solution. These chain reactions decelerate with time and an equilibrium iron concentration remains steady within the solution. As temperature increases at the same acidity the reaction kinetics fastens and more hematite is precipitated. They agree on that iron solubility increases with high acidity and low temperatures resulting in more hematite precipitation but high temperatures increases dissolution rate of goethite and hence nickel solubility which is a contradicting balance situation [49]

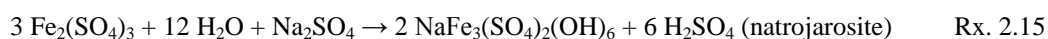
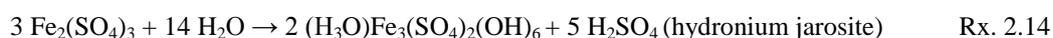
Another point of view is the effects of background salts and oxidation-reduction potential (Eh) of the solution. Tindall and Muir (1996) studied the effects of several sulfate salts including sodium, copper (II), aluminum and chromium within the temperature range of 230°C to 250°C. While sodium, copper and magnesium were found to be enhancing agents for goethite to hematite transformation, chromium and aluminum completely stopped the reaction even in minor/trace amounts. The positive effect resulted from sodium salt came from the formation of more stable jarosite that will be discussed later but the same effect of magnesium and copper could not be understood by the authors. It was commented on the base study by Tozawa and Sasaki that increasing temperature from 170°C to 200°C with the additions of these salts uplift the maximum acid concentration limit below which hematite can form. These salts decrease the free acid concentration by bisulfate-sulfate complex formations and cause this positive effect. On the other hand, detrimental effects of aluminum and chromium were related to hindered protonation of the iron oxide surface due to aluminum and chromium [47]. As it will be discussed in Chapter 3, both aluminum and chromium have stronger bonds with oxygen with respect to that of iron and block the goethite surface. Hence dissolution of iron becomes harder as surficial barrier by aluminum and chromium enlarged.

Loveday (2008) extensively studied the results of ferrous iron concentrations in pregnant leach solutions during pressure acid leaching. The first impression from their result is that the resultant leach liquor contained uncommonly high levels of iron concentration (11000 ppm) for a PLS from HPAL circuit. Expectedly iron was found to be in divalent state. That is because of the fact that ferrous iron requires higher temperatures to precipitate as hematite otherwise it remains within the solution as FeSO_4 causing acid consumption. In addition, ferrous iron is problematic for downstream applications which will be discussed in another section. Second impression was that the solution ORP (oxidation-reduction potential) or Eh value was 350 mV which is also evidence for high ferrous iron concentration (more reductive solution). He studied the behavior of such solution under oxygen

environment. Ferrous iron concentration drastically dropped to 1000 ppm and ORP values reached to 600 mV. By doing so, acid consumption was decreased whereas free acid amount was increased. The reaction that ferrous iron underwent during hematite transformation is given as follows [50]:



Apart from hematite and basic iron sulfate, there can be other iron compounds that are produced after pressure leaching. After the experiences obtained from second generation HPAL, it was found that the process water type used for slurring differentiated the leach residue contents from hematite to a different complex compound called jarosite at the expense of hematite. Jarosites are iron-containing members of a large mineral family called alunites with a general formula of $\text{AB}_3(\text{SO}_4)_2(\text{OH})_6$ where $\text{A} = \text{H}_3\text{O}^+, \text{Na}^+, \text{K}^+, \text{NH}_4^+$; $\text{B} = \text{Al}, \text{Cu}, \text{Fe}$. The most commonly observed jarosites are namely, hydronium jarosite, natrojarosite (Na-jarosite), jarosite (K-jarosite), ammoniojarosite with the respective anions given for A. The reactions of hydronium jarosite and natrojarosite formations are given by Rx. 2.14 and Rx. 2.15, respectively.



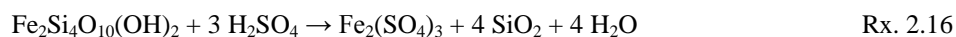
Relative stabilities of jarosites follow the order of jarosite>ammoniojarosite>natrojarosite. When compared to hematite, jarosites have several drawbacks. Primary handicap is the loss of acid into the residue within the jarosite structure (4/3 mole acid loss per 2 moles of goethite for hydronium jarosite, 1 mole acid loss per 2 moles of goethite for natrojarosite). As stated previously, basic iron sulfate is also responsible for acid loss by 1 mole per 2 moles goethite. Other advantages of hematite over jarosite can be listed as higher stability, inertness and being a potential by-product as saleable iron source. Jarosite on the other hand was found as scale former in several autoclaves. The transformation order in acid-iron sulfate solution between these products by temperature increase is as follows: hydronium jarosite formation between 50°C and 140°C, basic ferric sulfate and hematite formation between 150°C and 200°C. However, instead of hydronium jarosite formation, existence of potassium, sodium and ammonium produces more stable jarosites at elevating temperature. Jarosite formation requires acidity as an intermediate between low-acidity-favored hematite and high-acidity-favored basic iron sulfate. According to Kyle (2003), stable jarosite formation requires 20 to 60 g/L acidity in temperature range between 150°C to 250°C. Interestingly, at certain conditions jarosite formation can be created from conversion of hematite at 200°C but this is not possible at a temperature of 250°C [51]. Also, conversion of jarosite into hematite was readily attained by Dutrizac (1990) at temperatures above 220°C and even without any free acid amount. The higher conversion rates were achieved by hematite seed addition into the solution to enhance the rate. However, the increased amount of added free acid decelerated the conversion. At 50 g/L free acid amount hematite formation ceased and left its place to basic iron sulfate. In both cases, there were no residual natrojarosite left [52].

Scarlett et al. (2008) have shown that at lower acid ranges hematite slowly formed but higher acid charges transformed jarosite directly to basic iron sulfate without any hematite presence [53]. High acidity and short leaching durations favor basic iron sulfate domination by shifting Rx. 2.11 to the left whereas low acidity and long durations produce hematite-dominated leach residues [17,30]. As supporting evidence, basic iron sulfate scales were found in first autoclave compartment of Moa Bay plant where the acid was injected providing high acidity [54]. Moreover, high temperatures favor hematite precipitation rather than basic iron sulfate [55]. Additionally, inletting hematite seeds to the initial slurry reinforces the hematite conversion by Rx. 2.11 with stimulation of additional nucleation sites, hence eases the nuclei formation of hematite precipitates. In the same manner denser solid concentrations in slurry feed provides benefits. Secondary nucleation on goethite particles or on-growing hematite particles plays an important role. A decrease in secondary nucleation rate decreases iron precipitation and results in higher iron concentrations in solution at any temperature or acidity [49].

Unfortunately, limonitic ores do not contain iron only as its mineral forms described above but can also have in associations with clay silicates and/or magnesium silicates since there is no strict separation between the ore layers which was detailed in previous sections (faults, fractures, earthquakes, etc.). As it will be discussed further in Chapter 3, some of these “contaminating” minerals may contain iron in either ferric or ferrous or both states. Existence of iron within these minerals, namely, smectite group and serpentine group, is due to the substitution of iron for mainly magnesium and aluminum. These substitutions result from the close ionic radii of these elements which is also the reason for nickel and cobalt association with them (See Figure 2).

As an example from smectite group minerals, nontronites contain high amount of iron for aluminum replacement in its trivalent form whereas montmorillonites can contain it in the divalent state for aluminum and/or magnesium replacements. Scarlett et al. (2008) gives a complete formula for nontronite/beidellite structure $(\text{Mg,Ca})(\text{Fe,Mg,Al,Ni,Cr})_2(\text{Si,Al})_4(\text{O,OH})_{12} \cdot n\text{H}_2\text{O}$ which includes all possible substitutions [53]. Based on the dominating elements these minerals are sub-grouped as it will be discussed in Chapter 3. The important point is that nickel is also incorporated with these minerals that in turn necessitate the complete dissociation of these minerals for acceptable nickel extractions. Serpentine are generally open for ferrous iron substitution for magnesium only. As depicted by Scarlett et al. (2008) serpentine are given as a complete formula of $(\text{Mg,Fe,Ni,Al})_3(\text{Si,Al})_2(\text{O,OH})_9$ which is also important for both nickel, iron and other impurity elements [53]. Therefore, despite they were not investigated as extensively as goethites, at least some smectites and serpentine are iron-bearing and should be considered for iron chemistry. More critically, these groups contain major nickel bearing sub-members for their own domination zones in laterite ore bodies. Hence it is also important for nickel case.

Dissolution of nontronite under pressure leaching conditions was observed simultaneously by synchrotron-XRD method for two PAL experiments with two different acid concentrations: low acid (0.20 kg/kg acid/ore ratio) and high-acid (0.33 kg/kg acid/ore ratio). For the low-acid experiment, it was observed that the amount of nontronite initially increased for a very short time period possibly due to an increase in its crystallinity or its swelling behavior that caused its expansion. However, it quickly dissolved after this short expansion and basic iron sulfate was formed with poor crystalline jarosite phase. In high-acid tracking, there were no expansion but sudden collapse of layered structure of nontronite followed by basic ferric sulfate formation without any jarosite trace [53]. The reaction for nontronite dissociation is given as Rx. 2.16 as follows:



2.4.3. Aluminum Chemistry

Aluminum is another important element to be considered for pressure leaching kinetics. This is because aluminum is not only important for acid regeneration but also for its critical role in downstream operations within leach solution. Aluminum can exist in three forms within lateritic nickel ores. The first form is its simple hydroxide minerals such as gibbsite $[\text{Al}(\text{OH})_3]$ or boehmite (AlOOH) or rarely aluminum oxide (Al_2O_3) which are the most general cases especially encountered in first generation Moa Bay deposit. Another form is as a substitution element for iron in goethite (up to 6% mole) and/or less commonly in chromite $(\text{FeCr}_2\text{O}_4)$ structures as iron replacements. The last aluminum contribution comes from clay silicates such as smectites [48,51,56]. At high temperature conditions, the primary existence form which is gibbsite transforms into boehmite (AlOOH) with thermal dehydroxylation taking place at temperatures above 135°C. When acid is injected into autoclave boehmite dissolves according to Rx. 2.17 as follows:

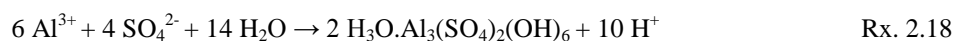


Once aluminum is released to the solution, it remains as a neutral complex form of $\text{Al}_2(\text{SO}_4)_3^0$ which does not dissociate further [45]. At that point there are three possible solid phases for aluminum to transform into in addition to stand as so-called complex in solution. The stable phase choice is generally determined by acidity of leach solution and temperature of the pressure leaching. Chou et al. (1976) proposed two different forms of aluminum sulfate hydrate at two temperature zones. At temperatures below 250°C to 220°C hydronium alunite is the stable phase formed by Rx. 2.18

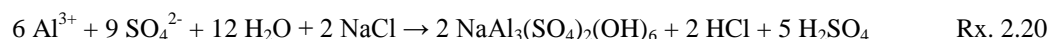
whereas at temperatures exceeding 280°C basic aluminum sulfate is the stable phase as in Rx. 2.19. He stated that at acidity between 20 g/L and 50 g/L alunite phase is the most stable product but formation of basic sulfate is favored with sufficiently high acidity (>50 g/L) in solution even at temperatures below 280°C. Increased acidity increases aluminum in PLS because the more acid provided the higher the aluminum to maintain its neutral sulfate complex and the higher its solubility in solution. Similarly, iron would behave in the same manner [30,41]. Whittington and Muir (2000) generalized the case for both aluminum and trivalent chromium such that soluble aluminum and chromium (III) hydrolyze to their respective sulfate salts but they do not further transform into a way to regenerate acid bond within their structure as in the case of iron [3].

According to Rubisov et al. (2000), aluminum generally reaches its solubility limit at pressure leaching conditions and unavoidably precipitates as hydronium alunite [46]. Moreover, the alkali ions that are supplied either externally (water source) or internally (ore minerals) can drop the aluminum concentrations of leach liquor dramatically. According to Krause et al. (1998) there are almost 2000 to 3000 ppm level differences in aluminum concentrations between the leach solutions obtained from fresh and saline water [38]. This situation arise from the fact that existing alkali ions promote the other stable alunite forms that can bear in pressure leaching conditions without dissolution. Despite the formation of alunite releasing a portion of acid, the net acid consumption will increase with increasing alunite formation. This is exactly the same negative effect caused by increasing jarosite and basic iron sulfate formations rather than hematite.

As can be seen from comparison of two reactions, formation of hydronium results in 4 moles of proton whereas it is 2 moles for aluminum sulfate. Despite aluminum chemistry offers regeneration of a portion of consumed acid, no matter what phase is formed, there exists a certain amount of acid loss. Hence aluminum is actually a net acid consumer as an intermediate between iron and magnesium.



Apart from acidity and temperature, ore feed and/or water salinity providing alkali ions in solution can alter the resultant stable phase just as in the case for iron. Depending on the head-cation ion in alunite formula $\text{AB}_3(\text{SO}_4)_2(\text{OH})_6$ where $\text{A} = \text{H}_3\text{O}^+, \text{Na}^+, \text{K}^+, \text{NH}_4^+$; $\text{B} = \text{Al}, \text{Cu}, \text{Fe}$, there are three types of alunite that are most commonly found in both leach residues and scales of HPAL circuit, namely, natro-, ammonio- and potassium alunite. More commonly occurring natroalunite formation in occurrence of neutral salt is given in Rx. 2.20.

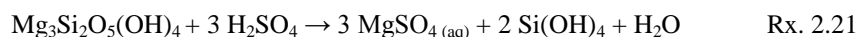


Generally, researchers refer to a combined alunite/jarosite formation which is hard to dissociate and designate each separately. Due to similarity in their chemical structure and multiple substitutions between Fe, Cr, Al and K, Na, H_3O their separation is hard by conventional characterization methods such as XRD and SEM. The most helpful signatures are that alunite is dominated by aluminum for B in chemical formula whereas it is iron for jarosite. Moreover, jarosites generally show up as cubic crystals whereas alunite particles are coarse and big [41]. Either alunite by itself or in combination with jarosite, it is generally found to be responsible for portion of the total nickel or cobalt losses due to multiple substitution case described above [39].

2.4.4. Magnesium Chemistry

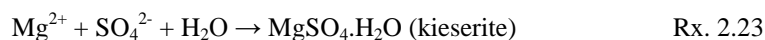
Magnesium has been one of the most problematic impurity metals for HPAL from the start which loads an importance for understanding of its chemistry during pressure leaching. By doing so the reasoning on acidity at pressure leaching conditions could be understood which in turn affects the other metals within the solution that are dependent on acidity. For example, at lower acidities the maximum nickel extractions remarkably decreases with decrease in the solution acidity [44]. Silva (1992) depicted that there should exist an available free acidity in solution media that could prevent nickel and cobalt from precipitation as their respective monohydrate sulfate salts [43]. At that point existence of magnesium plays an important role for valuable metal extractions that is discussed below.

As previously stated, limonitic laterite ores fortunately do not contain high portions of magnesium in their composition. Generally magnesium content in such ore feeds is close to 1.5% or less which is bearable for an acid consumption between 0.2 to 0.4 kg/kg. However, some HPAL operations prefer limonite/saprolite blends for extra nickel grade of saprolites at the expense of acid costs. In that situation acid consumption increases dramatically. Marshall et al. (2004) showed that an increase in magnesium content from 0.9 to 2.7% after blend operation, the acid to ore ratio required to attain the same extractions increased from 0.22 to 0.33 kg/kg [57]. As the main magnesium bearing mineral especially in saprolitic ore feeds, the dissolution of serpentines in simplified formula was given in Rx.'s 2.21 and 2.22:



Magnesium neither forms a neutral sulfate complex as aluminum nor precipitates in a way that regenerates acid as iron. Moreover, Baghalha and Papangelakis (1998) proposed a modeling on the behavior of magnesium at pressure leaching temperatures in which magnesium does not stand as simple cationic ion within the solution but rather form a basic sulfate-bisulfate or sulfate-bisulfate complex. Both complexes hinder hydronium ions and decrease the true acidity at the temperature of pressure leaching [45]. The dissolved magnesium content mainly remains in cationic state after releasing its SO_4^- into the solution that form sulfate complexes which result in a reduction in ion activity and free acid amount as described in acidity section. Since magnesium solubility is temperature dependent there exists an exact difference between the true acidity at operation temperature and terminal acidity once the leaching product is cooled to the room temperature [44]. As temperature decreases below 80°C, the solubility of magnesium sulfate complexes increases and hence there exist a magnesium concentration that actually does not truly represent the exact solution at the higher operational temperatures [45]. In that case 30 g/L free acid requirement is invalid and acidity requirement increases towards 50 g/L to suppress magnesium effect at high temperatures.

In several articles, magnesium precipitates were not mentioned in examinations of leach residues for these reasons. The only reported magnesium phase was magnesium mono-hydrate sulfate phase in leach residue that was reported by AMAX researchers which was formed as in Rx. 2.23:



However, this observation was for a limonitic-saprolitic ore blend that created an uncommonly high magnesium concentration (more than 12000 ppm). This is also in parallel with other studies such as one carried out by Marshall et al. (2004) which has proven that the extent of supersaturation is balanced with insoluble magnesium sulfate precipitations into the residue. Even if the precipitates of magnesium phase (kieserite) had survived on cooling they were probably in negligible amounts such that they could not have been detected by other respective researchers who conducted their examinations by conventional characterization methods after the sludge was completely cooled to room temperature and hence most of the magnesium sulfate were re-dissolved leaving no trace behind them.

However, Scarlett et al. (2008) actually observed the formation of kieserite mineral ($\text{MgSO}_4 \cdot \text{H}_2\text{O}$) while the leaching was in progress with the help of continuous synchrotron X-ray diffraction methodology [53]. What they observed was enlightening the scene after magnesium intake from the easily soluble respective source mineral (ferruginous lizardite with formula given previously in iron chemistry) into the solution. As lizardite dissolution commenced, initially iron ions precipitated as jarosite whereas magnesium was found to form the so-called sulfate hydroxide mineral kieserite subsequently dissolved on cooling. Another important observation was an increase in amorphous content as the lizardite dissolution was continuing. This amorphous phase was not quantified or qualified but its amount was decreasing with increased amount of crystallization of kieserite and jarosite. The so-called amorphous phase was possibly re-precipitation product as poorly crystallized silicon after polymerization of dissolved silica from lizardite structure (Rx. 2.22). Amorphous silica was mentioned in several articles and it is generally responsible for nickel losses into the leach residue. Mostly, silicon is in acid-resilient minerals such as quartz, kaolinite and talc. However, as in

the case for serpentine minerals, they may contribute into phyllosilicate minerals that can be destroyed easily by acid attack.

According to Whittington and Muir (2000), the solubility of magnesium sulfate salts (i.e. kieserite) in water media increases with acidity because at higher acidity equilibrium magnesium concentration increases within the solution [3]. Higher acid load will increase the serpentine dissolution and any nickel associated within it. But this revenue will come with increased acid cost. Resultantly, highly acidic leach solution will demand extra limestone consumption in downstream applications for mixed hydroxide precipitation route to be neutralized. However, there might be an important portion of nickel grade within these minerals even in limonitic ores that could not be spent as cut-off grade. Overall, as the revenue from nickel is the basic profit, the acid consumption due to these minerals should be studied with a careful economic study. For example, there was ore upgrade in Moa Bay and Ravensthorpe HPAL plants for serpentine rejections [58].

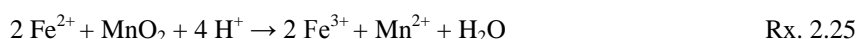
In literature there is no exact range of typical magnesium extraction. Whittington and Muir (2000) stated that normally 50 to 60% of magnesium extraction was observed whereas there are other operational reports that stated up to 90% magnesium extraction. This contradictory situation might be arisen from the problem resulting from re-dissolution of magnesium salts on cooling and/or the behavior of magnesium-dominated minerals against acid attack.

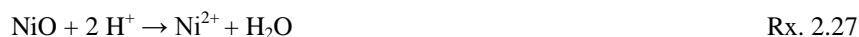
2.4.5. Manganese-Nickel-Cobalt Chemistry

Nickel and cobalt are the valuable target elements which form the basis of this research. Since manganese minerals or by description in geochemistry phylломanganate minerals are also responsible for being hosts especially for very high individual nickel and cobalt concentrations, their dissolution chemistry is of great importance. These oxyhydroxide minerals and their chemical formulae are given as asbolane $(\text{Co,Ni})_{1-y}(\text{MnO}_2)_{2-x}(\text{OH})_{2-2y+2x} \cdot n(\text{H}_2\text{O})$, lithiophorite $(\text{Al,Li})\text{MnO}_2(\text{OH})_2$ and birnessite $\text{Na}_4\text{Mn}_{14}\text{O}_{27}$. Other rarely encountered phylломanganates are not so important to mention here however, the higher the amount of these minerals within the ore deposit the more important is their chemistry [59,60].

Manganese dissolution generally resembles to cobalt dissolution but with slower rates [61]. This is because cobalt is associated with manganese minerals in great amounts. The other important mineral that can host cobalt is goethite but individual goethite particles are never capable of bearing as high cobalt amounts as manganese minerals can do. This is because of the fact that goethite contains cobalt as a substitution impurity element for iron that does not create significant structural deformations. On the other hand, cobalt and manganese generally behave in the same manner during weathering of laterites and accumulate in a solid solution. This similarity was described by a study of Manceau et al. (2000). Cobalt is selectively uptaken by these phylломanganates as both within the layer and between the layers as a substitution for manganese. The higher amounts were correlated to geochemical affinity of trivalent cobalt for both states of manganese at the laterite layer. Basically, soluble divalent cobalt is oxidized by Mn (III)/Mn(IV) to insoluble cobalt (III) by means of sorption into the structure. Unlike phylломanganates, goethite has not this ability and generally cannot individually uptake cobalt and/or manganese for iron replacement as high as manganese minerals (always less than 20%, if occurs at all) [62]. Some limonitic deposits contain manganese rich layers (generally close to lower end of limonite layer) some have manganese minerals as inclusion in other layers (such as limonite layer) rather than a separate layer. Although it will be detailed in Chapter 3, it should be mentioned that there exists some minor amounts of asbolane within the Çaldağ lateritic nickel ore sample. Hence, it is of concern to understand the basic chemistry if there happens to be some problems for unacceptable nickel and cobalt extractions.

To begin with, nickel, cobalt and manganese are generally assumed as simple respective oxides for chemistry. The dissolution reactions of manganese, cobalt and nickel are given in Rx's 2.24, 2.25, 2.26 and 2.27, respectively.





As a result of high iron content and positive response of manganese dissolution to acid amount, Gou et al. (2010) proposed that the extraction of cobalt is easier than nickel. However, there are some other studies that contradict this statement. Actually, the widely accepted behavior is that dissolution of manganese minerals in limonitic ores is low on the absence of reducing agents which is typically between 50% to 60% which confines the cobalt efficiencies at low levels [3,63]. These reducing agents are expectedly ferrous iron and trivalent chromium that are products of clay or clay-like silicates such as serpentines and smectites. Here, it might be seen that the reactions involve trivalent chromium and divalent iron as catalyzers. Despite manganese is in tetravalent state, the only state of manganese that was found in pregnant leach solutions was in the divalent state which is the evidence of that Rx's 2.24 and 2.25 occur with chromium (III) and ferrous iron media. Similarly, cobalt is initially in trivalent state and reduces to divalent state by iron contribution which is the only observed form of cobalt in PLS, too. It is noteworthy that iron and chromium can interchange their reactions and do not have to stick with one reduction reaction. The reduction mechanism of ferrous iron on tetravalent manganese was described within the iron chemistry section. However, at that point there is a cautious situation. While reducing iron-chromium ions are helpful catalyzers for manganese dissolution that provide higher nickel and cobalt extractions, the amount of these agents can exceed the manganese amount. At that point, these reducing agents decrease the iron transformation reactions into hematite. Remnant ferrous iron does not precipitate as hematite at pressure leaching conditions and will definitely be problematic in MHP route. Remnant trivalent chromium ions will tend to reduce trivalent iron ions mainly from goethite dissolution. This will increase acid amount bonded with ferrous iron (hence increases acid consumption), less hematite will be precipitated which will lower the settling quality of leach residue and once again problematic ion concentration amount will increase prior to MHP route. Hence there is once more a contradictory situation between profit and loss.

According to Whittington and Muir (2000) the studies conducted on several ore types gave very variable, ore-dependent manganese extraction efficiencies ranging from as low as 40% to as high as 100% [3]. Hence the behavior of manganese is highly dependent on the ore type. Georgiou and Papangelakis (2009) detected a manganese particle that survived untouched but was depleted from both nickel and cobalt within it. According to this study even if the manganese minerals might not completely dissociate by acid attack they may release all their valuable metal content which is the indication that high cobalt extractions do not require the same high extraction percentages of manganese. This is because of the fact that cobalt distribution is not necessarily homogenous in manganese particles but can heterogeneously concentrate towards the external surfaces of the particles that acid can easily sweep those surficial cobalt atoms [63].

2.4.6. Leach Residue Characteristics

In industrial applications of HPAL + MHP combined route, once the pressure acid leaching is conducted the leach residue is generally not separated from the sludge until the end of the first iron removal stage in mixed hydroxide precipitation process which means that the resultant sludge contains solid wastes of both stages that are dumped to the tailings. Despite that fact, there have been numerous efforts in literature that were focused on the resultant leach residue from pressure acid leaching separately. The reason for that importance of leach residues comes from the valuable information that could be gained from leach residues. Leach residues can give a backup for understanding of the kinetics and performance of the pressure leaching of the ore feed. The most commonly observed phases so far are alunite/jarosite, hematite, amorphous silica and a so-called alumino-silicate structure. Other less commonly observed phases are basic iron and magnesium sulfates. Apart from these minerals that are produced during pressure leaching, there have been untouched primary minerals such as maghemite, chromite, talc, kaolinite, quartz, etc. Moreover, goethite and manganese structures can be seen as undissolved particles. Within this section it will be tried to explain the form of these minerals as a guide for the characterization of the leach residue obtained at the optimum conditions of this study.

Although it was not studied under TEM within this study, it can be seen from Figure 14 that goethite has a structure of agglomerated needle-like particles. In bulk form, goethite is porous and can have poor to well crystallinity with several impurity substitutions potential. As the acid attack on goethite, the needle-like particles dissociate and due to its large surface area the whole structure is departed by surface interactions described in the free acid section. Goethite structure was further studied during pressure acid leaching by sample take in at specific time intervals. What this study showed that within time goethite particles are completely dissolved while spherical hematite nodules are simultaneously and rapidly precipitated.

Hematite can be seen as both primary (in run-of-mine ore) and secondary (precipitation of ferric iron after goethite dissolution) hematite. Secondary hematite particles were very uniform and fine in size and did not show any further growth with time. However, as the pulp density of slurry increased the shape of hematite particles became coarser with respect to one obtained in lower density. On the other hand, aluminum was only found as alunite structure in leach residue which was bigger in size with respect to secondary hematite. In all trials of the study, there was no basic iron sulfate. As can be seen in the same figure that a nickeliferous magnesium silicate structure (serpentine) was also imaged under TEM prior to the leaching and it was not mentioned further within leach residue which means it probably dissolved. In a second study, a manganese structure was imaged under TEM. It was shown that manganese particle was completely depleted of nickel and cobalt without any significant distortion in the structure. That means nickel and cobalt contents in the so-called manganese phase were actually easily leachable without a requirement for dissolution of whole structure.

Despite Georgiou and Papangelakis did not mention the alunite composition in detail, the structure of alunite is quite complex especially when jarosite is also formed during leaching [41]. According to Kyle (2003), jarosite does not form independently but rather is transformed from alunite by aluminum-iron substitutions [51]. As a result, the amount of alunite/jarosite formation is dependent on the aluminum content of the ore feed. The higher the aluminum content the higher the residue will contain alunite/jarosite which is also dependent on the water salinity of course. As can be seen in Figure 15, when hypersaline water is used in slurry formation the resultant leach residue contains large crystals of alunite/jarosite. On the other hand, tap water (closest water type to fresh water) results in fine grains of hematite and silica in leach residue. This is actually what was found in scales of the first and second generation plants. Among them Moa Bay and Murrin contains 4.8% and 3.16% aluminum while Bulong and Cawse follow with 2.75% and 1.71%. While Moa Bay extremely suffered from scale formation of natrojarosite/natroalunite, Cawse was not reported to have a significant scale problem [51].

Sobol (1969) figured all possible substitutions that might occur in alunite structure which can be summarized as Figure 16. However, he stated some boundaries for limitation in substitution amounts. Up to 30% of sulfate anion replacement and 30% OH⁻ replacement were stated by chromate and silicate ions, respectively. Moreover, up to 26% aluminum might be replaced by trivalent iron whereas it is 65% aluminum replacement by iron in natrojarosite. A correlation between chromate and silicate is rather linear such that for every two silicate there is one chromate incorporated in alunite structure. However, Whittington et al. (2003) pointed on cautions on the molar calculations by Sobol to be doubly applicable on other residues since these calculations were made for Moa Bay plant operations. As an example, unlike Moa Bay leach residue, when silica might be associated in other phases than alunite, the molar extent of silicate might vary from those Sobol dictated. Another point dictated by this study is that precipitation product hematite was barely responsible for nickel co-precipitation [39,56].

It is clear that, as pointed in previous sections, alunite precipitation can be responsible for nickel and cobalt losses within its structure. However, the less existence of chromate ions within the alunite structure decreases this tendency and improves the nickel-cobalt extractions. On the other hand, chromate ions are formed by oxidation of trivalent chromium by manganese dioxide which is a positive process for manganese mineral dissolution hence especially for cobalt extractions. Moreover, chromate reduces the polymerization amount of dissolved silica and decreases amorphous silica formation which is also responsible for nickel losses. For that reason, additional sulfur inlet within the slurry was found to diminish the negative effect of chromate for nickel losses into alunite structure [3].

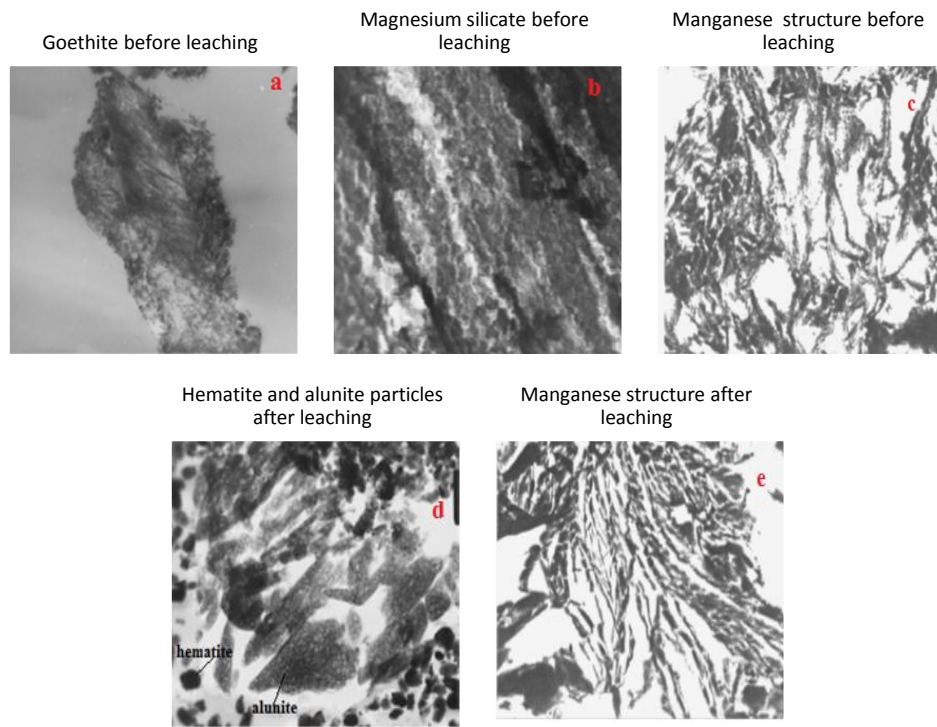


Figure 14 TEM images of different structures before and after pressure leaching [41,63].

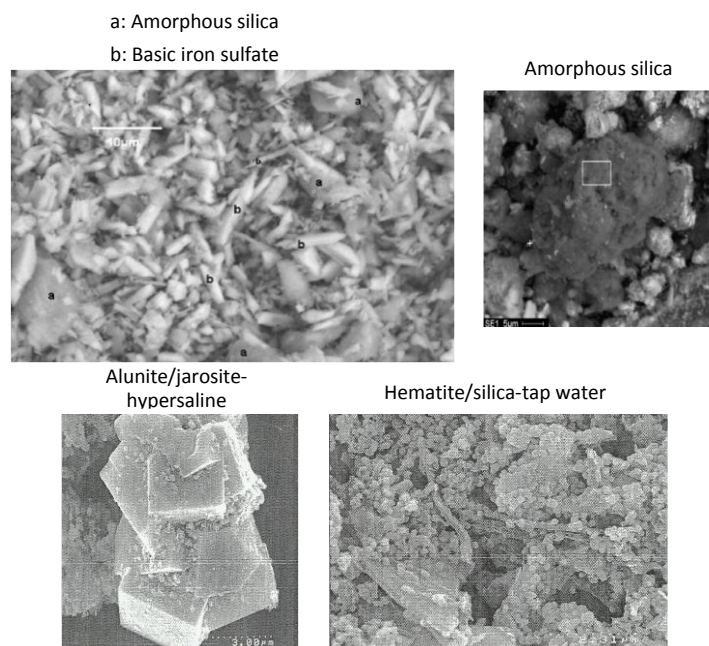


Figure 15 SEM images of amorphous silica and basic iron sulfate [54]; amorphous silica with higher magnification [17], large alunite/jarosite particles after hypersaline water HPAL, fine hematite-silica particles after tap water HPAL [51].

Amorphous silica is the product of soluble silica $\text{Si}(\text{OH})_4(\text{aq})$ re-precipitation by Rx. 2.22 given in magnesium chemistry. However, the choice of being precipitated as gel (gelation) or a precipitate depends on several factors. According to statements of Whittington and Muir (2000), these factors are supersaturation, seed particles that aqueous silica may precipitate on, temperature, and pH which are also rate determining of gelation process. Gelation of amorphous silica increases with increasing supersaturation, temperature and amount of active seed (in that case pulp density). They stated that hematite does not welcome the silica deposition on its own precipitation process. That is because, at sufficiently low pH values, the rate of metal hydroxide (i.e. goethite) dissolution in acid is much higher than silica re-precipitation on that hydroxide [3]. This information is crucially useful on SEM examinations. Muir et al. (2006) stated that due to its highly negative surface the ability of amorphous silica to absorb the soluble cations such as nickel and cobalt is high which in turn creates nickel and cobalt losses [64]. A schematic view of amorphous silica can be seen in Figure 15.

The situation of jarosite/alunite formation was investigated for pressure acid leaching conditions. After a significant number of studies it was found that the formation of jarosite is very dependent on process temperature, ore process water and ore composition [49,51,55,64–66]. Overall of all studies can be summarized as follows: First of all for any types of jarosite or alunite formation there should be external or internal anion (Na, K, NH_4 , etc.) sources within the reaction media as depicted by Rx's 2.14, 2.15 and 2.20. In HPAL case, these sources can be ore feed or water source and in the present case it can only be ore feed. As its composition will be given Chapter 3, the process water supplied for this thesis work was constantly fresh deionized water throughout the whole study. However, it was stated that despite nickel, cobalt, iron and manganese extractions are slightly higher whereas aluminum content significantly lower in salinity than in fresh water, residual free acid of pregnant leach solutions obtained in salinity decreases because of higher natrojarosite/natroalunite formation. The slight increases stated by Marshall et al. (2004) are due to faster reaction kinetics. Consequently acid consumption increases in the case of saline water usage. If sufficient backup for decreasing free acid could not be supplied then nickel and cobalt extractions will be negatively affected due to salinity. On the other hand, less hematite formation as a sacrifice for natroalunite/natrojarosite formation will drop the settling quality of the leach residue which in turn will require higher volume CCD and storages for disposals. These problems were encountered in Western Australian HPAL plants where hypersaline with 11 g/L Na (sea water, Bulong) to saline 6 g/L Na (sub-potable water, Cawse) water were utilized [65].

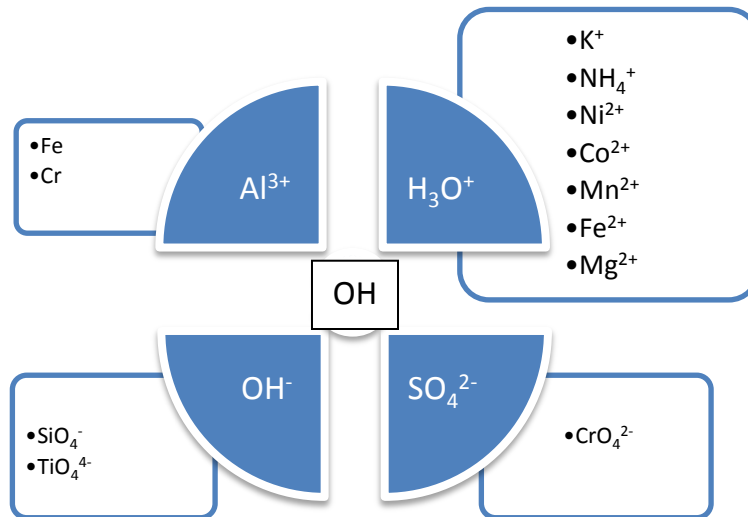


Figure 16 All possible ionic replacements within the alunite structure [39].

2.5. Downstream Processes on Pregnant Leach Solutions

After acid leaching (either AL or HPAL) the resultant product is a solution containing nickel and cobalt with several other contaminating elements such as iron, aluminum, chromium, magnesium, etc. In each upstream process type the further processing choice to remove these impurities and obtain a saleable product from PLS is somehow independent from the upstream choice. Despite HPAL plants start with autoclave processing, they do not necessarily follow the same downstream process train which is also valid for AL plants. That is because of the fact that there is once more no such option as exact winner over the other options. Each process type that will be discussed further has its own pros and cons. Hence, there is no absolute rule that a PLS obtained from either of the upstream processes is proper only one specific downstream choice. Being mainly dependent on its composition, the offerings of the nickel-cobalt loaded solution after a suitable choice must be considered well or it might even be tested for several routes to optimize the economic concerns.

Generally, pregnant leach solution obtained by atmospheric leaching (AL) of lateritic nickel ores contains 15000-30000 ppm Fe and 2000-5000 ppm Al while the solution is solid-free and it is at ambient temperature. Unlike the PLS obtained from AL process, at the end of the HPAL process the resultant solution is hot (operation temperature is 240-270°C) and comes out with 20-25% solid concentrations while the solution carries less than 8000 ppm iron and less than 3000 ppm aluminum [67]. Additionally, the PLS after HPAL can have 3000-6000 ppm nickel, 200-800 ppm cobalt, 10000-2000 ppm magnesium and 1000-3000 ppm manganese concentrations. Despite being in much less amounts there are also some problematic metals such as copper, zinc and chrome [68]. Chromium concentration in leach solutions may vary with the mineralogical existence of chromium (response of host minerals to acid attack) and the amount of chromium in run of mine ore as well as its behavior during dissolution-precipitation reactions of leaching. Within this study, the chromium concentration in leach solution ranged between 50 ppm to 200 ppm depending on the experimental conditions.

Up to now, researchers dealt with several problems encountered in developing purification routes to obtain a high quality and marketable intermediate or final product in the end. After several decades of efforts, there are now three well-developed and commercially utilized or is being utilized routes. These are namely, mixed sulfide precipitation (MSP), direct solvent extraction (DSX) and mixed hydroxide precipitation (MHP). Apart from those three routes, there have been other suggested new technologies such as molecular recognition technology (MRT), ion exchange (IX) and resin-in-pulp (RIP) that have not had a chance of commercial operation. The reason why all the nickel extracting companies behaved timid against these options lies beneath the fact that IX processes have never been

tried commercially before and unavoidably are hazardous for picking as primary extraction method while there are other alternatives that had already proven themselves to be beneficial [69].

Eventually, in his last review, Willis (2012) did not include these technologies probably due to that reason [6]. Hence it will be more proper to neglect these prematurely ceased options and concentrate on other more reliable new trends in addition to those routes already in commercial use. The trend in improvement is basically towards the refinement of the problems associated with well-developed routes especially for DSX method. For example, a recent development called synergistic solvent extraction (SSX) method has been proposed as an upgraded version of DSX.

2.5.1. Mixed Sulfide Precipitation (MSP)

Being the oldest, mixed sulfide precipitation method was first applied in Moa Bay process train which then spread worldwide by followers such as Murrin Murrin, Coral Bay, Syerston, Weda Bay, Ambatovy, Gladstone, Nonoc and Mindoro projects. As can be seen, the half-century experience proved the MSP process to be applicable to any PLS from any leaching process. High selectivity offered by this route for nickel and cobalt over other impurities such as iron, chromium, manganese and aluminum is the major highlight with respect to its less-selective competitive. Due to this higher selectiveness, there exist no precipitation steps in order to remove these impurity elements prior to intermediate product formation. According to Willis (2007), the MSP route is the best suitable method for laterites that have less than 3:1 ratio for Ni:Mn [67]. Higher manganese concentration within the ore feed will probably increase the manganese content which can create troubles in MHP production as it will be discussed further. Additionally, lower grade nickel laterites could be more proper for MSP route since the loss within the downstream will be lower and may offer higher profit than it would under MHP route conditions where nickel losses will be higher. However, the capital costs of MSP should also be considered and compared with the extra benefit from this revenue. A typical flowsheet for mixed sulfide precipitation can be seen in Figure 17.

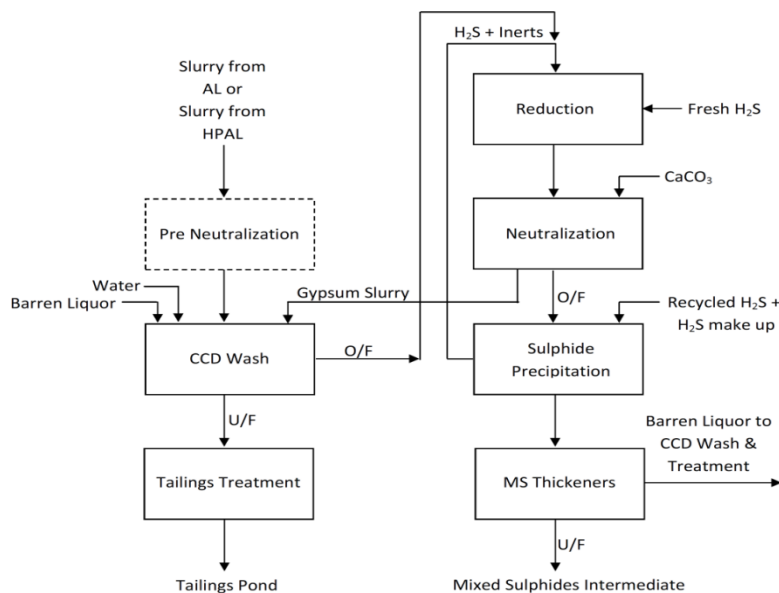


Figure 17 Typical mixed sulfide precipitation flowsheet.

After CCD wash circuit, the PLS from either AL or HPAL stage can be preferentially directed to a reduction unit where copper is selectively removed from the solution by controlled redox reduction with hydrogen sulfide gas inlet while simultaneously trivalent iron and hexavalent chromium also reduced to divalent and trivalent states, respectively. By doing so, the problematic behavior of divalent iron can be removed which is due to the close sulfide precipitation lines of Fe^{2+} , Ni^{2+} and Co^{2+} ions. If remnant divalent iron concentrations are not removed prior to sulfide precipitation of nickel and cobalt, the resultant intermediate will be contaminated by significant amount of iron which restricts the product market. This is especially crucial for PLS obtained from AL stages where iron is in higher amounts and mostly in ferrous form. Yet, the reduction of iron is not enough and demand a portion of it to be removed since the reduction of higher ferrous iron concentrations into ferric iron with higher hydrogen sulfide gas will increase the process cost. For that reason, a neutralization step is placed in order to drop the iron level below 200 ppm with limestone usage for pH increment in the range between 2.5 and 3.0. Operation temperature can range between 70°C and 90°C in order to fasten the reaction kinetics. Under these conditions most of the iron present in the solution can be removed with gypsum formation due to sulfuric acid neutralization [67]. The resultant sludge is passed through CCD washing circuit where solid wastes are disposed of and the leach liquor is forwarded to sulfide precipitation reactors or autoclaves to produce the so-called intermediate product. The operation conditions are 121°C, 1034 kPa, 10-30 minutes for autoclaves and 80-95°C, 200-400 kPa, 60-90 minutes for multiple reactors. Under these conditions more than 99% of nickel and cobalt precipitation can be achieved [70]. The discharge slurry from the precipitation unit is subjected to CCD wash circuit where solid saleable product is separated from barren overflow. The MSP product is then prepared for transfer to a refinery where the final product is obtained. Prior to refinement, a typical MSP composition can be seen in Table 6. As can be seen, the contamination by copper and zinc is unavoidable due to the same reason for divalent iron. The barren solution on the other hand might be disposed to the tailings or further treated for recycle purposes depending on the plant water source availability.

Table 6 Typical mixed sulfide precipitate composition [67].

Component	Unit	Value
Nickel	wt% (dry)	55-61
Cobalt	wt% (dry)	3-6
Zinc	wt% (dry)	2-6
Copper	wt% (dry)	1-5
Manganese	wt% (dry)	< 0.1
Magnesium	wt% (dry)	< 0.1
Iron	wt% (dry)	< 0.8
Aluminum	wt% (dry)	< 0.1
Sulfur	wt% (dry)	34-36
Moisture	wt%	10-15

2.5.2. Direct Solvent Extraction (DSX)

The first development and utilization of direct solvent extraction process was in Bulong HPAL plant. Despite the initially obscure performance of DSX by means of economic imbalance between process cost with valuable metal recovery and final product quality, it was managed to perform the process only for 4 years in plant. This was achieved by some advancement in process trains for several problems such as gypsum precipitation in Ni-solvent extraction circuit overcame by antiscalent agent, one of the most important problems. Unfortunately, the plant could not afford the economic outcome due to lower-than-expected production level and ceased its production. The process flowsheet from the Bulong operation can be seen in Figure 18 [71].

As can be seen, the PLS feed coming from HPAL unit is modified with neutralization in such a way that resultant PLS could carry a moderate level of acidic sulfate and low levels of Fe, Al, Cr. During

neutralization the solution is saturated with calcium. Resultant PLS is fed into cobalt-SX stage where the paths of nickel and cobalt are separated. To achieve that an organic material called Cyanex 272 was used in Bulong. Cobalt-rich strip liquor (LSL) is directed to cobalt precipitation where cobalt is separated from manganese and magnesium as sulfide while nickel co-precipitates with trivalent iron, zinc and copper. The filtrate of sulfide precipitation is directed to cobalt refinery in order to obtain cobalt cathodes as the barren solution containing manganese and magnesium is disposed to the tailings. Meanwhile, in the second SX circuit, the cobalt-SX raffinate is transferred to nickel-SX circuit where another organic material called Versatic 10 is utilized for nickel separation from calcium and magnesium. After this treatment, nickel rich organic strip is passed through electrowinning (EW) stage to obtain nickel cathodes.

The problems of Bulong process was two stages of SX circuit which caused large equipment and gypsum formation in the second circuit since Versatic 10 was not so selective for nickel over calcium. Despite the efforts to utilize better organics such as synergist Acorga CLX50 that improved the situation, the so-called organic was not commercially available. The criteria on selecting best organic reagent are the more affinity for nickel and cobalt over other impurities (including calcium) in addition to the natural request of fitting of the reagent to SX conditions. Despite the problems associated with the process, DSX still drags significant interests due to its lower capital and operation costs with respect to its competitive (MSP). This is because of the facts that in DSX process there are no necessities for intermediate precipitation; re-leach circuits or CCD separations as in the case of MSP. For that reason Vale Nouvelle-Caledonie (New Caledonia) plant currently operates DSX on their process train. In recent years there have been several organic materials tested for their efficiencies and selectivity for nickel and cobalt in DSX circuits. Within that manner synergetic organics such as Versatic 301, LIX63, TBP, etc. forms the basis of the new synergetic solvent extraction (SSX) method which is the new way of DSX out of the future [70,72].

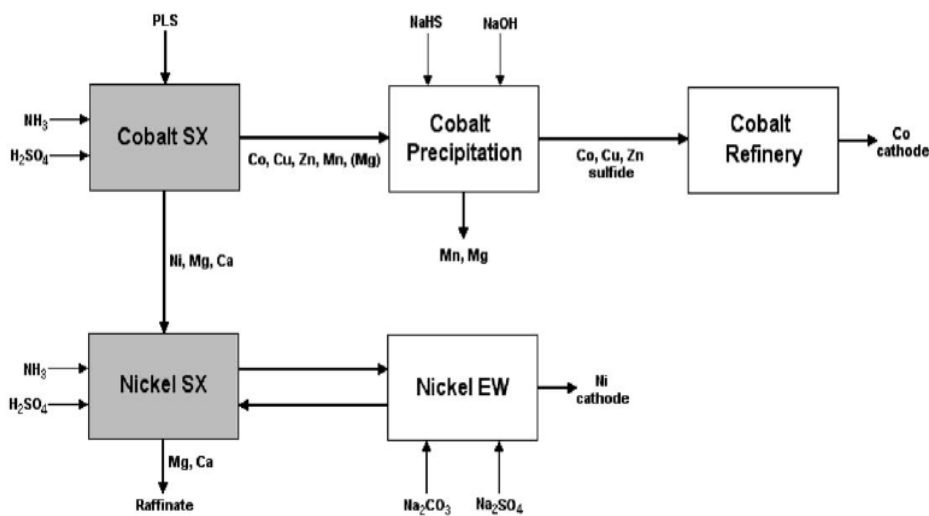


Figure 18 DSX flowsheet from Bulong operation [71].

2.5.3. Mixed Hydroxide Precipitation (MHP)

Mixed hydroxide precipitation is not as old as MSP process but has been a well-developed, proven flowsheet since its first application in Cawse plant. The proposed route was both simpler and inexpensive with respect to those proposed in Moa Bay and Bulong. The simplicity of the process lies beneath the fundamental logic of pH increment while the others deal with complex organic materials or risky gaseous sulfide gases. From the first applicant, this process widespread over several

operations despite Cawse plant could not survive from closure. Now, MHP process is currently utilized in Ramu (PNG) and Ravensthorpe (Western Australia) and is in progress for Vermelho (Brazil), Young, Mt. Margaret and Kalgoorlie (Western Australia). According to META Nickel and Cobalt Company they are also going to use the MHP process train as their purification and neutralization route [6,73]. The advantageous simplicity relied on the pH increment, however, comes with a price of lower selectivity of nickel and cobalt over several impurities that causes an enlarged process train to eliminate the problems related with. The absence of selectivity of nickel and cobalt over iron, chromium and aluminum necessitates a two-stage removal (i.e. FER 1 and FER 2) input to the process train whereas limited selectivity of nickel and cobalt over manganese necessitates additional precipitation step (i.e. MHP 2) after the actual precipitation step of nickel and cobalt by MHP 1 step. The schematic view of complete process train can be seen in Figure 19. As can be seen, after HPAL and/or AL the resultant leach solution passes through 5 major stages namely: recycle leach, two-stage iron removal, two-stage nickel-cobalt precipitation and manganese removal. Magnesium removal stage can be preferentially added to the end of the process to remove magnesium in case the overflow solution (barren solution) which is almost completely depleted from most of the impurities and highly loaded with magnesium is to be used as recycle water especially for thickeners. Magnesium removal is optional but can be a requirement if the plant is suffering from insufficient fresh water source. Within this study, however, magnesium removal stage will not be discussed.

Before the introductory for each and every step of the process, it will be more proper to discuss the logic beneath the process benefits. As depicted, a pH increment is utilized in order to conduct the so-called removal stages. As can be seen in Figure 20, Monhemius diagram pictures the scene of the stability regions of several impurity elements that limits their solubility [70]. Since the resultant pregnant leach solutions are bearing a certain amount of remnant free acid within them, the solution pH is generally within highly acidic region close to 1. Hence, from the figure, it can be seen that all of the impurity ions are already in their stability regions with no regard for their molarity amount (if exists though). The thumb rule is not to get across the line of the respective curve of an ion in order not to cause precipitation as its respective state/s (i.e. hydroxides). Based on this diagram, the first three relatively independent lines are owned by trivalent iron, chromium and aluminum ions all of which are targeted to be removed from the solution within the first two stage of the process following recycle leach. However this so-called thumb rule is not perfectly practiced in the real plants the case of which has been reported several times. For example, even this iron-removal zone is the stability region of cobalt and nickel, a negligible but certain amount of loss of these valuable metals during the first two stages of iron removal has been reported. Moreover, precipitation of nickel and cobalt will be impossible without co-precipitation of zinc, copper and divalent iron as they are closely neighboring the stability lines of nickel and cobalt. Their existence might obscure the success of the process but thankfully zinc and copper do not exist in significant amounts in ore feeds while there is a solution for ferrous iron elimination from the solution. Similarly, manganese and magnesium lines falls at higher pH ranges before where nickel and cobalt already tend to precipitate. Hence, both of them will not be readily removed prior to nickel-cobalt hydroxide precipitation and will partially contaminate the intermediate product from this hydroxide precipitation. The lack of selectivity of process more or less underlies beneath these problematic behaviors of impurity elements. Nonetheless, within certain limits these unsolvable problems can be tolerated by following refining processes of intermediate hydroxide product as these limits will be discussed later in this section.

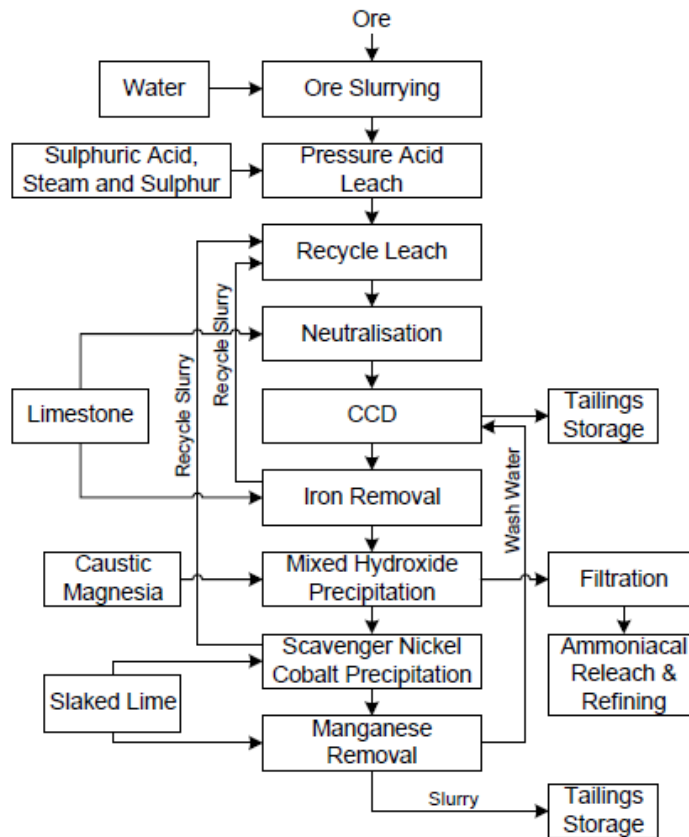


Figure 19 Schematic view of complete HPAL + MHP process train [74].

As stated previously, the kinetics of the process is based on pH increment. This is achieved by reagent additions to the acidic solution. The precipitation reactions are triggered from the fact that with pH increment, the solubility of respective ions becomes unfavorable which results in solid phase formations that separate the excess ion concentrations [75]. In hydrometallurgy, precipitation corresponds to physico-chemical process. Dissolved ions are contacted with externally introduced inorganic materials in order to obtain the conversion of these ions into insoluble precipitates by limiting the solubility of ions at lower levels. The lower the barrier for soluble ions concentrations the better the process efficiency by means of production of more resistant insoluble precipitates [75]. As an example for such a precipitation process, the reaction between iron sulfate and calcium carbonate can be seen in Rx 2.28 (imbalanced).



Despite there exists a significant pH value for an ion to precipitate at its significant respective molarity, there are other factors affecting the precipitation process. Above all, the desired pH range should be kept within a controlled narrow band in order not to cause supersaturation since MHP process is not so selective for nickel and cobalt. As the pH increment is attained by reagent addition, the inlet amount must be sufficiently high to both provide enough driving force for precipitation and prevent supersaturation. Any sudden increase in the reagent amount will locally raise pH value at that point and the precipitation reactions may shift to right unlike the general picture. This means that supersaturation can create a different local picture that triggers premature precipitation reactions that are supposed to occur at higher pH values which might not be observed by only general picture of the whole solution. Another important case is the complete utilization of the added reagent. Since the reactions starts at the interface between the reagent particles and solution the maximum utilization of contact area is very important for both precipitation efficiencies and also prevention of unreacted reagent within the precipitates. For that purpose generally the reagents are in fine grain sizes in order

to increase the interaction between particles and the feed solution. Moreover, these materials are prepared as slurry form instead of being injected into reaction tanks as dry particles. At dry state, fine particles are highly prone to agglomerate and even at high agitations of solution these particles may still stick together within the solution. Such a behavior causes the cancelation of available reagent surfaces for precipitation reactions. The less reaction surface on reagent particles may leave incomplete or completely untouched reagent materials in precipitates. This problem can be very crucial for quality of precipitates at certain MHP stages and also critical for the operation cost since the ineffective reagent addition will consume higher amount. For example, Pillay et al. (2012) showed that MgO in slurry or in finer sizes form produced better quality and less MgO contaminated MHP than in dry or coarse form while less MgO was consumed in former cases [76].

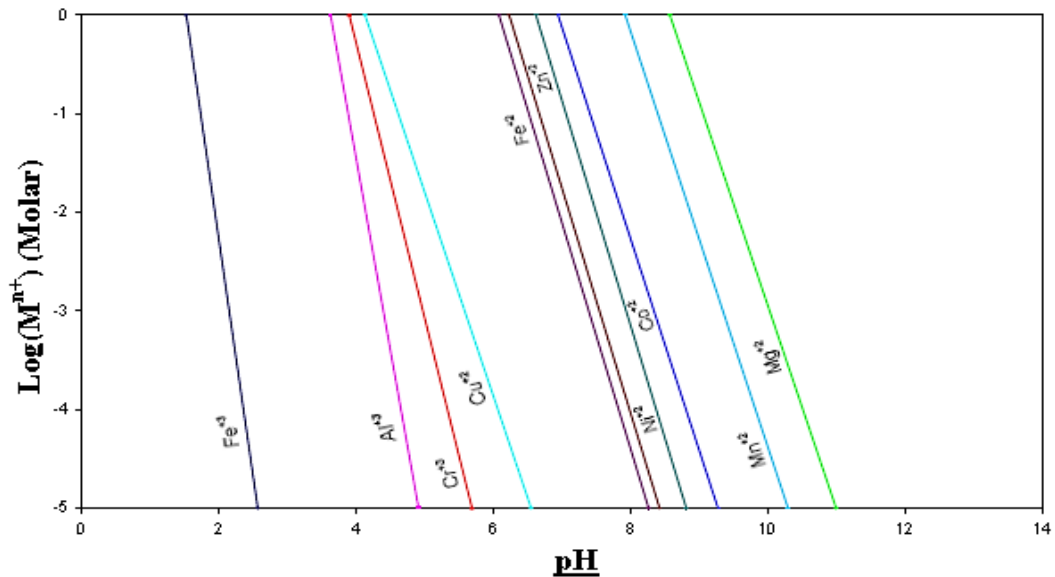


Figure 20 Stability curves for several ions with respect to molarity and pH at ambient conditions (25°C and 1 atm) [70].

Another important issue is the settling characteristics of precipitates formed by the precipitation reactions. At that point, reagents are once again played the major role. As they will be discussed further by their comparison for several issues, the only point mentioned here will be their observed effects on resultant precipitate products. Sodium, magnesium and calcium hydroxides and calcium-containing reagents are generally considered for MHP process. Lime (calcium oxide) and slaked lime (calcium hydroxide) generally improve the settling character of the precipitates by creating crystalline particles of calcium sulfate phases as by-products of reactions such as gypsum ($\text{CaSO}_4 \cdot 2\text{H}_2\text{O}$) or bassanite ($\text{CaSO}_4 \cdot 0.5\text{H}_2\text{O}$). On the other hand, these reagents are generally responsible for the contamination of so-called insoluble sulfates in MHP product. Lime can also be responsible for breaking the metal complexes in waste water discharged to nature. This can be a problem for environmental conditions but lime is the most economic choice within these options. Sodium hydroxide results in a bad morphology that is very problematic by means of extremely fine and slimy precipitates. Such precipitates occupy the CCD tanks for long durations due to difficult filterability [75,77,78]. As the intermediate product MHP is of concern for the whole process, nickel and cobalt hydroxide precipitates are generally gelatinous and problematic in washing steps. In order to improve the settling characteristics of MHP, Sist and Demopoulos (2003) proposed the heterogeneous precipitation route instead of homogenous precipitation. Since the latter produces irregular particles that results in longer filtration sessions, this can worsen the MHP settling. Another critical result is the higher impurity incorporation in precipitates. Since homogenous nucleation and growth entraps the surrounding solution more impurity ions will be captured by this method. For that reason they proposed two improvements to eliminate the homogenous precipitation amount as much

as possible. The first route is the seed material addition into reaction tanks (as MHP seeds) to enhance heterogeneous precipitation on the seed particles and to inhibit colloidal-like precipitate formation [77]. As an extra advantage, the heterogeneous precipitation can shorten the precipitation durations due to eliminated time period for homogenous nucleation by directly initiated growth process on the seed material. Another suggestion was the control over the supersaturation that can even sweep off the improvements achieved by seed material. As supersaturation favors the nuclei formation homogeneously the bad morphology and other negative effects of this precipitation type remains unsolved [78]. In summary, letting sufficiently long residence time for completion of precipitation reactions and controlling the pH increment and the terminal pH of the feed solution, poor selectivity of MHP process can somehow be improved.

In order to give an introductory for the MHP process each step will be detailed by means of abovementioned composition limits, operational conditions, cautions and their purposes in MHP route.

2.5.3.1. Recycle Leach

The process flowsheet starts with recycle leach which is a junction point where fresh PLS coming from the HPAL circuit is mixed with the solid underflows from second iron removal and second mixed hydroxide precipitation stages. Despite within this study recycle leach step is ignored due to lack of a continuous production in experimental studies; it is a standard stage in industrial MHP routes. Hence it will be necessary to briefly detail the step. The purpose of this additional step is only to recover the inevitable nickel and cobalt contents within these precipitates. Almost complete recovery of nickel and cobalt can be achieved by the help of this additional step. The process conditions are generally higher than 50°C temperature, between 60 to 120 minutes residence time and more than 20g/L acidity in solution. One or two tanks in series is/are used and the resultant stream is forwarded to first iron removal stage [67]. Despite the inlet of solid precipitates of so-called stages will increase the Fe, Cr, Al, Mn content by re-dissolution in free acid coming from fresh PLS discharge; it will not be a significant problem as these precipitates can be kept below a critical value in order not to cause accumulation of so-called impurity elements within the process train. Actually, the answer to why solid discharge from first iron removal step is not forwarded to recycle leach lies under this fact that the discharge of first iron removal is in great amount with respect to that obtained in second iron removal. The solid product of first MHP step is reserved for further refining in another flowsheet or prepared as a market value and sold.

2.5.3.2. First Iron Removal Stage (FER1)

The discharge coming from the recycle leach unit is introduced to the first iron removal stage where almost all iron together with some aluminum and chromium precipitate. The operation conditions can be summarized as a temperature range of 70°C to 90°C, a residence time between 90 to 180 minutes (including all residence durations in 3 to 4 tanks in series)[6]. Although Willis reported a pH range of 2.5 to 3.0 in his previous study (Willis, 2007), he stated that the new trend is the control of pH between 3.3 and 3.8 in his latest review (Willis, 2012) [6,67]. Generally, limestone is the preferred choice of reagent due to its lower cost since the major reagent consumption is observed at that stage. Temperature is actually effective only on the residence time by accelerating the reactions. However, at higher temperatures slurry viscosity decreases and hence homogenous stirring and more effective reagent-solution contact can be achieved. Due to these reasons, rather than ambient temperatures, it was found that in the above stated temperature range precipitation is more efficient.

Under ambient conditions (1 atm, 25°C), iron is stable and soluble in either divalent or trivalent state at a certain pH level of around 2 for trivalent and around 6 for divalent iron depending on the concentration. The concentration of iron within the solution is of concern since the major amount of the removal of iron is at this stage. Since iron in limonitic ores generally goes into solution in trivalent form, it is expected to remove most of the iron in the corresponding pH levels of the operation. Since saprolitic ore types are generally poor in iron concentrations, MHP utilization is better for the HPAL plants consuming this type of ore. However, the possibility of iron substitutions in clay minerals especially as ferrous iron can be problematic. As ferrous iron does not precipitate until a higher pH, there must be some additional treatment for oxidation of divalent iron to ferric form. The existence of

ferric iron is even worse for PLS obtained from AL circuits. As stated previously, iron concentrations are distinctively higher in AL circuits due to absence of iron hydrolysis reaction that re-forms consumed acid and leave an iron-dominated leach residue generally in hematite form. Utilization of an oxidative environment during leaching process or after discharging from autoclave has been studied in both leaching circuits. Loveday (2008) found that by creating an oxidative environment, ferrous iron concentration can be lowered to very low levels (from 10000 to 1000 ppm). This oxidative environment can be supplied by creating an oxygen atmosphere or adding manganese oxides into the solution [50]. Manganese oxide introduction can occur naturally, since manganese minerals serve in the same manner as described in the chemistry section. Another choice is SO_2/O_2 environment since it is more effective than pure oxygen atmosphere [79].

In the first iron removal step, simultaneous neutralization of high amount of free acid (30-50 g/L) takes place with the reaction given as Rx. 2.28. During these neutralization reactions, a great amount of hydrated calcium sulfate product is formed as by-product. Willis (2007) stated that in industrial applications of MHP route, air is injected into reaction tanks in order to eliminate the negative effect of bicarbonate buffering effect [67]. As it will be shown in Chapter 4, the pH profile observed in that stage displayed a very slow pH increment until a certain pH value. This is probably the buffering effect of product of the reaction between added calcium carbonate and free sulfuric acid.

Within this stage, it is desired to remove most of the iron (>90%) and some of the aluminum and chromium prior to last PLS-adjustment stage which is second iron removal. Additionally, dissolved silica can also be precipitated at an efficiency of 95% at pH level of 3.5 and 80-90°C with 1 hour precipitation duration [24]. More importantly, dissolved scandium was also found to co-precipitate or form its respective hydroxide in these pH regions. As a last note for the first iron removal stage, nickel and cobalt can also be lost due to co-precipitation. However, a negligible amount is generally reported as between 0.5-1.0 percent. The discharge of the products from reaction tanks is followed by thickening of the slurry. Then, the separation of solids in CCD tanks in order to wash off the precipitates and recover soluble nickel and cobalt values therein takes place. While the overflow is directed to the second iron removal unit, the underflow is either disposed to the tailings or filtered as a cake.

2.5.3.3. Second Iron Removal Stage (FER2)

During the first iron removal stage, significant amount of iron is removed from the solution. However, there still exists an intolerable amount of iron in the solution. The same situation of chromium and aluminum also requires an additional removal stage. The operation conditions of second iron removal can be summarized as follows: a pH range of 4.4 to 4.8, a temperature range between 70°C and 90°C, a total residence time between 60 and 120 minutes. The reagent utilized for that stage is generally once again limestone. The aim of this step is to remove all of the remnant iron, silica and chromium and dropping the aluminum levels below 50 ppm [67]. The necessity for a secondary removal stage is due to the high amount of solid mass that would be formed if the two-stage removal was combined as one. Instead the majority of iron and free acid which are highly responsible for the huge solid dispose can be discarded from the process train with a negligible revenue loss. Despite this additional stage enlarges the flowsheet and equipment requirement (more reaction tanks and more CCD tanks), at pH levels of 4.4 to 4.8, there would be unconvertible nickel and cobalt losses (as high as 10%) in other case. Since these losses cannot be restrained due to supersaturation of nickel and cobalt within the solution, it is more proper to revert only the low-in-mass solid product of this stage to recycle leach. Another reason for two-staged process is the improved control over the impurity concentrations. As FER2 is the last step towards the maximum purification of the PLS prior to mixed hydroxide product formation, the feed solution will not be wasted in case of any undesired PLS composition especially for iron, chromium, aluminum and silicon. Since chromium does not interfere with MHP due to its less existence in ore feed and low extraction percentages into PLS because of its existence in acid-resilient minerals; chromium is actually not so critical. Moreover, chromium at these low levels can be easily precipitated almost completely.

Iron, aluminum and silicon are problematic when present in MHP product. As it will be described later, MHP is further refined in complex subsequent options. One of these process routes includes ammonia re-leach where solid MHP is subjected to ammoniacal liquor (ammonia/ammonium

carbonate solution) in order to re-dissolve the nickel, cobalt, zinc and copper and reject iron and manganese. Indeed, aluminum creates a very troublesome situation during ammonia re-leach. According to Willis (2007), aluminum forms a gelatinous amorphous precipitate as oxide that surrounds nickel and cobalt precipitates [67]. The ability of gel formation of aluminum can be seen even in very low amounts (as low as 0.5%). Since these oxide precipitates are hardly soluble, nickel and cobalt recoveries in this step reported to be reduced by 10-30%. Due to a similar behavior, iron and silicon are also responsible for fewer recoveries of valuable metals in ammonia re-leach. Hence, primarily aluminum and secondarily iron and silicon concentrations must be reckoned to meet these limitations. Despite chromium would not be expected to cause a significant problem its concentration must also be adjusted to very low levels. Consequently, the terminal pH of the resultant PLS after this step is majorly dependent on the aluminum concentration [74,80]. According to Agatzini et al. (2009) aluminum and chromium are precipitated efficiently (>95% precipitation efficiency) at 3.5 pH, ambient pressure and 95°C conditions with 20% CaO pulp addition. The resultant precipitate phase is the jarosite/alunite with minor nickel and cobalt incorporation. They also stated that the mode of pH increment can also affect the amount of supersaturation that causes premature precipitation reactions. For example, keeping the increment rate as low in prolonged duration (up to 12 hours) assists prevention of supersaturation of several ions together with amorphous phase formations [81]. Amorphous phase formation can worsen the settling behavior of precipitates and can occupy CCD tanks in longer durations.

After the discharge slurry is thickened, the sludge is forwarded to CCD tanks where solid and liquid parts are separated. Soluble nickel and cobalt values are regained by washing off the solids and the overflow is directed to first mixed hydroxide precipitation stage. On the other hand, the underflow solid precipitates are recirculated to recycle leach unit in order to revert the precipitates and re-dissolve the nickel and cobalt precipitates into the circuit.

2.5.3.4. First Mixed Hydroxide Stage (MHP1)

After the two iron removal stages, the resultant leach liquor is expectedly diluted for several impurity ions and mostly acid-free. At that pH level there is no other precipitation stage until where nickel and cobalt are precipitated in their original pH zone. Hence the pH level of the solution is gradually raised to around neutral levels by reagent addition. The temperature range is between 50°C and 70°C while this range is not a strict limitation since higher temperatures favor higher precipitation rates. Total residence time in reaction tanks is generally between two to three hours.

The function of this step is to practically precipitate nickel and cobalt ions with 90-95% efficiency while keeping the manganese content of the final solid product below 5% with a typical precipitation of 20-35%. Unavoidably zinc and copper also co-precipitate by other remnant ions such as iron, chromium, and aluminum within these pH levels, however their concentrations are generally not so high to be of concern. Since MHP process is not selective for nickel and cobalt over manganese, the control over the pH increment is critical as there is no recycle step for the MHP process. Actually, this is the reason for conducting MHP in two stages. As can be seen both removal and hydroxide precipitation processes are divided into two separate stages. That is because of the nickel and cobalt interactions with the solid precipitates and also premature or tardy precipitations of them at lower and higher pH values than the expected pH ranges. The same issue is valid for other impurity elements especially premature precipitations of manganese and retarded precipitation of aluminum in MHP 1 stage. Since aluminum is already dropped to lower levels, by keeping the pH level close to neutral, manganese contamination can be controlled in these desired levels and a solid product with >35% nickel and 3-5% cobalt can be obtained. However, the control over manganese contamination becomes harder as its concentration in the incoming PLS solution increases. As stated by Willis (2008, 2012), MHP is best suited for laterites having a Mn:Ni ratio below 1:3 which once again makes saprolitic ores a better choice if the MHP route is to be conducted [6,70].

Problems related to contamination are not only regarding the incoming PLS but also the reagent utilized for the precipitation reactions. Generally, alkaline type reagents are preferred that contain several sub-choices with their own advantages and disadvantages. For example, a choice for reagent usage for MHP 1 stage was covered within the study by Willis (2007) [67]. As he stated, caustic soda (sodium hydroxide), lime (calcium oxide), soda ash (sodium carbonate), hydrated or slaked lime

(calcium hydroxide) and magnesia (MgO) are the practically tested reagents for MHP process. It is preferential to use these reagents as blend to combine their advantages. Theoretically, any alkaline reagent can be used for any stage of MHP process but it must be considered with its advantages and problematic results generally on the intermediate product MHP. Generally magnesia is the preferred choice for the first stage of nickel-cobalt hydroxide precipitation due to lower cost than both caustic soda and soda ash. The product quality is better than that for calcium hydroxide. However, the reactivity of magnesia is stated to be 0.7 to 0.9 and can decline more with aging. As a result of that, an excessive amount of magnesia should be inlet into the solution to recover the non-performance of unreacted magnesia particles. This will lead magnesia contamination in the product as brucite [Mg(OH)₂] and hence excessive magnesium contents can be problem for market concerns. On the other hand, insufficient supply of magnesia will leave more nickel content to be precipitated in the second mixed hydroxide precipitation solids which are recycled. This will cause recirculation of nickel in the circuit and increase in nickel losses in former removal stages as well as higher reagent consumption in MHP 2 stage [82]. In order to prevent these as much as possible, magnesia should be used as fresh slurry and when it is in dry form, it should not be exposed to humidity. Caustic soda does not offer any contamination but results in a better selectivity of nickel over manganese with more controllable pH increment. Despite these offerings that produce higher quality MHP than magnesia can, it is generally very expensive. Introduction of lime as reagent increases the calcium concentrate and results in gypsum precipitates that contaminates MHP product. The problem associated with soda ash is the lowered selectivity of nickel over manganese. That is because of the resultant products to be carbonates and nickel carbonate is not more soluble than manganese carbonate [67]. Overall, the general main problem is the contamination of MHP product by Mn, Ca and unreacted MgO. A typical saleable mixed hydroxide precipitate with MgO utilization expectedly has the composition that can be seen in Table 7.

After the first mixed hydroxide precipitation, the overflow from thickener is directed to the second mixed hydroxide precipitation unit whereas the solid underflow is separated for ammoniacal re-leaching unit or shipped to a refinery unit or directly prepared for the market. In order to obtain better settling and filterability in MHP 1 tanks, some portion of solid underflow might be fed into thickeners as seed material. Due to its high moisture content, mixed hydroxide precipitate will cause some transportation problems that will increase the operation costs. This could be problematic especially when the refinery unit is far from the HPAL+MHP plant. Hydrometallurgical refinery options include the following three possible routes all of which are initially aimed to selectively re-dissolve the MHP 1 solid so that nickel and cobalt with some impurities can be treated to final product.

- Ammonia leach followed by ammoniacal solvent extraction and electrowinning
- Ammonium sulfate leach, cobalt solvent extraction and hydrogen reduction
- Acid leach, cobalt solvent extraction and electrowinning

After either of these treatments nickel and cobalt are obtained in almost completely pure metallic forms.

Table 7 Typical MHP composition [67].

Component	Unit	Value	Component	Unit	Value
Nickel	wt% (dry)	30-39	Iron	wt% (dry)	< 0.5
Cobalt	wt% (dry)	2-5	Aluminum	wt% (dry)	< 0.5
Zinc	wt% (dry)	1-4	Sulfur	wt% (dry)	3-5
Copper	wt% (dry)	1-4	Moisture	wt%	35-45
Magnesium	wt% (dry)	3-5	Manganese	wt% (dry)	4-9

2.5.3.5. Second Mixed Hydroxide Stage (MHP2)

After the MHP 1 step the overflow liquid is injected to reaction tanks of MHP 2 or Scavenger precipitation unit. Despite this feed solution is mostly depleted from nickel and cobalt, there is still a need to recover these remnant values into the circuit. The reason for sacrificing these remnant values are due to manganese limitation of being less than 5% in intermediate MHP 1 product. Typically the depleted feed solution contains 200 ppm nickel and much less levels of cobalt while the aim is to recover all of these values in the precipitate product. These precipitates are not saleable because of the high manganese content (typically 7-20%). Rather than marketing, this solid product is recycled to the recycle leach unit to recover the precipitated nickel and cobalt. As expected there is a manganese circulation due to this recycling. Hence, the manganese precipitation levels should be kept between the ranges of 20-30% in the precipitates that would not cause accumulation of manganese. Operation conditions are generalized as 7.5 to 8.0 pH values, 60° to 80° temperature and 60 to 80 minutes residence time. Due to its lower cost, calcium hydroxide is preferred instead of magnesia since the product quality is not of concern. After this treatment, it is expected to decrease the levels of nickel and cobalt in the resultant barren solution to less than 10 ppm. The discharge slurry is thickened and overflow solution is directed to the manganese removal unit whereas the solid part is sent back to the recycle leach unit. In order to improve settling characteristics, here again some portion of solid product can be used in thickeners as seed material [6,67].

2.5.3.6. Manganese Removal Stage

The solution obtained from MHP 2 unit is now highly dominated by manganese and also magnesium (if magnesia was used in MHP 1 unit) with other insignificant impurity levels of previously existing elements. Despite most of the lateritic nickel deposits are in tropical or sub-tropic regions can enable the sufficient water supply to the operating plant, there are regulations for manganese level of disposed waste water stream that should be met. Moreover, as stated in previous sections, not all the laterite deposits especially those in arid-region laterites such as Western Australian ores are that lucky to have sufficient nearby water supply that would not necessitate the circulation of waste water. Hence generally this barren solution coming from MHP 2 unit is used as wash water in CCD tanks or in thickeners. However, the high levels of manganese are to be lowered in order not to cause the accumulation of manganese in the process train. After all, this excessive manganese levels will cause supersaturation in MHP 1 stage and more premature precipitation of manganese will occur that will contaminate the MHP 1 product. In order to achieve that pH of the incoming solution, it is adjusted between 8.5 and 9.0 at 50°C-60°C for 0.5 to 2 hours of residence time. By doing so, the remnant manganese content can be decreased to below 100 ppm. If lower manganese concentration is required then oxidative treatment by means of air or dilute sulfur dioxide can be applied in order to precipitate manganese dioxide. If this treatment is included, the residual manganese concentration is lowered to 10 ppm. The resultant discharge slurry is thickened and overflow of the thickener either recycled to wash liquor or disposed of as waste water. Preferentially, the barren solution can be subjected to magnesium removal in order to improve its quality but generally this step is skipped due to high amount of reagent consumption (calcium hydroxide) especially when magnesia was utilized in MHP 1 step. Underflow, on the other hand, is used as seed material or disposed to the tailings.

2.6. Previous Studies on Çaldağ Ore Deposit

Being the first atmospheric acid heap leaching project, Çaldağ lateritic nickel deposit has owned a worldwide fame and it is presently owned by a company called VTG Holding. Additionally, having the highest amount of proven ore reserve according to the State Planning Organization (DPT) which is about 33.3 million tons, this lateritic deposit is still one of the most important nickel reserves of Turkey with a reasonable grade as can be seen in Table 8 [4,5]. Due to these facts, it was noticed that a great deal of attention has been paid for research and investigation of this reserve when literature was searched. Several studies have been done so far for the geological and mineralogical characterizations of the deposit or its leachability under atmospheric conditions together with its characterization. Despite these efforts, none has been made for the leachability of this deposit under high pressure and high temperature conditions. In this section, most of the up-to-now studies will be mentioned as briefly as possible.

Table 8 Nickel reserves of Turkey [5].

Region	Proven Reserve (t)	Probable Reserve (t)	Possible Reserve (t)
Manisa Çaldağ	33300000	37900000	-
Manisa Gördes	32000000	40000000	70-80000000
Eskişehir Yunusemre	10000000	86625000	231000000
Uşak Banaz	-	11601500	30937500
Bursa Yapköydere	-	82000	81000
Bitlis Pancarlı	-	-	15500

2.6.1. Geological and Mineralogical Characterization Studies

After its exploration at early 1940s and first mining operations at early 1950s, Çaldağ deposit was thought as an iron deposit which can be understood by the focuses of first studies on the iron formation understanding of the deposit [83]. However, it was not until late 1970s that this idea was shifted by the recognition of existence of nickel and cobalt in the reserve by the Mineral Research and Exploration Institute (MTA) [84]. In the meantime, some of the members of MTA delivered their geological survey reports about this site. Overall consequence of the authors was that the laterization of the main rock (serpentinite) was believed to be responsible for the formation of Çaldağ nickel-cobalt ore. All these mineralogical and geological studies were previously summarized by Özdemir (2006) [85] in his thesis work. A more contemporary geological study was done by Tavlan et al. (2011) where Çaldağ was included as another station of a lateritic belt that starts from the Balkans, passing through Greece and extends to Iran over Turkey. It also includes the chronology of most important geological occurrences throughout a 50 Ma (mega annum) geological time zone and is concluded with a reasoning that depth of the ore profile would be 1 km (which is well above the real value, 69 m) only if the weathering of the uplifted base rock had not been fluctuated or interrupted by geological occurrences such as erosion within this time zone. A general view of the deposit taken from the study can be seen in Figure 21 [86].

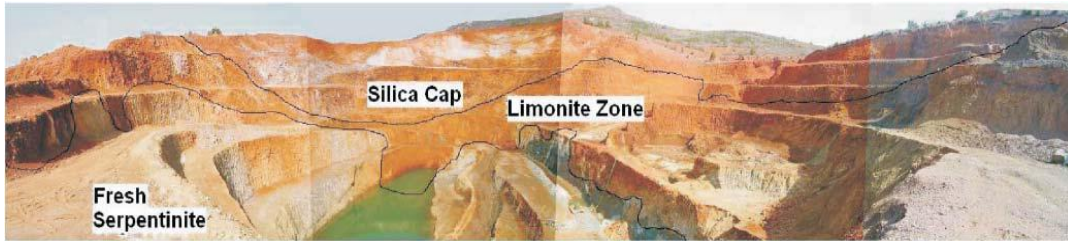


Figure 21 Superimposed horizons of the Çaldağ laterite: silica cap, limonite zone and fresh serpentinite [86].

In order to characterize the ore sample used throughout this thesis study, it will be more rational and helpful to utilize more of the mineralogically focused studies rather than those related to the geological background of the ore since mineralogy is a direct factor on the leaching efficiency. For that purpose, the first attempt for description of mineralization of the ore was by Çağatay et al. (1983). In this study, ore site was hypothetically divided into 4 distinguishable zones with distribution of manganese, nickel, cobalt and iron within these zones as can be seen in Figure 22. Each zone separately was described in terms of their mineral content, the existence forms of these minerals (as veins or fillers in cavities) and their correlations with each other. In both limonite zones, the major minerals were found as limonite and goethite with minor amounts of asbolane, quartz, chromite,

calcite and clay minerals, namely, montmorillonite and halloysite. Asbolane zone, on the other hand, was described as a mineral mixture of serpentine (frequently as crystalline antigorite and rarely as bastite) and locally enriched asbolane (enriched at upper parts of the zone) together with calcite, chlorite (up to 3-4% of bulk as nickel containing phyllosilicate), limonite (as goethite), magnetite and hematite (both in minor amounts), chalcedony and clay minerals (halloysite, montmorillonite and nontronite). At the bottom of the ore, unweathered serpentinite layer which is the source rock of deposit was found to contain very small amount of nickel, cobalt and chromium. Moreover, the study pointed on the fact that asbolane is the main source of nickel and cobalt which was found contradictory to other lateritic deposits originating from nickel silicates (i.e. garnierite). This fact was also interpreted as an indication of the incomplete laterization process of the deposit since completely progressed laterites generally enriched in nickel as nickel silicates at lower sections of asbolane zone.

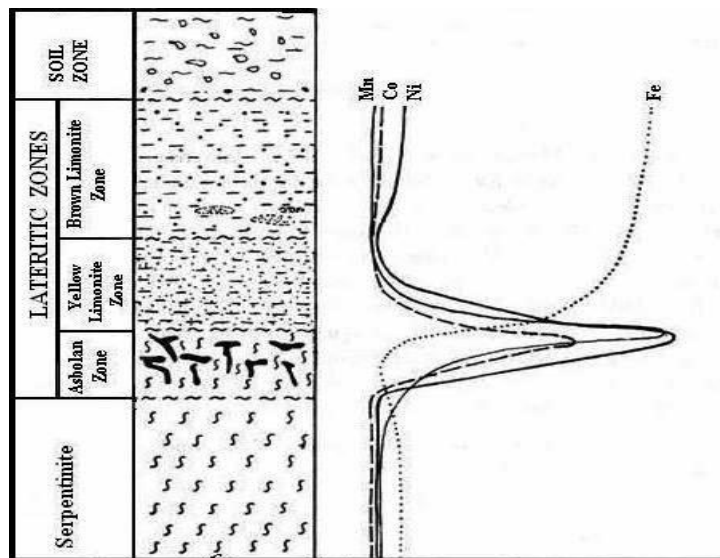


Figure 22 Lateritic profile of Çaldağ nickel-cobalt ore with nickel, cobalt, iron and manganese distributions [84].

A similar hypothetical division of the profile of the deposit site was given in a study by Thorne et al. (2009) with a brief geological introductory about history of Çaldağ laterite. In that study, however, the division was rather correlated with the textural, mineralogical and morphological contrasts between the so-called “pits”. What Thorne and his co-workers did was instead of generalizing the concentration profile throughout the deposit; they decided to define the site in terms of pits and further defined these pits by their own profile variations which provide more realistic estimations on the plant operations. Images of in-situ sub-divisions of the pits, namely, hematite, north and south, can be seen in Figure 23 with their locations on the deposit site.

As emphasized by the study, Çaldağ lateritic nickel ore has no saprolite zone that is generally constituted by secondary silicates such as garnierite found in most of the nickel deposits which in turn caused a clear transition between a limonite zone and the base rock region (serpentinite) marked by a sudden decrease on magnesium oxide content. This is also a correction of the study by Çağatay et al. However, the variations could not be generalized throughout the laterite deposit due to additional fluctuations (mechanical weathering) on profile that have been caused by several transportation mechanisms of mass soil (i.e. faulting) during laterite development and after it. In all pits, limonite zone seemed to be consistent to include limonite in the form of fine grained goethite as dominating mineral with only one exception of south pit containing carbonate (in the form of calcite) more commonly with respect to other pits. The highest nickel content in limonitic zone was found in hematite pit. Distinctions between pits are generally due to the levels above the limonite zones. While uppermost levels are dominated by siliceous materials in hematite pit, it is the calcite for the south pit.

The northern profiles, on the other hand, display no distinct hematitic sections as the other two pits and these sections generally accompanied by limonite together with hematite. Despite the fact that each and every data provided within this study is so valuable to mention, the summary of these distinctions can be visualized in Figure 24. Finally in this study, the nickel content was found to diminish with height since silica influences the nickel content within the profile [87].

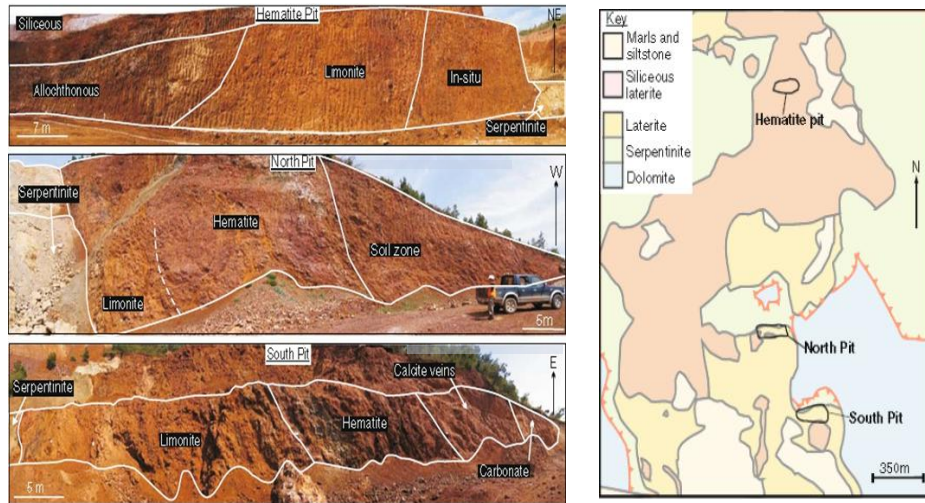


Figure 23 In-situ images of hematite, north and south pits of Çaldağ ore (left) and location of the pits on a map (right) [87].

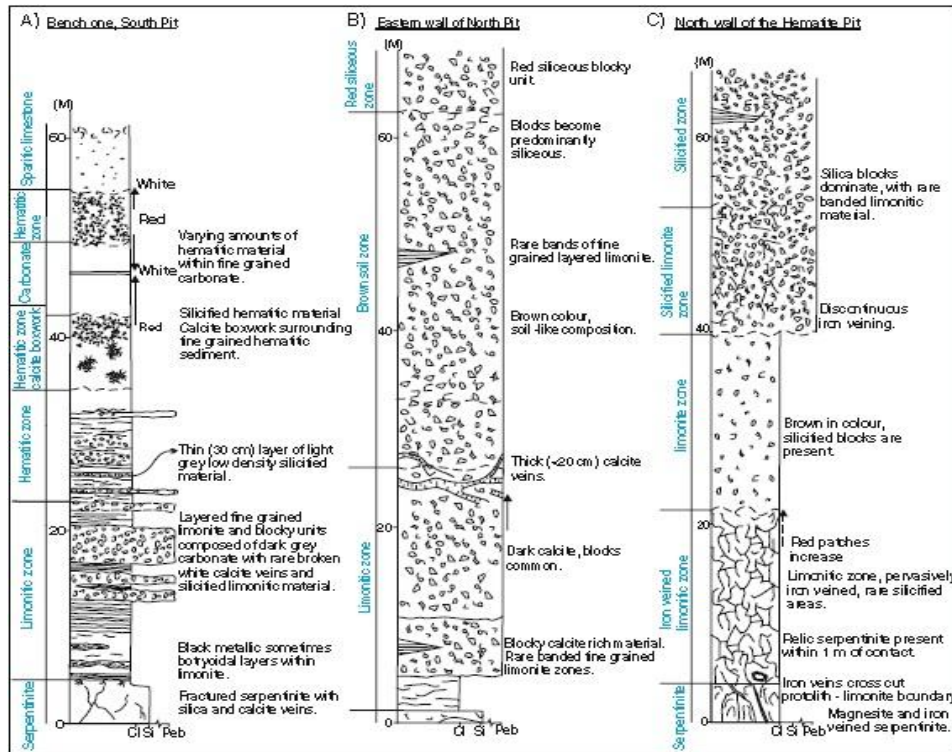


Figure 24 Profile variations of three pits in Çaldağ nickel deposit [87].

One last study worth to mention was performed by one of the most widely used automated characterization systems that makes use of energy-dispersive scanning electron microscope (SEM-EDS). This system, trademarked as QEMSCAN[®], was performed on samples from Çaldağ (limonite zone of hematite pit), Acoje (the Philippines) and Devolli (Albania). Samples taken from Çaldağ were found to contain goethite as the major nickel (locally up to 4%) and cobalt (up to 0.03%) source together with asbolane. However, manganese was found not only in asbolane and goethite but also in manganese silicate form. Chromium, on the other hand, found mainly within goethite not as chrom-spinel. Wide nickel concentration differences between and within the goethite particles confined the writers to a classification of goethite as low-, medium- and high-nickel goethite. Whilst high nickel content in goethite existed with elevated SiO₂, CoO and MnO amount, the low nickel content was associated with high Cr₂O₃ and Al₂O₃ amount. Iron oxides (hematite and magnetite) were found to be minor in all samples but clay minerals were found in significant amounts. As in the previous studies, there was no garnierite within the samples which is identification of absence of saprolite layer beneath the limonite zone. Concentrations of these and other minerals and their distributions can be seen in Figure 25 [88].

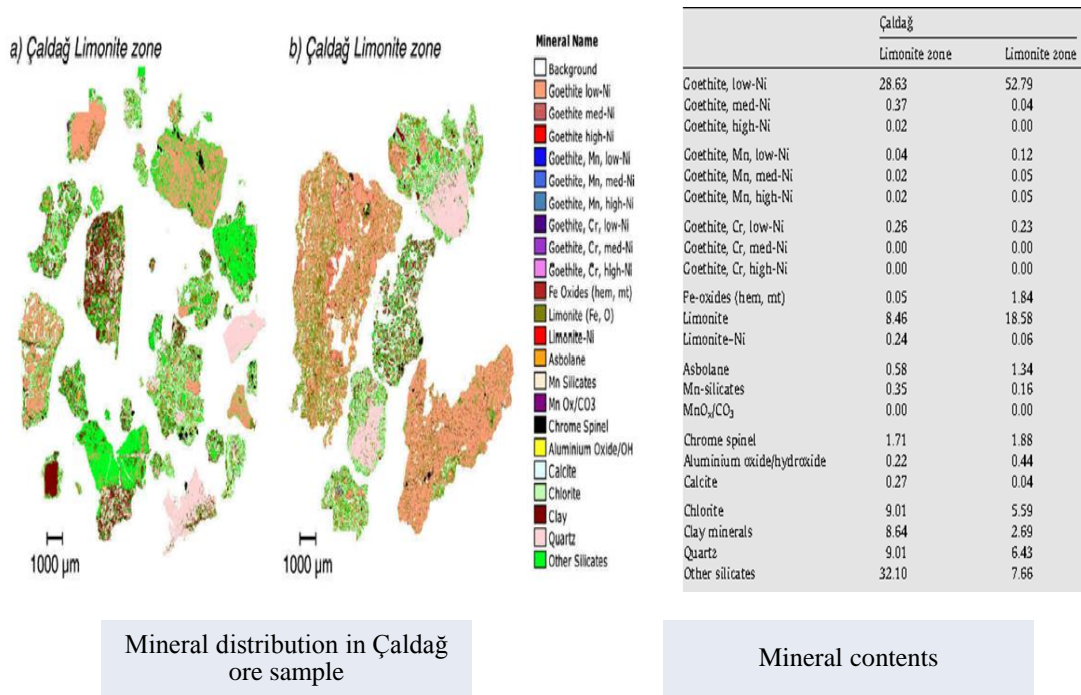


Figure 25 Mineral contents (wt. %) (right) and their distributions (left) in samples taken from Çaldağ ore by use of QEMSCAN method (5000 counts) [15].

2.6.2. Atmospheric Heap/ Column Leach Studies

The story of Çaldağ had just paused for two decades after the studies of MTA for its re-consideration as a nickel and cobalt source. In early 2004 the European Nickel PLC started their pilot plant preparations in Turkey under the name of Bosphorus Nickel Madencilik Ticaret A.Ş. (later on changed to Sardes Nickel Inc.) in order to test the leaching efficiency of the ore under atmospheric conditions from the start to the end where a saleable mixed hydroxide precipitate was gained. In late 2004, the initial acid contact of the first heap was started which was followed by the irrigation of two more heaps within 4 months. After a 2-year-long trial period, the results of tests were shared with the relevant scientific world in several congresses and symposiums [19,89–91].

In all the documents, the lithology of ore profile was simplified from surface to bottom as red limonite, yellow limonite, weathered serpentinite and serpentinite. In a comparison between the two limonite levels, nickel and cobalt contents were richer in yellow limonite as in the case of asbolane. However, goethite dominated both zones and contained more than 80% of the total nickel content by itself while asbolane individually contained the highest amount of nickel (locally 30% of its composition) but was found in minor amounts. In a brief summary, apart from goethite and asbolane, minor contributions to ore grade from hematite, chlorite and clay were also detected.

After 548 days of atmospheric leaching of the first heap which was the most representative of the ore site, the recoveries of nickel, cobalt, iron, manganese and aluminum were 79.4%, 82.7%, 30.0%, 78.9% and 37.1%, respectively. The sulfuric acid concentration had been kept at 75 g/L and the total sulfuric acid consumption for these extraction values was calculated as 528 kg/ton of dry ore. The resultant pregnant leach solution was then subjected to mixed hydroxide precipitate (MHP) processes which was composed of (1) iron removal and acid neutralization, (2) first stage nickel precipitation and (3) second stage nickel precipitation steps. In the first stage they preferred limestone addition to adjust pH of high acid pregnant solution (HA PLS) so that iron, aluminum and other impurities could be removed before sequential nickel precipitation steps. The resultant low acid pregnant leach solution (LA PLS) with pH= 4.8 was transferred to iron precipitation tanks and iron thickeners to separate iron hydroxide, gypsum, aluminum hydroxide and other impurity hydroxides by vacuum belt filtering

where iron cake was produced. The impurity-free PLS was then adjusted to a pH value of 7.6 by sodium carbonate addition. By doing so, underflow nickel was filtered and pressed to produce primary nickel product (PNP) while overflow of thickener was further processed by pH increment to 8.5 and similarly filtered to form secondary nickel product (SNP). PNP composition was given as 27-34% Ni, 1-1.3% Co, 0.90-3.7% Fe and 0.58-1.26% Mn. SNP composition was reported as 13-29% Ni, 0.60-1.30% Co, 0.03-0.24% Fe and 4.90-13% Mn. These products were shipped to several countries for refinement of nickel. The process is expected to be sustained by the new owners of the ore site.

In the meantime, Arslan et al (2006) presented their findings of agitation leaching experiments in another symposium. The utmost nickel and cobalt extractions of the experiments were given as 90.2% and 96.8%, respectively under the conditions of 80°C temperature, 200 g/l sulfuric acid concentration and 8 hours of leaching duration. Comparison of the results and benefits offered by the study covered in this thesis with the results obtained by the processes mentioned above will be discussed in the following chapter. Yet, it is also worth to mention about their optical mineralogical investigations. As a sum up of all previous studies, they found that the ore sample contained limonite, hematite, goethite, lepidocrocite, magnetite, asbolane, chromite, serpentine, chalcedony, quartz, chlorite, calcite and clay minerals. Mineral assemblages once more were found to exist as in the previous studies. While on one side asbolane was found to seizure in cracks and veins within the texture together with limonite, serpentine and clay type minerals; on the other side chromite, chalcedony, quartz, calcite and chlorite were detected through the cracks and fractures of serpentine and clay type minerals. On the contrary to QEMSCAN analysis, hematite was also found widely in their sample with other iron oxides (limonite and goethite) [92].

CHAPTER 3

SAMPLE CHARACTERIZATION, EXPERIMENTAL SET-UP AND PROCEDURE

3.1. Sample Description

Throughout this thesis study, the experimental procedure was practiced on a sample that was obtained from limonitic nickel laterite ore from Çaldağ, Manisa. At the time of receiving the sample, dated back to 2007, Çaldağ nickel ore was owned by the European Nickel PLC and the sample was given by the company for the aim of determination of the optimum conditions for nickel and cobalt extractions in a column leaching experiment series as a part of a project supported by TÜBİTAK. On the other hand, in this thesis, the ore sample was subjected primarily to high pressure acid leaching and subsequently to mixed hydroxide precipitation experiments. The sample was brought and has been kept in conventional, permeable linen bags which in turn caused a continuous decrease in actual humidity of the sample during this 5-year-long time period. In this respect, the sample cannot be considered as representative of its climatic environment.

3.1.1. Sample Preparation and Physical Characterization of Ore Sample

At the very first step, it was decided to check the physical conditions of the remaining sample. The sample in all linen bags weighed together about 220 kg with the largest particle size being -10 mm and with a colour range from light yellow to dark brown. It was informed by the company that each linen bag was filled with the ore samples from different locations of the mine. In order to satisfy the real-life conditions especially mineralogically, the whole sample had to be homogenized so as to obtain representative samples for the HPAL experiments. The homogenization of the whole sample, or in other words, sampling must be handled so carefully that any individual sample taken from the gross should be able to represent the proven reserve (33.3 million ton).

One of the widely accepted and industrially utilized studies put forward for sampling is by Gy which correlates the minimum weight of the sample from an ordinary ore to some characteristics of that ore. According to the equation proposed by Gy (1979) and revised by Smith (2001), the minimum weight of a sample is directly proportional to a sampling constant that is dependent on several factors (particle shape, particle size range, liberation factor and mineralogical composition) and the cubic size of the largest particle; and inversely proportional to a standard deviation of sampling [93]. Based on this study several calculations were carried out to find the necessary amount of sample in accordance with its particle size which is the most important parameter. In Table 9, the minimum required weight values for samples with respect to their particle sizes can be found whose range also includes the samples prepared during all crushing, grinding and sampling processes.

Table 9 Minimum weight of sample for ordinary ores with respect to particle size¹.

Diameter of Largest Particle		Minimum Weight of Sample	
Inch	Millimeter	Pound	Kilogram
0.010	1.02	0.0625	0.0286
0.083	2.11	0.5	0.227
0.167	4.24	4	1.814
0.313	7.94	32	14.51
0.500	12.70	125	56.80
0.625	15.88	256	116.12

At this point, it is essential to mention the necessity of reduction of particle size of samples that were subjected to high pressure acid leaching experiments. The effect of particle size of the slurry on leaching kinetics and extractions of nickel and cobalt has been described in the literature part. There one may find the physical reasons for that necessity. Since the ROM ore obtained was at -10 mm, the required amount of sample to be truly representative corresponds to a value between 14.51 kg and 56.80 kg. Additionally, as it will be discussed in the part subtitled as the effect of particle size on nickel and cobalt extractions in Chapter 4, the larger the particle size of ore feed, lower is the efficiency of extraction of these metals. More importantly, many chemical analysis techniques (i.e. AAS, ICP, etc.) use chemical reagents to dissolve the sample in very small amounts (2-10 g) for analysis which means both input and output samples would require further grinding and sampling operations for each experiment. Finally, Chou et al. [30] and Seçen [94] found that discarding the coarser particles increases the nickel and cobalt grades of ore with a manageable loss as the finer particles are less contaminated by gangue minerals such as quartz. Even decreasing the particle size from run-of-mine state (40 to 100 mm) to below 30 mm resulted in an increase in nickel grade from 0.7% to 1.3% for trial heaps of the European Nickel PLC [19].

With all the reasons stated above, 220 kg ROM ore was decided to be reduced in size from -10 mm particle size to -1 mm in a sequential, step-by-step crushing, grinding, screening and sampling processes that are summarized in Figure 26. Unfortunately, it is not possible to practice physical concentration operations to enrich the valuable metals on this kind of ores since nickel and cobalt do not have distinct minerals in the ore.

In accordance with these principles, total of 220 kg ROM ore was first mixed on a flat surface by forming of a cone with its top flattened with a shovel and divided into four quadrants with a cross. The rest of the procedure was exactly same as commercially known coning and quartering step and the same procedure was repeated until a satisfactory amount of sample was obtained. After coning and quartering of the initial sample, its particle size was decreased from -10 mm to -8mm with a jaw crusher and the output was subjected to coning and quartering again. The remainder sample was then reduced in size first to -4mm and then to -1mm with a roll crusher without sequential coning and quartering steps. This was so because of the final sample weight was approximately 25 kg and it was enough for high pressure acid leaching experiments as planned.

¹ 1 inch = 25.4 mm
1 pound = 0.45 kg

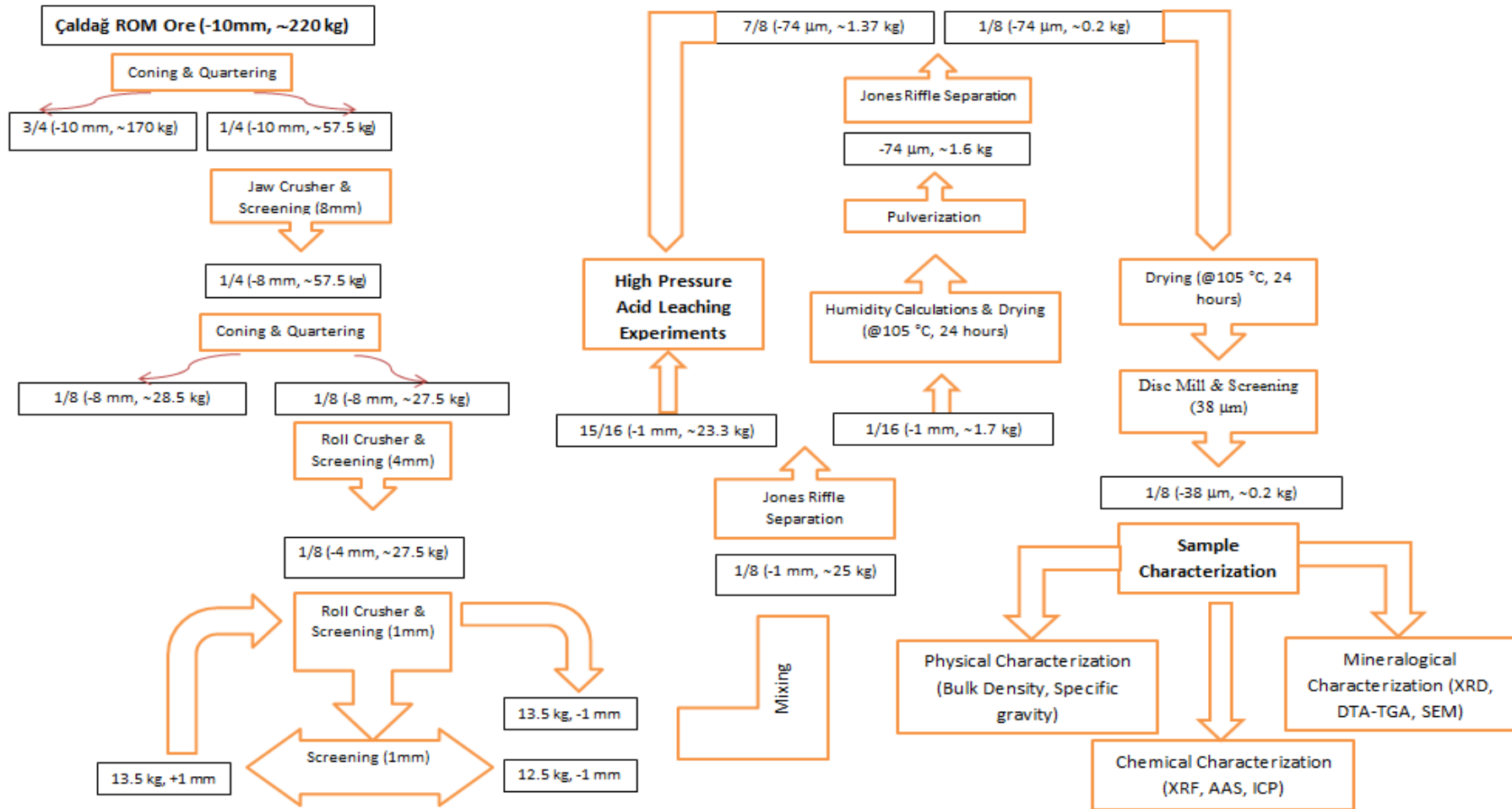


Figure 26 Crushing, grinding and sampling processes of Çaldağ lateritic nickel ore.

Despite the ore sample achieved target particle size (-1mm), there was a need for further sampling to prepare samples for humidity determination and several characterization tests that require lesser amounts of sample. Total of 25 kg sample was subjected to Jones riffle splitter which, unlike coning and quartering process, divides the sample into two equal parts and also guarantees the minimization of loss of sample. In each separation, one half was separated for further splitting whereas the second half was collected and bagged for further sample needs. After the first splitting stage, the last half of last separation was in -1mm particle size and 1.7 kg weight which was used for humidity determination. The sample was dried at 105°C for 24 hours and humidity of the sample is given in Table 10. This amount of moisture is generally well below the actual humidity of a fresh ore which is dependent on location and climatic environment of the deposit. In the study by Oxley et al. the moisture content of the ore was given as 18%, 20% and 17.9% for the three different trial heaps tested which are much higher than the value given in Table 10 [19].

Table 10 Moisture content of ROM sample.

Representative Ore Sample	Moisture Content (wt. %)
-1 mm ROM sample	5.4

After the humidity determination, the dried sample was ready for pulverization to decrease further its size. With a second Jones riffle separation after pulverization, the resultant last half was in the condition of -74 µm and 200 g in weight. In order to increase the accuracy of tests for the characterization of the sample, this amount of sample was subjected to utmost reduction in size to -38 µm with a laboratory disc mill. All characterization tests were conducted on the samples taken in small amounts from this finely ground ore.

The other factor, apart from the moisture content, that is important for storage of the ore is its bulk density. It correlates necessary volume of tank storage with the maximum amount of ore that is going to be stored in. In order to calculate the bulk density, 250 g of -10 mm ROM sample was filled into 1000 ml measuring cylinder with a diameter of 6.2 cm. The cylinder was shaken to flatten the upper surface of the ore. The height of the ore in the cylinder and its weight were noted for calculations and then the same sample was kept in a drying oven at 105°C in order to find its moisture content. After 7 hours drying, calculated bulk density of the ore can be seen in Table 11. According to Oxley et al. the bulk density values measured were 0.95, 1.10 and 1.24 ton/m³ for the three different heaps [20].

Table 11 Bulk density and specific gravity of ROM samples.

Representative Ore Sample	Bulk Density (g/cm ³)	Specific Gravity
-10 mm ROM sample (wet basis)	1.22	-
-38 µm ROM sample (dry basis)	-	3.22

Another important physical characteristic of the ore is its specific gravity which was measured in the central laboratory of METU (MERLAB) with a helium pycnometer at 24.4 °C and in order to prevent the moisture pick up, the sample was dried overnight before it was tested. The result is also given in Table 11. This value is the true density of ore without any air between particles or within the pores. It is the overall density to which each mineral present in the ore contributes.

After a sufficient amount of sample with the target particle size was prepared for high pressure acid leaching experiments as given in Figure 26, it was necessary to determine the particle size distribution of the sample. The variations in size of particles are due to the differences in hardness of the minerals

they contain. For example as a member of serpentine minerals, lizardite has a Mohs hardness of 2.5 whereas it is 7.0 for quartz. Instead of hardness values, the term, the Bond work index, is generally used in mining industry for comparison of grindability of several materials. As a result of that fact, one may only define an ore sample quantitatively by its largest particle size and its particle size distribution. Generally, the sieve analyses (wet or dry) are carried out with small amount of representative samples. Particle size distribution of the sample with –1mm particle size was determined with a nest of ten sieves as given in Table 12. While the sieves were shaking, 100 g of sample was poured on the uppermost sieve and water flow was continuously applied at the top in order to ease the passage of particles and reduce the blockage of sieve apertures and also to prevent the loss of fine particles as dust by vibration action. After wet screen analysis, the sieves were detached from each other, the oversize particles on each screen were collected in separate plates in which they were dried at 105°C overnight and then weighed separately. The results are also drawn as Gates-Gaudin-Schuhmann graph in logarithmic scale in Figure 27 which gives a straight line instead of a curve; hence one can easily interpolate or extrapolate weight percentages to any particle size within the size range or outside [93].

Table 12 Particle size distribution of -1 mm Çaldağ ore sample.

Mesh Size (micron)	Oversize weight %	Cumulative Oversize Wt. %	Log Particle Size (micron)	Cumulative Undersize Wt. %	Log Cumulative Undersize Wt. %
850	5.39	5.39	2.93	94.61	1.98
600	8.64	14.03	2.78	85.97	1.93
425	6.75	20.78	2.63	79.22	1.90
300	7.50	28.28	2.48	71.72	1.86
212	6.48	34.76	2.33	65.24	1.81
150	5.87	40.63	2.18	59.37	1.77
106	5.93	46.56	2.03	53.44	1.73
75	1.74	48.30	1.88	51.70	1.71
53	5.37	53.67	1.72	46.33	1.67
38	1.33	55.00	1.58	45.00	1.65
-38	45.00	-	-	-	-
TOTAL	100.00	-	-	-	-

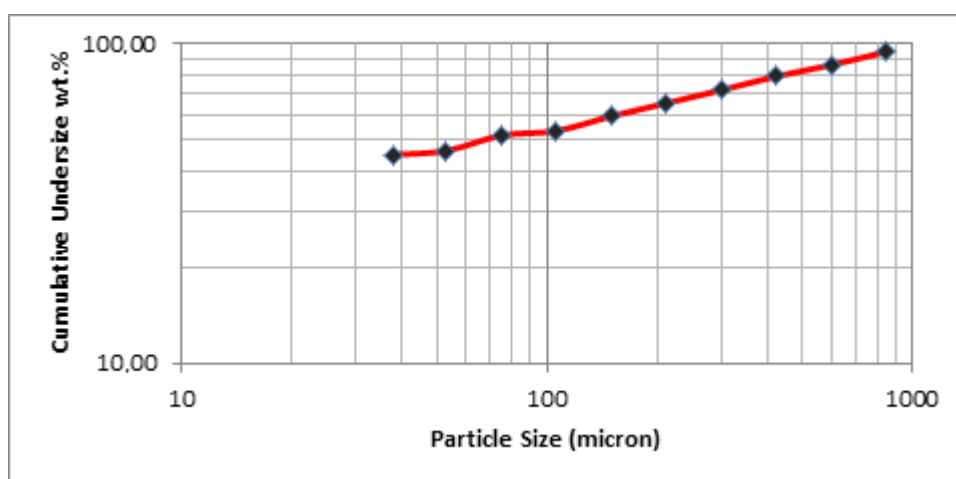


Figure 27 Particle size distribution of -1 mm Çaldağ ore sample (logarithmic scale).

Within this study, in order to understand the effect of particle size on the nickel and cobalt extractions, two more samples with 0.5 mm and 1.4 mm largest particle sizes were prepared in addition to the major sample prepared for the whole high pressure acid leaching experiments and the same wet sieve analysis that is described for -1mm sample were performed on these samples too. However, depending on the largest particle size of the sample, the minimum required amount of the sample to be truly representative varies for 1.4 mm particle size for which 150 g sample was found to be sufficient. The results of wet screen analysis of each sample are given in Tables 13 and 14, respectively. Similarly, the log-log plots are drawn and given in Figures 28 and 29 as follows:

Table 13 Particle size distribution of -0.5 mm Çaldağ ore sample.

Mesh Size (micron)	Oversize weight %	Cumulative Oversize Wt. %	Log Particle Size (micron)	Cumulative Undersize Wt. %	Log Cumulative Undersize Wt. %
425	0.24	0.24	2.63	99.76	2.00
300	1.75	1.99	2.48	98.01	1.99
212	5.36	7.35	2.33	92.65	1.97
150	10.17	17.52	2.18	82.48	1.92
106	9.69	27.21	2.03	72.79	1.86
75	8.63	35.84	1.88	64.16	1.81
53	7.07	42.91	1.72	57.09	1.76
38	1.48	44.46	1.58	55.54	1.74
-38	55.61	-	-	-	-
TOTAL	100.00	-	-	-	-

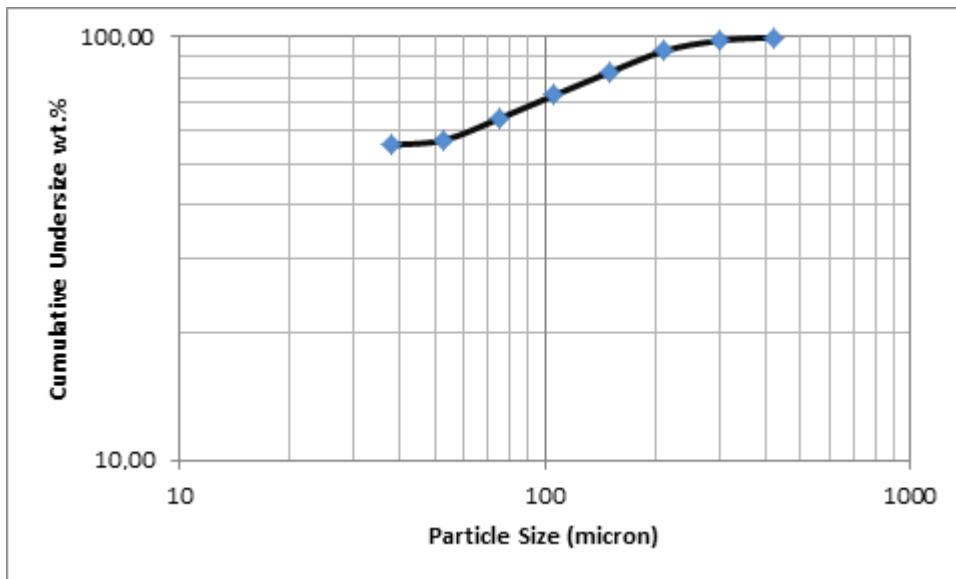


Figure 28 Particle size distribution of -0.5 mm Çaldağ ore sample (logarithmic scale).

Table 14 Particle size distribution of -1.4 mm Çaldağ ore sample.

Mesh Size (micron)	Oversize weight %	Cumulative Oversize Wt. %	Log Particle Size (micron)	Cumulative Undersize Wt. %	Log Cumulative Undersize Wt. %
1168	2.80	2.80	3.07	97.20	1.99
850	8.07	10.87	2.93	89.13	1.95
600	7.20	18.07	2.78	81.93	1.91
425	5.94	24.01	2.63	75.99	1.88
300	6.62	30.63	2.48	69.37	1.84
212	5.47	36.10	2.33	63.90	1.81
150	5.40	41.50	2.18	58.50	1.77
106	7.67	49.17	2.03	50.83	1.71
75	8.67	57.83	1.88	42.17	1.62
53	7.57	65.40	1.72	34.60	1.54
38	0.74	66.14	1.58	33.86	1.53
-38	33.86	-	-	-	-
TOTAL	100.00	-	-	-	-

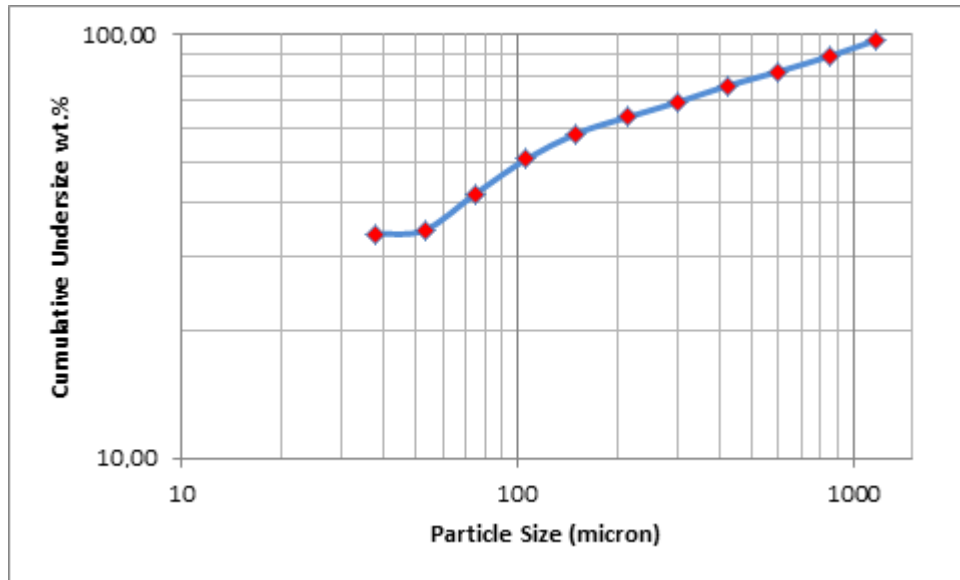


Figure 29 Particle size distribution of -1.4 mm Çaldağ ore sample (logarithmic scale).

The particle size distributions of all samples gave somewhat similar results since each ore sample had almost one half of its content with very fine particles (finer than 38 μm) while the remaining half of it consisted of relatively coarser particles.

3.2. Chemical Characterization of Ore Sample

Laterite ores can contain several elements all of which have individual importance in regard to their abundance. The chemistry of most important and most commonly encountered ones were described in the literature part. Related to these chemistry concerns during leaching, it is also important to know the chemical composition of the ore in order to predict its theoretical acid consumption which gives a general idea of where to start the high pressure acid leaching experiments. This theoretical approach is based on the assumptions of how much percentage of elements or their ions are extracted and in what amount they are responsible for the sulfuric acid consumption during leaching. The recommendations

for the assumptions put forward by the Sherritt-Gordon Company with their previous experience and the details will be given in Chapter 4.

The chemical composition of Çaldağ ore sample was determined by two different methods in order to cross-check the accuracy. The first method used was Inductively Coupled Plasma Atomic Emission Spectroscopy (ICP-AES) which was carried out by ALS Analytical Chemistry and Testing Services, Canada. Afterwards, the same ore sample was analyzed with X-ray Fluorescence (XRF) method using Bruker S8 XRF analyzer in the Metallurgical and Materials Engineering Department of METU, Turkey. The theoretical acid consumption calculations were based on the results obtained by ICP-AES. The results of both analytical methods are given in Tables 15 and 16.

As can be seen in Tables 15 and 16, the chemical analysis results of the two methods are different for some elements because of the calibration problems and yet can be considered as consistent within a negligible error band. On the average, the ore grade was 1.238% Ni and 0.069% Co. However, for the experimental calculations, Çaldağ ore sample was accepted to have the composition listed beneath the ICP –AES title. Moreover, the most abundant elements were found to be iron and silicon which were in parallel with the mineralogical characterization results that will be discussed in the next section.

Table 15 Chemical composition of Çaldağ lateritic ore sample

Element	ICP-AES (wt %)	XRF (wt %)	Element	ICP-AES (wt %)	XRF (wt %)
Ni	1.215	1.26	Zn	0.04	0.04
Co	0.078	0.060	Na	0.04	-
Fe	32.70	33.21	Cu	0.055	0.06
Al	1.66	1.92	Si	13.39	11.19
Mn	0.349	0.340	As	0.01	0.01
Mg	1.62	2.17	K	0.2	0.12
Cr	1.01	0.94	Ti	0.06	0.04
Ca	0.60	0.70	S	0.11	0.13

Table 16 XRF and ICP analysis results of scandium.

Element	ICP-MS & ICP-OES (mg/kg)	XRF (mg/kg)
Scandium	65 (\pm 0.2)	61

3.3. Mineralogical Characterization of Ore Sample

To know the mineralogy of a lateritic ore sample is very crucial for many aspects of the operation of high pressure acid leaching plants. It has broad affects at several stages throughout the process flowsheet. The first concern is of course at the first stage of HPAL process where hot acid is introduced to ore slurry. The mineralogy has an important role for especially leaching kinetics and extraction efficiencies of not only valuable nickel and cobalt but also the other elements including iron, aluminum, and chromium and so on. Apart from that the solid waste produced at this stage is in correlation with the mineralogical content of ore feed. Scale formation in the autoclave is hugely affected by the mineralogy that was discussed previously in Section 2.4.6. After the upstream stage, the mineralogy either directly or indirectly affects the efficiencies of each downstream process.

Initially the resultant free acid within metal loaded leach solution is of concern in neutralization step for reagent consumption whereas the extraction performances of each impurity metal are of concern in removal stages for high quality saleable product. Hence, it is quite important to determine the existing minerals in lateritic ores and if possible to quantify them as accurately as possible. According to the latest survey, the frequency of minerals that have been recorded in 117 different laterite deposits can be seen in Table 17. Here the nickel bearing minerals are grouped according to their composition and laterite subtype except for those minerals belonging to serpentine group, talc and chlorite since they are dispersed and scattered and hence can be seen within any laterite type. Additionally, accessory minerals are not included in any sub-type because they display no correlative pattern with ore type. Another point is the minerals belonging to clay silicates. Despite the clay silicate sub-types of nickel laterites are the lowest one, the minerals of this type are highly frequent in ore deposits. This is because of the absence of exact and pure clay silicate layers but rather their distribution in almost all parts of laterites. As can be seen from the table, the leading minerals according to their frequency of detection in laterite deposits are goethite and limonite with hematite for limonitic ores.

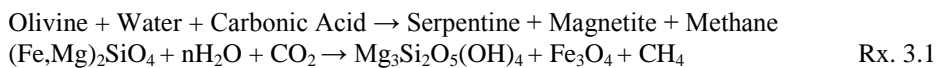
Table 17 Frequencies of detected nickel-bearing minerals by their counts and percentage of deposits containing minerals among all 117 laterite deposits (Adopted from [14]).

Minerals	Counts	% of deposits containing mineral
Ore Sub-type: Fe and Mn oxides		
Goethite	92	77
Limonite	88	73
Hematite and maghemite	72	60
Mn-oxide (including cryptomelane, pyrolusite, ramsdelite)	20	17
Todorokite and chalcophanite	8	7
Lithiophorite	5	4
Ore Sub-type: Hydrous Mg-silicates		
Serpentine (undifferentiated)	77	64
Garnierite	40	33
Talc	38	32
Lizardite	11	9
Antigorite	10	8
Kerolite	19	16
Pimelite	16	13
Nepoulite	13	11
Ore Sub-type: Clay silicates		
Smectite and illite	92	77
Nontronite	88	73
Gibbsite	72	60
Clay minerals (undifferentiated)	20	17
Kaolinite	8	7
Montmorillonite	5	4
Other Accessory Minerals (Non-nickeliferous)		
Quartz	78	65
Chromite and Cr-spinels	70	58
Magnetite	65	54
Chalcedony	21	18
Opal	19	16
Magnesite	21	18
Dolomite	8	7
Siderite	11	9
Calcite	7	6

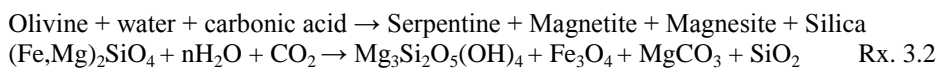
3.3.1. XRD Examinations

In order to characterize Çaldağ ore sample mineralogically, the first step was XRD (X-Ray Diffraction) examination. For that purpose a very small amount was taken from 200 g ground sample prepared for the characterization as summarized in Figure 26. XRD analysis was carried out with Rigaku D/MAX2200/PC model X-Ray Diffractometer with a Cu-K α X-Ray tube working under 40 kV and 40 mA. XRD result is given in Figure 30.

As can be seen from the XRD pattern, the major peaks were due to the presence of quartz and goethite with hematite. This was expected as the chemical analysis of ore indicated that it was dominated by iron and silicon. Apart from these major phases, it was also detected that serpentine (possibly lizardite), smectite (either beidellite or nontronite or both), calcite, dolomite and asbolane phases existed in relatively minor amounts. As it will be discussed with the results obtained from the SEM examinations of sample, it was probable that a spinel form of iron chromium oxide, which was possibly chromite, might also have existed within the sample. It was also found that at around 28° the two very small peaks neighboring to major quartz peak at 26° were found to match two different types of silica with card numbers of 79-1913 and 81-0068. In the previous optic mineralogy studies, the existences of chalcedony and opal were mentioned [92]. As chalcedony and opal are varieties of quartz with the same chemical compositions but with different crystal structures, the differentiation of them is only possible by detailed optical mineralogy study. Hence, the so-called peaks were also classified as quartz. Similarly, chlorite existence was also mentioned but neither of the members of this clay group was found to have a quite match with respect to XRD pattern. After detection of serpentines the existence of magnetite was questioned since it is known that during the serpentinization of olivine where it transforms into serpentine according to one of the reactions magnetite can be formed as by product.



Or,



As the characteristic peaks of chromite, magnetite and hematite are very similar to each other due to their similar structures (both are spinels) their quantification is rather difficult [53]. In Çaldağ case, the combined existence of gross goethite, quartz and hematite peaks have made the situation even worse as they might have suppressed the chromite from its reflections. Chromite and magnetite was reported in several studies that they are very refractory against acid attack [48,95,96]. As a result, their detections are quite possible when the leach residue of the pressure leaching experiment is subjected to XRD where it is expected to see a more clarified pattern by removal of most of the pre-existing ore minerals such as goethite. However, when chromite and magnetite also dissolve in acidic media they release undesired divalent iron (ferrous) ions. Ferrous iron concentration must be treated with oxidative environment during pressure acid leaching so that it can be oxidized to trivalent iron (ferric ion) prior to downstream processes. That is because ferrous iron is hard to remove later on in downstream processes (i.e. MHP) as its precipitation line is extremely close to nickel and cobalt. Ferric iron can also readily be reduced to ferrous iron in the presence of sulfur and/or with SO₂ gas [79]. Existence of chromite and magnetite will be further mentioned in SEM examinations.

Existence of clay-like minerals can be a problem due to divalent iron concentration similar to chromite. However, their situation is more of concern because these types of minerals generally readily dissolve and might be responsible for high ferrous iron concentrations as well as amorphous silica formation. On the other hand, they can contain valuable metals within their structure. If a general picture can be drawn that includes their compositions, the results after HPAL tests can be more truly commented. For example, a high ferrous iron concentration in the absence of manganese agents (i.e. asbolane) will be commented as complete serpentine and/or smectite dissolution. On the other hand, higher than reported manganese dissolution in serpentine and/or smectite media will possibly result in a low ferrous iron but high hematite precipitation amount with high cobalt extractions. Correlation of other elements in their structure will also be related to their behavior against acid attack such as magnesium, chromium, nickel and alkali ions like potassium and sodium.

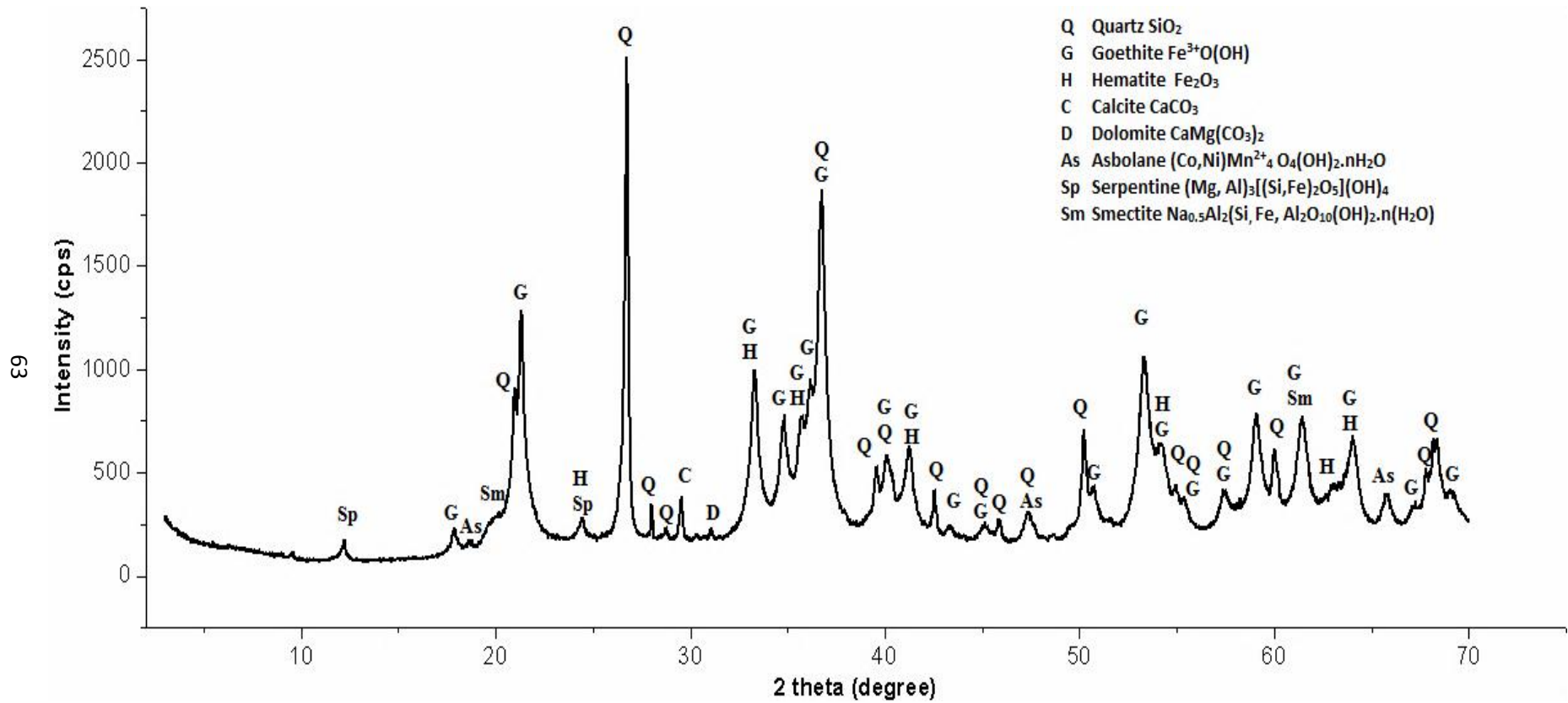


Figure 30 XRD results of Çaldağ run of mine sample.

3.3.2. DTA-TGA Examinations

In order to confirm the identified phases within the ore sample so far, the thermal analysis by means of Differential Thermal Analysis (DTA) and Thermo Gravimetric Analysis (TGA) was conducted at MERLAB. The analysis were performed under the conditions of 10°C/min heating rate within the temperature range of 35°-1000°C in air atmosphere. DTA-TGA analysis result can be seen in Figure 31.

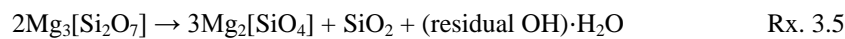
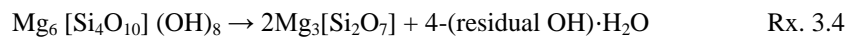
As a broad definition, the loss of physically present water with increasing temperature is called dehydration whereas for the loss of chemically bound water the term dehydroxylation is used. Many minerals (phyllosilicates, oxides, hydroxides, etc.) contain physical water within their bulk form which in turn causes an endothermic peak at around 100°C in their DTA curves associated with a decline in their TGA curves. The endothermic peak observed for Çaldağ sample at around 110°C was believed to be due to the dehydration of the ore sample.

Hematite as pure substance gives only a small peak at 675°-680°C which is the Curie point of the mineral. However, the existence of hematite was found to affect the behavior of goethite. Goethite, when pure, gives an endothermic peak between 385 and 405°C depending on its fineness and gives no more peaks between 500°C and 1000°C. As goethite is blended, hence diluted with hematite the endothermic peak of pure goethite is depressed and shifted to lower temperatures with increasing amount of hematite. This case is valid when goethite exists with thermally inert minerals other than hematite. Moreover, the natural goethite is amenable to impurity atom substitutions for Fe by Ni, Co, Al, Cr, and Mn. These substitutions may affect its dehydration temperature. In literature there are several studies on the thermal behavior of natural goethite. According to Lopez et al. (2008) under oxidative environment goethite loses its chemically absorbed water and transforms into hematite with Rx. 3.3 at around 300°C [97]:



Hence, the endothermic peak observed for Çaldağ ore at around 290°C was due to thermal transformation of goethite associated with a distinctive mass loss as a result of water release. Landers et al. described this thermal dehydroxylation of goethite as topotactic transformation which initially starts at the surface of goethite and moves inward through the voids created as a result of volume shrinkage since hematite has lesser volume than goethite [98].

Being the second most significant peak, the exothermic peak at around 820°C was the evidence for the existence of serpentine mineral in Çaldağ ore. According to Földvári (2011), Mg-serpentine undergo two thermal reactions: one between 640°C-820°C displays as an endothermic peak and the other between 800°C-840°C displays as a sharp exothermic peak. In the first step, the dehydroxylation takes place according to Rx. 3.4 and in the second, the decomposition of serpentine and formation of forsterite take place according to Rx. 3.5 [99].



As seen in Figure 31, there was a continuous mass loss with almost steady slope of TGA curve as temperature was raised from about 330° to about 750°C. Yet, from the DTA curve of this temperature range, it was hard to detect a clear endo- or exothermic peak except those endothermic peaks at about 590°C and about 660°C. The broad peak at 590°C might be the signature of allotropic transformation of quartz from trigonal α -quartz to hexagonal β -quartz which occurs at 573°C \pm 40°C [100] or endothermic dehydration of kaolinites (including halloysite) between 530°C and 590°C.



However, the associated exothermic peak at 900°C-1000°C corresponding to transformation of kaolinite into a spinel form by Rx. 3.6 was not observed [99]. Hence it might be a sign for the absence of kaolinites. As further evidence enhancing their absence was the information that kaolinites are acid

resilient and also they are reluctant for impurity metal substitutions. For this purpose, as it will be discussed in Chapter 4, the XRD examination of leach residue produced at the optimum conditions was also searched for kaolinite existence. On the other hand, the other endothermic peak at about 660°C might be due to previously mentioned serpentine dehydroxylation by Rx. 3.4.

It is obvious that the continuous mass loss within this temperature range could be related to the existence of clay minerals and/or carbonates within the ore sample that were losing their chemically bonded CO₂ or H₂O with increasing temperature. Members of many groups of clay minerals actually suffer from dehydration and/or dehydroxylation within this temperature range that could cause such a steady mass loss. Apart from the previously mentioned clay sub-groups like kaolinites and serpentines; smectites also exhibit thermal activities at that range. According to Földvári (2011), montmorillonites (either Ca or Na) display an endothermic dehydroxylation peak at about 700°C and endothermic-exothermic peak system between 850°C to 1000°C for their structural decomposition. Nontronites display an endothermic dehydroxylation peak at about 400°C to 500°C with the same system later on in the same range as smectite minerals. As a result, the response at 660°C might also be the evidence for the existence of smectite minerals. In conclusion, it can be said that the thermal analysis of the original Çaldağ sample was helpful to a limited extent. There was a clear evidence for the presence of goethite and serpentine minerals but blurred evidences for the existence of smectite and absence of kaolinite.

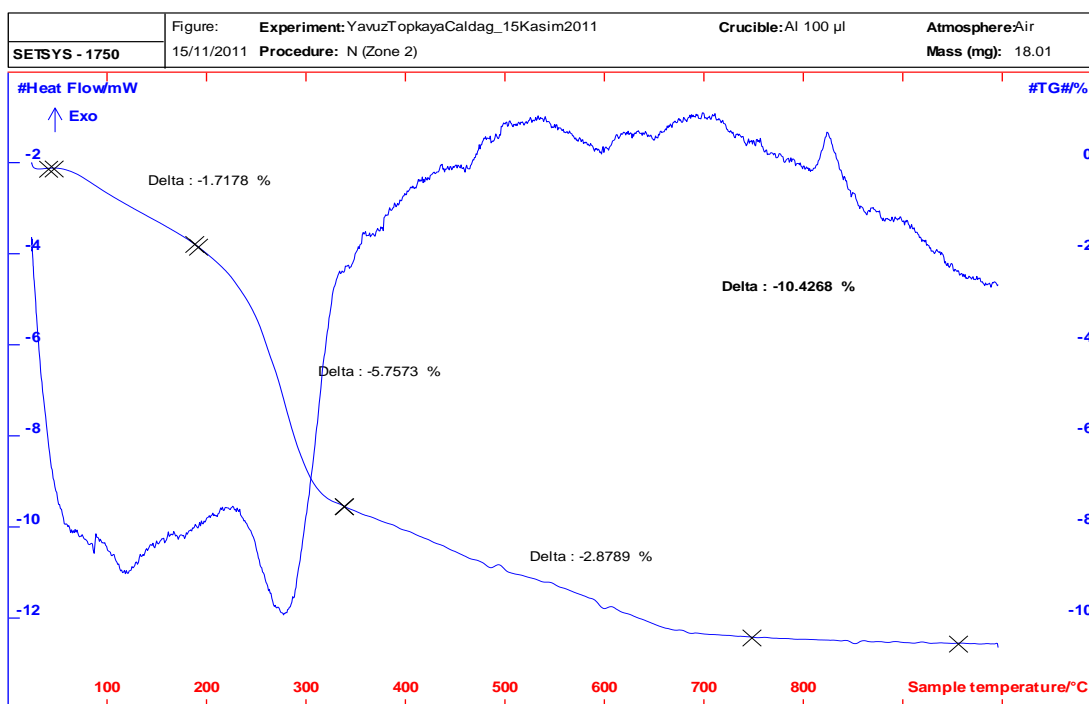


Figure 31 DTA-TGA analysis result for Çaldağ lateritic sample.

3.3.3. SEM Examinations

Due to the insufficient data obtained from the thermal analysis, a confirmation for the results obtained from the XRD data tried to be checked by utilization of scanning electron microscope (SEM) with the aid of energy-dispersive X-ray spectroscopy (EDX) unit. At the same time, an effort towards detecting the possible nickel and/or cobalt bearing minerals in the ore sample was made. By doing so, the extraction of these valuable elements entrapped within these target minerals can be understood by considering the dissolution behavior of these minerals. Additionally, commenting on the expected and the actual efficiencies on extracting these elements through high pressure acid leaching experiments

could be easier and more realistic. For example, the determination of serpentines ($(\text{Mg}, \text{Fe}^{2+})_3\text{Si}_2\text{O}_5(\text{OH})_4$) and their quantities within the nickel laterites are of great importance for the determination of the optimum conditions since serpentines are one of the acid consuming minerals due to their magnesium content [101]. Clay silicates and clay-like minerals are expected to dissolve more easily. According to Canterford and Griffin et al. smectites, serpentines and sapolites are readily leached even at atmospheric leaching conditions and their complete dissolution is important for many elements forming their structure [21,102]. On the other hand, nickel bearing chromium rich hematite can be resilient against acid attack while spinels such as chromite are known to be refractory against acid dissolution requiring higher acid to ore ratios and longer leaching durations [95] [103].

In addition to these direct outcomes, some indirect conclusions might be related to mineralogical findings. For example, the divalent iron concentrations in pregnant leach solutions are generally desired to be negligibly low. If not, the creation of oxidative environment either during autoclave operation or during first iron removal together with neutralization steps is generally the applied solutions. Iron-spinels such as magnetite or iron-bearing clay minerals such as ferruginous smectites and serpentines could be responsible for high ferric iron concentrations in pregnant leach solutions. Nontronites are rich in iron and contain it predominantly in the trivalent state whereas montmorillonites can include it in divalent state as substitutions for Mg [104]. Serpentines can also include ferric iron in their complex nature as substitutions for magnesium however during acid attack some of the divalent iron oxidizes to trivalent form.

The ferrous iron concentration is not only related with the source minerals but also existence of other ions that can oxidize ferrous ion to ferric iron. As an example, when divalent iron concentration is considerable, tetravalent manganese come into contact with divalent iron and reduction to divalent manganese occurs which enhances manganese dissolution. According to the study by Tindall and Muir (1997), despite manganese-bearing minerals display low extraction tendency, nontronitic ore feed (rich in clay minerals and hence Fe^{2+}) containing lithiophorite showed high extraction efficiencies for both manganese and cobalt elements during pressure acid leaching [42].

As a consequence, the detection and -if possible- quantification of these minerals are crucial for the determination of choice of parameters throughout the process train. Furthermore, the detection of minerals with acid consuming elements such as magnesium and aluminum is of concern since acid consumption is one of the most important operational parameter for pressure acid leaching. For example, after it was found that considerable amount of serpentine existed within the ore profile of Ravensthorpe in West Australia; serpentine rejection during ore preparation prior to acid leaching has been applied in process train of this ore.

With all these purposes SEM-EDX examinations were initiated. In order to achieve that, small amount of -75 micron ore sample taken from 200 g that was prepared for the characterization purposes was used initially. However, EDX analysis could not be interpreted sufficiently as it was found that interactions between surrounding particles and electron beams were unavoidable. EDX mapping trials for these samples were also found to be not very useful. Fine particles were quite close to each other (despite ultrasonic agitation of sample in acetone was applied prior to examination) and mapping of each element resulted in the dots all over the sample holder. Besides, due to agglomeration of fine particles and also coating of dusty particles on relatively larger particles the analysis results were not very reliable. Instead, it was decided to prepare relatively coarse particles that would prevent agglomeration. 100 g of run of mine sample with -1mm particle size was sieved and particles larger than 850 micron were washed with tap water so that the removal of sticking very fine particles was achieved. Washed sample was dried in oven at 105°C overnight.

Before SEM analysis, carbon tapes were cut into quarters and the particles were randomly selected by nipper and classified into quarters with respect to their color ranges. The reason for classifying them in color was to use the color differences when necessary. It is known that iron oxides are generally brownish to reddish, asbolane is known to be black, and serpentines are yellowish to light green whereas quartz and calcite are known to be white or transparent. Lastly, the samples were coated with gold in several nanometers in order to satisfy the working principles of SEM as the samples were in oxide form. Samples including particles used in the examinations can be seen in Figure 32 prior to gold coating. As it can be seen some particles were decreased in size into smaller particles while glued

on carbon tape. This behavior indicated that such particles contained softer minerals such as smectites (i.e. nontronite).



Figure 32 Images of sample holders prior to gold coating.

Each quarter was studied separately and within each quarter, the particles were grouped as smoothly as possible in order to ease the location of particles during examination and to compare their colors with literature when necessary. A general EDX was taken from each group so that the elements detected in this EDX results were selected for elemental mapping. Since the sample holders were known to be Al-Mg alloy, these elements were added into mapping. One of the main research purposes of SEM-EDX examination was the detection of Ni-Co bearing minerals. After mapping, each particle within each group was subjected to one to three EDX analyses in order to confirm the homogeneity of particles. However, some of the particles were found to contain two or rarely more phases within them. The most obvious mixture of two phases can be seen for particle 1 in Figure 33 where a white region (as quartz) is joined with a darker region (iron-oxide). Actually, that was an expected problem as the particles were chosen from relatively larger particles but still it was possible to detect pure particles of minerals that will be given in detail as follows.

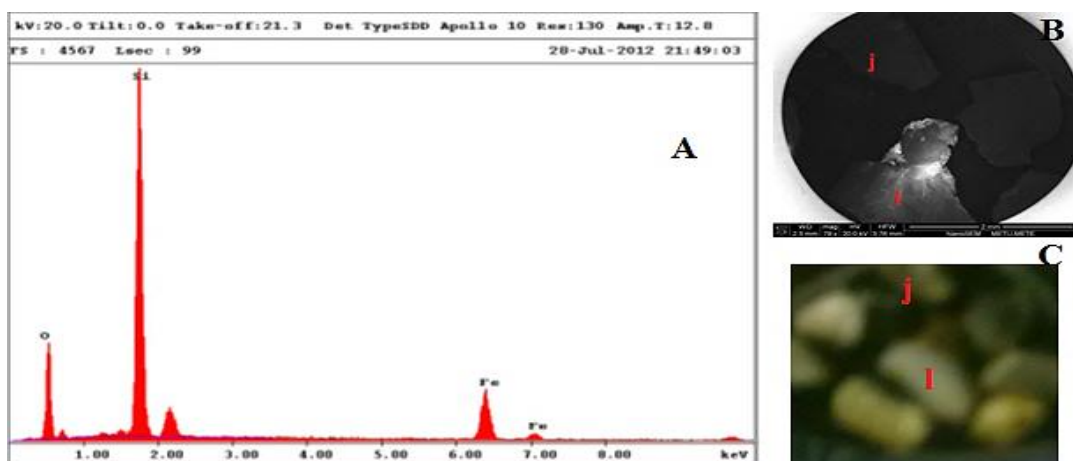


Figure 33 Two intercalated phases in particle 1: prior to gold coating (C), SEM image (B) and EDX result taken at the junction region (A).

3.3.3.1. SEM Examinations on Particles of First Sample Holder

A typical procedure taken can be described through Figures 34-36. In Figure 34, one of the studied quarters of first sample holder was divided into two groups and each particle was labeled including un-grouped single particle (particle h). SEM views of each group were listed next to the un-coated sample scheme. Prior to mapping a general EDX of particles were taken as in Figure 35 in order to determine the elements that would be mapped within the particles. Later, mapping was initiated for these elements as in Figure 36. Degree of coloring of regions for respective elements is commented as their concentrated or major phases. EDX results of particles were grouped in Appendix C.

In all mapping results, it was once again confirmed that neither nickel nor cobalt were concentrated on a particle but rather were found to distribute over several particles. On the contrary, both iron and silicon were the most abundant elements in particles as their own phases and in others they contribute in varying amounts. This result was expected on considering the chemical analysis.

Chromium was generally found to be correlated with iron oxides along with ferruginous smectite particles which caused doubt on probability of chromite mineral existence. Within this examination, once again distinctive evidence could not be found. Nonetheless, this does not necessarily mean that chromite did not exist within the mineral as the particles were randomly selected and examination purpose was search for proofs for existence of detected phases rather than proving their absences. Overall, when the XRD result of original sample is considered, it is believed that either chromite contribution in sample is in minor or trace amounts or even it is completely absent but rather chromium is incorporated with iron oxide/hydroxides and ferruginous smectites. Manganese was found to exist in two forms. One form is its own mineral form which is thought to be asbolane (based on the XRD results) and the other form is as a substituting element within iron oxides. Aluminum and magnesium were generally associated with clay minerals. However, gibbsite form of aluminum and aluminum substituted goethite has been mentioned in several articles. Gibbsite could not be detected in XRD examinations while aluminum substituted goethite was also questionable as iron oxides were generally associated with clay minerals in most cases. On the other hand, serpentine particles were found rich in magnesium but poor in aluminum and for all serpentine particles this situation was quite steady and consistent. On the other hand, smectite particles were rich in aluminum alongside the other dominating element silicon while magnesium content was quite low. Additionally, some smectite particles (especially those in second sample holder) were richer in iron content. Calcium was found to contaminate almost all particles in minor amounts. As mentioned previously, smectites can contain either calcium or sodium as their exchange cation element. Asbolane can also be host mineral for calcium at about 2%. In this study, sodium was rarely found while calcium was generally the abundant one for smectites. Fortunately, it was possible to detect separate calcium mineral, namely calcite particles as can be seen in Figure 37. In addition to calcite mineral, in some EDX analysis sulfur was found to associate with calcium which pointed to the existence of calcium sulfates (i.e. gypsum, anhydrate or bassanite). Trials for XRD matching were negative which meant that these calcium sulfates were in lesser amounts than detection limit. Nevertheless, sulfur contribution in these calcium sulfate particles during pressure leaching process is a side benefit as calcium is one of the consumers of acid during pressure acid leaching. As a footnote for EDX graphs, the unlabeled peaks are due to carbon (from carbon tape) and gold (from coating) that were excluded for clarity.

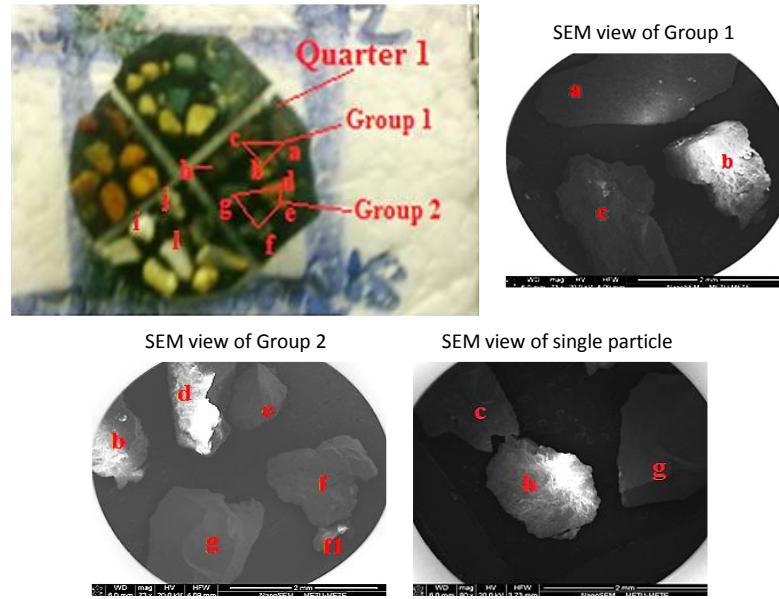


Figure 34 SEM views and classifications of particles in a quarter of first sample holder.

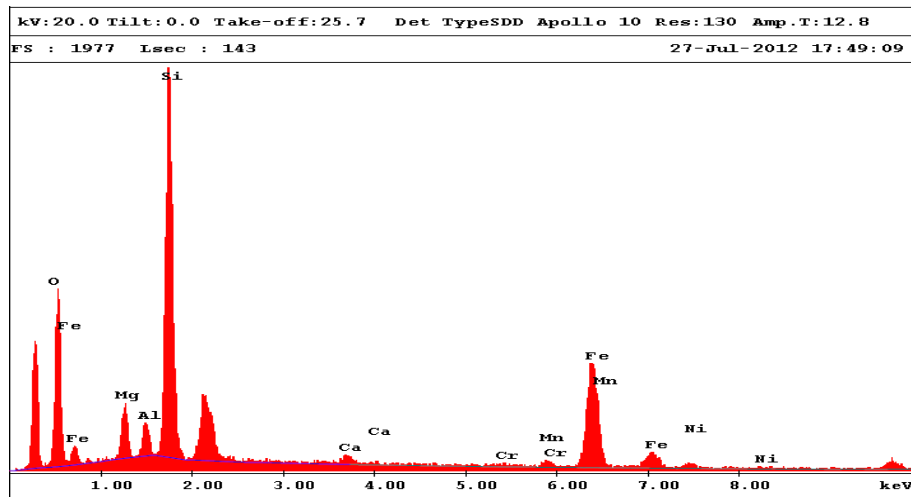


Figure 35 EDX result of general view of Group 1 for mapping of existing elements.

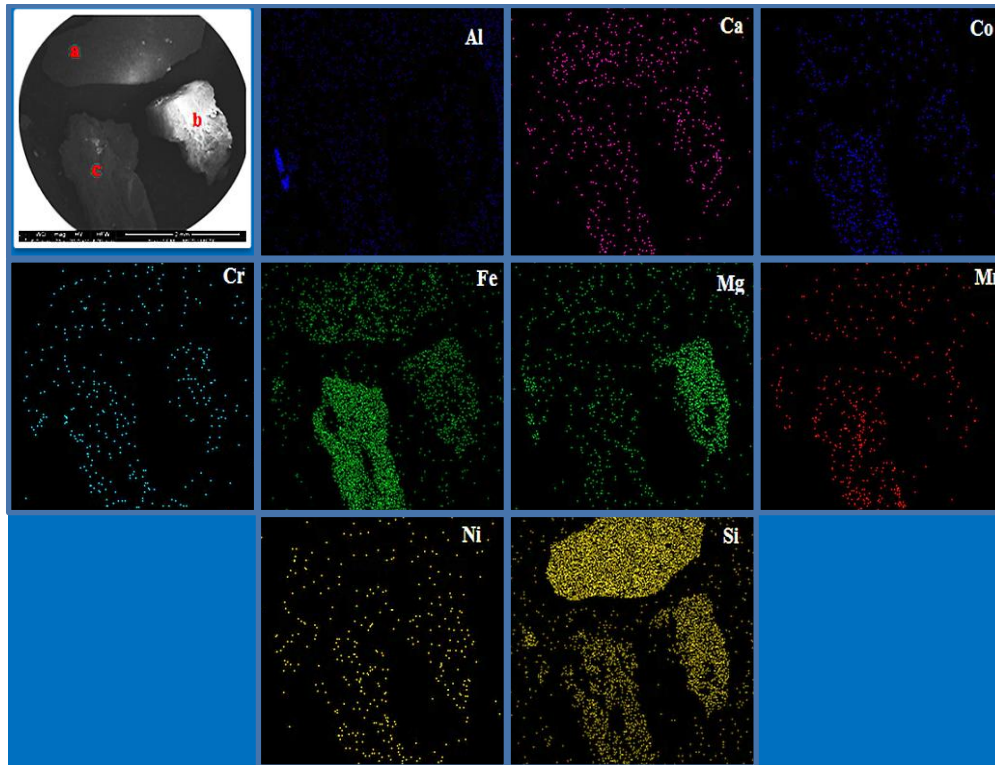


Figure 36 Mapping results of Group 1 for detected elements.

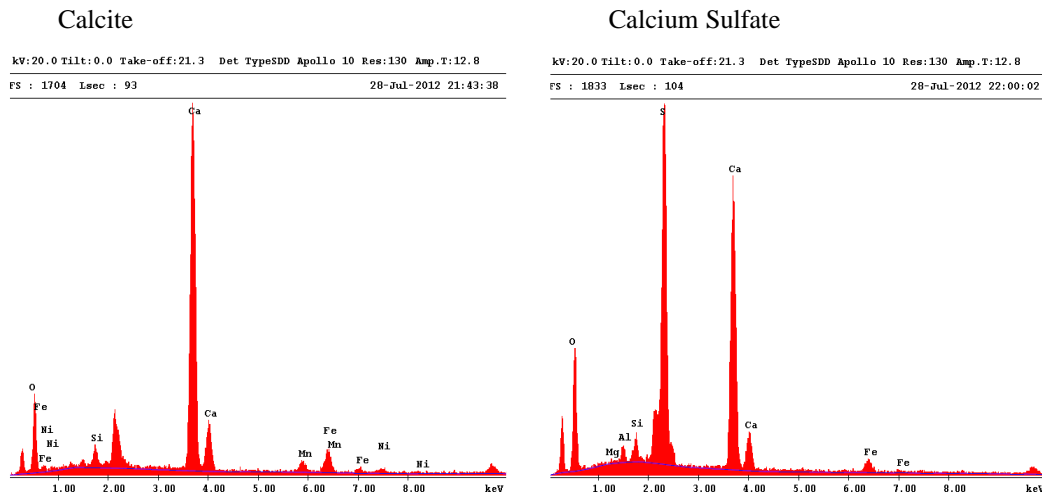


Figure 37 EDX results of particle i (Calcium Sulfate) and particle j (Calcite).

As can be seen from the elemental mapping of particle a, the particle region was dominated by silicon with a high concentration. As expected, the EDX result in Figure 79 confirmed that this particle was a pure quartz particle with some iron and calcium inclusions. In addition to such solid, coarse quartz particles as silicon mineral, there were other phases that were found to host silicon within their structures. Quartz existence can drop the grade of the feed ore. As a result of that the discarding of

coarser particles is carried out for mainly lessening the quartz content of ore feed in some operations of HPAL plants.

When the elemental mapping of particle b is observed, it can be seen that the region for that particle was dominated with magnesium and silicon with less intensity of iron. This particle is definitely a member of easily leachable mineral group called serpentines. Serpentines are generalized with the formula of $(Mg, Fe)_3(Al, Si)_2O_5(OH)_4$ and generally occur as lizardite and antigorite with less commonly as chrysotile. Various amounts of Fe^{+2} and Al^{+3} substitutions for Mg^{+2} are common while Ni, Mn and Zn substitutions for magnesium are less common. On the other hand, Si replacement with trivalent aluminum and less commonly trivalent iron can occur in some species. These substitutions are due to close ionic radii of the so-called elements. In addition to these replacements trace or minor amounts of calcium might be seen in some serpentine samples. As a general rule for sub-members, lizardite is more substituted in Fe and Al than chrysotile but when compared with antigorite, it contains less aluminum [105]. This was observed in SEM examinations of serpentine particles in Çaldağ sample. Serpentine particles were found with a composition that Al was in trace amounts while Fe content was up to 10% in EDX results of particles in this sample holder. The case for serpentines in later sample holder was different and will be discussed in the next section. Moreover; matching of XRD peaks of lizardite in run-of-mine sample were better than antigorite. As a result, it is believed that rather than antigorite the so-called serpentine mineral was possibly lizardite.

Existence of iron oxides in laterites (especially in limonitic ones) is a very common case. Among these oxides, goethite together with some hematite is the most common for iron oxides that can be seen in natural lateritic nickel ores followed by less common maghemite and magnetite. Due to their nanometric crystal size, large specific surface area and high surface reactivity, these iron oxides are amenable to substitution of several metals as they are acting as a sink for these trace metals. Substitution of iron with aluminum is very common as mentioned previously. Additionally, other metals including Cr, Mn, Ni, Co, Cu, Zn, V, Sc, Ti etc. were also found to obey this substitution-mechanism in synthetic goethite and hematite formed in several studies [62,106]. According to Xie and Dunlop (1998), incorporation of trace metals can be either by isomorphic substitution of iron in lattice structure or sorption of these metals by the structure during crystal growth by means of diffusion [107]. In both case, the substitution of elements has great effect on leaching behavior of goethite and hematite.

Within this study, either being goethite or hematite, iron oxide particles were found with some chromium or manganese separately or both apart from nickel as can be seen in Figures 81-82-83. Since goethite and hematite are compounds of iron and oxygen (also hydrogen for goethite) in varying contents their separation by means of EDX analysis might not be safe especially when there is the contribution of other particles or substituting metals such as chromium. Theoretically, hematite is composed of 70% iron and 30% oxygen while goethite has a composition of 63% iron, 36% oxygen and 1% hydrogen (cannot be detected by EDX). Hence, within the SEM examinations, usage of the term iron oxide will be more proper unless it is clear that the so-called particle is goethite or hematite.

As mentioned, the existences of substitution elements are of concern when acid attack is considered. During leaching of goethite, the dissolution of structure is greatly dependent on these metal substitutions. Aluminum and chromium are stabilizing elements for goethite and hematite against proton attack which is the basic kinetic of leaching. Liu et al. (2009) describes this behavior by comparing the bond strengths between Fe-O (390.4 kJ/mole), Al-O (512.1 kJ/mole) and Cr-O (429.3 kJ/mole) [108]. Both aluminum and chromium have higher bond strengths than iron which is the main reason why aluminum or chromium substituted goethite is more difficult to dissolve. This can be a problematic behavior especially when nickel contributions in such particles are high which might cause low nickel extraction during pressure acid leaching. On the other hand, divalent metal ion substitutions such as nickel and cobalt result in more readily dissolved goethite samples [95]. McDonald and Whittington (2008) stated that nickel presence in goethite structure is not only by substitution but also in two additional modes. The first mode is association of nickel with amorphous or poorly crystalline goethite and the second one is adsorption of nickel on highly crystalline goethite surface with weak bonds [1]. Manganese on the other hand has a positive effect on dissolution behavior of goethite. Alvarez et al. (2008) described the reactivity of cobalt and manganese substituted goethites with respect to pure goethites. According to his study dissolution rate of cobalt goethite is increased with increasing cobalt substitution for iron. The reason for this behavior was

stated as an interdependent effect of increased surface area due to reduced crystal size that was caused by increased cobalt substitution. All these together created a perfect media for acid to more rapidly break Co-O bonds than Fe-O bonds. Additionally, he regulated the reactivity of goethites in acidic media as Co-goethite>Mn-goethite>Goethite. Although it is not mentioned in this study, it is believed that a similar mechanism results in the positive effect on dissolution behavior of goethite when it is manganese or nickel substituted [109].

In order to keep the SEM examination results short it will be more proper to move on the examinations of second group of the same quarter. The same procedure mentioned above repeated for Group 2 particles. The general EDX result is given in Figure 38 and the corresponding mapping result is given in Figure 39.

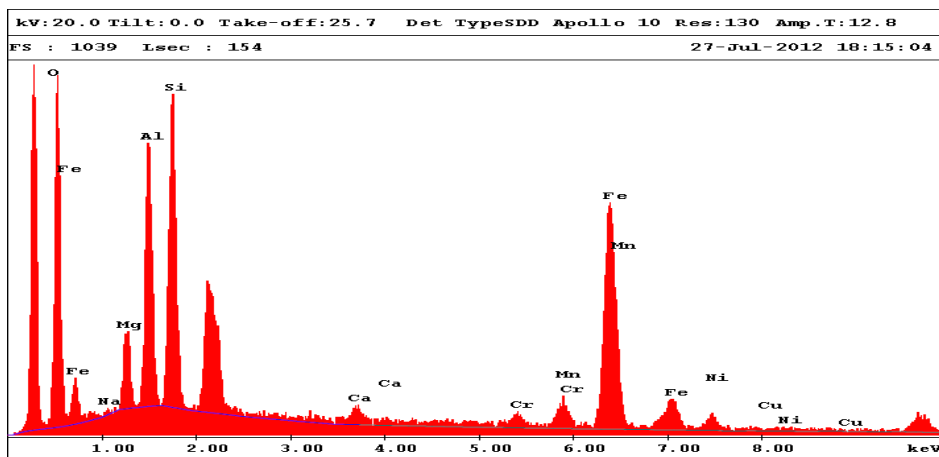


Figure 38 EDX result of general view of Group 2 for mapping of existing elements.

Before sharing the results it is important to describe the smectite family as brief as possible. Smectites are a wide class of clay minerals that have relatively more complex structure with respect to kaolinites or serpentines. They are the most diverse clay group that extends from Al-rich (montmorillonite or beidellite-like) to Mg-rich (saponite-like) to Fe-rich (nontronite-like) forms and each sub-group contains its own sub-members. Sub-groups of smectites that are generally encountered are as follows [110][111]:

- Saponite with ideal formula of (X) $[\text{Mg}_3(\text{Si}_{2.7}\text{Al}_{0.3})\text{O}_{10}(\text{OH})_2]$
- Montmorillonite with ideal formula of (X) $[(\text{Al}_{1.7}\text{Mg}_{0.3})\text{Si}_4\text{O}_{10}(\text{OH})_2]$
- Beidellite with ideal formula (X) $_{0.5}\text{Al}_2(\text{Si}_{3.5}\text{Al}_{0.5})\text{O}_{10}(\text{OH})_2 \cdot n(\text{H}_2\text{O})$
- Nontronite with ideal formula of (X) $[\text{Fe}_{2.0}(\text{Si}_{3.7}\text{Al}_{0.3})\text{O}_{10}(\text{OH})_2]$

Here (X) represents the exchangeable cation most commonly alkali earth or alkaline elements. Each sub-group member was subjected to XRD examination for run-of-mine ore sample. Among them, saponite was irrelevant to XRD data while montmorillonite was found to miss some characteristic peaks. Beidellite and nontronite was found to be more proper. However, smectites in lateritic nickel ore deposits rarely have ideal end-member compositions during laterization which allows a perfect media for severe elemental substitutions within smectite structure. Generally nontronite-like smectites contain more iron with very low aluminum and magnesium content. Beidellite-like smectites are generally aluminum dominated while montmorillonite-like smectites are also generally known by their aluminum compositions with significant magnesium content. Saponite on the other hand is magnesium dominated. Overall, at least some ferrous/ferric iron occurs in various smectites including most montmorillonites and nontronites as its dominant central atom in octahedral sheets is generally trivalent iron [112].

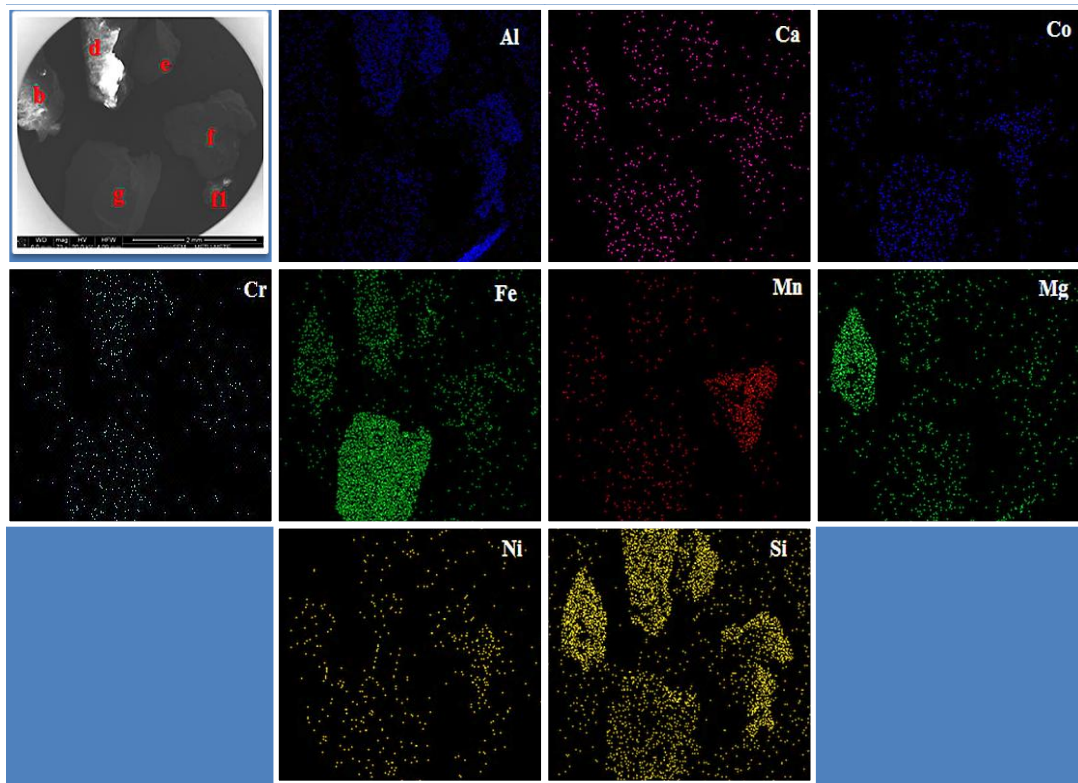


Figure 39 Mapping results of Group 2 for detected elements.

Another problem causing smectites to diverse from their ideal structure is that they can also form inter-mixed layers with other clay minerals most commonly with chlorites. Despite all these problems, it is a known characteristic of all smectites that they are in abundance of exchangeable cation elements such as calcium, potassium and sodium as interlayer cation. As long as there is no intergrown calcium or less likely sodium or potassium phases within smectites, this information is helpful for their distinction. Under the light of XRD examination and thermal analysis results, it is believed that one or two sub-groups of smectites exist within the ore feed. As a consequence of problems discussed above, smectite-like particles are termed as nontronite-like smectite or beidellite-like smectite depending on their iron and aluminum content since magnesium content was always negligibly low which vanish the saponite existence. Despite the mentioned chlorite existence was searched in XRD examinations after their possible correlations with smectites, none of them (nimite, clinochlore, etc.) were found to match for run-of-mine ore. Yet minor or trace amounts of chlorite group members might occur below detection limit of XRD or they might be masked by smectite layers from XRD reflections.

When EDX mapping of particle e is observed it can be seen that it is highly dominated by aluminum and silicon with lesser regional intensifications of magnesium, chromium and iron on the particle. As discussed above magnesium contribution in smectites are in minor amounts when it is an Al-rich smectite. Chromium existence brought the idea of intergrown chromite particles associated with smectite particles. On the other hand, McDonald and Coelho et al. reported that chromite can be hosted within smectite and goethite as substituting element in lateritic nickel ores in addition to its own spinel [95] [113]. However, a deep insight on the particle showed an interesting situation.

An EDX taken from the upper section of the particle can be seen in Figure 84. It can be seen that chromium is relatively high and in a correlation with iron by a ratio of Cr: Fe as 7.2:1 (wt %/wt %) which is well above the theoretical ratio of 1.85:1 within ideal chromite. Another EDX taken from lower section of the particle gave a reversed situation where iron is now dominating over chromium as can be seen in the figure. This situation casts doubt on existence of chromite and probably resulted

from interchanged position of one by another during weathering of laterite. When the neighboring particle d is subjected to EDX analysis it was found that a similar situation existed with particle e which can be seen in Figure 85. However, in this particle aluminum content was lessened with increased iron amount with substitution and got closer to nontronite-like smectite. This increment of iron might have also caused the charging of particle under electron beams but the reason for that could not be understood.

Detection of cobalt was quite hard as its content in ore sample was only 0.078% and the characteristic peaks of cobalt generally were suppressed when iron content was dominating. However, as an exception, a relation between cobalt and manganese could be seen in both mapping figures. Actually, these particles where manganese was found to be concentrated were the only particles that cobalt peaks from EDX results were detected with no doubt. These particles were believed to be a form of manganese oxide. On the basis of XRD results and previously mentioned study by Çağatay et al., these particles were representing asbolane mineral. However, as can be seen in Figure 86, the particle f was found to be composed of two types of minerals. EDX result of particle f can be seen meaningless at first sight. However, when the EDX result of particle f1 that was disintegrated from the main particle f was considered, it can be seen that Al-Si-Fe contribution was due to smectite. Here again the particle f1 showed that a competing replacement between aluminum and iron existed. As a general rule, the lower the iron content within smectite the higher the aluminum content within them and the more it is beidellite-like since magnesium content is generally below 1 wt%.

3.3.3.2. SEM Examinations on Particles of Second Sample Holder

Similar procedures for SEM-EDX examinations of the previous holder were conducted in order to extend and confirm the research by XRD examination. However, the particles were not as homogenous as those in previous one. Deep insight enabled detection of some individual compositional variations within minerals that were found in previous ore sample. In this step, it would be more helpful to divide the quarters by the dominating minerals or elements. As can be seen in Figure 40, the left half of the sample holder was completely invaded by serpentine particles with varying color from slightly white-yellow to slightly green-yellow. The other quarter was dominated by iron-rich oxides/hydroxides whereas the right hand side quarter was expectedly occupied by asbolane and manganese rich iron oxide/hydroxides. Since the particle selections were completely random somehow enrichment of some phases occurred in this sample holder. However, this does not necessarily mean that serpentines are more in amount than XRD represented. As stated previously, rather than any quantification or proving absence of minerals, the aim was to confirm the existing minerals offered by XRD. EDX results of particles were grouped in another appendix, Appendix D.



Figure 40 Image of second sample holder with particles prior to gold coating.

To begin with, the dominant phase in half of the sample holder was found as serpentine. Here again, serpentine mineral was the most consistent one that had almost steady composition. The only exception was the increased but now slightly varying iron content in a range from 10% to 17%. As in the case for previous particles, calcium was found to associate with them at about 1%. Since the particles were so steady in composition it would be adequate to display the mapping result of lower most quarter of the sample holder including particles m and n as in Figure 41. As can be seen these particles are literally shining for Mg, Si and Fe. Additionally, calcium and nickel mapping gave meaningful results while aluminum was once again in minor amounts. This is actually consistent with the serpentine formula that was previously detailed.

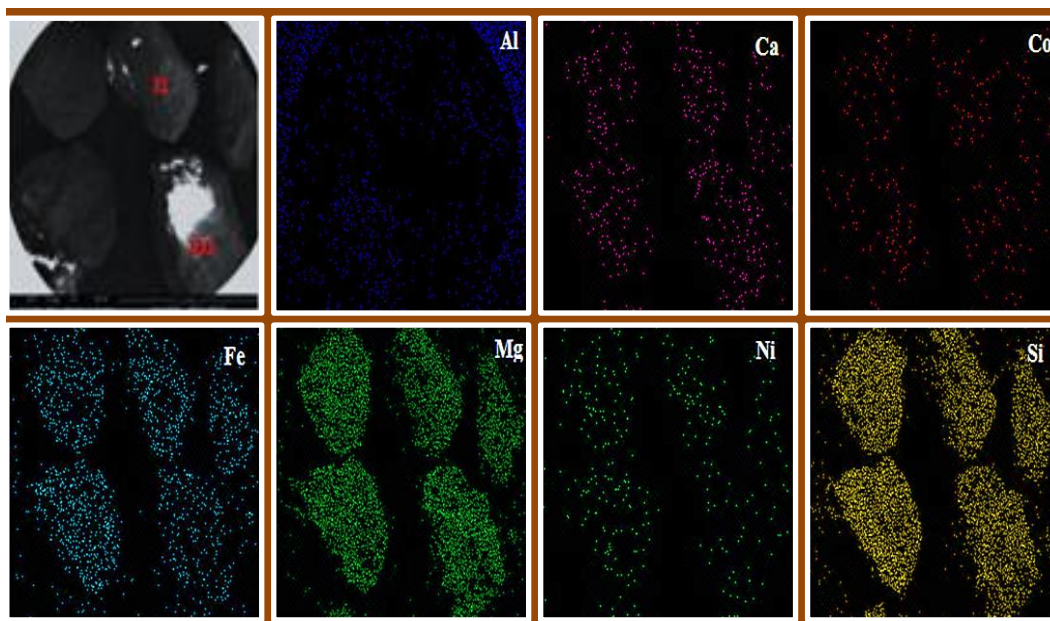


Figure 41 SEM image and elemental mapping of lowermost quarter having full of serpentine particles.

In Figure 87 where the EDX result for particle m is given, the iron contribution was 10% with less than 1% of nickel contribution. On the other hand, in the same figure the result for particle n showed that the increased amount of iron somewhat enhanced the nickel sorption into serpentine lattice structure both at the expense of magnesium content. This might be caused by more distorted structure by more iron substitution and smoothing nickel sorption. In this examination, there was a parallel correlation between iron and nickel contributions in serpentines such that the higher the iron content the higher the nickel within the particle. However, a generalization for that the rule over the complete ore feed requires further mineralogical analysis since within these SEM examinations randomly selected particles were used. But it is quite clear that serpentines are the most reluctant phase to host other mineral phases to intergrowth with and also to host other impurity metals apart from iron. As another important point to mention for serpentines was the magnetic behavior of serpentines with respect to their iron contribution.

When literature was further searched for specific iron contribution in serpentines, it was found that when the product of serpentinization is a high-iron (approximately 6% to 17% Fe end-member), yellow-colored lizardite, very small or no magnetite is produced as by-product. Moreover, once lizardite is produced the contained iron is generally in its trivalent form rather than its divalent form [114]. This could be the explanation of magnetite absence within the ore sample and is actually important as ferrous iron content was previously mentioned to be as low as possible. In the case of

particle p, it had the lowest iron amount (10%) just like nickel content within all serpentine particles of this group.

The second quarter to mention was manganese rich quarter that was quite important for nickel and cobalt extraction efficiencies. Actually this was expected since it is known that manganese rich phases are generally in dark colors. Among them, asbolane was already mentioned to exist in first holder but intercalated with less iron containing phases. Here again it was found with smectite but with more nontronite like form. Additionally it was found with intercalation of serpentine. It is believed that these phases were intergrown during laterization since the mapping results of particles such as s and t in Figure 42 seemed to have homogenous distribution of respective elements.

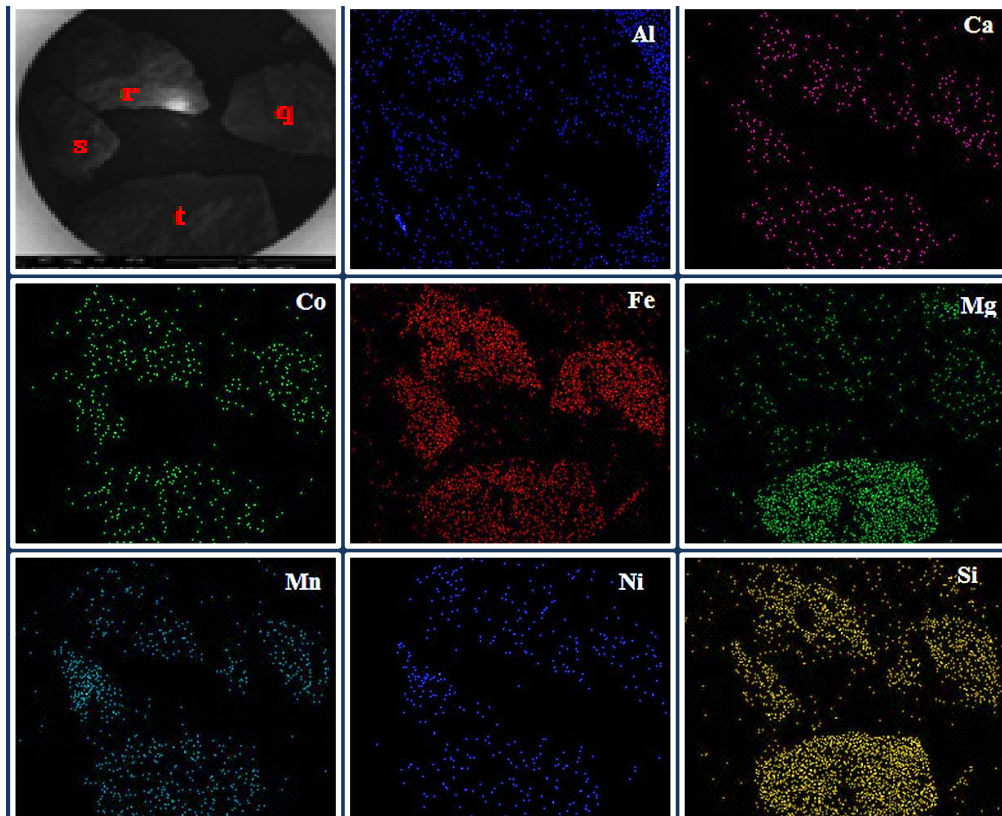


Figure 42 SEM image and elemental mapping of manganese-rich quarter without particles u and v.

In EDX result of particle s, Figure 89, one can see a similar situation that was for particle f but here this particle was coherent and not separated. The calcium contribution might exist due to smectite or asbolane or both. The nickel content was 20% while cobalt was 10%. A similar intergrowth asbolane case was seen in the same figure for particle t. At first sight, it might seem that there existed a serpentine phase intercalated with a manganese rich iron oxide. However, iron contribution was only 12% whereas manganese was 14%. Hence it is more likely to be an intercalated asbolane and serpentine particle. A similar situation was encountered in other quarters of sample holder that will be discussed as follows.

In this quarter apart from intercalation between asbolane and other two phases, a different combination was found that was not encountered so far. This is a confirmation of other undetected but of course can be existing combinations in the ore feed. As can be seen in Figure 88 where the results of particle q and r were given, the first impression was some kind of iron silicate phase such as fayalite (Fe_2SiO_4) exists. Fayalite and other possible minerals were searched for XRD examination but

did not match at all. Since aluminum, magnesium contributions were as low as 2% with calcium (also potassium) content of less than 1% while silicon content was 14%, it is believed that the whole iron content was separated for a nontronitic smectite phase leaving the higher rest part for chromium containing iron oxide/hydroxide phase. This was because of the high iron content that was impossible for even ideal nontronites to handle. As a result these particles are stated to represent a more iron containing nontronitic smectite (due very low aluminum and magnesium content) and one of the iron oxide/hydroxide with low chromium contribution which is consistent with the data from characteristic peaks of phases. A similar case mentioned right above for Figure 89 (particles s and t) is seen for particle u with the exception that one side of intercalation is now asbolane instead of iron oxide. If the EDX results for asbolane are focused closely, manganese peaks follow the order that the first peak at 6 keV (Mn K α) is always higher than the second one at 6.5 keV. However, this situation is reversed now. This is the sign for contribution of iron from nontronitic phase. Additionally, nickel and also cobalt contents are extremely high for a nontronitic smectite encountered so far (both above 5%). This described case is exactly the same for the neighboring particle v whose EDX result was not put here for clarity.

The last quarter studied during these examinations was the uppermost quarter titled as iron-rich quarter. The overall color of particle was very close to brown which is typical for iron minerals such as hematite and goethite. Actually the only phase was iron oxides/hydroxides with some quartz inclusions. Hence, it was thought to be unnecessary to display the elemental mapping of whole quarter group by group as done for other quarters.

As can be seen in Figure 90, there are three quartz-contaminated iron oxide/hydroxide mineral particles. Both particles are containing considerable nickel content (>2%) without any other metal impurities such as chromium and manganese that were seen previously. Considering their iron percentages the first particle (y) is less quartz contaminated but already with 63% iron content. Without silicon contribution it is quite close to hematite composition so that this particle is more probable to be hematite. Similarly particle z and w are both with quartz load in higher amount than particle y. However, these particles are representing goethite family. This is because even when regarding the absence of silicon and addition of whole silicon content (approximately 11-12%) to only iron (54-55%) content, the result is still a lower iron composition than a usual hematite composition. These particles are helpful in understanding of hematites that they are also contributing into nickel grade of ore feed. However, the extent of such hematite particles requires more examinations to be generalized over the ore sample. Another important implication from these particles is the fact that there are goethite particles that are only nickel carriers and are free of other impurity elements. Unfortunately, the quantification of these goethite particles is also requiring further examinations. Nonetheless it is valuable to observe their existences since nickel substituted, chromium and/or aluminum free goethites are amenable to dissolve in acid leaching even in a few minutes.

3.3.4. Conclusions of the Characterization of Run-of-Mine Samples

- XRD examination of original run-of-mine ore revealed that major phases were goethite, quartz and hematite and minor phases were serpentine, smectite, asbolane, calcite, dolomite and other two forms of quartz.
- The existence of chromite and magnetite could not be proven by XRD examination since its characteristic peaks were suppressed by other iron minerals. Further examinations were only helpful to cast doubt on chromite existence and to remove magnetite existence by lizardite formation. It was indicated that chromium was rather associated with iron oxides and ferruginous smectites.
- Thermal analysis was helpful to a limited extent giving a clear evidence of goethite and serpentine existences with a blurred designation of smectite occurrence and kaolinite absence within the ore feed.
- It was found that smectites in second holder were more nontronite-like by means of higher iron but lower aluminum content. Serpentine was found to occupy half of this sample holder with a consistent composition including >10% iron content. Asbolane was once again associated with smectitic phase and here also with serpentine.
- SEM-EDX examinations have shown that nickel was entrapped within the minerals asbolane, iron oxide/hydroxides, smectites and serpentine. When individual contribution is considered

asbolane was found to bear the highest nickel (also cobalt) amount of ore followed by iron oxide/hydroxides. It was indicated that some of the hematite particles are also nickel contributor but generalization in terms of its relative amount in ore feed was not possible.

- Nickel sorption in smectites and serpentines were related to iron content within them. Beidellite-like smectites and less than 10% iron containing serpentine particles were containing trace amounts of nickel whereas nontronite-like smectites and more than 10% iron containing serpentines were richer in nickel content.

3.4. Experimental Procedures

3.4.1. Procedure for High Pressure Acid Leaching (HPAL) Experiments

In this thesis study, Çaldağ lateritic nickel-cobalt ore was first acid leached under high pressure and high temperature conditions in order to dissolve nickel- and cobalt-bearing minerals that were determined by the mineralogical characterization of ore sample. The experiments were carried out in METU Hydrometallurgy Laboratory with a Parr-4532 model, grade-4 titanium autoclave with a capacity of 2 liters. While the reaction vessel was heated or cooled to stabilize the experiment temperature via an automated control system, a magnetically driven stirrer was set to 400 rpm for all of the HPAL experiments since it was previously reported that the agitation speed has negligible effect on the valuable metal extractions and 400 rpm was proven to provide enough mixing that maximizes the acid-ore contact and hinders agglomeration of colloidal batch composition at the bottom of the reaction vessel. The autoclave with its crucial parts that was used throughout this experimental part can be seen in Figure 43.

However, the utilized autoclave lacked the ability of acid injection system that enables the acid addition right before or just at the aimed process temperature which can range between 240 to 270°C. Such a system is what is generally observed in literature and also in industrial applications. However, the operation of such an autoclave equipped with acid injection system requires not only a considerable expense of investment and of maintenance but also great care for prevention of possible life-threatening situations in case of failure. Any failure of injection system due to lack of maintenance during operation under acidic media with extreme pressures could greatly endanger the researcher's life. Therefore, the absence of acid injection system at temperature did definitely effect the reaction duration that will be mentioned in following paragraphs.

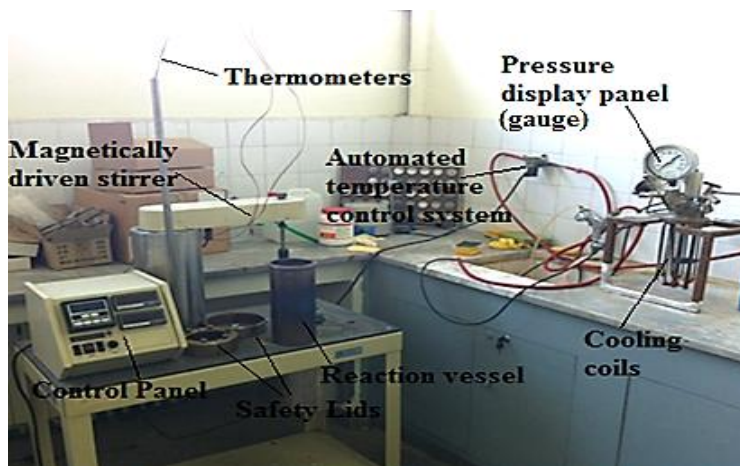


Figure 43 Titanium autoclave used in HPAL experiments.

The original input of each experiment was Çaldağ ore sample and deionized water (which are together termed as slurry hereafter) along with concentrated sulfuric acid (Merck grade 0713). If the response of ore sample to acid leaching is observed to be problematic in terms of extraction efficiencies, there might be additional inputs including some possible reagents or additives such as metal salts or elemental sulfur to improve the leachability of ore by means of changing the oxidation or reduction potential of the leach solution. A typical input composition in accordance with pre-determined solid concentration for this study can be seen in Table 18. Throughout the HPAL experiments, the solid concentration of each batch was kept as 0.30 or 30% as given in the table while the acid contribution to liquid volume was excluded.

As a result of the absence of acid injection system described earlier, the procedure was slightly adjusted to capability of the autoclave. Rather than injecting the pre-determined amount of acid to the slurry “at the experimentally planned temperature”, it was decided to add the acid to the slurry “at the outset” of experiment (i.e. at room temperature). Once the slurry according to the batch composition given in Table 18 was prepared and mixed with the given acid amount within the reaction vessel, the lid of the autoclave was closed and carefully tightened in order to prevent any gas leakage during the operation which may affect the experimental data. After setting experimental conditions (i.e. temperature, stirring speed), the autoclave heating was started.

Table 18 A typical composition of input for HPAL experiments.

Input Materials	Weight (g)
Ore sample (dry basis)	150
Deionized Water	350
Sulfuric Acid	48.75*
*according to Sherritt calculation	

All of the experiments were always assumed to start off right after the temperature of vessel reached the aimed temperature. Eventually, during the time period between acid addition at room temperature and the time when autoclave achieved the aimed temperature, there had been leaching reactions to some degree between the added acid and the ore minerals. This time period had to be taken into consideration especially when the leaching duration parameter was studied. As a result of this necessity, the heating curve of autoclave up to the highest temperature that was studied in the experiments was determined and is drawn in Figure 44. As can be seen from the heating curve, heating of loaded autoclave took approximately 45 minutes to achieve 250°C. Moreover, to understand the extraction behavior of ore sample until the reaction vessel reached the optimum temperature one experiment was done for that purpose after the optimum conditions were determined. The results will be discussed in Chapter 4. The “zero point” for all experiments was noted as the time when the autoclave achieved the experimental temperature and only after then the experiment was assumed to start.

After the pre-determined leaching duration of experiment was reached, the autoclave temperature controller was re-set to room temperature and the system was let to cool down approximately for one hour by tap water circuiting within the cooling coil of vessel. The autoclave was then disassembled from its lid and the reddish sludge in the vessel was subjected to filtration where solid and liquid parts were separated. Filtering flask sealed with a Buchner funnel on top was used for filtration purposes. Whatman grade-40 filter paper was placed in the funnel. In order to accelerate the solid liquid separation, a vacuum pump was used which was connected to the filtering flask. While the sludge was being poured onto the filter paper, a greenish pregnant leach solution (PLS) was collected within the flask leaving the accumulating reddish leach residue on top of the filter paper. After the separation step, the flask containing the metal loaded pregnant leach solution (PLS) was disconnected from vacuum pump for various measurements such as density, oxidation-reduction potential (ORP), etc.

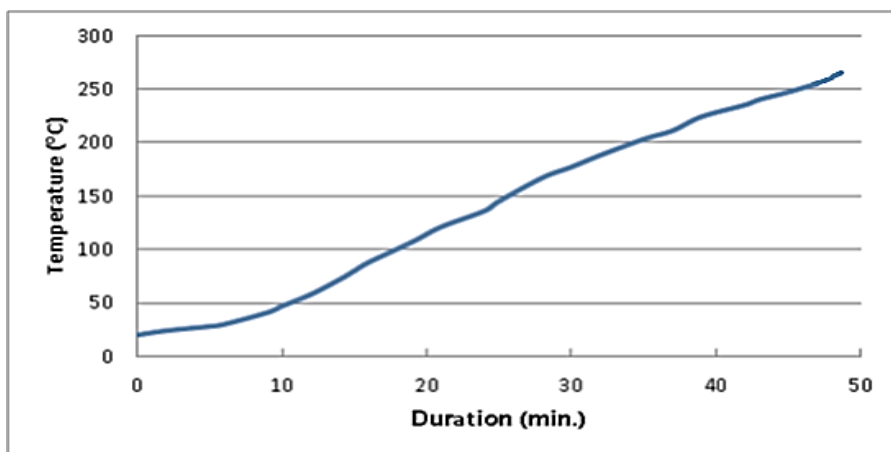


Figure 44 Heating curve of loaded autoclave to the highest temperature (260°C) studied.

Filtration system was re-set with another filtering flask for washing each leach residue out of any remnant PLS portion that might have been remained within the residue particles. Such an entrapment within the leach residue particles may cause errors in the chemical analyzes of solid products which in turn results in errors in solid based extraction calculations of metals. Another important point to mention at that step is the need for low-pH wash water. As it was discussed more specifically in the literature part that the iron precipitation commences at around pH=2 depending on the molarity. For deionized water with a pH of higher than 6 to be used as wash water will definitely mean an increase in basicity of remnant PLS. Such an increase is crucial especially for iron that will enhance the conditions for its precipitation from the remnant solution and once again will lead to mistakes in the extraction calculations for iron. On the other hand, an extreme acidity of wash water might lead to re-dissolution reactions of precipitates in solid residue giving wrong extraction percentages. Consequently, the used deionized water that was intentionally acidified by sulfuric acid addition to pH=2 was used for washing of leach residues. The resultant PLS-free leach residue was kept at 105°C in a drying oven overnight in order to remove its moisture content.

Chemical analysis of each product of all experiments was done for the determination of extraction efficiencies. Leach residues were analyzed by META Nickel and Cobalt Company with both XRF (Niton X-Met 820) and AAS methods. Pregnant leach solutions were analyzed by AAS method in the Chemical Engineering Department of METU. Both products of experiment that was chosen as the optimum test were additionally sent to MERLAB for ICP analysis. ORP of pregnant leach solution was determined by Pt-Ag/AgCl electrode that was saturated with 3 M KCl solution (free of Ag⁺ ion). One can find the equivalence of measurements in the Standard Hydrogen Electrode potential by adding 198 mV to the measured values. ORP value taken from solution in continuous systems can be used as an identification of the progress of the on-going leaching process after its measurement at the critical stages such of pilot testing or actual plant operation. The last measurement in each experiment was the free acid determination of PLS. For this purpose, 0.2 M sodium hydroxide (NaOH) solution was prepared in order to neutralize the free acid. However, while neutralization is performed some metallic ions (for example divalent/trivalent iron) in solution can interfere with titration of acid. To overcome this problematic behavior of such ions in solution, diluted di-potassium oxalate monohydrate (K₂C₂O₄.H₂O) was used as chelating agent. The procedure started with preparation of a so-called reference solution by adding 28 gr of K₂C₂O₄.H₂O (Merck grade 5072) into 100 cc deionized water. While this solution was magnetically stirred, the calibration of pH-electrode with respect to a buffer solution of pH=7 was performed at room temperature. In a beaker, 20 cc of reference solution and 5 cc of deionized water were placed and mixed by magnetic stirrer during the measurement. The calibrated electrode was placed in this solution and the pH value was noted as target pH which had to be re-achieved after the expected drop in pH of the solution due to the addition of 5 cc acidic PLS. Once the total of 30 cc solution was homogenized, the titration process was initiated by previously prepared NaOH solution. The amount of NaOH solution that was consumed by

the solution to re-achieve the target pH value was noted and from this value the amount of free acid in PLS was calculated.

3.4.2. Procedure for Downstream Experiments

During high pressure acid leaching of laterite ore, the major portion of nickel and cobalt content of the ore can be extracted by complete disintegration of lattices of the host minerals and release of these elements or by surficial sweeping of these atoms that are physically absorbed by these minerals after acid attack. Unfortunately, during this acid attack, not only nickel and cobalt but also several impurity atoms are also extracted. Despite some or most portion of these impurities (also valid for nickel and cobalt) precipitate according to the thermodynamics of precipitation reactions or cannot even be extracted due to refractoriness of some minerals (i.e. chromite, talc, etc.) there will always be a considerable amount of impurities within the resultant pregnant leach solution that prevents this product to be saleable. For example in this study, while only 1-2% of chromium was extracted at all of the experimental trials, up to 90% of magnesium was observed to pass into the pregnant leach solution. This problem will remain no matter which operational conditions are chosen as long as hydrometallurgical routes are chosen since the selective leaching of nickel and cobalt is not possible due to the absence of any nickel or cobalt minerals.

As a consequence of this unavoidable problem, the researchers have developed several methods to purify this metal loaded solution and the most important and industrially applicable ones were already given in detail in the literature part. In this study mixed hydroxide precipitation (MHP) route was chosen to be used after the removal of most of these impurity metals enabling production of a saleable intermediate product. As described earlier this route contains 4 main steps unless manganese and magnesium removal steps are required.

The first two steps are for removal of the most crucial impurities. The main target is separation of all of iron and most of aluminum and chromium as their respective hydroxides with very small amount (less than 10%) of nickel and cobalt losses within the solid part. To achieve that, pH of the leach solution is increased with the aid of several possible types of reagent addition. Simultaneously, these removal stages also achieve the complete neutralization of typically 30-50 g/L free acid within the pregnant solution which in turn causes the pH level of leach solution initially to be less than 1. The reason for iron, aluminum and chromium ions to be removed first among the others can be explained by Monhemius diagram. From highly acidic to basic order, possible ionic impurities are listed with respect to the pH values at which their respective hydroxides start to precipitate under ambient conditions. As can be seen Fe, Al and Cr ions are the first three to be removed by pH increment from 1. A critical presence of divalent iron within the pregnant leach solution must be considered during these stages since the existence of such ions in solution prior to mixed hydroxide precipitation stage can cause contamination of product by iron. To avoid these problems, if necessary, the treatment of leach solution prior to iron removal stages by SO_2/O_2 mixture must be applied in order to oxidize divalent iron ions to trivalent iron.

In the next two steps, the main target is the precipitation of as high amount of nickel and cobalt as possible from the solution as a mixed hydroxide product with as low amount of contamination by manganese (<5% of solid product) as possible. Unfortunately, contamination of this product by copper and zinc is almost unavoidable since the pH ranges for the precipitation of these elements are very close to those for nickel and cobalt. However, these impurities within the leach solution are generally present in minor amounts so they can be tolerated. Similar to the previous two stages, the pH increment is implemented by reagent additions. Once the MHP is separated, the treatment of barren solution for manganese and magnesium removal stages are possible with further increase in pH of solution by reagent additions. The preferences of these stages depend on the balances of operational profit/loss analysis and water supply of project.

3.4.2.1. First Iron Removal and Neutralization Step (FER 1)

In literature review for solution purification of nickel laterite liquors some studies were mentioned for the selective precipitation of nickel cobalt hydroxides. General trend in these studies was utilization of synthetic solutions obtained by mixing metallic salts of commonly found metals in real pregnant leach

solutions. Unlike these cases, a real pregnant leach solution stock was produced in this study under the optimum conditions of high pressure leaching process and used in the downstream experiments. As it will be discussed in detail in the results and discussion chapter, the optimum conditions of HPAL were found to be 250°C, 0.325 (kg/kg) acid to ore ratio at -1mm particle size and 1 hour leaching duration. Under these conditions a total of 4.6 liters of pregnant leach solution was prepared for the completion of all downstream experiments. After each experiment carried out for the stock preparation, the same route described in Section 3.4.1 was followed and the solid leach residue of each experiment was also stocked after washing and drying treatments. Some of the properties of PLS stock prepared under the optimum conditions of HPAL for downstream experiments are given in Table 19.

Table 19 Some properties and respective measurements of pregnant leach solution stock.

Property of PLS Stock	Measurement
Volume (L)	4.6
Density (g/L)	1.10
ORP (mV)	443
Free Sulfuric Acid (g/L)	46.2

In industrial application of MHP process, it can be seen that the output from autoclave contains both solid and liquid parts and this output is directed to the first iron removal and neutralization section. Only after the first iron removal with neutralization step, the separation of PLS from solid leach residue and iron-dominated precipitates are performed within 6 or 7 counter-current-decantation (CCD) tanks in series. The reason for this is to decrease the processing cost and corrosion of the thickeners. Then, the solid precipitate and leach residues are disposed to the tailings dam. Subsequently, the pregnant leach solution from this section is forwarded to the second iron removal section.

However, the presence and importance of scandium in PLS has recently shifted this trend to a partially new route. Nowadays, it is known that scandium is also leached during high pressure acid leaching of nickel laterites (if exists in ROM) and ends up in PLS in varying amounts. Scandium co-precipitates with iron during first iron removal and neutralization stage. If it is precipitated with iron then it will be lost to tailings. As a solution, after HPAL, the solid-liquid separation by means of CCD units can be applied in order to avoid the complete loss of scandium to the tailings. After the separation of the leach residue by means of CCD system, scandium can be recovered from the PLS by solvent extraction and then the first iron removal by precipitation can be applied to the scandium free PLS.

By taking this point into considerations, the experimental procedure chosen was as follows: 100 cc of PLS taken from the stock was replaced into a 250 or 500 cc Pyrex balloon having 4 necks with a magnet in it. As can be seen in Figure 45, the balloon was placed on a hot plate with a magnetic stirrer. Also, reagent slurry for the first iron precipitation and neutralization was freshly prepared before each experiment. The prepared slurry was continuously stirred during each experiment with a magnet on a magnetic stirrer at room temperature. For the first iron removal with neutralization stage, limestone was decided to be used as slurry with a 25% weight/volume concentration. In order to prepare this slurry, 100 cc deionized water was mixed with 25 g CaCO₃ (Merck grade 2066/ ~14 micron).

On one neck of Pyrex balloon, a condenser was placed in order not to lose any input as steam by evaporation during experiment. Another one was sealed with placement of a contact thermometer that controlled heat supply of hot plate with respect to the actual temperature of the PLS during the experiment; hence stabilized the experimental temperature at the aimed value. A pH-meter (NEL 890) was utilized through all downstream experiments and it was equipped with a pH-electrode (WTW Sentix 82) capable of measurements at up to 100 °C. At the beginning of each experiment, pH-meter was calibrated with a buffer solution of pH=4 at room temperature before the electrode was installed through the third neck in order to observe the change in pH level of PLS with CaCO₃ slurry addition.

When the input PLS gained the experimental temperature after heating, the pH-meter was then calibrated for that temperature to read accurate pH values since pH and temperature are known to be correlated.

The last neck of the Pyrex balloon in the center was closed by a stopper and reserved for the addition of slurry at the same pre-determined rate throughout the experiments. The important point about slurry addition into PLS during experiment is that any highly-concentrated CaCO_3 addition can cause a sharp local increase in pH of solution that will cause unnecessary nickel and cobalt precipitation at the contact region. At that point, homogenous mixing of the added reagent must be achieved to prevent any accumulation of calcium carbonate in a localized region. This may result in errors in the experimental calculations due to unnecessary nickel and cobalt precipitations or presence of unreacted reagent amount. For that reason, the slurry was added drop by drop by a micropipette with an adjustable volume between 0 to 1000 μL . Moreover, as a result of troublesome behavior of CaCO_3 slurry (solid limestone particles have a great tendency to quickly separate from water and settle at the lower section of pipette causing concentration differences between the first and last drops) rather than using a normal glass pipette, a micropipette was used which was found to ease the control over the addition process.

Once the CaCO_3 slurry was prepared and the PLS within the 4-necked Pyrex balloon has reached the experimental temperature, the addition of slurry was initiated at a rate of 1000 μL per 5 minutes until the required pH was obtained. Added amount of slurry to the PLS was noted after this operation. Experimental duration was then started at that time and the solution was tried to be stabilized at a certain pH level and temperature throughout the experimental duration. However, it was almost always observed for all the experiments that the pH level of the solution-slurry mixture to be somewhat instable; mostly a tendency towards a decrease in pH value from target pH was observed. When such a decrease was observed slurry addition (in 100 to 500 μL volumes depending on the necessity) was continued to maintain the pH level at the target value during experimental duration.

After the experimental duration was reached the hot plate was turned off and the balloon was disassembled from its components. The total CaCO_3 slurry addition was calculated including the afterward additions to maintain constant pH level. The brownish to yellowish sludge present in 4-necked balloon was then subjected to filtration operation in order to separate the precipitate from partially purified pregnant leach solution that was lower in iron concentration. For this purpose, the same setup described for the filtration of leach residue was used. After filtration, it was noted that the new filtered solution was less greenish than the input PLS and the precipitate was less in amount with respect to leach residue of HPAL.

Each solution obtained after the first iron precipitation was used for the measurements of ORP, volume, etc., and the pH of solution was checked by a pH paper in order to make sure that the experiment was completed in the desired pH range. Then, a new flask was connected to vacuum pump in order to wash out any remnant solution within the precipitate particles. Once again deionized water used for washing was intentionally acidified to pH=2 so as to not to cause any afterward precipitation of iron from the remnant solution. When the filtered washing water became clear, the setup was dismantled and the solid precipitate on the Buhner funnel was dried overnight in an oven at 105°C.

Solid precipitates were analyzed by META Nickel and Cobalt Company with both XRF (Niton X-Met 820) and AAS methods for the mass balance calculations. Pregnant leach solutions that were partially purified of iron were sent to the Chemical Engineering Department of METU for AAS analysis for the same purpose. Also, the precipitate and partially purified solution obtained under the optimum conditions of first iron removal was analyzed by ICP in MERLAB.

The new pregnant leach solution was finally subjected to free acid calculations. Although highly acidic pregnant solution was simultaneously neutralizing during the first iron removal experiment, the complete neutralization of the solution requires higher pH values. Yet, it was observed that the free acid amount of solution was greatly decreased with increasing pH as expected. After all the necessary measurements were completed, the new pregnant leach solution of lower iron concentration was stocked for any future use. For stocking purposes, the solution was acidified by a single drop of concentrated sulfuric acid. That was done because the solution pH was still high enough for iron precipitation to take place while waiting.



Figure 45 Experimental set-up for downstream experiments (CaCO_3 slurry is replaceable for upcoming steps).

In this stage one set of experiments was done at a pH range of 2.50 to 3.25 (with 0.25 increments) at the fixed conditions of 90°C and 2 hours in order to observe the effect of pH on precipitation percentages of metals in solution. A second set of experiments was done for leaching durations of 1 to 3 hours (with 1 hour increments) in order to observe the effect of duration.

3.4.2.2. Second Iron Removal Step (FER 2)

After determining the optimum conditions for the first iron removal with neutralization step, a new stock of pregnant leach solution of this stage was prepared for the upcoming second iron removal step. It is important to mention that for all experiments conducted for stock preparations prior to this step; the volume of input PLS was increased to 350 cc at the same time the constant rate of reagent addition was shifted to $3500\ \mu\text{l}$ per 5 minutes. After the experiments for stock preparation each resultant pregnant leach solution and solid precipitate were sent for chemical analysis. The 3.5-fold increased amount of addition in stock preparation experiments proved itself to have no negative effect in terms of consistency and reproducibility of the original experiments done for the determination of the optimum conditions. The results will be given in Chapter 4 in detail. Some of the measurements of resultant pregnant leach solution stock can be seen in Table 20.

Table 20 Properties of pregnant leach solution after the first iron removal with neutralization step.

Property of PLS Stock	Measurement
Volume (L)	2.45
Density (g/L)	1.054
ORP (mV)	271
Free Sulfuric Acid (g/L)	2.35

The experimental setup for this stage was the same setup used for the prior step that can be seen in Figure 45. The experimental procedure was also the same as the prior one. The exceptions were the decreased concentration of calcium carbonate slurry which was 12.5% weight/volume and the fixed temperature condition that was 70°C. The reduction in reagent concentration from 25% to 12.5% was done for the purpose of prevention of an uncontrollable, very rapid increase in pH of the input solution. Otherwise, a sudden local increase in pH would occur due to prior neutralization of most of the free acid that created a buffering effect during slurry addition in first iron removal stage and slowed down the pH increase. Hence, in the absence of high free acid concentration, the pH control of input PLS could be difficult during slurry addition. In order to prepare the slurry in reduced concentration; 12.5 g of fresh CaCO₃ was added into 100 cc deionized water and allowed to mix by a magnetic stirrer throughout the experiments. Once again the addition of the slurry was done at a constant rate of 1000 µL per 5 minutes with the same micropipette in Figure 45. This rate was once more served as a useful method for controllable pH increment. Once the aimed pH of the experiment was attained, the experimental duration was started. During this duration both pH of the solution and the temperature read from contact temperature were followed. When a decrease in the pH of the solution from the aimed pH was observed, the addition of reagent slurry was done in lower amounts depending on the necessity (100 µL to 250 µL).

For the determination of the optimum parameters in this stage, a set of experiment was conducted at a pH range of 4.00 to 5.00 (with 0.25 increments) at the fixed conditions of 70°C and 3 hours. A second set of experiments were conducted for the observation of effect of duration that ranged between 1 to 3 hours with 1 hour increments at the fixed conditions of 4.50 pH and 70°C. After each experiment, the same filtration method as in prior steps was applied in order to separate liquid and solid products. The precipitates accumulating on filter paper were washed with acidified deionized water (pH=2). After washing, the solid precipitates were dried in an oven at 105°C overnight. New pregnant leach solution was stocked after some measurements (volume, ORP etc.) were done. Both products were sent for chemical analysis separately as detailed in the previous section. In case of future necessities for chemical analysis, PLS of the parameter determination experiments were intentionally acidified by a single drop of sulfuric acid to prevent any precipitation while waiting during storage.

3.4.2.3. First Mixed Hydroxide Precipitation (MHP 1)

After the variables of second iron removal step were studied and the optimum parameters were decided, stock preparation experiments at the fixed optimum conditions were initiated in order to obtain a stock of new pregnant leach solution that would be used as input feed for the first and subsequently second mixed hydroxide precipitation stages. After the stock was prepared some of its properties were determined as can be seen in Table 21. One thing to mention is that the free acid in the new pregnant leach solution could not be measured with the previously described titration method since it was almost completely neutralized with the two-stage calcium carbonate additions. The second point to mention is the continuous decrease in density of pregnant leach solution obtained after the two iron removal steps. This is actually what it should happen as some portion of impurity elements were removed as precipitates in these steps.

Table 21 Properties of new pregnant leach solution after the second iron removal stage.

Property of PLS Stock	Measurement
Volume (L)	1.70
Density (g/L)	1.041
ORP (mV)	210
Free Sulfuric Acid (g/L)	-

During the first mixed hydroxide precipitation experiments, the same setup given in Figure 45 was used again. Here once more there were exceptions. The first exception was the replacement of CaCO₃ by MgO (98-100.5% MgO of Merck 5862 grade) in very fine size of powder form as reagent. The choice of MgO was described earlier in comparison with the other possible reagents. The other

exception was experimental temperature which was decreased to 60°C as the fixed condition throughout this stage. The last and the most important exception was the concentration of MgO slurry. Now the solution was mostly purified leaving only nickel, cobalt and manganese as majority cations within the solution. So the amount of reagent addition to be added was rather predictable based on the theoretical calculations. These calculations will be discussed in Chapter 4 but here it is important to indicate that based on these calculations at least 34 cc of slurry must be added into input PLS. Based on that volume it was decided to prepare a slurry with a doubled volume of this necessity in order both to ease the addition and to consider any further necessities for addition during experiments. Therefore, 0.68 g of fresh MgO was mixed with 68 cc deionized water to prepare slurry with 1% (wt/vol.) concentration and used without delay. The reason for preparation of slurry with such a low concentration is related to the same reason described for the second iron removal step. Here again, the rate of addition was kept constant at 1000 µL per 5 minutes with the same micropipette.

In this stage, a set of experiment was conducted for a pH range of 7.00 to 7.20 (with 0.10 increments) at the fixed conditions of 60°C and 1 hour duration. After each experiment, the same filtration method used for the prior steps was applied in order to separate liquid and solid products. The precipitates accumulating on filter paper were washed with deionized water without acid addition. After washing, the solid precipitates were dried in an oven at 105°C overnight. New pregnant leach solution was stocked after the critical measurements (volume, ORP etc.) were done. Both products were sent to MERLAB for chemical analysis by ICP separately. As the MHP 1 solid product is highly important, the chemical analyses were done as soon as possible in order to prevent its oxidation or moisture pick up. The new solution was not acidified since no precipitation concern was seen due to highly purified resultant solution.

3.4.2.4. Second Mixed Hydroxide Precipitation (MHP 2)

As the last step conducted in this thesis work, a stock with a low amount of Ni and Co in solution obtained from the optimum MHP 1 precipitation experiment conditions was prepared and subjected to MHP 2 experiments. Some of the properties of the stock produced at the optimum conditions for this step can be seen in Table 22.

Table 22 Properties of new pregnant leach solution after the first mixed hydroxide precipitation stage.

Property of PLS Stock	Measurement
Volume (L)	0.55
Density (g/L)	1.029
ORP (mV)	142

The procedure was almost the same as that used for MHP 1 stage with again the exceptions of reagent type and slurry density. In these experiments, instead of MgO, fresh calcium hydroxide (Merck grade 2047, >96% Ca(OH)₂ and <3% CaCO₃) was used as reagent. The slurry was prepared based on the theoretically necessity amount and kept constant for each experiment. Based on the calculations, 0.61 gram of Ca(OH)₂ was mixed with 61 cc deionized water and stirred until the end of the experiments. Slurry addition rate, temperature and other variables were the same as before.

In this step, a pH range of 7.5 to 8.0 was studied with 0.25 increments at the fixed conditions of 60°C and 1 hour residence time. The procedure for liquid/solid separation and chemical analysis were the same with the previous step. As a last table to give about the experimental setup and procedure of both HPAL and MHP experiments, it is important to list composition of the deionized and distilled water source as in Table 23.

Table 23 Chemical analysis of deionized water source utilized both in HPAL and MHP experiments.

Element	Concentration (ppm)
Na	20
K	3
Ca	0.264
Mn	0.023
Mg	0.719
Fe	ND*
*Not detected	

CHAPTER 4

RESULTS AND DISCUSSION

4.1. High Pressure Acid Leaching Experiments

As explained before, the operational conditions of the HPAL circuits of several operating or operated plants are in a narrow range. However, there are several possible combinations of conditions that can be tested since there are several important parameters as detailed in literature review. Initially, a rough but instructive theoretical calculation can be helpful to start with the study. After several years of experience gained some assumptions for the behavior of elements against acid attack can be made. For example, while ferric iron content of an ore feed can be as high as 50%, the regeneration of acid results in only a maximum of 5% iron extraction that can be responsible for acid loss. On the other hand, some of the acid-locking elements can be assumed to be completely leached and consume the acid with respect to their content in the ore feed such as magnesium. Another assumption is made on the negligibly extractable elements such as chromium and silicon due to their general existences in acid-resilient minerals like chromite and quartz. Although these assumptions are quite helpful, in many cases it might be different from the real case since rarely nickel and cobalt can be extracted by 100% and almost always manganese extraction is below 90%. However, the net picture that can be drawn from Table 24 is the major advantage of HPAL circuit on AL option. As can be seen, the atmospheric conditions quadruple the theoretical acid requirement. This is due to the partial acid release by aluminum and only 5% acid consumption by the dominant element iron under the pressure leaching conditions due to iron and aluminum hydrolysis reactions.

According to Sherritt-Gordon assumptions and the respective elemental content of Çaldağ limonite sample, the necessary theoretical acid consumption was calculated to be approximately 300 kg acid per ton of dry ore in order to completely dissolve nickel and cobalt as can be seen in Table 24. Within these assumptions, it was estimated that the resultant pregnant leach solution should have a free acid of 40 g/L with respect to our experimental batch composition (350 cc deionized water plus 150 g of dried ore feed) which corresponded to about 93 kg per ton of dry ore. Hence, as a starting point the chosen acid to ore ratio for the first experiment was 0.30 kg/kg and the first set of experiment series done was for acid to ore ratio optimization as follows.

Table 24 Theoretical sulfuric acid consumption per ton of dry Çaldağ ore sample.

	Çaldağ Limonite Ore	Limonite Ore AL conditions	Sherritt-Gordon HPAL conditions	
Element	ALS (Weight percent)	Sulfuric Acid Consumption (kg) / Ton of Ore	Percent Extraction	Acid Used (kg/ton)
Fe ⁺³	32.7	861.5	5	43.1
Fe ⁺²	0	0	0	0.00
Ni	1.215	20.3	100	20.3
Al (dissolved)	1.66	90.7	25	22.7
Al (precipitated)	1.66	40.3	75	30.2
Co	0.078	1.3	100	1.3
Mn	0.349	6.2	100	6.2
Ca	0.600	14.7	100	14.7
Mg	1.628	65.3	100	65.3
Cr	1.01	19.1	5	0.95
As	<0.01	-	0	-
Si	13.39	-	0.9	-
Na	0.04	1.7	45	0.77
Cu	0.055	-	100	-
Zn	0.04	0.6	100	0.60
Free Acid 40 g/L	350 cc L/ 150 g S=2.33	93.2	-	93.2
Total Acid Consumption (Kg/Ton of Dry Ore)		1214.9	-	299.3

4.1.1. Effect of Acid to Ore Ratio on Metal Extractions

Although the a/o ratio could be theoretically calculated, the other parameters could only be selected from the previous experience gained in HPAL plants at least as starting assumptions. When the literature was searched for the operational temperature values of previous or on-going HPAL plants, it was seen that generally a temperature close to 250°C was the more preferred one certainly with exceptions. For example, in the first and second generation HPAL plants like Cawse and Bulong used 250°C while Moa Bay and Murrin chose to operate at 246°C and 255°, respectively [58][115]. As an intermediate between these values, it was decided to start with 250°C so that later on an experiment series for only optimization of temperature (lower or higher) could be done. Another starting point to be decided was for residence time of the first experimental set. In literature, it was seen that the duration of autoclave operation ranged between 30 minutes to 90 minutes. After taking into consideration the heating curve of the autoclave vessel utilized in this study, it can be seen that approximately 40-50 minutes duration of acid-ore contact was present until the reactor reached 250°C. Consequently, rather than 90 minutes of actual reaction duration, it was thought to be more appropriate to study not more than 60 minutes under the stated conditions. As it will be explained in the following sections, half an hour might not be so effective on the extraction of nickel and cobalt despite most of these metals are generally extracted from easily leachable host minerals within a short time period. In summary, for the first set of the experiments, it was decided to study the most important operational parameter that is acid to ore ratio at the fixed conditions of temperature, leaching duration, particle size, solid concentration and stirring speed with the values given in Table 25.

As can be seen from Table 25, five experiments were planned for the determination of the optimum acid load with 0.025 kg/kg increments. Extraction efficiency calculations of the experiments are given in detailed in Appendix A.

Table 25 Experimental parameters of the first set of experiments for the optimization of acid load.

Parameter	Value/Amount
Acid to Ore ratio (kg/kg)	0.25, 0.275, 0.30, 0.325, 0.35
Leaching Duration (minute)	60
Temperature (°C)	250
Particle Size (mm)	100% - 1
Solid Concentration	30% (excluding acid volume)
Stirring Speed (rpm)	400

The extraction results for nickel, cobalt and iron can be seen in Figure 46. As can be seen from Figure 46, with increasing acid load the extraction values for all three metals is increasing. The behaviors of nickel and cobalt seem to resemble each other. However, the amount of increase in extractions somehow decreases on passing from 0.30 to 0.325 a/o ratio and stay almost steady with further increases in acid load. This result is consistent with the literature. According to Guo et al. (2011), both the nickel and cobalt extractions increase rapidly up to a certain acid load and further increases bring a marginal effect on the extractions [116]. Probably in the present case this value was 0.35 kg/kg acid to ore ratio.

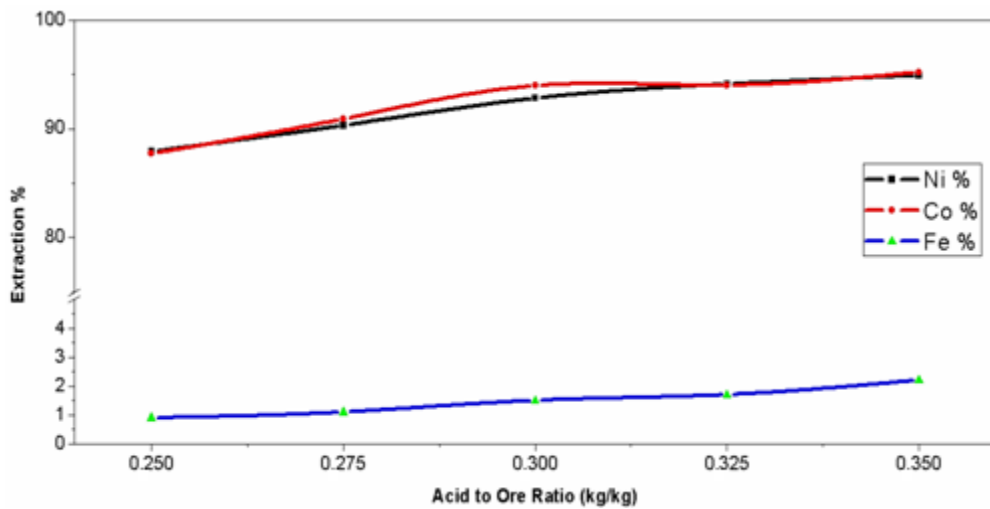


Figure 46 Effect of acid to ore ratio on nickel, cobalt and iron extractions.

As discussed in the characterization of the ore feed, nickel and cobalt are always within more than one mineral either by surficial adsorption or entrapment within the lattice structure. As long as the so-called minerals are not contacted by acid and leached, it is impossible for them to lose their nickel and cobalt content. The destruction of these particles requires hydrogen activity which in turn requires sufficient acid amount in the solution. Hence at least some acid is necessary in media in order to take nickel and cobalt values into solution. This result is consistent with the literature as increasing acid amount will further destroy the untouched regions of host particles or more resistant host minerals within the particles [3].

When Figure 46 is studied, it can be seen that although it was below the calculated value in 250 to 275 kg per ton of dry ore acid range, it was still possible to extract a significant amount of nickel and

cobalt. This might be a sign of that both nickel and cobalt values of ore feed were entrapped within relatively easy-to-leach minerals. However, for economic concerns, a value greater than 90% extraction is generally required for nickel and cobalt extractions. On the other hand excessive acid load would require further neutralization in downstream applications if MHP route has to be followed. Expectedly, higher acid consumption would be more costly if it was not balanced with the revenue of nickel and cobalt extractions. At that point, the acid to ore ratio of 0.35 was seemingly pointless since approximately the same revenue could be obtained at lower acid loads without higher remnant free acid to neutralize. Overall, there existed some sort of competition between 0.30 and 0.325 a/o ratios to be selected as the optimum acid load. However, the amount of remnant impurity in pregnant leach solution is also important for the intermediate MHP production. Since these impurities are to be removed in sequential downstream steps, it is desired to lower their quantity as much as possible. Hence, the selection of an optimum acid load is dependent on the highest valuable metal revenue, the lowest possible free acid and the lowest possible impurity concentrations in the PLS.

As the major impurity, the situation of iron is given together with nickel and cobalt. As stated previously, with increasing acid load there was an increase in iron concentration in PLS. This is an expected result as Whittington reported [3]. Likewise for nickel and cobalt, the main iron bearing minerals goethite and hematite require at least a certain level of acid amount. Specifically, with higher acidity the amount of protonation of goethite surface will increase and iron hydrolysis reactions will be further enhanced by increasing acid-goethite interaction amount. This will favor hematite precipitations at higher acidities at a certain acid level because further acidic solutions enable basic iron sulfate formation as described in the literature review. The reason for this behavior is that hematite forming reactions are hindered by excessive hydrogen activity. Rather than separating to leach residue, iron remains dissolved in the solution. When the solubility of iron in that form is also achieved then iron precipitates as basic iron sulfate. As mentioned previously, when iron precipitates as basic iron sulfate there should be a drop in acidity level (if other acid-locking metals are not changed in concentration), in other words, the free acid amount must drop when this formation is observed.

Expectedly, the increasing acid load will increase the free acid in PLS however, simultaneously higher load will extract more nickel and cobalt and also other impurity elements thereby which in turn means further acid consumption by these freed metals. On the other hand, the behaviors of iron, aluminum and magnesium are the major dominators for the terminal free acidity as described in the literature review. Hence, the concept of free acid with metal extractions is rather interactive. When the problematic case after HPAL for neutralization is also considered, the free acid change becomes complicated. The free acid change with acid load is given in Figure 47.

As can be seen from the mentioned figure, with increasing acid load, the resultant PLS became more acidic. There existed a continuous acidity increase from 34.7 g/L to 50.5 g/L; hence the iron concentration was also increasing meaning basic iron sulfate was probably still not favored. As indicated in the literature, a free acidity between 30 to 50 g/L is a must in order to prevent solid nickel and cobalt sulfate formations. Hence the situation for low nickel and cobalt extractions for all trials in this set was probably due to insufficient acid contact or highly resilient host minerals. However, it must be taken into consideration that the secondary nickel and cobalt losses are also possible due to formation of alunite/jarosite, amorphous silica, etc. as discussed in the leach residue characterization. The distinction can only be understood by successive leach residue characterizations that will be explained in following sections.

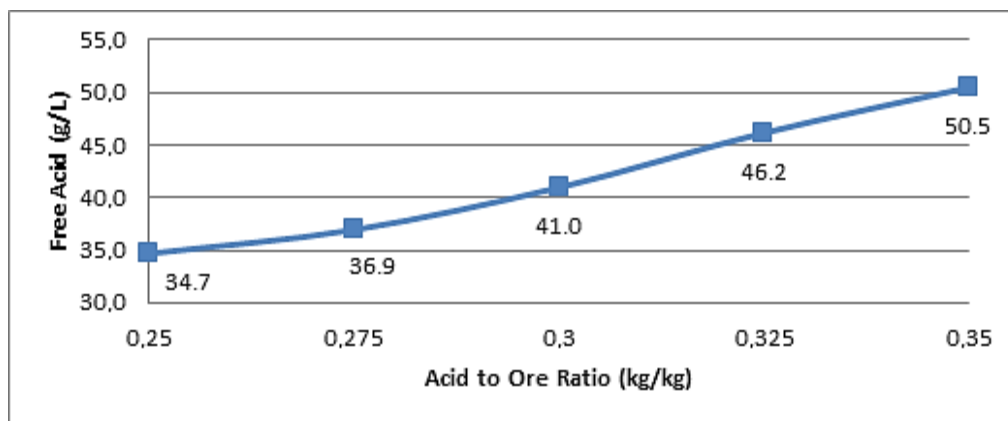


Figure 47 Terminal free acid changes with acid load.

The behaviors of the other impurity elements are given in Figure 48. As stated by Krause et al. (1998) and Georgiou (1995) higher acidity will unavoidably improve the extractions of aluminum and chromium. Indeed, the behavior of aluminum reveals that it is the most sensitive element to the media. As in the case of iron, aluminum hydrolysis reactions are also favored by increasing hydronium ion concentrations. It was mentioned that dissolved aluminum remains as neutral complex with sulfate bond. Hence higher amount of acid will cause higher aluminum to remain as neutral complex in the solution. This situation will continue until the aluminum solubility limit is not exceeded. However, as can be seen even at the highest acid load aluminum extractions could not go beyond 55% which was probably due to alunite and/or jarosite precipitations. Although their effects were not included in extraction calculations, sodium and potassium were shown to exist in minor amounts of 0.04% and 0.2% in Çaldağ ore, respectively. In considering that at least some portion of these alkali elements were leached and Na and/or K-alunite/jarosite formations were possible which are more stable than hydronium alunite. Alternatively, according to Rubisov et al. (2000), aluminum generally reaches its solubility limit at pressure leaching conditions and unavoidably precipitate as hydronium alunite [46]. As discussed in the literature review, the most stable phase at 250°C is alunite for solid state of aluminum. In the same manner chromium extraction was showing a slight but steady increase with increasing acidity. Such a low amount of chromium extraction is questionable. If it exists in a resilient mineral such as chromite, this situation is acceptable and chromite peaks should reveal themselves in leach residue X-ray data. On the other hand, if chromium is associated with relatively readily dissolving minerals such as smectite, then chromium should precipitate as its own basic chromium salt or together with iron in hematite structure. This issue will be discussed further in SEM examinations of leach residue. Whatever the reason for low chromium extraction was, it is quite desirable for goethite dissociation because both chromium and aluminum can lock the goethite surface for protonation which prevents the release of nickel and cobalt entrapped within goethite. The same reasoning is also valid for aluminum.

Another point that can also effect the transformation amount of soluble iron into hematite or basic iron sulfate is the background salts of such as zinc, copper (II), magnesium. Their effects are the uplifting of the maximum stability level of hematite in the solution media and hence hematite formation becomes more stable. As can be seen from Figure 48 that the extraction ranges for copper, zinc and magnesium were about 8%, 60% and 85%, respectively. All of these elements were hardly affected by increasing acid amount but their existences in solution might have helped in prevention of higher iron concentrations in solution (especially in divalent form) and also basic iron sulfate formation that would be responsible for acid loss to the leach residue. The situation of magnesium did not follow a regular pattern. In the literature, it was mentioned that magnesium generally differs in extraction behavior on cooling the reactor to room temperature which might cause this situation. Moreover, it was described that neither magnesium nor free acid display the exact situation of solution at the exact operation temperature due to this problem. However, it is highly extractable with respect to the rest of the impurity elements. That was probably due to its existence in readily soluble minerals such as serpentine.

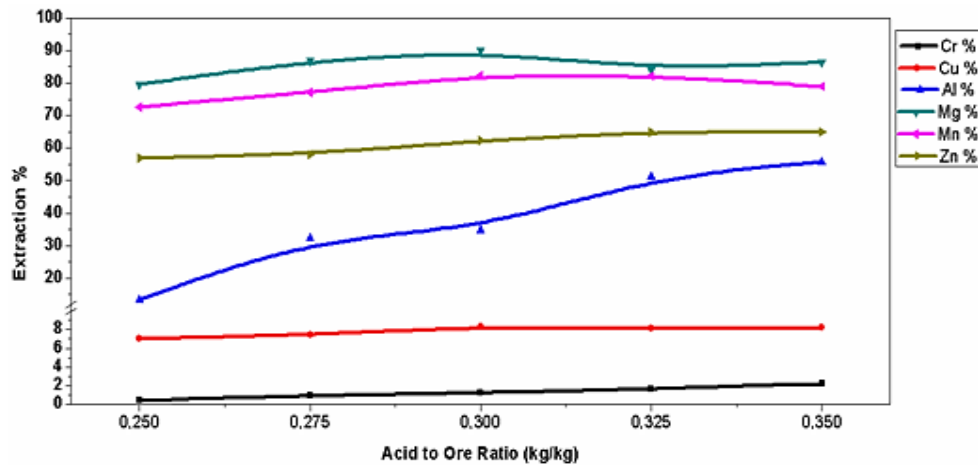


Figure 48 Effect of acid to ore ratio on other impurity metal extractions.

Manganese extraction on the other hand was more than the literature reported values with some exceptions. Guo et al. (2011) obtained similar behaviors for both manganese and magnesium. Magnesium extractions were always close to 90% even at 0.10 kg/kg acid to ore ratios whereas manganese was initially limited until a certain acid load was achieved. At that acid load and higher than that point, manganese was close to 90% extraction [116]. At this point it is worth to mention that the existence of ferrous iron in serpentine and possibly in smectite minerals of the ore feed should have improved the dissolution of manganese oxyhydroxides so that the cobalt extractions would also be positively affected. As can be seen from Figures 46 and 48, there was about ten point difference between the cobalt and manganese extraction percentages throughout the extraction curves. Remembering the information given in Section 2.4.6, i.e. the study of Georgiou and Papangelakis (2009), for complete cobalt delivery it is not strictly necessary for manganese structure to be completely leached especially when the cobalt concentrations are close to particle surfaces (i.e. heterogeneous distribution) [63]. This might be the reason for that difference.

As can be seen from the whole picture, there were slight differences between 0.30 and 0.325 kg/kg a/o scenarios in the way valuable metals and impurities behaved. In order to observe all possibilities with a significant noticeable change on behaviors of primarily nickel and cobalt and secondarily other impurities including iron, it was decided to select both 325 and 275 kg acid per ton of dry ore and conduct comparative tests by changing the other parameters including temperature, particle size and leaching duration.

4.1.2. Effect of Temperature at Two A/O Ratios

The first variation was decided to be done on temperature since it is also an important issue for both heat energy consumption and autoclave design. As mentioned previously, the correlation of temperature and pressure continue exponentially after about 150°C and after that point an every 5 degree increase in temperature can result in more difficult conditions by means of pressure increase. As a result, before the autoclave manufacture for an HPAL plant, the optimum temperature with a tolerance band should be decided for design of autoclave. As the situation for the acid to ore ratio was described above, it was decided to decrease temperature in steps of 5 degree in 0.325 kg/kg a/o ratio experiments while it was increased in the same steps for 0.275 kg/kg experiments. Based on the literature, it is known that temperature increases would expectedly increase the efficiencies of nickel and cobalt extractions. However, rather than both increasing acid load and temperature it was decided to lower one while increasing the other in order to decrease the operational costs while searching for a junction point where nickel and cobalt could be extracted with acceptable values. The studied conditions are summarized in Table 26 as follows:

Table 26 Experimental conditions of effect of temperature series.

Acid to ore Ratio (kg/kg)	0.275	0.325
Temperature (°C)	250, 255, 260	250, 245, 240
Leaching Duration (minute)	60	
Particle Size (mm)	100% - 1	
Solid Concentration (%)	30	
Stirring Speed (rpm)	400	

The temperature effect is basically seen on reaction kinetics in general. According to Krause et al. (1998), the effect of temperature on reaction rates was very dramatic such that for a 93% Ni extraction, 50 minute duration at 240°C was necessary, whereas the same extraction was obtained by just 10 minute retention time at 280°C [38]. In the present study, the extraction behaviors of nickel, cobalt and iron were plotted together at two different acid to ore ratio as can be seen in Figure 49. On both acid load cases, nickel was more sensitive to temperature increase whereas cobalt lost its sensitivity at lower acid load. These results are in agreement with the literature. Chou et al. (1976) stated that for rapid leaching, temperatures close to 250°C are required but higher temperatures will increase the initial rate up to 275°C. On the other hand, 300°C will just lower the nickel extraction [30]. According to the study by Georgiou and Papangelakis (1998), an increase in temperature from 230°C to 270°C results in a steep increase of nickel and cobalt extractions during initial temperature ranges. However, this increase decelerates and further temperature increases beyond 260°C have no significant influence on extraction values. [41]. It is worth to mention that both at 0.325 a/o and 0.275 a/o ratios neither nickel nor cobalt dropped below 90% extractions even at the lowest temperature studied which is quite interesting in terms of mineralogy. It is quite clear that the major amounts of nickel and cobalt were in leachable state in the host minerals. On the other hand, for 0.275 kg/kg acid load, reaching to 260°C did not result in an expected satisfactory situation for cobalt extraction which meant that acid load was not enough for higher cobalt extractions even with the aid of faster reaction kinetics. Actually this was expected since the effect of temperature on cobalt is negligible unless it is not high enough to enable reactions (i.e. below 230°C). That is because extractable cobalt is readily and rapidly dissolves in former leaching durations and does not improve after a certain level by just increasing temperature [63]. Chou et al. (1976) generalized this case for both nickel and cobalt such that increasing temperature from 250°C to 275°C had a pronounced effect on extraction rate during the first ten minute duration and after that point they became almost temperature independent [30].

Generally, there exists a correlation between leaching duration, acid load and temperature. Higher temperatures reduce both the required leaching durations and required acid load to obtain the same efficiencies at lower temperatures. Similarly, increasing acid addition is also effective on leaching duration reduction. Lower acid addition will not only decrease the maximum nickel and cobalt extractions but also the initial rate of nickel and cobalt extractions. Here, it is worth to mention the effect of acid load on the necessary residence time of leaching. Krause et al. (1998) showed that at the same given temperature an increase in acid addition by 15% shortens the required leaching duration by 20% to obtain the same extraction values [117]. Chou et al. (1977) also described a similar situation for Moa Bay ore that decreasing the a/o ratio from 0.30 to 0.27 meant an increase of 3-fold in residence time to achieve 90% extraction of nickel at 250°C. Hence during the decision-making situation this knowledge could be helpful to balance the acid consumption cost with capacity-decreasing residence time [3,30].

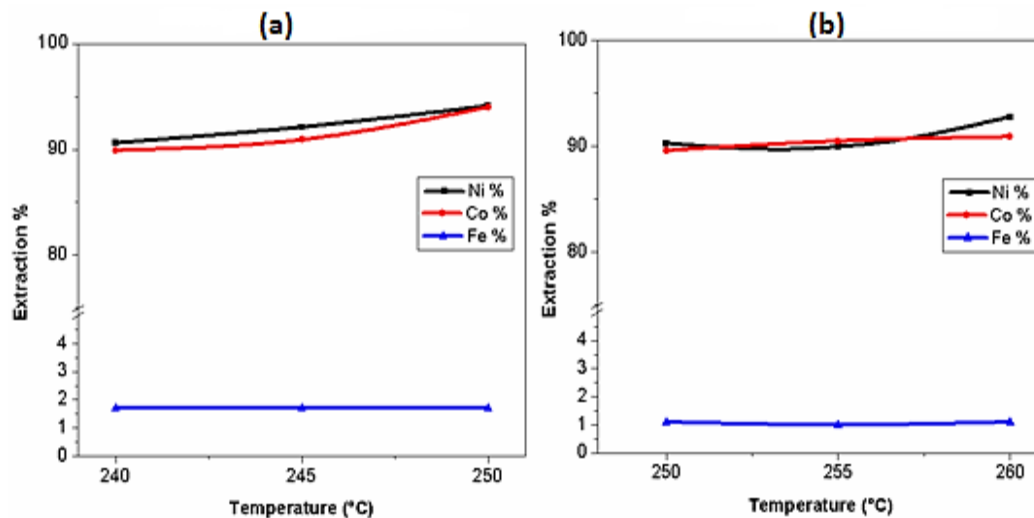


Figure 49 Effect of temperature on nickel, cobalt and iron extractions at 0.325 kg/kg (a) and 0.275 kg/kg (b) a/o ratios.

The behavior of iron can be seen in the same figure for nickel and cobalt. Although there was a slight increase in extraction efficiency for 0.325 kg/kg acid to ore ratio than for 0.275 kg/kg, iron seemed to be immune against temperature changes for both acid levels at least in these temperature ranges. In the literature, the behavior of iron with respect to temperature was described as follows. Papangelakis et al. (1996), Georgiou and Papangelakis (1998), Chou et al. (1977) and Guo et al. (2011) reported that increasing temperature will decrease the iron concentrations in pregnant leach solutions at the same acid level [30,41,49,116]. The reason for this behavior is stated to be due to the enhanced kinetics of goethite dissolution and hematite precipitation with increasing temperature. As an example, Guo et al. (2011) showed that increasing temperature from 230°C to 270°C decreased the iron dissolution from about 4% to about or less than 1%.

Other authors rather preferred to describe the situation as nickel and cobalt selectivity over impurity levels by means of $(Ni/Co):(Fe+Al)$ concentration ratios. Hence, it is more appropriate to refer to Figure 50 where the aluminum extractions are given. As can be seen from this figure although iron did not show any sensitivity with respect to temperature, the situation was different for aluminum. Actually, increasing acidity and temperature both or separately, decreased the aluminum extraction efficiencies. As in the case for iron, aluminum precipitation reactions were also favored by increasing temperature where it precipitates as either hydronium alunite or more stable Na or K alunite. Chou et al. (1977) stated that increasing temperature from 250° to 275°C decreased the impurity level (iron and aluminum) and increased the quality of PLS obtained at constant leaching duration and acid level. He also stated that, the sulfur assay of the leach residue also increased with higher temperature. That was probably due to higher alunite formation that entrapped sulfates in its structure (rather than due to hematite precipitation) although he did not mention this reasoning. Georgiou and Papangelakis (1998) enlarged the temperature range from 230°C to 270°C and showed that the selectivity of nickel and cobalt over impurities are exponentially increasing with respect to temperature after 250°C to 275°C during one hour leaching.

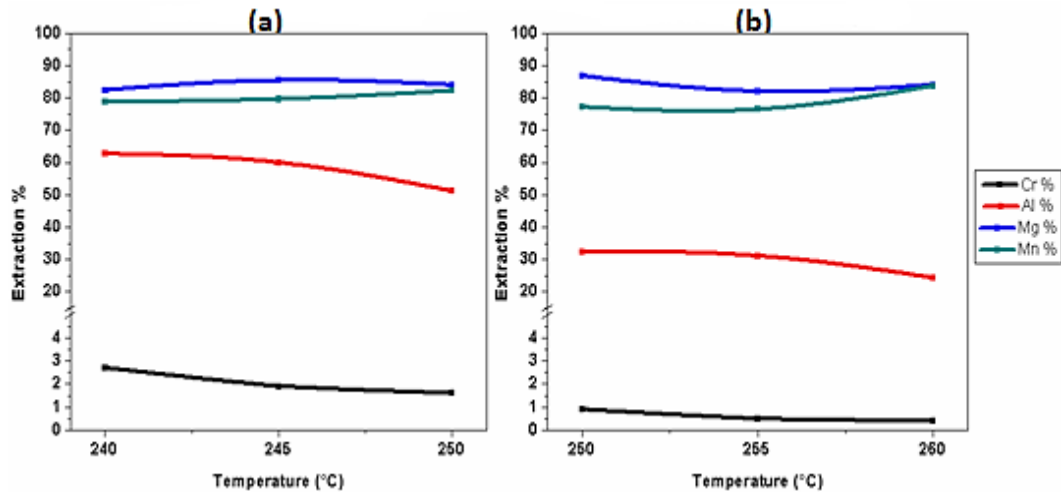


Figure 50 Effect of temperature on other impurity metal extractions at 0.325 kg/kg (a) and 0.275 kg/kg (b) a/o ratios.

Rubisov and Papangelakis (2000) on the other hand, detailed the situation with consideration of free acid change. They stated that the free acid should be temperature independent at lower acidities (0.320 kg/kg and lower). The reason for that behavior was found to be rather complex. Since at higher temperatures iron and aluminum solubility limits are lower, more precipitates will be formed and more sulfate will be injected to solution rather than losing in leach residue. Similarly, at these high temperatures, magnesium solubility will also be lowered and hence magnesium will also tend to precipitate which will decrease the magnesium concentration in solution. Magnesium is explained to be in the form of sulfate complexes that entrap free hydronium ions and lower the actual acidity at temperature. Precipitation of magnesium will favor the free acidity in solution which means free hydronium concentration will be increased. These free ions will then lock the soluble aluminum and iron and keep them in solution hence increase their concentration. By doing so, the direct effect of temperature on solubility of Al and Fe will be vanished and free acid should stay still [46]. It seems that this tangible but fragile balance is highly dependent on the concentrations of all three metals at the exact temperature. On the other hand, Chou et al. (1977) stated that the equilibrium free acid concentration that is gained after several initial minutes should be independent of temperature variations from 250°C to 270°C. Overall, it can be seen from Figure 51 that the free acidity was in agreement with the findings of Rubisov et al. (2000) and Chou et al. (1977) especially for lower acid load. Both iron, free acidity, aluminum (slightly) and magnesium (slightly) remained almost constant with temperature increases. On the other hand, at the highest acid but the lowest temperature case, the free acidity was lower than its neighboring values. Despite iron and magnesium extractions were steady; the aluminum concentration was high at that temperature. This might be caused by more amount of free hydronium concentration locked with neutral aluminum sulfate resulting in lower acidity.

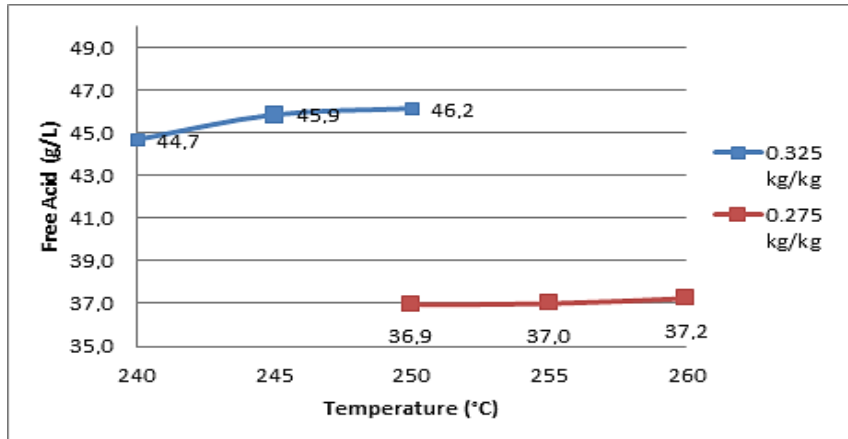
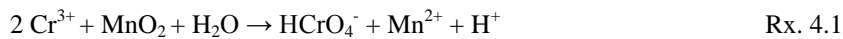


Figure 51 Terminal free acid change of solution with temperature obtained at different a/o ratios.

The effect of temperature on chromium concentration was similar to that of aluminum. As stated by Whittington (2000) chromium is actually important to be considered especially when manganese is also in the scene. When chromium hosting minerals dissolve such as chromite or goethite or even smectite, chromium stays in solution in simple ionic trivalent form. However, when there exist some manganese oxides (MnO_2) in media, following reaction proceeds:



It can be seen from Rx. 4.1 that chromium basically acts as a reducing agent that resultantly extracts manganese in divalent form and actually helps the manganese mineral dissolution which in turn liberates entrapped cobalt. In the absence of chromium and existence of trivalent iron a similar reaction occurs as given in the literature review. As Rubisov and Papangelakis (2000) stated, both chromium (III) and Mn (IV) have negligible solubility under high temperature pressure leaching conditions [61]. As discussed above, the metal solubility limits generally tend to be lowered which is also valid for chromium. When chromium is reduced after interaction with manganese dioxide, it generally precipitates within alunite structure or less commonly within hematite for iron replacement (if remains as trivalent ion). Hence chromium behavior is not only dependent on the operational conditions but also behaviors of manganese and aluminum. Overall, it can be seen that the chromium concentration decreased with increasing temperature with all the precipitation-favoring reasons explained above. However, both in acid to ore ratio section and here, while the chromium extraction decreased to lower amounts manganese amounts increased which might be by the help of chromium.

In summary, there are three possible options until the end of these two sets of experiments. These three options and their respective extraction percentages are given in Table 27. Since the nickel and cobalt extraction efficiencies are directly related to the business profit, the first comparison should be made on their extractions. As can be seen all three options suggest more than 90% extractions for each hence at that point the acid and temperature requirements should be considered. As can be seen at 245°C, 0.325 kg/kg acid load offers almost the same benefits for nickel and cobalt as that are possible to gain at lower acidity (0.275 kg/kg) but at higher temperature (260°C). On the other hand, at higher acidity but medium temperature (250°C), the highest possible extraction efficiencies can be gained. At that point, the decision-making process is still early since the particle size and leaching durations can reverse the picture. However, it is clear that 260°C is a high temperature for operation that will increase the operation costs despite its offering of lower acid consumption and relatively lower impurity levels (a significant decrease in aluminum and chromium can be seen). Moreover, decreasing temperature by 10-15 degrees and increasing the acid load by only 50 kg per ton of dry ore, it is still manageable to keep the same revenue or reach higher than that.

Table 27 Three most highlighted choices with operational conditions and respective extraction efficiencies after temperature and a/o ratio experiments.

Parameters/Metal Extractions	Choice 1	Choice 2	Choice 3
Acid Load (kg/kg)	0.325	0.325	0.275
Temperature (°C)	245	250	260
Leaching Duration (minutes)	60	60	60
Particle Size (mm)	100% -1	100% -1	100% -1
Ni %	92.1	94.1	92.8
Co %	90.9	94.0	90.9
Fe %	1.7	1.7	1.1
Cr %	1.9	1.6	0.4
Cu %	7.8	8.1	7.6
Al %	59.9	51.1	24.3
Mg %	85.4	84.0	84.0
Mn %	79.6	82.2	83.7
Zn %	60.1	64.9	63.0

Despite it does not seem quite a remarkable difference in temperature, 10-15 degrees temperature increment will bring higher standards for autoclaves which are already expensive. Titanium clad steel autoclaves are actually the most important and the most costly investment of HPAL plants. Actual pressure measured during the present experiments was about 50 atm at 260°C whereas it was about 38 and 42 atm for 245°C and 250°C, respectively. With increase in the pressure the thickness, quality and grade of titanium clad on the inside wall of the autoclave increases in order to bear with the steam pressure and heat inside of the autoclave [118]. Steam pressure is necessary for the prevention of boiling of the slurry components and also for more efficient penetration of acid into the slurry [3]. Moreover, at higher operational temperatures, the steam consumption will also increase which will be an additional load on the operation and lower the operational benefits.

4.1.3. Effect of Leaching Duration at Two A/O Ratios

As a result of discussion above instead of considering 260°C, it was decided to keep the temperature at or below 250°C. Before completely ruling out the 0.275 kg/kg acid load option, it was decided to conduct a series of tests on leaching duration to observe any improvement in such a case. For comparison, the same conditions were chosen for 0.325 kg/kg acid load experiments. The experimental conditions can be seen in Table 28. Here, the so-called 0-minute experiments actually represent the heating of autoclave reactor with the complete batch contents to the experimentally planned temperature. Once the planned temperature was reached, it was cooled to room temperature without waiting. By doing so, the effect of coexistence of acid and ore feed during heating on metal extractions could be observed.

Table 28 Experimental conditions of leaching duration experiment series

Acid to ore Ratio (kg/kg)	0.275	0.325
Leaching Duration (minute)	0, 30, 60, 90	0, 30, 60, 90
Temperature (°C)	250	
Particle Size (mm)	100% - 1	
Solid Concentration (%)	30	
Stirring Speed (rpm)	400	

The experimental series were conducted at 250°C in order not to cause a decrease in already low extraction efficiencies of 0.275 k/kg acid load. The results for nickel, cobalt and iron are given in Figure 52 whereas the rest of impurity metals can be seen in the following Figure 53. As can be seen in Figure 52, during heating of the reactor, there were reactions which were occurring at some rate that enable the extractions of nickel and cobalt as well as the other metals. As a result of these reactions about 70% of each metal could be readily taken into the solution. After the reactor reached the actual temperature further duration enabled the rest 20-25% of extractions with gradual and continuous increment. In general, the leaching duration had a positive effect on the extraction behaviors of valuable metals up to a certain level after that the effect was rather marginal. These results were consistent with the literature. As stated, significant amounts of nickel and cobalt (especially those surficial values) were already extracted into solution at very early stage of leaching. This increasing trend continued up to 1 hour leaching duration after that time the effect of duration was rather insignificant [116].

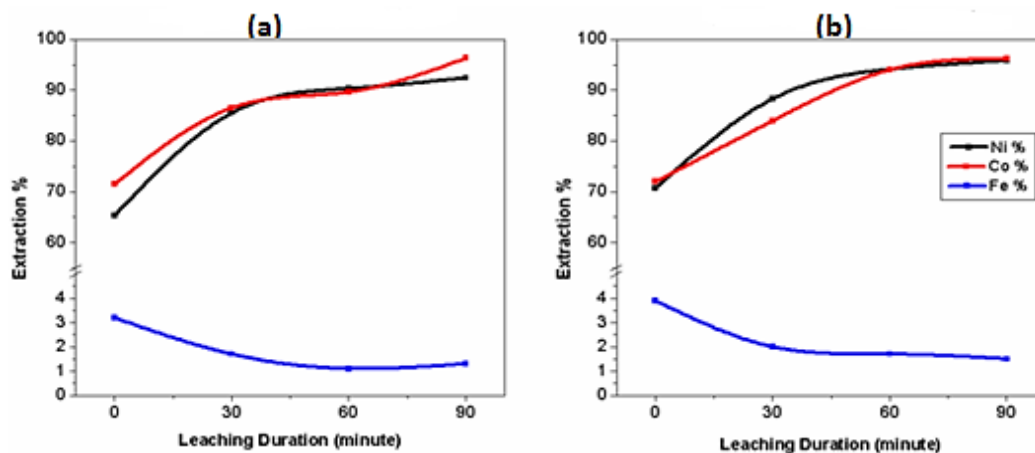


Figure 52 Effect of leaching duration on nickel, cobalt and iron extractions at 0.275 kg/kg (a) and 0.325 kg/kg (b) a/o ratios.

As can be seen at higher acidity, the effect of extending the leaching duration from 1 h to 1.5 h just caused an approximately 2-point increase in extraction efficiencies. Likewise, at lower acidity the nickel extraction was improved by the same low amount. The most pronounced effect was on the cobalt extraction at this acid load which increased to 96% that could be obtained by higher acidity at the same duration. This situation indicated the possibility of that some minor portion of the cobalt was probably entrapped within more resilient and less porous structure. As described in the characterization part, cobalt was highly associated with manganese oxyhydroxide mineral called asbolane and goethite. If at least some part of cobalt was heterogeneously distributed and specifically cumulated in core of these asbolane and/or goethite particles, the low amount of acid load could not reach to the core and might have needed longer leaching duration to extract cobalt from the core of these particles. This situation was less likely to occur for goethite due to its highly porous and extensive surface area in bulk form but the same statement could not be true for manganese minerals since they were coarser and less porous. However, there were still a portion of the cobalt (4%) that could not be extracted at even higher acidity and same long period which brought another question in mind. This seemingly untouched cobalt values could be related to secondary losses that might be entrapped with after-leaching phases such as amorphous silica or alunite or even hematite. The same situation was valid for nickel with exactly the same reason as given of cobalt. So far, nickel could not be extracted above 95% which will be investigated in the following sections. The worst situation was observed by Kaya (2011) in his thesis study where hematite was believed to be responsible for low (85%) nickel extraction efficiencies [5].

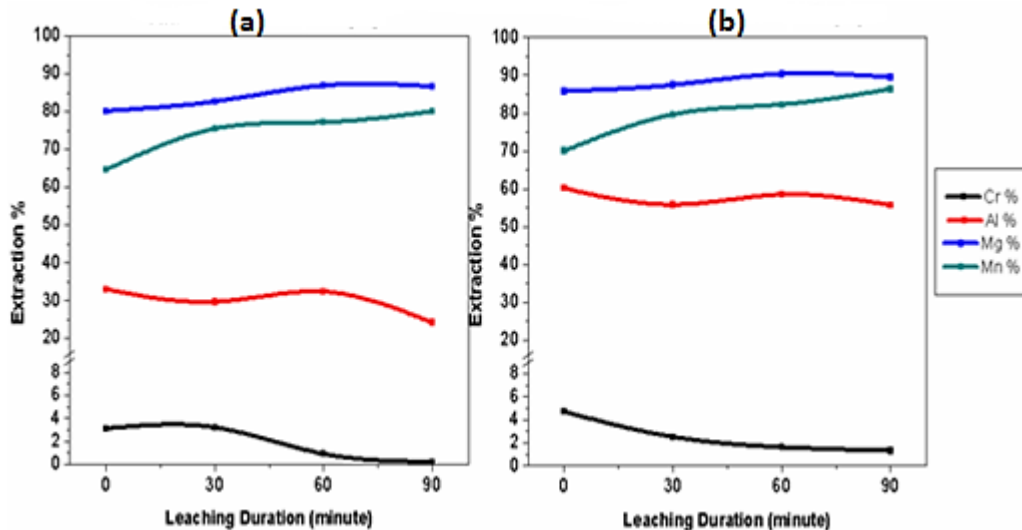


Figure 53 Effect of leaching duration on other impurity metal extractions at 0.275 kg/kg (a) and 0.325 kg/kg (b) a/o ratios.

On the other hand, the extraction of iron was inversely affected by the extended durations. Logically the longer is the time allowed; the higher will be the leached iron amount that will be precipitated. As it can be seen in Figure 52 that at 0-time experiments there existed the highest recorded amounts of iron extractions that were observed so far. This is because of the fact that at the initial period of leaching, the high concentration of hydronium actively and quickly dissolving porous goethite particles cause a supersaturation of solution by iron. These rapid dissolution reactions affected the free acidity level as can be seen in Figure 54. At the 0-time, the free acidity was at its lowest value due to soluble iron that locked the hydronium ions prior to precipitation. Additionally, goethite-hematite transformation rate is still dependent on goethite dissolution rate at that time. As the hematite precipitation increases, the free acidity recovers itself and tends to increase with acid regeneration in time. As can be seen this supersaturation was balanced with rapid hematite precipitation within the 30 minutes duration and remained constant at each acid load experiments. On the other hand, after 60 minutes, there was a tendency for further increase in acidity. This was because of the continuing alunite formation since aluminum concentration was still decreasing until 90 minute duration was reached. Here once again, it can be seen that alunite precipitation rate was slower than that of hematite. Moreover, the magnesium and manganese dissolutions slightly increased with the additional 30 minute duration. As can be seen, chromium behaved in the same manner as iron. The solubility of chromium decreased with time and probably precipitating with alunite since there was no change in the iron concentrations. In order to understand the manganese and relatedly cobalt behavior, it might be helpful to refer to the oxidation reduction potential of the solutions obtained during this set of experiments.

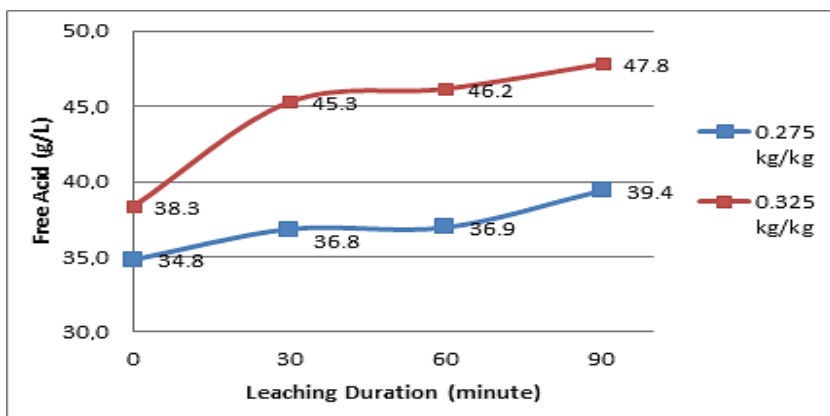


Figure 54 Terminal free acid change with respect to leaching duration at two different acid loads.

Some researchers believe that the oxidization-reduction potential of solution can influence the goethite to hematite transformation rate. According to Stopic (2004), ORP is directly correlated with ferric-to-ferrous iron concentration ratio whereas Tindall and Muir (1996) included the manganese oxide as oxidant into the scene. They both agreed on that the lower is the ORP, the higher will be the electron transfer into the goethite structure and hence the higher is the dissolution rate of goethite and hematite precipitation. In latter study, manganese oxide and ferrous iron were separately added into the solution deliberately. As ferrous iron (Fe^{2+}) concentration increases, ORP values of the solution decreases (more reductive) which is vice versa for both Mn (IV) and ferric iron additions (See Figure 55). Added ferrous iron fastened the dissolution of goethite whereas manganese oxide addition resulted in incomplete transformation even after 90 minutes duration. This situation is extremely important for the ores containing manganese oxide minerals. The extent of the manganese content within an ore is crucial for both nickel and manganese extractions (hence cobalt recovery) and also leaching duration. The decrease in the oxidation-reduction potential will effect leaching in two ways. First it converts the manganese dioxide into Mn (II) and more Mn goes into solution in divalent form (so also cobalt), then it will increase ferrous iron content which in turn will fasten the dissolution of goethite and release more nickel (and associated cobalt) [40,47]. In the absence of ferrous iron concentration, the rate of transformation is dependent on the goethite dissolution (Rx. 2.7) rather than hematite precipitation (Rx. 2.9) [119]. Despite ferrous iron concentrations are desired to be low for downstream applications (especially for MHP and DSX) the positive effect of its high concentration is helpful in autoclave performance. A similar situation for chromium was already detailed in the previous section.

Based on this knowledge, it can be seen that there should exist initially a ferrous iron concentration that might come from the complete dissolution of serpentine and possibly smectite mineral. This unknown amount then interacts with manganese oxides and transforms into ferric iron. Hence, the remnant amount of ferrous iron in terminal solutions of the present case should be minor. Chromium had always about 1.5% extraction values which was low but also important for manganese dissolution. Probably, the co-existence of soluble chromium and ferrous iron had been the reason for the manganese extractions to be higher than reported in the literature.

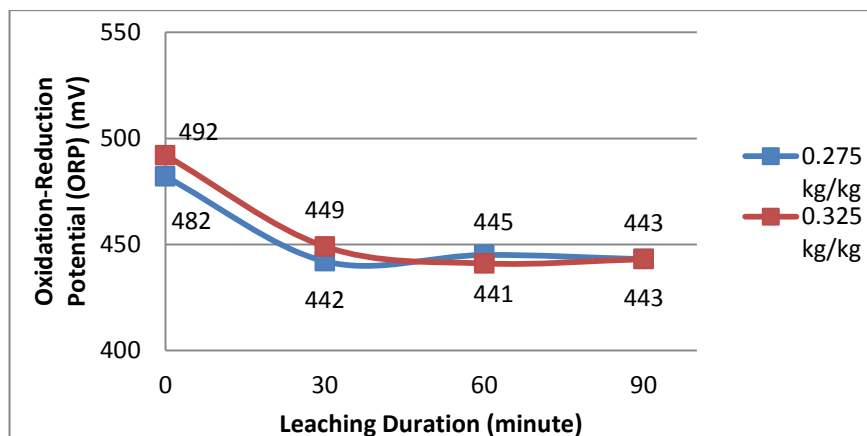


Figure 55 Oxidation-reduction potential of solution with respect to leaching duration at two different a/o ratios.

After these experiments, the possibility of 0.275 kg/kg acid load to be the optimum a/o ratio became less possible. Both at higher temperature (260°C) or longer duration (90 minutes) this acid load seems to be replaceable by other alternatives that offer higher nickel and cobalt revenues with lower temperature and shorter durations despite the attractiveness of lower impurity level, lower free acid content in PLS and lower acid consumption (50 kg/kg per ton of dry ore). After consultation with META Nickel and Cobalt Inc. rather than sacrificing the nickel and cobalt revenues, it was found to be more beneficial to consume additional 50 kg sulfuric acid per ton of dry ore. Consequently, it was decided to move on with the first two choices in Table 29 and conduct one more test in order to observe any improvements especially in Choice 1 so that the acid consumption could be balanced with 5 degree decrease in temperature.

Table 29 Four most highlighted choices after three sets of HPAL experiments.

Parameters/Metal Extractions	Choice 1	Choice 2	Choice 3	Choice 4
Acid Load (kg/kg)	0.325	0.325	0.275	0.275
Temperature (°C)	245	250	260	250
Leaching Duration (minutes)	60	60	60	90
Particle Size (mm)	100% -1	100% -1	100% -1	100% -1
Ni %	92.1	94.1	92.8	92.4
Co %	90.9	94.0	90.9	96.3
Fe %	1.7	1.7	1.1	1.2
Cr %	1.9	1.6	0.4	0.2
Cu %	7.8	8.1	7.6	8.1
Al %	59.9	51.1	24.3	24.2
Mg %	85.4	84.0	84.0	86.6
Mn %	79.6	82.2	83.7	80.0
Zn %	60.1	64.9	63.0	61.0
Free Acid (g/L)	45.9	46.2	37.2	39.4

4.1.4. Effect of Particle Size at Two Different Temperatures

To investigate the effect of particle size, a set of experiments was conducted based on the conditions given in Table 30. In order to conduct the experiments of this series, new sample stocks were prepared at -1.4 and -0.5 mm particle size. The sample preparation steps were given in detail previously in Chapter 3. In the mentioned chapter, one could see the particle size distribution of the so-called samples prior to conducting the pressure leaching experiments.

Table 30 Experimental conditions for particle size experiments.

Particle Size (mm)	100% -1.4, 100% - 1, 100% -0.5	100% -1.4, 100% - 1, 100% -0.5
Temperature (°C)	245	250
Acid to Ore Ratio (kg/kg)	0.325	
Leaching Duration (minute)	60	
Solid Concentration (%)	30	
Stirring Speed (rpm)	400	

Particle size effect is simply related to the acid-ore feed interaction amount. Smaller is the particle size the higher will be the specific surface area of the particles; hence more reaction sites will be available for acid attack. Higher amount of acid attack will eventually mean higher mineral destructions and resultantly more nickel and cobalt liberations to the solution will occur together with more impurity metal passages into the pregnant leach solution. The results of particle size effect on the nickel, cobalt and iron extractions are given in Figure 56, whereas the behaviors of other impurity metals are given in Figure 57. As can be seen from the mentioned figures, there is a dramatic effect of reduction of particle size on especially the cobalt extractions at both temperatures. At higher temperature and the lowest particle size, cobalt was almost completely extractable which was also valid for the lower temperature but with a slightly lower extraction efficiency. Therefore, it was possible to leach cobalt from ore feed with extraction efficiencies between 96-99% by reducing particle size below 0.5 mm. On the contrary to this promising result for cobalt, the nickel extraction was actually not too much affected by particle size reduction. This behavior of nickel that persistently remained around 95% was tested with one more experiment as it will be discussed later on. In order to understand the effect of particle size, the literature was specifically searched for these varying behaviors of nickel and cobalt.

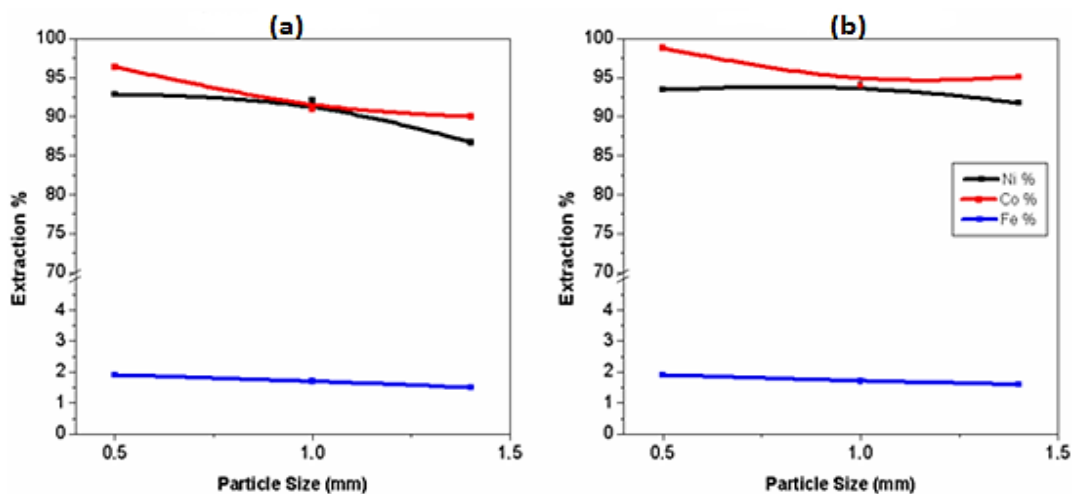


Figure 56 Extraction efficiencies of nickel, cobalt and iron with respect to particle size at 245°C (a) and 250°C (b).

In the literature review, it was previously stated that ore feed for HPAL is best suited at a size of 0.25 to 0.5 mm but this was not a strict limitation. As reported by Chou et al. (1976), the grinding of the ore feed down to smaller sizes had no effect both to dissolution-precipitation reactions and to extraction efficiencies of nickel and cobalt [30]. However, this observation was ore-specific as the studied ore was obtained from Moa Bay which is a limonitic ore site probably containing most of its nickel grade in already finer particles (i.e. goethite) and further reduction in particle size could not cause any improvements. As evidence to ore-dependency of particle size effect, Kaya (2011) studied the effect of particle size reduction down to 38 micron from 2 mm which caused a remarkable increase in the extracted of nickel and cobalt amounts from 85% to more than 92% with the same constant parameters. He indicated that the particles of Gördes limonitic laterite ore that were classified above 425 micron were also nickel contributor and needed to be treated with increased acid contact area [5]. This was explained by the nature of the nickel-bearing minerals. From the distribution of particle sizes given before for Çaldağ, it can be seen that the weight percentages of particles in each sample that were less than 38 micron particle size, were 33.9% for -1.4 mm, 45% for -1mm and 55.6% for -0.5 mm. Therefore, as the upper particle size of the sample decreased the amount of fine particles was expectedly increasing. Actually it can be observed from Figure 56 that about 90% of the total nickel content was present within these fine portions of the ore feeds and the remnant nickel composition was probably in more resilient minerals of coarser size.

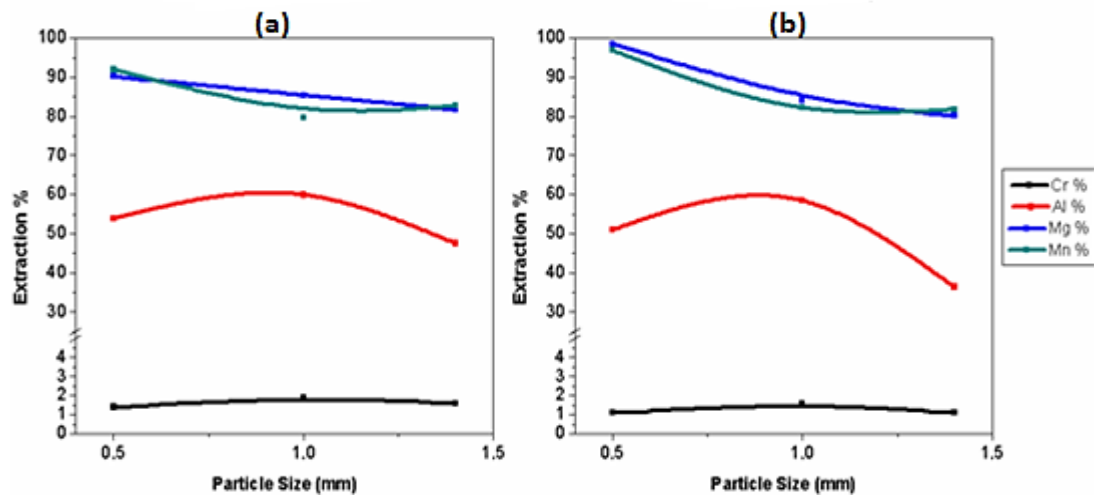


Figure 57 Extraction efficiencies of other impurity metals with respect to particle size at 245°C (a) and 250°C (b).

This reasoning was validated by Whittington and Muir (2000) since as the cobalt liberation increases the extraction percentage of cobalt also increases with finer particle sizes [3]. This impact on cobalt extraction is probably due to the characteristics of host mineral asbolane. As previously mentioned asbolane occurs as coarse grains and could be problematic during extractions. Hence, as in the present case too, the mechanical reduction of its grain sizes could increase the acid performance in cobalt extraction. Evidentially, the amount of manganese extraction reached above 90% for the first time in these experiments. Hence, there should be some asbolane mineral present that was heterogeneously containing some minor amount of cobalt. By reducing the ore size, not only the cobalt leaching from these particles became possible but also with increment in acid-particle contact other manganese containing minerals were probably destroyed and released manganese into the PLS.

The average size of particles in ore feed is not only important for extraction efficiencies but also for impurity levels of resultant liquor. Since goethite is the main nickel bearing mineral in limonite, finer grain sizes of goethites can serve as enlarged nucleation and acid attack area for sequential ex situ

hematite precipitation on acid attack consequently reducing soluble iron concentration in liquor. Since there was no such change in iron extraction which was already in very small amount according to Figure 56, it is probable that majority of goethite phase had already been reduced under 0.5 mm and did not experience any difference. On the other hand, a similar behavior to iron was also valid for aluminum during its precipitation reactions. When Figure 57 is observed, it can be seen that aluminum did not follow a meaningful path at both temperatures but a peaking was observed in both cases. This can be explained as follows: The lower extraction values of aluminum at coarser grains were probably due to insufficient acid contact with aluminum-bearing minerals. As shown in Chapter 3, even at particle sizes between 1.2 to 0.85 mm there were interlocked particles with each other. The reason for low extraction amount was probably due to that fact. On the other hand, a second decrease in aluminum extraction was seen for the finest particle size. As discussed above, that might be due to the increased nucleation site for alunite precipitation rather than low amount of aluminum extraction from aluminum minerals. Together with these reasons, excessive grinding of ore feed is beneficial for both increased valuable metal extraction and the increased Ni:(Fe+Al) ratio leading more easily treatable leach liquor in downstream processes [3,30]. However, it can also be seen that both manganese and magnesium were also positively influenced by this trend which meant that the impurity level might not be reduced with respect to their final concentrations in PLS, indeed they might significantly increase in amount and the final solution could be more contaminated.

4.1.5. Optimum Conditions for HPAL Experiments

In HPAL plants treatment of tons of coarse ore feed with particle sizes as high as 20 mm, requires cost-intensive processes in order to reduce coarse grains to extremely small sizes. On the other hand, coarser ore feed will influence the rheology and (in turn) stirring concerns apart from lower extraction values (still mineralogy dependent though). Therefore, an optimum value for particle size has to be chosen to balance the costs. In the present study, the reduction of particle size from -1mm to -0.5 mm created extra nickel and cobalt extractions at two different temperatures which are given in Table 31.

Table 31 Four most highlighted choices for the optimum operation conditions of HPAL.

Parameters/Metal Extractions	Choice 1	Choice 2	Choice 3	Choice 4
Acid Load (kg/kg)	0.325	0.325	0.325	0.325
Temperature (°C)	245	245	250	250
Leaching Duration (minutes)	60	60	60	60
Particle Size (mm)	100% -0.5	100% -1	100% -0.5	100% -1
Ni %	92.9	92.1	94.0	94.1
Co %	96.4	90.9	98.8	94.0
Fe %	1.9	1.7	1.9	1.7
Cr %	1.4	1.9	1.1	1.6
Cu %	9.0	7.8	9.4	8.1
Al %	53.9	59.9	51.0	51.1
Mg %	90.2	85.4	98.5	84.0
Mn %	92.0	79.6	96.9	82.2
Zn %	69.7	60.1	71.7	64.9

As can be seen from the table, the reduction in particles size at the lower temperature resulted in extra 6% cobalt extraction only whereas that of nickel was slightly improved. At higher temperature, the reduction of size provided once again about 5% more cobalt extraction whereas in the nickel case once more did not change at all. Hence by only gaining about 5-6% cobalt extraction, the extensive grinding operation costs could be or could not be balanced depending on the grinding operations used in an actual plant and general cobalt price. As can be seen, the impurity levels were not so helpful by means of creation a distinctive contrast between the choices. Since it is not so possible to determine the real cost balance of an HPAL plant under the laboratory conditions, it is quite hard to make a decision. What it could be done within this study was that the most attractive choices could be

visualized as in Table 31. It is quite possible to operate at either of these choices since all of them offered some advantages and disadvantages coherently in their own way. However, it is possible for a plant to operate at rather coarser sizes since the cobalt cost might be variable especially in economic crisis times. Hence, rather than choice 1 and 3, the other two choices are more attractive. Yet there have to be made one selection between choice 2 and 4. Between these choices differences are 5 degree temperature change and 2% nickel and 3% cobalt revenues from their extra extractions. As in the case of particle size reduction, a 5 degree temperature change could or could not be balanced with these revenues depending on the autoclave quality requirements for 5 degree temperature increase and nickel-cobalt prices. Overall, it was decided to select choice 4 for the sake of nickel and cobalt revenues and at the expense of heat and autoclave savings.

Hereafter the optimum conditions for HPAL process are chosen as 0.325 kg/kg acid to ore ratio, 250°C for temperature, 60 minutes for leaching duration, 100% -1 mm for particle size and 400 rpm for stirring speed. After this determination, a stock with the given properties in Chapter 3 was prepared in order to conduct the downstream experiments and for producing an intermediate saleable nickel-cobalt mixed hydroxide precipitate. In Table 32, the composition of pregnant leach solution with the extraction percentages under the optimum conditions is given. The resultant leach residue composition is also included in the same table. As can be seen from Table 32, the terminal divalent iron concentration was extremely low which meant that most of the divalent iron coming from serpentine and/or smectite phases contributed the oxidation-reduction reactions that enhanced manganese dissolution. Another important point was that, at the optimum condition, scandium was highly extracted from ore feed and ended up in the PLS.

Table 32 Extraction efficiencies at the optimum conditions, leach residue and pregnant leach solution compositions obtained at these conditions.

Element	HPAL Extraction (%)	Leach Residue (%)	Pregnant Leach Solution (ppm)
Ni	94.1	0.082	4564
Co	94.0	0.0053	294
Fe	1.7	36.5	2231
Al	51.1	0.922	3296
Cr	1.60	1.129	64.8
Mg	84.0	0.2950	5460
Mn	82.2	0.0705	1150
Cu	8.1	0.0574	18.6
Zn	64.9	0.0160	104
Si	6.8	14.2	364
Sc	90.9	<0.0001	24.1
Fe ²⁺	0.0003	-	0.324
Free Acid	-	-	46200

4.1.6. Leach Residue Characterization

The characterization of leach residue after pressure leaching could give valuable information and could reveal answers to problems encountered especially when nickel and cobalt losses are significant. Although Çaldağ nickel ore sample was very leachable and in several cases gave more than 90% nickel and cobalt extractions, there was still a special problem about nickel. As mentioned previously, the nickel extraction values could not go beyond the 95% barrier in all of the experiment done during pressure acid leaching. As discussed in the characterization section of the ore sample, there can be some possible reasons for such an extraction. The first possibility is the primary losses or in other words losses that are due to unleached original minerals. For example, aluminum and/or chromium contributions in nickel hosting iron oxide/hydroxides minerals and in solution media could be

detrimental by means of formation of barriers by aluminum and chromium against protonation of these metal oxide/hydroxide minerals due to stronger oxygen bonds. Additionally, spinel forms are generally non-reactive with acid and they are reluctant to release their nickel content if they have. As example for these spinels; chromite, hematite, maghemite and magnetite can be given. On the other hand, Liu et al. (2009, 2010) gave a leachability order for several minerals as follows [17,108]:

Lizardite>goethite>maghemite>magnetite>hematite>chromite

As they stated, while clay like minerals can be dissolved easily during acid attack (that is the reason why magnesium extractions have never been lower than 80%) it can take longer durations and consume higher acid loads when those more resilient minerals are present in ore feed. Such a problem was encountered in the study of Kaya (2011), where it was found that hematite was responsible for lower than 90% nickel extractions [5]. If these minerals are actually responsible for these nickel losses, it might be helpful to conduct an experiment that has the harshest operation conditions tried so far by allowing all possible positive effects observed on the basis of the results obtained up to this stage. With this aim, a single ultimate test was conducted in order to see whether nickel can reach higher than 95% extraction values. The operation conditions and the final extraction values are given in Table 33. As can be seen once again, the nickel was lost by about 5%. In order to be sure of whether primary or secondary losses or both are responsible for that problem, it will be more proper to refer to the XRD data of the leach residue obtained at the optimum conditions as can be seen in Figure 58. XRD result of ROM sample was also included to the figure in order to see the disappeared peaks and newly formed others.

Table 33 Experimental conditions and respective extraction efficiencies of the ultimate test.

Parameters/Metal Extractions	Measurements/Extraction Efficiencies
Acid Load (kg/kg)	0.35
Temperature (°C)	260
Leaching Duration (minutes)	90
Particle Size (mm)	100% -0.5
Ni %	95.1
Co %	98.8
Fe %	1.9
Al %	45.4
Free Acid (g/L)	54.9

4.1.6.1. XRD Examination of Leach Residue

When XRD result of the leach residue obtained under the optimum condition is observed in Figure 58, it can be seen that it has only three phases whereas there are eight for the original ore feed. As can be seen from the XRD pattern goethite, serpentine, smectite, asbolane, calcite and dolomite phases did not exist within the leach residue anymore. Actually disappearances of some of these minerals were expected since clay-like serpentine and smectite phases, calcite and dolomite minerals are readily leachable in acid media under pressure. However, their complete dissolution would also mean high magnesium, aluminum, calcium and silicon concentrations within the pregnant leach solution. Complete goethite and asbolane dissolutions are extremely important since goethite was the major nickel-cobalt carrier in cumulative whereas asbolane had the highest nickel and cobalt contents as individual particles. Since goethite was completely dissolved, the reasoning for aluminum/chromium substituted goethite case became invalid now. If it was true, then goethite peaks would be preserved in their positions but decreased in intensity. On the other hand, contrary to the literature, the complete dissolution of asbolane was probably due to the release of divalent iron and trivalent chromium into solution from their corresponding host minerals which temporarily dropped the ORP of solution and enhanced the dissolution of asbolane. As a result of goethite and smectite dissolutions, aluminum and iron were released to aqueous media and during pressure leaching some portion of these metals (49%

of Al, 99% of Fe) precipitated as alunite and hematite which can be seen in Figure 58. Newly formed alunite peaks indicated that alunite was present in minor amounts with respect to newly formed hematite amount due to lower aluminum content of ore feed. As can be seen from the figure, the hematite peaks were highly sharpened and dominated the leach residue while goethite and asbolane and other minerals peaks had completely vanished. As stated previously, K-alunite is more stable than hydronium alunite which can stand more severe conditions of pressure leaching than hydronium alunite. Alunite was found to have a perfect match for K-alunite which is expected since the utilized water was fresh; acidity was high (not as high as to cause basic iron sulfate formation) and did not cause any co-precipitation of jarosite together with alunite. The existence of potassium in alunite was due to ore feed containing 0.2% K once again mostly coming from smectite. Hence, rather than alunite/jarosite compound mixture it was alunite itself since jarosite could not be found as large cubic crystals in leach residue examination by SEM. On the other hand, the complete dissolution of serpentine created an increase in magnesium concentration (whereas some portion of this increase is due to dolomite and smectite dissolutions) and yet did not result in any distinctive magnesium phase in leach residue.

As it will be explained in the following papers, the magnesium concentration was present in the resultant solution being about 5000 ppm which was actually high for magnesium concentrations (it was 11000 ppm for AMAX situation as discussed in literature where they observed simple magnesium sulfate salts in leach residue). This was probably due to re-dissolution of magnesium sulfate salt complexes on cooling the reactor to room temperature since the XRD peaks for kieserite phase were not present. However, Scarlett et al. (2008) actually observed the formation of kieserite phase ($\text{MgSO}_4 \cdot \text{H}_2\text{O}$) while the leaching was in progress with the help of continuous synchrotron X-ray diffraction methodology [53]. What they observed was enlightening about the scene after magnesium intake from the easily soluble respective source mineral (ferruginous lizardite with formula given previously in iron chemistry) into the solution. As lizardite dissolution commenced, initially the iron ions precipitated as jarosite whereas magnesium was found to subsequently form the so-called sulfate hydroxide salt which later dissolved on cooling. Another important observation was an increase in amorphous phase content as the lizardite dissolution was continuing. This amorphous phase was not quantified but its amount was decreasing with the increasing amount of crystallization of kieserite and jarosite. The so-called amorphous phase was possibly re-precipitation product as poorly crystallized silica after polymerization of dissolved silicon from lizardite structure (Rx. 2.22). Amorphous silica was mentioned in several articles and it is generally responsible for nickel losses into the leach residue. Mostly, silicon is in acid-resilient minerals such as quartz, kaolinite and talc. However, as in the case for serpentine and smectite minerals, they may contribute to phyllosilicate minerals that can be destroyed easily by acid attack. It is surprising to see that the major quartz peaks were significantly decreased in their intensities in leach residue. Hence, apart from serpentine and smectite, that quartz dissolution would definitely have increased the silicon concentration in solution.

Whether amorphous silica precipitated and if so at which quantity it is actually not so easy to answer. Depending on its crystallinity, amorphous silica can be or cannot be traced with XRD examination. Liu et al. (2009) stated that after serpentine dissolution, a blurred, irregular and overlapped peak series between 15° to 30° was the evidence of amorphous silica in leach residue [108]. Its characteristic broad and irregular peak at around 20 degree (2 theta) might be the result of amorphous silica rather than crystalline quartz. Indeed, Luo et al. (2009) spotted amorphous silica at exactly the same point in their study of a lizardite containing saprolitic ore [120]. Therefore, it should be more proper to refer to the SEM results to ensure that amorphous silica was precipitated during pressure leaching.

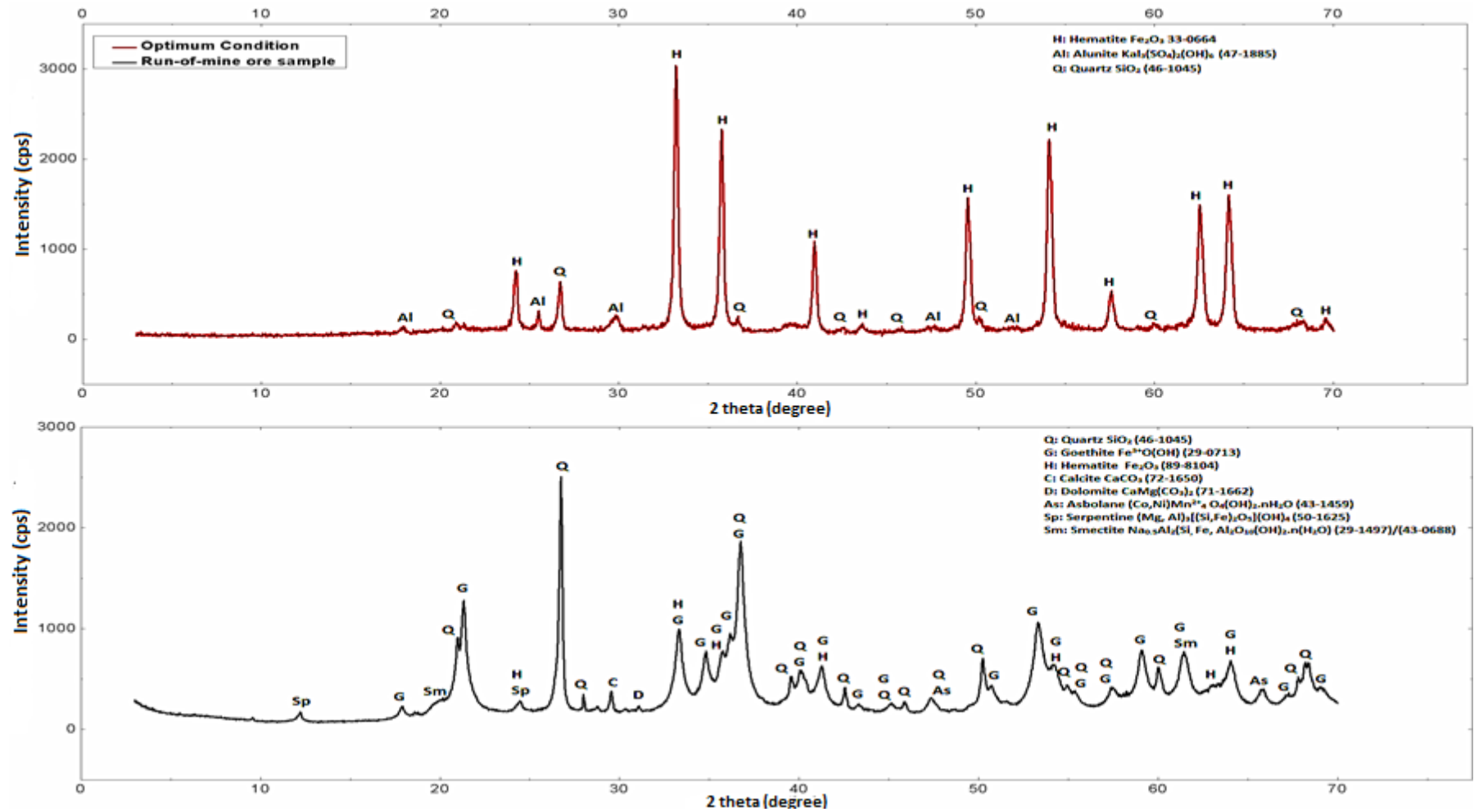


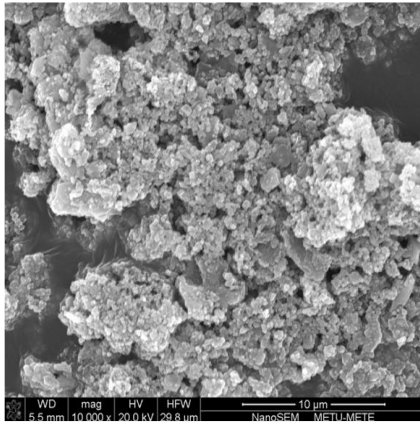
Figure 58 XRD results of leach residue obtained at the optimum HPAL conditions and of original ore sample.

Since the sharp quartz and goethite peaks were off the scene now, it was possible to comment on chromite existence. As can be seen in Figure 58, the chromite did not have any matching XRD peaks in leach residue. If chromite was in ore feed (at least in separate amounts) it would not be possible to miss its characteristic peaks since in the present case chromite was extracted at particularly low values (about or less than 1%). Then, the fed chromium amount (1.01%) should exist in leach residue as it was not so high in concentration in the PLS. There are two possibilities for chromium to incorporate with solid phases in leach residue. It can be either within the primary hematite phase or secondarily formed phase/s. Here again another two possibilities arise for chromium; the first one is being in alunite structure as a replacement for OH⁻ which was detailed in the literature and the second one is less likely to be within hematite structure as iron replacement. To observe which one occurred once again SEM examinations were utilized. Overall it was not possible for nickel losses to be primary unless hematite was containing nickel and was resilient. This distinction is quite hard since the distinction between primary and secondary hematite can be hard especially when the whole leach residue will be expectedly dominated by secondarily formed fine hematite clusters. Among the possible responsible secondary phases there were amorphous silica, alunite, and secondary hematite in the present study.

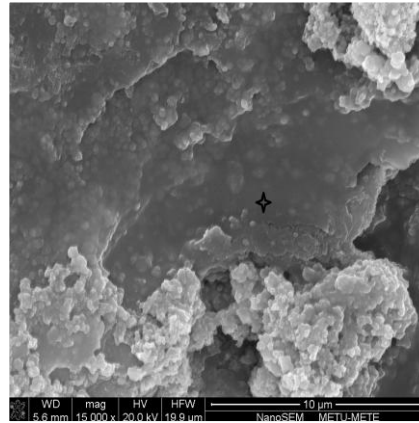
4.1.6.2. SEM Examination of Leach Residue

Since there were three phases in XRD pattern, it was rather easier to study the leach residue than run-of-mine ore. However, there was not any chance to select coarse particles as in the prior case since the leach residue particle size was dependent on the leaching process and most of the phases had been secondarily formed under these conditions. Since most of the minerals had disappeared, the leach residue was containing only the remnant quartz, amorphous silica, secondary and/or primary hematite and alunite particles. A general image taken from the ore sample can be seen in Figure 59. As can be seen in (a), the leach residue was actually made up of clusters of highly agglomerated particles. As it can be seen more closely in the right side (b) of the figure, there was some sort of contrast in regions of the pictures. On one side there existed a more bright fine particle clusters and on the other side there was a darker region that was formed by some sort of gelatinous matrix encapsulating spherical particles. The EDX results taken from the points approximately designated by stars showed that the gelatinous section was actually rich in silicon and oxygen only with some pure iron contribution. This meant that the dark material was probably amorphous silica that surrounded and held the bulk particles and even clusters (c) together and the iron contribution came from the spherical hematite particles it covered. As stated previously in the literature review, hematite does not welcome the silica gelation while its own dissolution-precipitation reactions are in progress. In fact that is what it was observed in both pictures. While the brighter region showed no trace of gelated silica, the dark region shows that gelation probably occurred after the hematite cluster ceased growing. Another point to mention, this gelatinous matrix was not found to contain any amount of nickel. In order not to generalize this with one spot, this gelatinous structure was searched in different regions of sample holder and fortunately it was observed that this matrix did not contain any nickel at all. Despite it is stated that amorphous silica is generally responsible for nickel losses, in this case it was not. The reason for this finding can be more than one. First, a slight chromate concentration could prevent the nickel adsorption in amorphous matrix as stated in the literature. Second, the excessive hematite precipitation might have retarded silica formation and have confined the silica precipitate. Third, as Lou et al. (2009) stated, high acidity can prevent amorphous silica adsorption of nickel due to more amount of free hydronium ion that can neutralize its surface.

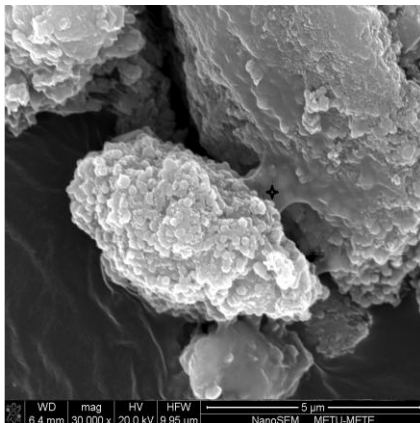
a) General view



b) Contrasting region



c) Canal formation



d) Notched Quartz

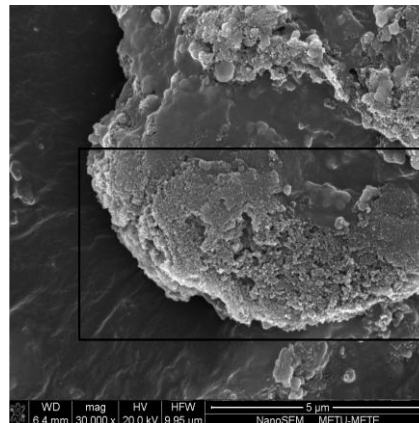


Figure 59 Several SEM views of leach residue obtained at the optimum conditions of HPAL.

Hence, in combination with all possibilities, the free acidity had the chance to recover itself to its equilibrium concentration during this prolonged period and might have instantly neutralized the lately formed negative charge of amorphous surface before nickel re-adsorption [120]. After all, the possibility that the amorphous silica may be responsible for nickel losses was out. Before moving on the search for other possibilities, it is worth to mention that, in Figure 59 (d), there was a squared region where it was found another silicon containing phase. As can be seen from the figure, these notched area belonged to primary silica which was the unleached part of remnant quartz. However, the notching effect of acid was evidence for the reduction in quartz peaks that showed one of the sources of the laterally formed amorphous matrix.

As explained before the hematite precipitation is rapid and ex-situ while goethite dissolves. Primarily precipitated hematite particles do not grow further but act as secondary nucleation sites. Due to this continuous pile up of simultaneously nucleating and growing hematite particles, the originally depleting goethite particle is rapidly surrounded and finally replaced by layers of growing hematite particles. In a similar manner, non-reacting particles will also be perfect heterogeneous nucleation sites for ferric iron and will probably be surrounded. Due these reasons, it was not possible to get deeper into particles to detect them especially when this gelatinous matrix was covering the clusters. Consequently, the existence of primary hematite was actually questionable. The only image that could

be obtained for a primary phase can be seen in Figure 60 (b) where EDX results showed that this particle was an iron oxide containing aluminum (5%), silicon (1%) and nickel (1.5%).

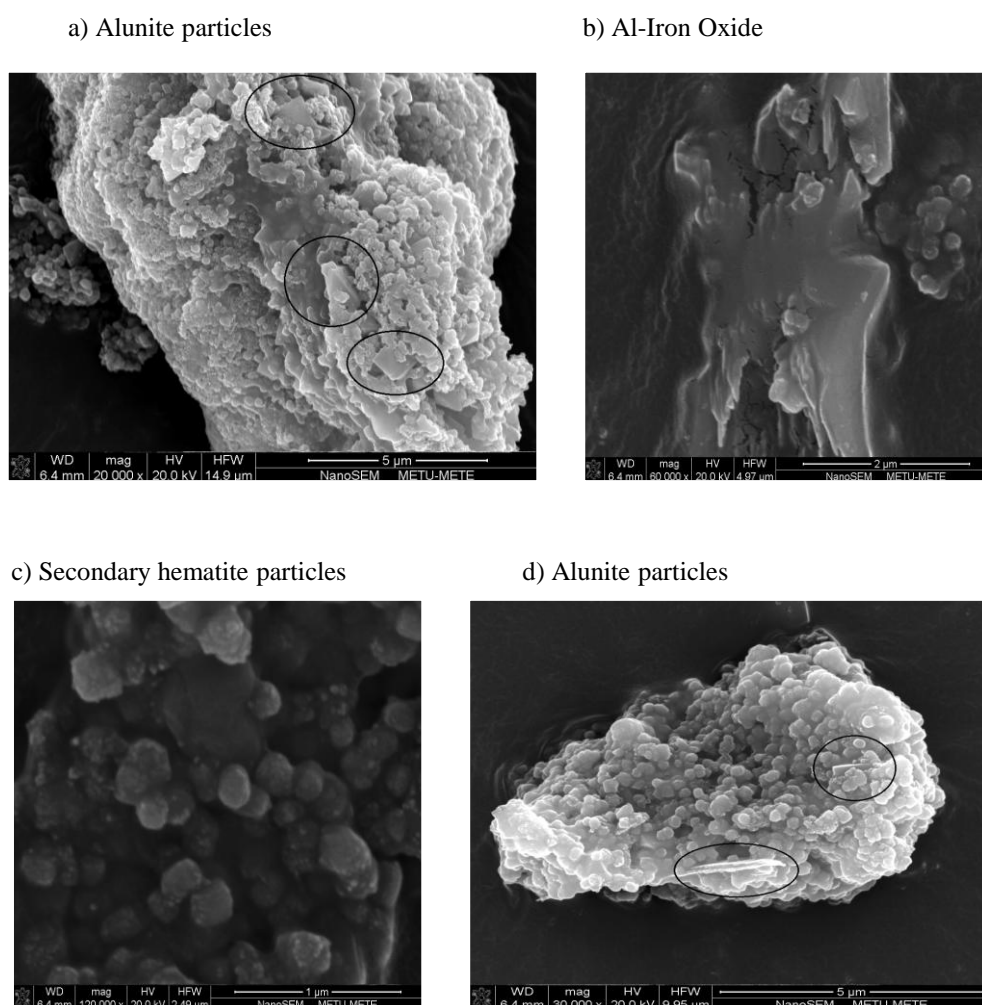


Figure 60 Primary and secondary hematite (b, c) and alunite (a, d) particles.

The absence of sulfur element ruled out the presence of alunite but silicon presence could be due to a thin layer of amorphous silica or less likely as a substitution. Hence this particle might represent the primary hematite containing significant nickel. The reason for its presence in the leach residue was probably due to aluminum substitution which could cause a problem as stated previously. In pictures (a) and (d) it can be seen that there were some cornered, coarse alunite particles that had intergrown with hematite particles. Alunite particles were also containing nickel together with some silicon and chromium as expected. However, it was hard to make a generalization whether it was the major phase responsible for total nickel loss since these particles were outnumbered by hematite and rarely found on surface of clusters. In parallel with the XRD results, alunite particles were also found to contain potassium rather than sodium or ammonium. As a last comment, picture (c) of the same figure indicated the only section that could be found for secondary hematite without any silica and alunite. In EDX of these particles also nickel was found in minor amounts (<0.5%). As a general comment for chromium, with increasing iron or aluminum in particles, chromium was also found to follow this trend but in a limited extent. Chromium content of particles never exceeded 1.5% in EDX results but almost always found in all of the secondary hematite and alunite particles. Co-precipitation of chromium with the secondary hematite and alunite might explain the results of HPAL experiments

where chromium extractions were always in minor amounts. In summary of the leach residue characterization, most of the primary phases that were goethite, asbolane, serpentine, smectite, calcite and dolomite, were completely leached during pressure acid leaching whereas it was not easy to comment on the primary hematite behavior. Amorphous silica was most likely not responsible for nickel losses whereas both alunite and secondary hematite were found to contain in varying amounts of nickel in their structure. Secondary hematite particles were not so willing to adsorb nickel in their structure unlike rare alunite particles.

4.2. Downstream Experiments

Once the optimum conditions of pressure leaching were determined and the pregnant leach solution stock was prepared with the composition given in Table 32 then, the downstream experiments were initiated in order to remove the impurity elements step by step and obtain a saleable intermediate product. The first step taken for that purpose was the first iron removal together with neutralization while the rest sequential process have been already described in the literature part. After each experimental step, once again the precipitation efficiencies were calculated based on solid composition analysis and checked with liquid based analysis and calculations. An example of this calculation is given in Appendix A. It is important to mention that the pH values given throughout the results of all downstream steps were terminal actual pH values at the so-called operational temperatures of the so-called steps. In other words, mentioned pH values were not the pH values that were read when the resultant new PLS cooled down to room temperature.

4.2.1. First Iron Removal Experiments

Although the iron extraction was close to 1% in HPAL, since the percentage of iron was so high in the feed that it still resulted in the presence of some iron in the pregnant leach solution (PLS) which was about 2300 ppm. On the other hand, the content of divalent iron was negligible to be concerned about so pre-cautions such as oxidation to trivalent iron was not taken. Fortunately, neither aluminum nor chromium was not that much extractable to contaminate the solution. However, probably due to the presence of very high magnesium in solution, free acidity (46.2 g/L) was very high almost close to the upper limit of 30-50 g/L. As it was confirmed by the results that will be given below, the reagent consumption as CaCO_3 powder was expectedly high due to simultaneous neutralization of this high amount of free acid.

According to Monhemius diagram, the first three removable impurity ions are trivalent iron, aluminum and chromium. However, due to supersaturation and adsorption, nickel and cobalt also precipitate together with these impurity ions. In the search for the optimum conditions, the main parameters studied were the terminal pH and leaching duration. Since it was planned to remove in this step, almost all of the iron and some of the aluminum with chromium, the optimum conditions were decided by the resultant iron concentration in the purified pregnant leach solution with tolerable nickel and cobalt losses not higher than 0.5%. It would be an extra benefit to remove as high aluminum and chromium as possible in this step since in the second iron removal the resultant precipitates would circulate in the process train due to high amount of nickel and cobalt contents in precipitates. Hence, the lower their concentration was in the solution feed prior to the second iron removal, the less they would accumulate in circulation. As a result of that, during deciding of the optimum conditions their concentrations should also be considered.

As the main driving force of precipitation reactions and also the most important parameter that dictates the required reagent consumption, the first parameter was pH to be studied. According to Willis (2007, 2008) 90°C and 120 minutes residence time are generally considered as the optimum conditions [67,70]. Hence, for the pH experiments, these fixed conditions were chosen. Iron precipitation commences at about pH=2.00 but in order to remove the desired amount of iron, precipitation with varying pH must be considered. Hence, it was decided to search the pH effect on precipitation efficiencies from 2.50 to 3.25 with 0.25 increments. The results obtained from this set of experiments are given in Figure 61.

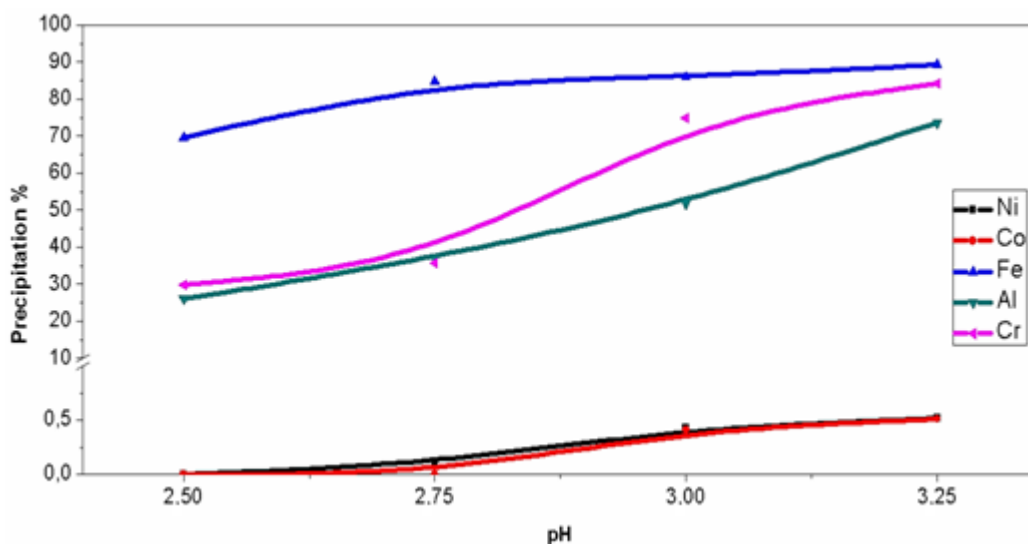


Figure 61 Precipitation of important metals with pH increase at the fixed conditions of 90°C and 120 minutes in FER 1.

As can be seen from Figure 61, nickel and cobalt behaved in the same manner with increasing pH. Valuable metal losses in this stage are non-recoverable since the huge precipitate amount of this stage could cause significant iron, aluminum and chromium circulation with pointless minor recovery of nickel and cobalt. As a result of that fact, both nickel and cobalt should be lost at the minimum amount in this waste product. On the other hand, even at the maximum pH value studied, the nickel and cobalt losses remained below 1% which was one of the most important targets to achieve. On the other hand, the iron precipitation started with about 65% at pH 2.5 and abruptly increased to about 85% with only 0.25 increases in pH after which it was not affected too much with further reagent additions. In studies of Seçen (2011) and Köse (2011), it was seen that increasing pH from 3.25 to 3.50 and 4.00 resulted in exponential increase in the nickel and cobalt losses. As can be seen in Figure 61, since it was already 0.52% and 0.51% for nickel and cobalt precipitations, respectively at pH=3.25, further increase in pH would probably exponentially increase the precipitation amounts of nickel and cobalt. This would certainly increase the nickel and cobalt losses that are unrecyclable. Hence, further increase in pH beyond 3.25 was not an option.

In each aluminum and chromium precipitation amount there was a continuous increase with pH increase which was unlike the case for iron. Initially low values of Al and Cr precipitation amounts at the lowest pH value showed an increase by 50% and 55%, respectively, from these initial values. This result is consistent with the findings of Agatzini-Leonardou and Oustadakis (2001) [121]. When Monhemius diagram is referred to for aluminum and chromium, it can be seen that their natural precipitation zones come after that for iron. On the other hand, the behavior of iron in the present study is quite unexpected. At first thought, it was suspected that divalent iron concentration was somehow responsible for this behavior but as it is given in Table 32; its concentration was too low for being a problem. It was believed that the reason for lower-than-expected iron precipitation could have been caused by the slow rate of initial homogenous nucleation or not so high enough iron concentration since in previously mentioned studies the utilized pregnant leach solutions were different in composition or state. Seçen (2011) has added leach residue to his batch composition in order to match the industrial MHP flowsheet and Köse (2010) had used a PLS stock obtained from atmospheric leaching that contained extremely high concentration of iron in his MHP study [73,94]. In the first study, the initially added leach residue particles were already very fine with large surface areas and created a perfect media for precipitation reactions. On the contrary to this study, in the present batch composition there were not any primary particles that could enhance the precipitation amounts. The secondary heterogeneous nucleation was only possible after some primary precipitates were created. As it will be mentioned in SEM images, these major primary particles were initially hydrated calcium sulfate particles that were produced during pH increment while neutralization of free

acid was ongoing. In the second study by Köse (2010), 38600 ppm of iron concentration was probably responsible for supersaturation of iron even at lower pH values which eventually resulted in 99% of iron removal at pH= 2.50. PLS of Seçen's (2011) study was containing 6658 ppm Fe prior to the first iron removal which was higher than that of PLS in this study. Despite this positive effect of leach residue, Seçen also could not increase the iron precipitation values above 90% even at pH=3.50. Hence it can be seen that the effect of supersaturation is more pronounced than the effect of heterogeneous nucleation. The reason for such a great difference caused by concentration can be explained by Monhemius diagram. As can be seen from the diagram, the lower the ion concentration is the more right the stability line shifts hence the higher is the pH for the ion to precipitate as hydroxide. In the present case, the initial iron concentration was 2231 ppm before first iron removal step and after the precipitation of iron by 86%, a small amount of remnant iron might have caused this shifting occurrence. The lower the concentration of remaining iron in solution, less sensitive is the iron to precipitate with small pH increments. However, these small increases in pH will certainly mean higher losses of Ni and Co to the precipitate during risky effort for further iron removal.

For the optimum pH value, it was decided to be 3.00 for this step. The reason why pH =3.00 instead of 3.25 was chosen as the optimum condition was due to less than 0.5% nickel and cobalt losses and this pH value was found to be more safer than the latter one which might cause beyond 1% losses if pH increment was not handled carefully. At both pH values the iron precipitation amounts were similar but it is obvious that higher pH will remove extra 20% aluminum and 10% chromium than lower one. However, for the sake of less riskier valuable metal losses and less reagent consumption, these extra values were not taken into consideration. Yet it is certainly possible to choose 3.25 as the optimum pH condition depending on the targets of the hypothetical HPAL plant on Çaldağ lateritic nickel ore. Then, it was decided to find out whether changing residence time could be helpful to remove more iron at lower pH. In order to observe that an additional experiment was conducted at pH=3.00 and 3 hours of residence time at 90°C. As can be seen from Table 34, the iron precipitation did not differ at all with 1 hour extra duration whereas a slight increase in nickel loss occurred. This result directly indicated that the only way of increasing iron precipitation was to increase pH as described above. Hence it is pointless to both decrease the capacity of reaction tanks with extra one hour occupation by slurry and also cause slight but important nickel loss. Consequently, two hours of precipitation duration was chosen as the optimum condition. It is also possible to utilize precipitation temperatures higher than 90°C in order to increase the reaction kinetics and also decrease the viscosity of slurry for better agitation.

Table 34 Effect of additional 1 hour residence time on nickel and iron precipitations in FER 1.

Element	Precipitation % (t= 120 minutes)	Precipitation % (t= 180 minutes)
Ni	0.43	0.60
Fe	86.0	86.0

This additional increase will increase the interactions between reagent and the ions and may help the removal efficiency. However, as summarized in the literature review, generally temperatures beyond 90°C are not welcome by HPAL plants since it will cause evaporation losses and result in higher operational costs. As a result of these discussions, the optimum condition for this step was chosen as in Table 35 with respect to precipitation efficiencies. In the same table it is possible to observe the composition changes between feed solution and product solution of the first iron removal step.

Table 35 The optimum conditions, precipitation efficiencies and compositional changes of FER 1 step.

Optimum Conditions: pH=3.00, T= 90°C, t=120 minutes		Solution Compositions	
Metals	Precipitation %	Feed Solution (ppm)	Product Solution (ppm)
Ni	0.43	4564	4541
Co	0.41	294	268
Fe	86.0	2231	285
Al	51.8	3296	1450
Cr	74.9	64.8	14.8
Mg	0.66	5460	4952
Mn	0.41	1150	1045
Cu	12.9	18.6	14.8
Zn	0.07	104	97.4
Si	59.4	364	135
Sc	86.4	24.1	3.0
Free Acid (g/L)	-	46.2	2.35
ORP (mV)	-	443	271

As can be seen from Table 35, there is a significant drop in the free acidity and iron concentration in PLS after the first iron removal step. During the iron removal step, a significant portion of free acid was also neutralized by the reactions between CaCO_3 and H_2SO_4 where carbon dioxide and hydrated calcium sulfate phases were formed. Carbon dioxide generally left the system by bubble formation while calcium sulfate phase crystallized during precipitation duration and acted as heterogeneous nucleation sites. Hence, by allowing sufficient time it was possible to reduce both acidity and iron content of solution by the first iron removal step with less than 0.5% valuable metal losses. Expectedly both manganese and magnesium precipitations were negligible since the terminal pH level of the solution was far from their precipitation zones. Moreover, it was possible to remove a small portion of copper and zinc by this step. As can be seen both were in very low concentrations and were expected to decrease further during the second iron removal step.

The precipitation of scandium is also included to Table 35. About 86% of scandium already present in low concentration precipitated possibly together with iron or as its own hydroxide and only 3 ppm was left in PLS. Hence, the suggestion to separate the solid and liquid parts prior to the first iron removal was necessary in order not to lose valuable amount of scandium to highly iron containing solid waste.

During the first iron removal step, it is important to calculate the consumed reagent amount since it is one of the operational costs even though calcium carbonate is cheaper than the rest of the possible reagents. At the optimum conditions, the consumption of CaCO_3 slurry was 26.1 cc (25% weight/volume) which corresponds to 6.53 g CaCO_3 per 100 cc PLS or 163.25 kg CaCO_3 per 1 ton of dry ore. It is important to note that 4.47 g per 100 cc PLS of this consumption was due to reduction of 46.2 g/L free acid to 2.35 g/L that occurred during neutralization reaction as follows:



As can be seen more than half of the total reagent consumption was due to the partial neutralization of excessive residual free acid. In Figure 62, the increase in the pH with increase in CaCO_3 addition can be seen. The curve follows an exponential pattern whose slope is initially small. As can be seen, after about pH=2.00 where theoretically iron commences to precipitate, pH increase is almost directly proportional to the added slurry amount. However, this does not necessarily mean that the precipitation reactions are not in progress prior to that pH value is reached. But it is possible that the added reagent is more efficiently used by remnant impurity metals as the solution is being neutralized.

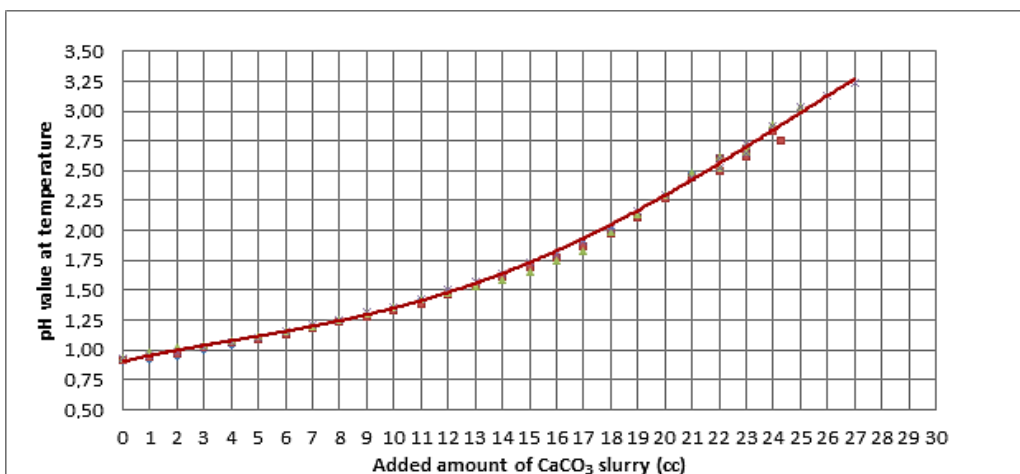


Figure 62 pH variation with constant rate of 1000 µl per 5 minutes CaCO₃ addition at 90 °C in FER 1.

Another point to mention is the reproducibility of the experiments at the optimum conditions. During a stock preparation for the second iron removal step, nine experiments were conducted and very close results were obtained as tabulated in Table 36. In Chapter 3, it was mentioned that the rate of addition was 1000µl per 5 minutes for 100 ml input PLS feed. For the stock preparation experiments, this rate was multiplied by 3.5 for 350 cc input feed. Expectedly, the resultant dry leach residue and other important parameters were approximately multiplied by the same factor. As can be seen, even under the laboratory conditions there might be small fluctuations probably due to addition mode. These fluctuations will certainly be in a larger tolerance band in industrial applications due to greater amount of feeds into reaction tanks. Hence, this was the reason for choosing a safer pH value of 3.00 as the optimum condition.

Table 36 Reproducibility of the optimum condition experiments of FER 1 step (wt.%).

Element	Test 1	Test 2	Test 3	Test 4	Test 5	Test 6	Test 7	Test 8	Test 9
Ni	0.40	0.36	0.34	0.38	0.66	0.39	0.34	0.76	0.60
Fe	86.1	85.5	86.2	86.6	86.8	84.8	84.9	86.9	87.1

4.2.1.1. Characterization of Precipitates of First Iron Removal

Although the nickel and cobalt losses were negligibly low at this step, the characterization of solid residues can be important in determining the settling characteristics of the solid phases. Since the resultant residue was enormous in amount of hydrated calcium sulfate crystals, it offered better settling characteristics since limestone was chosen as the precipitating reagent. Moreover, the resultant product was also of concern for the environmental standards especially for iron phases as discussed in the previous sections where hematite, jarosite and goethite were compared. Chemical analysis result of precipitate obtained at the optimum conditions is given in Table 37.

Table 37 Chemical composition of precipitate obtained at the optimum conditions of FER 1 step.

Element	Weight %	Element	Weight %
Ni	0.032	Mn	0.008
Co	0.002	Cu	0.004
Fe	3.15	Zn	0.0001
Al	2.80	Ca	27.4
Cr	0.08	Sc	0.0159
Mg	0.059	Si	0.36

Iron removal has been an important issue especially in zinc industry so most of the proposed methods were modified for the purification of pregnant leach solutions obtained by AL or HPAL of nickel laterite ores and were studied extensively. These methods are namely, jarosite, goethite, hematite processes and introduce different parameters for their own conditions [122]. In Figure 63, the stability regions of respective iron phases in iron-water system with 0.5M iron sulfate concentration is given with respect to pH-T [123]. Under the circumstances of the so-called optimum conditions, the stability region indicates that the soluble iron is expected to precipitate as goethite in this step (as well as following second iron removal step) with the reaction as follows:



However, Köse (2011) reported that apart from goethite phase, additionally hematite may also be observed in precipitate which is formed by the following reaction [73]:



As can be seen in Figure 64, the XRD result of precipitate sample obtained at the optimum conditions showed that both of the iron phases co-existed in minor amounts. According to the chemical analysis of this solid, iron content was actually not so high due to its relatively low levels in input PLS. A similar situation was also valid for aluminum where a similar reaction resulted in the formation of aluminum hydroxide phase which was bayerite. Since it had lower concentration its precipitation amount was also in minor amounts. As can be seen in Figure 64, the domination of hydrated calcium sulfate phase which was bassanite created a difficulty to detect these minor amounts by suppressing the characteristic peaks of these minor phases. In order to visualize the situation, the SEM image taken at 1000x magnification can be seen in Figure 65.

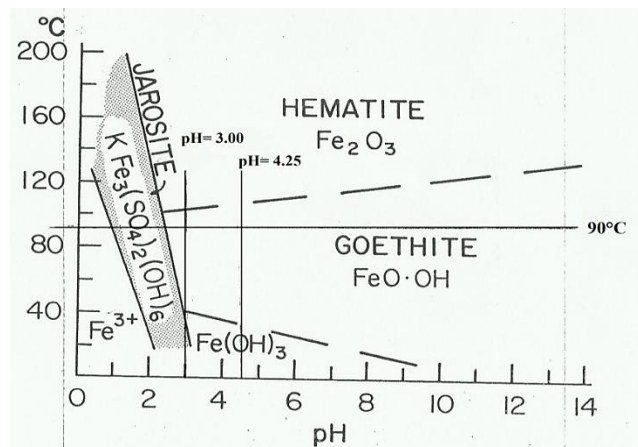


Figure 63 pH vs. temperature stability diagram for iron-water system in 0.5 M $\text{Fe}_2(\text{SO}_4)_3$ solution [123].

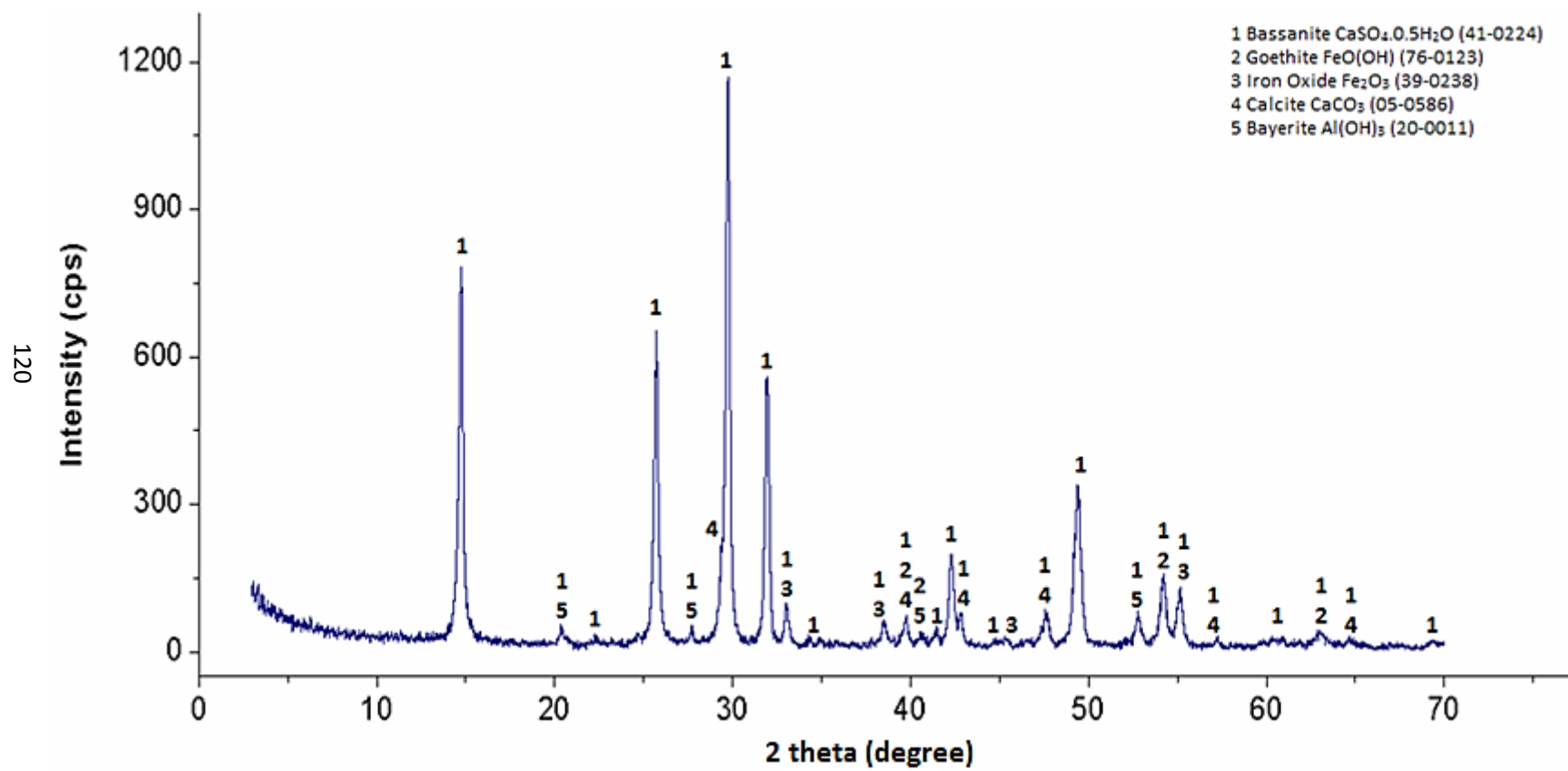


Figure 64 XRD result of the precipitate sample obtained at the optimum conditions of FER 1 step.

Expectedly, the crystalline bassanite needles covered all over the sample holder. In several junction points of these needles, the precipitates of iron, silicon and aluminum phases settled as an adhesive. On the other hand, none of the chromium, nickel, cobalt, manganese or other negligibly low concentrations in precipitate was found as a distinctive individual phase. Since the nickel and cobalt were extremely low in these precipitates, it was hard to comment on the precipitating phases. According to Cheng et al. (2009), the nickel losses occur by two mechanisms: adsorption or co-precipitation by chemical or physical bonding. It was difficult to state whether nickel was captured by the lattices of solid phases or adsorbed by the surface of these particles or precipitated in a separate hydroxide form. Fe:Ni ratio prior to removal has an important effect on nickel loss. Higher this ratio, higher is the nickel losses and more sensitive to pH change of the solution [124]. Although it is not so clear from the XRD, the characteristic peak at around 20° might once more be a representative for amorphous silica formation. Moreover, the XRD result showed that solid waste product also included calcite peaks probably due to unreacted limestone particles. As can be seen in Figure 65, it was possible to detect some of these calcite particles that were a muddy agglomerate of several fine limestone particles formed due to initially being in slurry form.

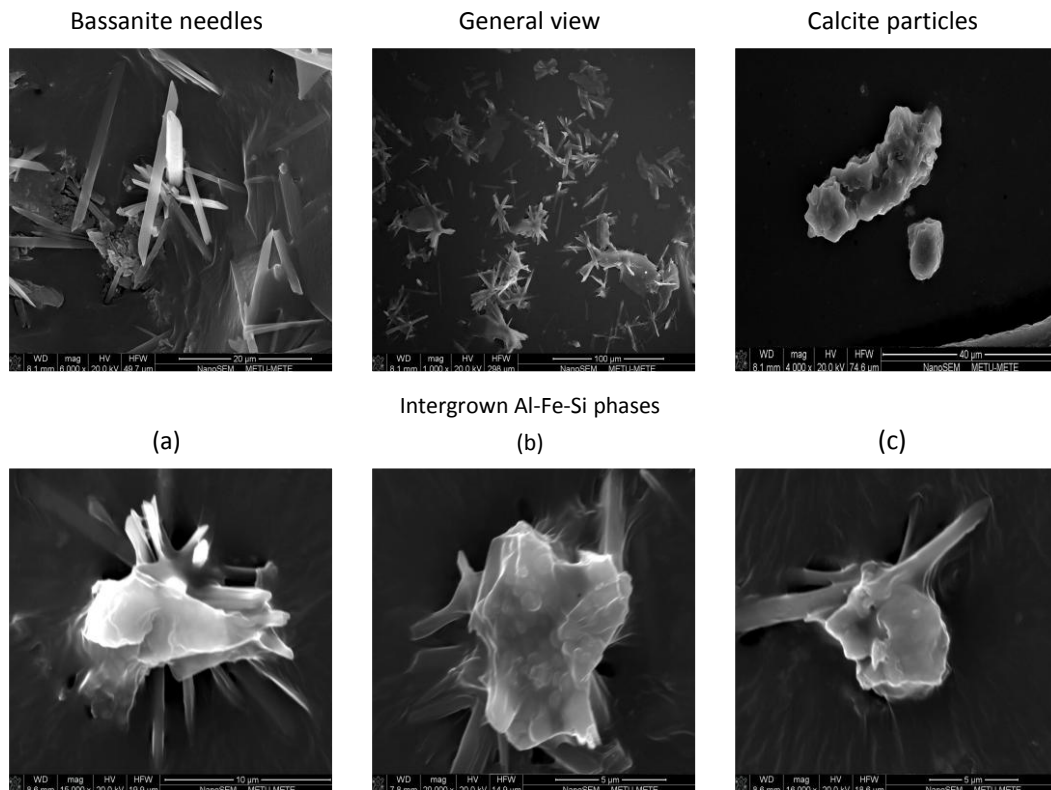


Figure 65 SEM images of several phases in the precipitate sample of FER 1 step at the optimum conditions.

The situation of particles that were found at the junction points of bassanite needles were quite complex especially when the behavior of iron was considered. Some authors described the precipitation route of iron oxides and hydroxides starting with the formation of an active amorphous iron hydroxide, $\text{Fe}(\text{OH})_3$, which transforms into inactive form by aging. Further transformation of this inactive amorphous phase results in goethite, hematite or jarosite formations as seen in Figure 63. Jarosite formation is favored at < 3 pH and more than 4 g/L ferric iron concentrations whereas at higher pH levels, there is a competition between goethite and hematite [125][51]. Cudennec and Lecerf (2006) disagreed on that initially known $\text{Fe}(\text{OH})_3$ which was misused for ferrihydrite for a long

time period but the latest researches showed that the transformation of goethite and hematite starts from ferrihydrite transformation rather than iron hydroxide [126]. Dutrizac (1980) described that despite the stable phase in Figure 63 is goethite, at certain circumstances hematite can be slightly more stable due to thermodynamics. This might explain the reason why goethite and hematite commonly precipitated in several cases including the present study. He described that goethite stability is dependent on the morphology of both goethite and hematite. If hematite is finely divided and goethite is coarsely crystalline, decrease in size of goethite particles will favor goethite stability. However, if goethite is also finely divided then hematite also increases in stability with decrease in particle size. Since initial particles are in very fine form then goethite can only be a metastable phase which is created due to kinetic barriers ahead of hematite formation [127]. Wang et al. (2011, 2013), described a more complicated situation. In his literature review for iron precipitation, he stated that in goethite process there may have been other reported phases which were hematite (α -Fe₂O₃), lepidocrocite (γ -FeOOH), akagenite (β -FeOOH), maghemite (γ -Fe₂O₃) and poorly crystalline phases that were later named as ferrihydrite and/or schwertmannite rather than conventional goethite (α -FeOOH). It was reported that these amorphous phases later transformed into more stable and crystalline goethite and/or hematite with increase in temperature or duration. Due to their lack of order in their structure, they might exist without any signature on XRD data of precipitates. In order to remove the domination of gypsum they used a specialized technique in which precipitates were washed off by a complex solution for gypsum removal and subjected to several characterization techniques after that treatment [128,129].

In this study the complex solution treatment was not done but SEM examination was utilized to observe whether these so-called iron phases could be differentiated. As can be seen in Figure 65 (a) and (b), there were some spherical phases within the transparent gelatinous matrix. This formation resembled the situation that was discussed in the leach residue characterization of the HPAL process. EDX results taken from the lower darker region of (a) showed that this region was dominated by 50-55% iron while the following contaminating elements were aluminum and silicon with about less than 10%. This situation was quite interesting. Since the morphology of particle resembled that of fine hematite and composition resembled aluminum substituted goethite with amorphous silica coverage; it was hard to comment whether these spherical particles were goethite or hematite. In central region of section (b), EDX results showed that the darker region was formed by aluminum with no trace of silicon but minor iron, calcium and sulfur contributions. As can be seen, this region could represent bayerite with background bassanite and iron phase contribution. However, in section (a) there was a brighter section atop of this combination. EDX result of that section showed aluminum-silicon domination with small calcium, sulfur and iron incorporation. On the other hand it was aluminum and silicon with minor calcium and sulfur for the case of (c). Hence the former case in section (a) was more probably hematite particles that were intergrown with little bayerite and amorphous silica. In correlation with the XRD data, the darker regions were generally representing aluminum domination whereas brighter regions represented aluminum-silicon domination. Spherical particles were most probably hematite particles while gelatinous matrix might have included very fine needles of goethite that could not be observed by SEM and intergrown with bayerite and/or amorphous silica. Overall, due to extremely fine precipitates and perfectly crystalline bassanite needles, settling behavior of the overall precipitate was quite good and easily filterable for that reason.

4.2.2. Second Iron Removal Experiments

Although the pregnant leach solution stock produced after the first iron removal stage was mostly purified from iron contamination there were still intolerable concentrations of iron together with chromium and aluminum that had to be removed prior to mixed hydroxide precipitate production. As mentioned previously, trace amounts (<0.5 wt %) of aluminum can be extremely problematic during ammoniacal leaching of MHP. That is because aluminum results an insoluble phase formation that can surround nickel and cobalt precipitates like a core shell and prevent the release of these valuable portion to the solution. Since chromium concentration was lowered to very small values, it was expected to be not so problematic. While these remnant impurities were removed as precipitates into solid product, nickel and cobalt concentrations would also experience a reduction which would be higher than those observed in the first iron removal stage. Since the product weight was typically about 10% of previously created solid waste of the first iron removal, the circulation of solid product of this step back to recycle leach unit was possible. As long as nickel and cobalt losses were not in

extreme amount (less than 10% precipitation), the optimum conditions are generally dependent on the composition of resultant new solution for iron, chromium and aluminum. Additionally, as an extra benefit, the higher precipitation values that might be offered by these optimum conditions were also important for copper and zinc concentrations. Although, this stage was not expected to completely remove these two contaminants, the more they were removed the better would be the quality of intermediate precipitate product.

As in the previous step, the first studied parameter was terminal pH of solution at a fixed temperature. Manipulation of pH was in the range of 4.00 to 5.00 with 0.25 increments. In order to determine the other fixed conditions literature was reviewed. According to Willis (2007, 2012), a temperature range between 70°C and 90°C, a total residence time between 60 and 120 minutes are generally utilized as the optimum conditions for this step [6,67]. In order to lower temperature to its lowest value in the above mentioned range, the residence time was increased to 3 hours since the remnant iron concentration was relatively high that might not be removed to the desired levels due to low precipitation achieved in the first iron removal. For the desired levels to be achieved, it was somehow inevitable for the optimum condition to provide at least 95% of iron precipitation for that step. It was also possible to reverse the situation since temperature increases would cause faster reaction kinetics that would shorten the necessary residence time.

As can be seen in Figure 66, the increasing pH expectedly increased the precipitation of all important metals in this step. Actually chromium and aluminum were already almost completely removed at the lowest pH as seen in this figure. However, in order to pass to the desired precipitation zone of iron, at least pH=4.50 should be obtained by limestone addition. Although nickel and cobalt losses below that pH level were negligibly low, iron, copper and zinc removals were not so satisfactory. On the other hand, it was obvious that beyond pH 4.50 dramatic increases in nickel and cobalt losses passed the 10% maximum loss limit even though other impurities such as copper and zinc were also noticeably removed. According to Zhu et al. (2010), zinc and valuable metals behave in the same manner with pH increment up to 6.50 whereas copper is more sensitive to pH in that range and completely removed before that value which confirms the results obtained here [130].

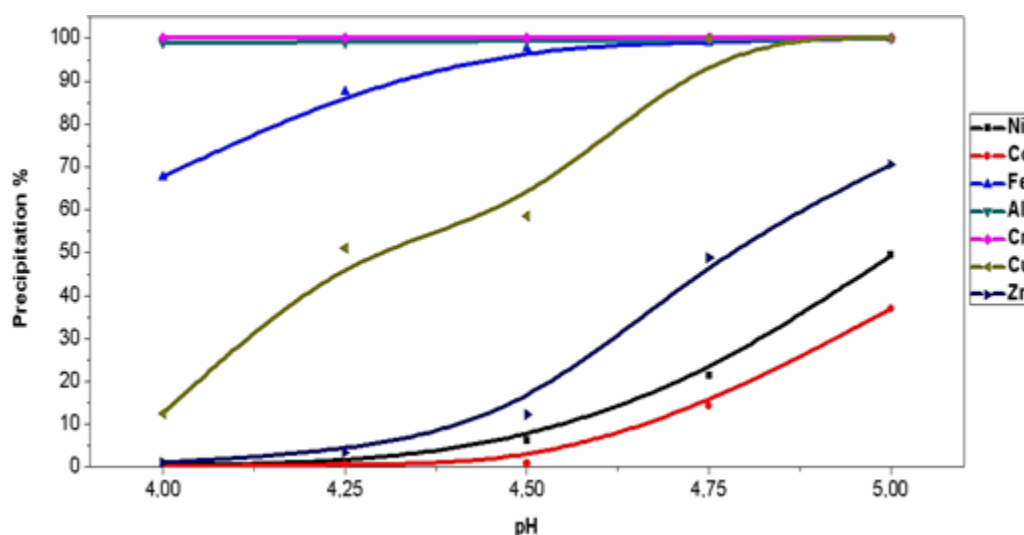


Figure 66 Effect of pH on precipitation of several metals in FER 2 step.

As can be seen in Figure 66, the nickel and cobalt precipitation values were 6.32 % and 0.95% at pH=4.50 which increased with just 0.25 pH increment to 21.35% and 14.32%, respectively. Since most of the free acid had been neutralized in the previous step, its buffering effect was not present here. Besides variation in the amounts of impurity levels of iron, aluminum, etc., inhibited a perfect pH control of the solution during reagent addition. So this step was somehow a transition zone

between the first iron removal and mixed hydroxide precipitation steps. Excessive precipitation reactions in the mixed hydroxide step and neutralization reactions in the first iron removal enabled a more controllable pH increment with reagent additions. Consequently, safety bands for nickel and cobalt losses were believed to be more important for second iron removal step. As a result a pH value equal to 4.50 was chosen as the optimum condition for the second iron removal step. After observing that pH=4.5 was adequate for successful iron removal in 3 hours, it was decided to see whether the residence time could be shortened still at 70°C. The results are given as in Figure 67. As can be seen neither 1 hour nor 2 hours residence time was not long enough for acceptable iron precipitation probably due to insufficient reaction rates at 70°C which was relatively low. Although it was not studied in this thesis, Seçen (2011) showed that by increasing temperature from 70°C to 90°C at constant pH=4.25 within 1 hour duration, it was possible to remove iron by 99% with 15% nickel and 7% cobalt precipitation losses [94]. Similar dramatic increases by the same temperature change were reported in the literature [73]. Hence, the increasing of temperature at constant pH level would probably mean further nickel and cobalt losses in our case. Overall, in order to obtain a pregnant leach solution with the least possible nickel and cobalt losses and the maximum possible iron, copper and zinc removal, it was decided to choose pH=4.50, 3 hours of duration and 70°C temperature. The remarkable differences in nickel and cobalt losses between this study and the above mentioned studies are due the initial Fe:Ni and Fe:Co ratios (also valid for other precipitating impurities). The higher are these ratios; it is more likely for nickel and cobalt to be absorbed by these impurities.

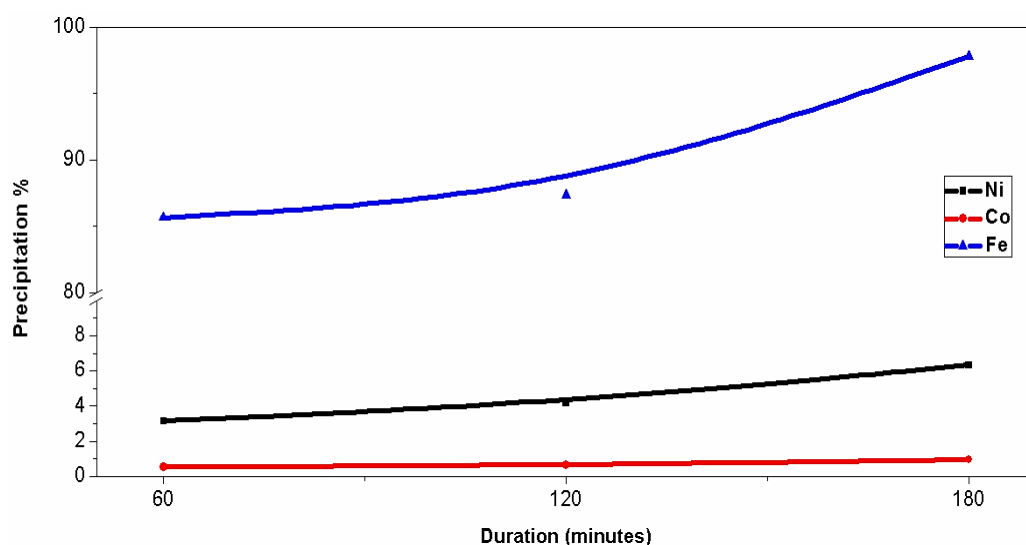


Figure 67 Effect of precipitation duration on nickel, cobalt and iron precipitations in FER 2 step.

As in the previous step, the consumption of limestone slurry is important but it was much less than that was consumed by feed solution in the first iron removal. Due to the reasons of more difficult pH control described above and as mentioned previously in Chapter 3, the slurry composition of calcium carbonate was 12.5% (weight/volume). At the optimum conditions the added slurry amount was 6.35 cc per 100 cc input PLS which corresponded to 0.794 g CaCO₃ per 100 cc input PLS or 21.68 kg CaCO₃ per ton of dry ore reagent consumption. It is important to note that 0.240 g CaCO₃ per 100 cc PLS reagent consumption was due to complete neutralization of remnant 2.35 g/L free acid. Neutralization reaction was given previously by Rx 4.2.

In Table 38, the precipitation values of several important metals and their compositional changes before and after the second iron removal step are summarized. As can be seen from the mentioned table, the majority of iron, aluminum and copper were removed such that remaining concentrations of these metals were below the desired 10 ppm level. As expected, chromium was completely precipitated but the residual zinc concentration was not so low after this step. Since this step was the

last one in order to purify the solution prior to the mixed hydroxide precipitation, all of the impurity concentrations should be reduced to very low values otherwise the residual iron, aluminum, copper and zinc would almost completely co-precipitate with nickel and cobalt during MHP 1.

Table 38 The optimum conditions, precipitation efficiencies and compositional changes for FER 2 step.

Optimum Conditions: pH=4.50, T= 70°C, t=180 minutes		Solution Compositions	
Metals	Precipitation %	Feed Solution (ppm)	Product Solution (ppm)
Ni	6.3	4541	3738
Co	0.95	268	255
Fe	97.8	285	6.0
Al	99.3	1450	9.2
Cr	100	14.8	0
Mg	3.08	4952	4381
Mn	0.80	1045	996
Cu	58.6	14.8	5.9
Zn	12.2	97.4	82.1
Free Acid (g/L)	-	2.35	-
ORP (mV)	-	271	210

4.2.2.1. Characterization of Precipitates of Second Iron Removal

As a follow-up stage of the iron removal series, the resultant precipitates of second iron removal were not expected to differ much from that those obtained in the initial step since the major impurities to be precipitated were still those considered in the first iron removal step. As can be seen in Table 39, the chemical composition of precipitate had a similar composition of the previous one. The only exceptions were the increased content of nickel and aluminum. Actually, aluminum was now one of the dominating elements in the precipitates due to its almost complete removal as solid phase. Nickel on the other hand precipitated at a remarkable percentage. Regarding these differences, it was expected that at least one distinguishable phase for each element could be detectable in the XRD results. Nickel was found as theophrastrite which is simply nickel hydroxide as can be seen in Figure 68. This phase was actually present in minor amounts. However, the expectation for aluminum was not actualized. Indeed once again the only phase containing aluminum was only bayerite which is simple aluminum hydroxide previously found in minor amounts within the first iron removal precipitates. There was no possibility of this minor amount of bayerite to bear the precipitated amount of aluminum by itself. Then, the question of where the rest of the aluminum went needed to be answered. In order to answer this question, SEM examinations were made on the precipitates obtained under the optimum conditions of second iron removal.

Table 39 Chemical analysis of precipitate obtained at the optimum conditions of FER 2 step.

Element	Weight %	Element	Weight %
Ni	3.37	Mg	0.25
Co	0.03	Mn	0.001
Fe	3.28	Cu	0.10
Al	16.95	Zn	0.14
Cr	0.17		

It is important to mention that despite almost complete neutralization in the first iron removal, the domination by bassanite was still valid for the second step. Remnant 2.35 g/L free acid consumed a significant amount of added slurry (30% of total added dry CaCO_3) and resulted in a significant amount of hydrated calcium sulfate formation. However, in several cases of SEM examinations, it was observed that rather than previously seen needle-like bassanite formation, the resultant bassanite particles of this step were thicker, bulkier and in quadratic or rod-like shapes which can be seen in Figure 69. It was interesting to see that unlike the case before, agglomerates of particles of precipitated phases were not stuck with these rods/quadrangles all the time. Instead there was some sort of pile-up of particles just like the hematite growth in HPAL leach residue. This might be probably due that even during reagent addition; impurity metals caught the same pace with the acid neutralization for the first time at that step. Regarding the pH increment figure shown in previous section, the pH increment of this step was more rapid due to less interference of sulfuric acid neutralization, even though it was harder to control. As a result of that fact, as the primarily nucleated bassanite particles were being created while homogeneously nucleating and growing particles were also precipitating at the same time. Consequently, the direct interaction of impurities with calcium carbonate particles resulted in surrounding of these reagent particles and externally growing of pile-up precipitate structure. This homogenous growth process resulted in extremely fine particles. As can be seen even the agglomerates were in very small sizes. On the other hand, as a result of homogenous nucleation, the co-precipitation and growth of several phases were more severe than the previous situation. Search for nickel phase was the primary target while the above mentioned question about aluminum was the other important point of search. Meanwhile, whether these precipitates were in hydroxide or sulfate forms was another point of search.

In SEM studies, it was seen that there existed a phase that was composed of only aluminum and sulfur with oxygen together with minor amounts (<10% wt %) of nickel, iron, silicon and calcium. Since hydrogen is not detectable with SEM it might or might not contain hydroxide part. According to the chemical analysis of precipitates, 16.5% aluminum was found in precipitates which made it one of the dominating elements. Despite this domination in chemical analysis, a distinctive phase of aluminum with dominating sharp peaks like for bassanite could not be seen in XRD result. However, it was obvious that there was a certain amount of noise in background of XRD result. Several EDX results taken from the prepared sample did not come up with a noticeable silicon content which eliminated the existence of amorphous silica. Besides, the remnant silicon content of input solution of that step was poor in concentration. Actually, the only silicon contribution was along with the aluminum-sulfur phase mixture as can be seen in Figure 69. It is believed that this amorphous contribution was unaccounted for so-called aluminum-sulfur phase.

Despite all trials for several Al-S containing phases (including oxides, hydroxide, oxyhydroxides, sulfates, etc.) in XRD data, none has been found as a match including several types of alunite, aluminite, alunogen or jurbanite. The case of bassanite domination was not helpful either. Nonetheless it was certain that there existed an unknown phase of aluminum with sulfur that was not possible to identify by the help of XRD. Under these circumstances, a clear determination of any iron or nickel phases by SEM was not possible due to domination of so-called amorphous phase on agglomerates. However, as a useful property of nickel phase, it was somehow possible to find a correlation between nickel and the agglomerates. As can be followed in the next figure, brighter was the precipitate agglomerates, more was the nickel + iron contribution within them. This behavior was probably due to charging of nickel hydroxide under electron beam.

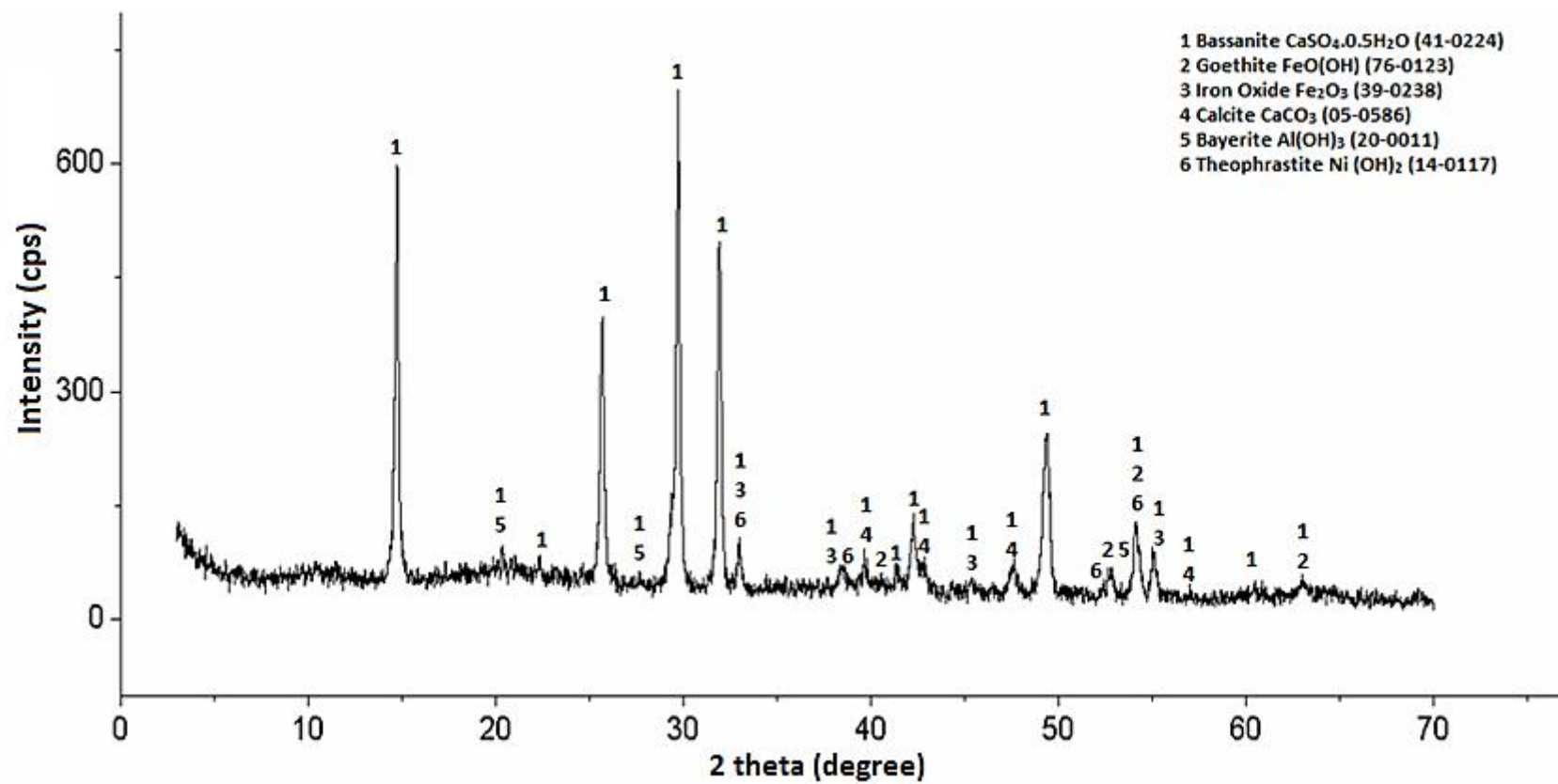
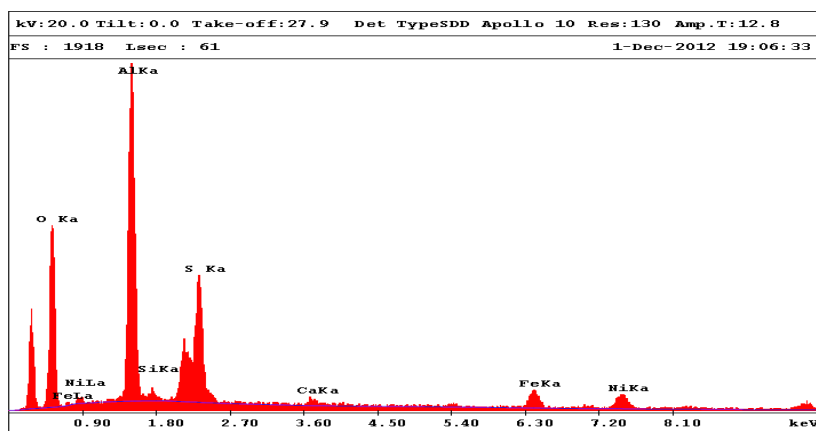
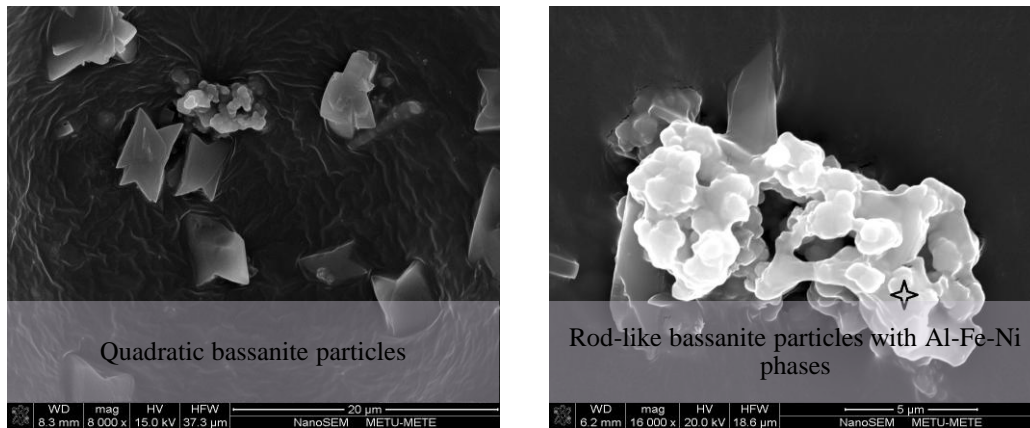


Figure 68 XRD result of precipitates obtained at the optimum conditions of FER 2.



EDX result of the designated point

Figure 69 SEM images of bassanite particles and agglomerates of phase mixture in FER 2.

According to Zhu et al. (2010), there are two chemical forms of nickel and cobalt to co-exist in precipitates that are obtained below and above pH=5.7. They can either be precipitated as their respective hydroxides by co-precipitation or as respective sulfates by adsorption. As they stated, since pH levels below 5.7 are far from their normal precipitation values and co-precipitation pH level of single metal in a solution is higher than in a polymetallic solution, it is more probable for nickel and cobalt to be adsorbed as sulfates within the precipitates [130]. Hence, negligible nickel and cobalt losses in the first iron removal were probably adsorption in sulfate forms whereas in this second stage, where 4.5 was the optimum pH, the situation was not so clear. Which phase was predominant over the other was changeable. According to their statistics, at pH=4.5 about 25% of total Ni/Co precipitates were in hydroxide form whereas the rest were in sulfate form. Overall, it was probable that a majority of nickel losses could be due to adsorption of so-called aluminum-sulfur phase. Actually, when Figure 70 is studied, it can be seen that there was a distinctive relationship between iron-nickel-chromium-sulfur contents of the agglomerates.

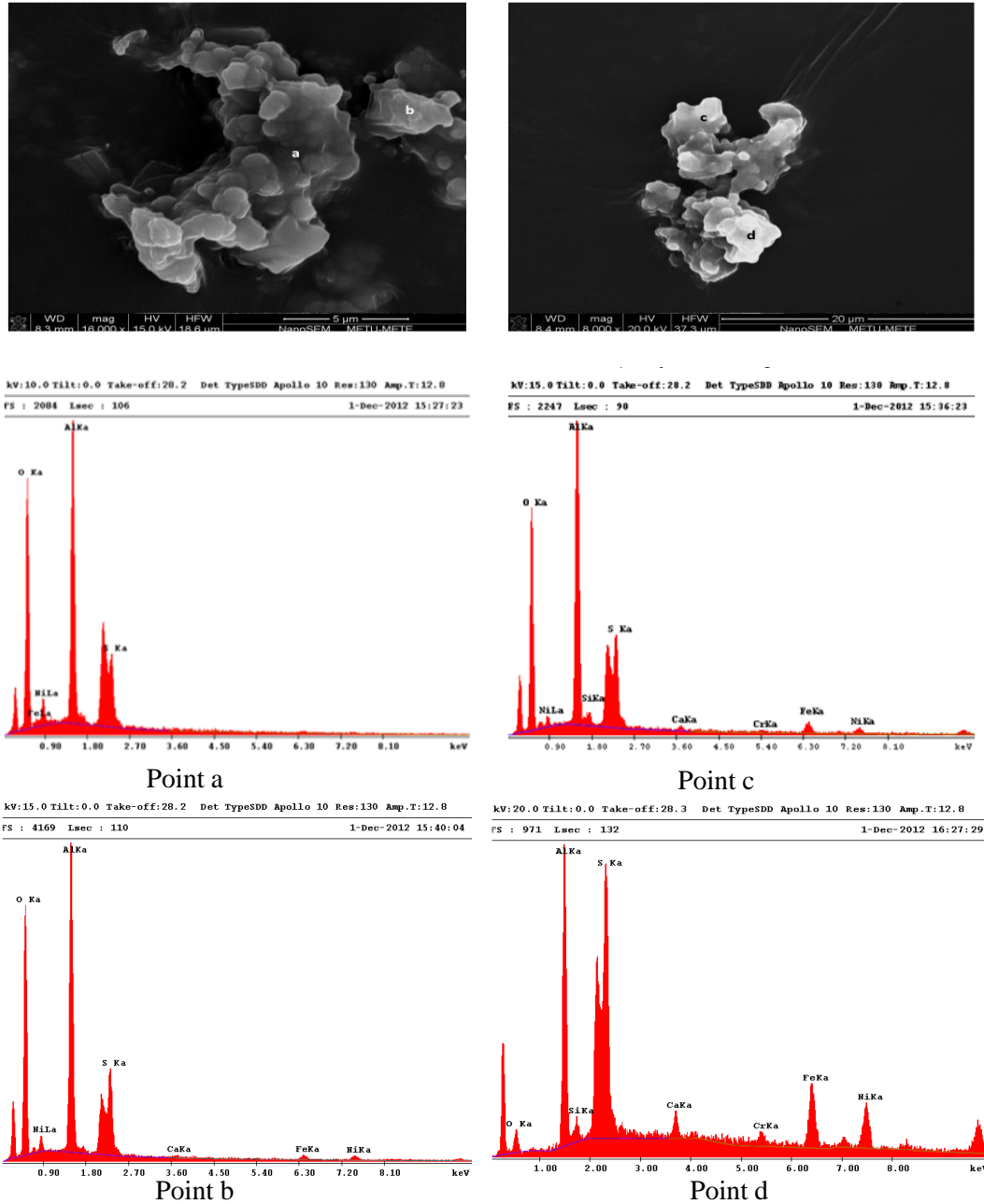
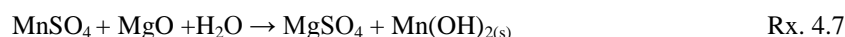
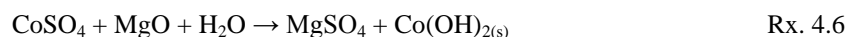


Figure 70 SEM images and EDX results of two different agglomerates of FER 2.

All of these increased together in the same way. Hence it seems nickel was not only precipitated as simple hydroxide but also adsorbed by the amorphous sulfate phase. Moreover, it was probable for nickel and cobalt to be adsorbed by iron precipitates. White et al. (2006) mentioned the possibility of nickel adsorption by goethite during precipitation but cobalt is much less sensitive to co-precipitation. That is because of the fact that nickel co-precipitation is more than simple anion-hydroxide precipitation system such that it is also more probable to be absorbed by surrounding solid phases which is not valid for cobalt [131]. This might explain the reason why cobalt losses in both steps were well below the precipitation losses of nickel.

4.2.3. First Mixed Hydroxide Precipitation Experiments

After the majority of impurities were precipitated by the first and second iron removal, it was aimed to produce a saleable quality intermediate product by increasing the terminal pH level of solution to the range between 7.0 and 7.20 with 0.10 increments. Now that the solution could be considered as a quaternary system including nickel, cobalt, manganese and magnesium (excluding zinc and other low-concentration impurities) it was possible to estimate the reagent consumption by the theoretical calculations based on the reaction series given below since magnesium was not expected to experience a significant precipitation within that pH range.



During these calculations it was assumed that all nickel, cobalt and manganese in feed solution would precipitate by the reactions given above. Based on these assumptions, it was found that the maximum MgO consumption by 100 cc input PLS was calculated to be 0.34 gr dry MgO. Magnesia slurry was prepared with respect to this amount. Slurry concentration was 1% weight/volume (0.68 gr MgO per 100 cc deionized water). In order to ease the addition and considering the slight possibility of any excess addition amount (in case pH of the solution could not be raised to 7.0 or more) prepared slurry was twice as much as it would theoretically be consumed. Hence, according to this slurry concentration, the theoretically calculated necessary slurry amount was expected to be about 34 cc. However, the calculation is for an idealized situation. First of all, MgO reactivity is a variable factor between 0.7 and 0.9 which means an additional amount of magnesia is required to suppress this effect [80]. This also means that at least some portion of the prepared magnesia will not be consumed by precipitation reactions and contaminate the precipitates. Second, 100% precipitation of manganese is actually impossible at the chosen pH range which means consumption will be less than the calculated amount. That is because manganese was reported to precipitate about 20-30% at about pH 7 [6]. In addition to manganese, neither nickel nor cobalt will probably precipitate completely. Overall, the actual consumption could be more or less than the value given above depending on the results of these reasons. Generally, in the first mixed hydroxide precipitation it is desired to precipitate nickel and cobalt by 90-95% while keeping the manganese content of the final product of this step below 5%. Resultant precipitate called MHP1 is expected to contain 30-39% nickel, 2-5% cobalt with variable magnesia contamination as magnesium hydroxide or unreacted magnesia. As stated previously, the mixed hydroxide precipitation is best suited for ores with Ni:Mn ratio more than 3:1. In the present case, despite there had been several nickel losses until this step, the input solution still had the quality to satisfy this requirement as can be seen in Table 38. In this step, the only parameter optimized was the pH. In literature, it was mentioned that generally the MHP precipitation temperature is between 50°C and 70°C while the total residence time is between 2 and 3 hours. With respect to this information, it was decided to do the experiments at 60°C and 1 hour residence time to balance the shortened residence time with medium temperature value. The results of precipitation for several important elements can be seen in Figure 71.

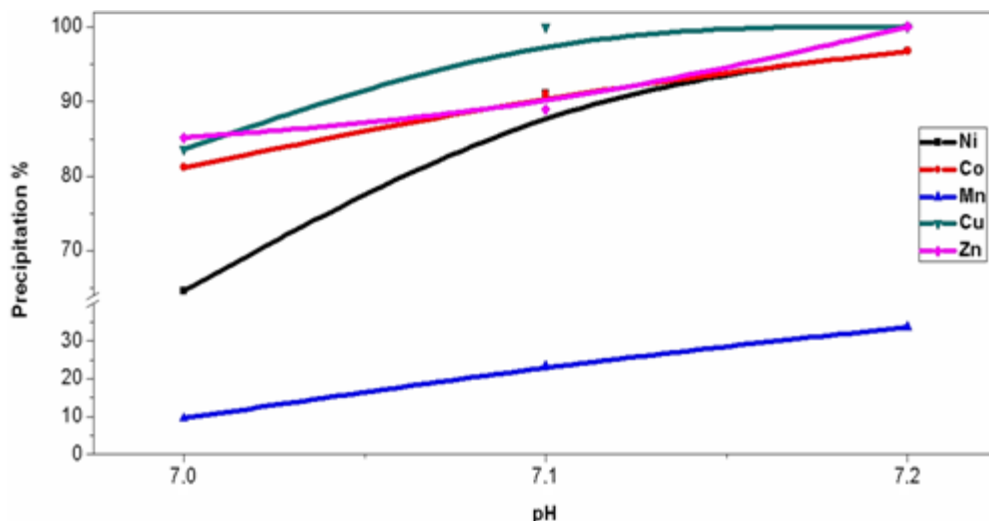


Figure 71 Effect of pH on precipitation of several metals in MHP 1 step.

As can be seen from Figure 71, all considered metals precipitated more with increasing pH level as expected. Nickel was more sensitive to pH change with respect to cobalt but by the end of the curves they reached the same precipitation values together. The reason for initially higher cobalt precipitations are due to faster reaction kinetics than nickel although thermodynamically nickel is expected to precipitate first. Moreover, co-precipitation of cobalt is easier than nickel at the corresponding pH levels. This difference between cobalt and nickel precipitations was observed even before the magnesia slurry addition where some portion of previously created MHP fed into the solution batch as seeds to improve precipitations [74]. On the other hand, manganese followed almost a steady increase in precipitation up to 33%. As can be seen copper was removed completely by pH=7.1 while this could not be achieved for zinc until the highest pH value was reached. The corresponding results should be considered together with the chemical compositions of precipitates obtained at the studied pH levels so that the optimum pH value can be determined. With respect to Table 40, the chemical compositions of all precipitates were actually in the required ranges for nickel, cobalt and manganese as stated by Willis (2007, 2012). Hence, all these precipitates were in saleable quality. However, the low precipitation efficiency of nickel and cobalt at the lowest pH would cause nickel and cobalt carry over to MHP 2 step where they would both consume more calcium hydroxide (slaked lime) and precipitates would contain more nickel and cobalt remnants. As the solid product of MHP 2 would be recycled back to the recycle leaching unit, nickel and cobalt accumulation in process train would occur and their corresponding loss amounts would increase in the first and second iron removal steps together with increased reagent consumptions (limestone) within these steps. Hence, the low precipitation values of pH=7.0 was not selected as the optimum for that reason.

On the other hand, the relatively high content of manganese in the precipitate of the highest pH level might surpass the 5% manganese rule if pH control is poorly handled. If this happens then the quality and salability of MHP product will definitely be difficult. Overall, all these reasoning highlighted the pH=7.1 as the optimum condition. As can be seen from Table 40, when the theoretical magnesia was added to the solution, the pH level reached to the highest studied value. On the other hand, the reagent consumption difference between the optimum and the lowest pH tests showed that the precipitation reactions were more severe on passing through this range which meant that most of the precipitation reactions were initiated when pH levels was close to 7.0 and increased in amount with increasing reagent addition. More reagent addition resulted in more magnesium content within the precipitate which might be due to more magnesium hydroxide precipitation or more unreacted magnesia contamination that could not be differentiated.

Table 40 Chemical compositions of MHP 1 precipitates (dry) obtained at different pH values.

Metals	pH=7.0	pH=7.1	pH=7.2
Ni	44.6	44.3	42.7
Mg	1.74	2.29	2.32
Mn	2.10	3.06	4.74
Co	3.81	3.01	2.74
Zn	1.29	0.95	0.96
Cu	0.091	0.070	0.069
MgO slurry consumption (cc per 100 cc input PLS)	22	29.5	34

As the optimum conditions were as stated in Table 41, the respective reagent consumption was 29.5 cc per 100 cc PLS or 0.295 g MgO per 100 cc PLS or 8.38 kg MgO per 1 ton of dry ore. Compositional changes within the solution prior to and after the MHP 1 step are given in Table 41.

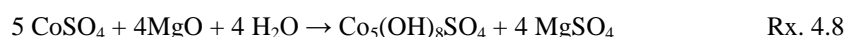
Table 41 The optimum conditions, precipitation efficiencies and compositional changes for MHP 1 step.

Optimum Conditions: pH=7.10, T= 60°C, t=60 minutes		Solution Compositions	
Metals	Precipitation %	Feed Solution (ppm)	Product Solution (ppm)
Ni	91.1	3738	250
Co	91.0	255	17.8
Fe	95.6	6.0	< 0.2
Al	78.6	9.2	1.5
Cr	-	< 0.02	< 0.02
Mg	4.0	4381	3263
Mn	23.5	996	590
Cu	100	5.9	< 0.07
Zn	88.9	82.1	< 0.2
ORP (mV)	-	210	142

As can be seen from Table 41, in the resultant solution after the removal of majority of metals, there were only magnesium and manganese with remnant nickel concentration. Concentration values that were designated by (<) represents that the corresponding metals could not be detected by ICP MS or in other words their concentrations were below detection limit as given in table. As can be seen, the oxidation reduction potential of the solution continuously decreased after 3 stages of downstream application. That is because; the solution had decreased in ion concentrations over the stages. Since most of the metals were separated from the solution, the density of resultant solution became closer to that of the initially used deionized water.

4.2.3.1. Characterization of Precipitates of First Mixed Hydroxide Precipitation

Since the precipitate obtained from this step is the resultant main product of the downstream process, its characterization is rather important in order to understand the form of nickel and cobalt whether being present as sulfate or hydroxide or both. Although the free acid of the solution had decreased to undetectably low levels, there was still some sulfur content bonded to the dissolved ions. On precipitation, the sulfur content of the solution had decreased as the chemical composition of solid product contains 4.01% sulfur which can be seen in Table 42 together with the other elements. That is because some of ions precipitate as sulfate rather than pure hydroxide. For example, Pillay and Pawlik (2012) proposed that when magnesia is used as precipitating reagent cobalt or other base metals do not precipitate as pure hydroxide but more probably as a hydroxy-sulfate by the reaction given below:



However, higher is the sulfur content more is the loss of ammonia during re-dissolution process of mixed hydroxide precipitate. Moreover, the state of contaminating elements such as manganese and magnesium are also important. According to Pillay and Pawlik (2012), the detection of brucite within MHP is the sign for unreacted magnesia and reduction of the reactivity of the reagent. This is also an indication of aging of the magnesia slurry. In order to prevent this problem, the magnesia slurry should be prepared right before the addition to the reaction tanks [76]. Moreover, silica contribution into MHP was reported by authors due to magnesia grade. Although it was not detectable from XRD data due to extensive amorphous structure of all phases; there might or might not be silica within the precipitate. Manganese is generally found in its hydroxide form and more commonly related to a process called oxidative precipitation. As explained above, the reaction kinetics of nickel and cobalt are fast at their normal precipitation zones. On the other hand, this fast reaction kinetics along with the air environment during precipitation is thought to be responsible for oxidative precipitation of manganese at the normal precipitation zones of nickel and cobalt which results in manganese hydroxide particle formation [74,132].

Table 42 Chemical composition of the solid product obtained after MHP 1 step.

Element	Wt. %	Element	Wt. %
Ni	44.3	Mg	2.29
Co	3.01	Mn	3.06
Fe	0.08	Cu	0.01
Al	0.09	Zn	0.95
Cr	< 0.0023	S	4.01

As can be seen in Figure 72, XRD result obtained from the precipitate of first mixed hydroxide precipitation revealed these expected phase formations. Since almost half of the precipitate amount was composed of nickel by itself, majority of the peaks were owned by three nickel phases namely nickel hydroxide hydrate, jaborite and theophrastite. Pourbaix diagrams of nickel and cobalt in water system and at 25°C (see Appendix B) suggested that at pH level about 7.0 and corresponding potential level both nickel and cobalt should be in Ni(OH)₂ and Co(OH)₂ forms [133]. However, in our case, there was an additional precipitate forming anion other than OH⁻ which was SO₄⁻ and the temperature was higher which increased the reaction kinetics. When supersaturation of so-called metals was included into the situation, it was reasonable to expect other anionic forms of nickel and cobalt. As an example for that, jaborite was detected. Jaborite is a variable mixture of several elements as anions or cations but the major constituent is nickel with 42-49% (wt.%) whereas other minor contributions can be listed as 3.5% S, 1.9% Co, 0.9% Fe and less than 0.2% Mg [134].

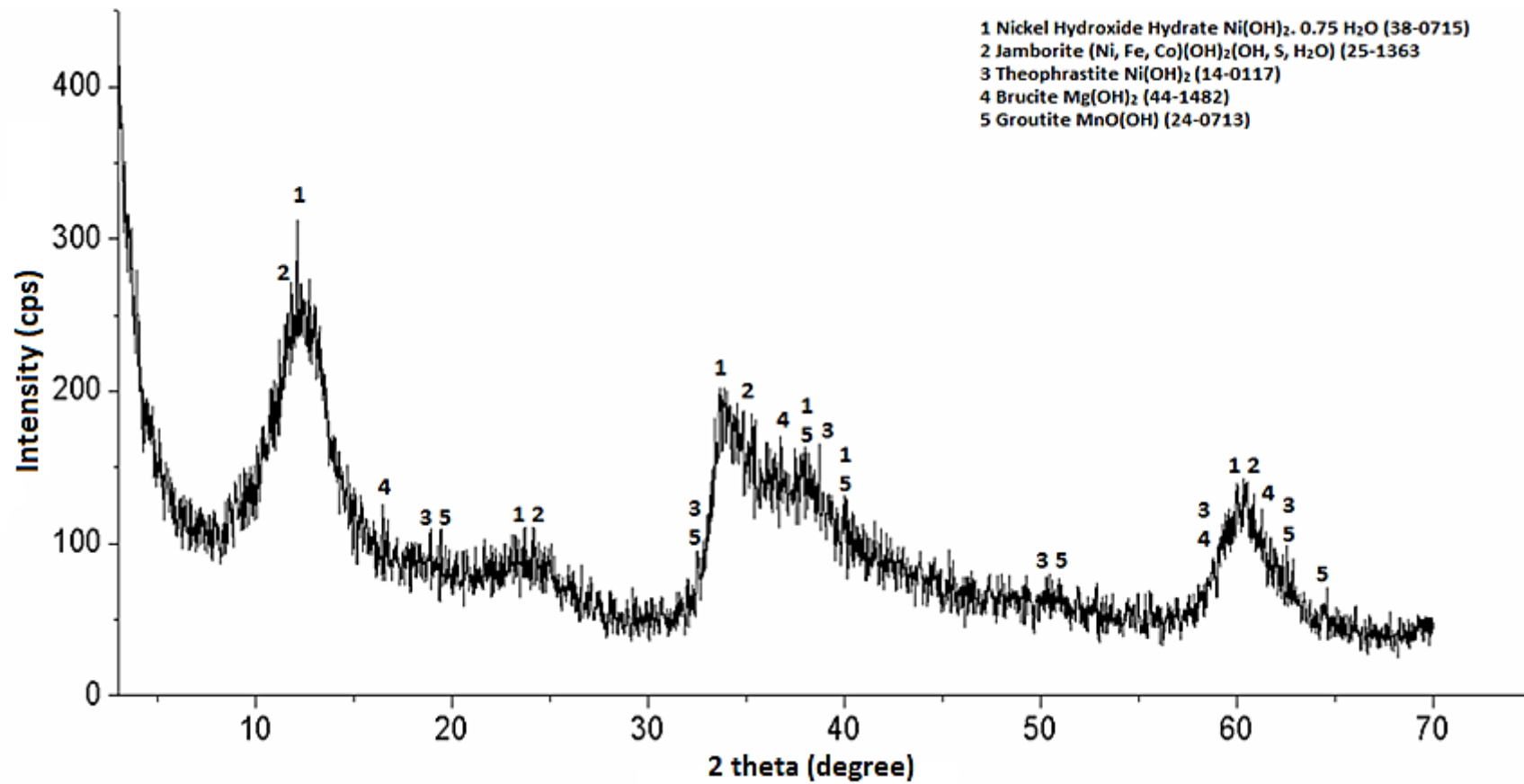


Figure 72 XRD result of the precipitate obtained at the optimum conditions of MHP 1.

Moreover, the chemically bonded water to nickel hydroxide that forms nickel hydroxide hydrate could not be understood but it was also found to match the XRD result. Rajamathi et al. (1997) synthesized a different nickel hydroxyl-sulfate with 0.44 mole chemically bonded H₂O to Ni(OH)_{1.82}(SO₄)_{0.09} in an aqueous sulfate solution which did not reveal the usual 53° (2-theta) peak of neither α- nor β-Ni(OH)₂ (Theophrastite). Hence, the chemically bonded water might be due to sulfate system and blurred designation of this peak in Figure 72 might somehow be the evidence for the so-called phase existence [135]. Manganese on the other hand was found as a minor phase in the form of groutite which is manganese hydroxide produced as a result of oxidative precipitation of manganese. Brucite contamination into the precipitate could not be prevented but its broadened characteristic peaks were the confirmation of low magnesia contamination.

Study of Oustadakis et al. (2006) revealed an XRD data with sharp brucite peaks at about 20°, 40° and 50° (2-theta degree) resulted by 26% Mg content in precipitate [75]. There is a contradictory explanation for the relation between brucite and nickel precipitates among authors. White et al. (2006) suggested that MHP particles are rarely found to be grown around on a magnesia particle and the structure is basically amorphous with appearance of agglomerates [131]. On the other hand, Oustadakis et al. (2006) included micrographs of thin sections of MHP and showed that unreacted brucite particles were surrounded by MHP phases [75]. As can be seen from Figures 73 and 74, the situation of MHP particles obtained by this study was more like the case described by the former author. As can be seen in Figure 73, there was porous, non-uniform, amorphous agglomerate. Although the agglomerate was coarse it can be seen that separate particles were not so easy to differentiate. In the following figure, it can be seen that the upper agglomerate was brighter than lower one. Despite the EDX results taken from designated points included more or less the same metal members; lighter agglomerate was more nickel and magnesium rich. This shows that the precipitation reactions occur more on the surface of previously formed MHP particles rather than on the surface of magnesia particles. Besides the sulfur contribution, EDX results show that the agglomerate was not so pure. Perhaps, these agglomerates contained both jamborite and the other two nickel hydroxide phases together. Since it was hard to dissociate these agglomerates even after 20-minute shaking in ethyl alcohol, there was no chance of comparison with rather pure agglomerates. However, the general scenario was almost always the same as the EDXs given in Figure 74. Silica contribution was probably introduced by the reagent itself since there were negligible amount of silicon concentration within the feed solution.

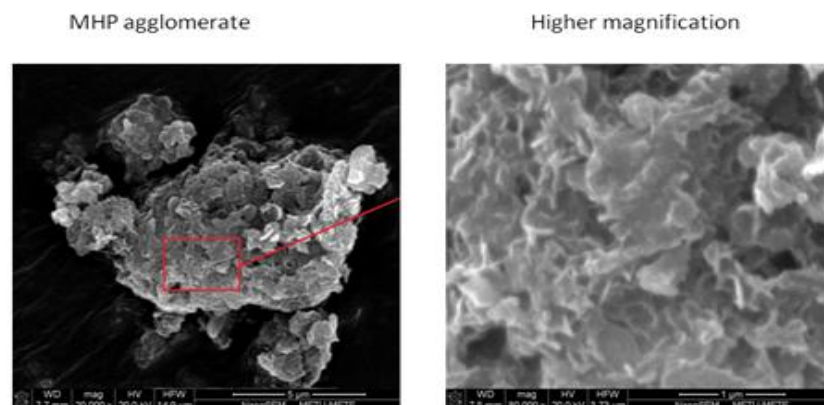
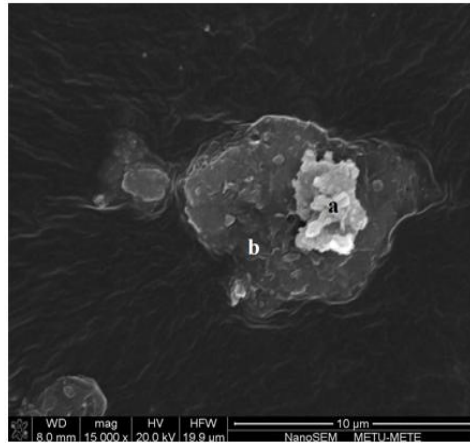


Figure 73 SEM images of MHP 1 agglomerate.



Point a

Point b

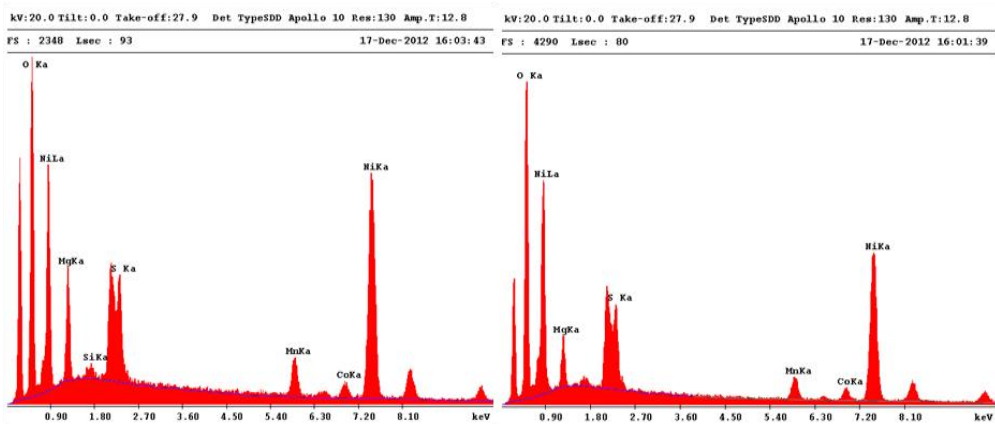
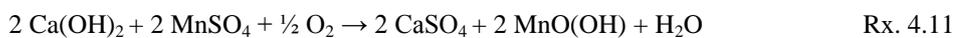
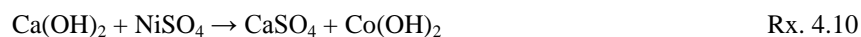
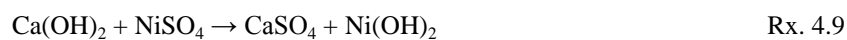


Figure 74 Two agglomerates of MHP 1 with respective EDX results.

4.2.4. Second Mixed Hydroxide Precipitation Experiments

After the first mixed hydroxide precipitation the resultant new solution was highly depleted from nickel and cobalt. However, the remnant concentrations were still needed to be recovered until concentration of these valuable metals dropped below 1 ppm. Hence, an additional precipitation process was required. The reason for not taking the precipitation process of nickel-cobalt in single step so that resultant solution contained the so-called remnant concentrations was simply due to controlling of manganese in the first mixed hydroxide precipitate. Operation conditions for MHP 2 are generally given as 7.5 to 8.0 pH values, 60° to 80° temperature and 60 to 80 minutes residence time [6]. Due to its lower cost with respect to magnesia and there are no quality restrictions as in the case of MHP 1 precipitate, slaked lime is preferred as reagent. Once again it was possible to calculate the necessary reagent amount for complete precipitation of remnant nickel, cobalt and manganese values based on the reactions as follows:



Despite not given in the reaction series above, magnesium also precipitates with similar reactions of nickel and cobalt, however it was excluded from the theoretical reagent consumption calculations due

to its low precipitation expectations. It can be seen that manganese reaction included oxygen which means manganese undergoes an oxidative precipitation pattern as in the previous step. Based on these reactions and assumptions, necessary slaked lime amount was approximately 0.123 g $\text{Ca}(\text{OH})_2$ for 100 cc input PLS. In order to prepare slurry with 1% weight/volume concentration, about 12-13 cc deionized water was required. Since this amount of slurry was quite small and hard to handle, it was decided to increase these amounts 5 times. Hence, the prepared slurry was 0.61 g $\text{Ca}(\text{OH})_2$ per 61 cc deionized water. A pH range of 7.50 to 8.00 was studied with 0.25 increments at fixed conditions of 60°C and 1 hour duration. The results of nickel, cobalt and manganese precipitations are given in Figure 75.

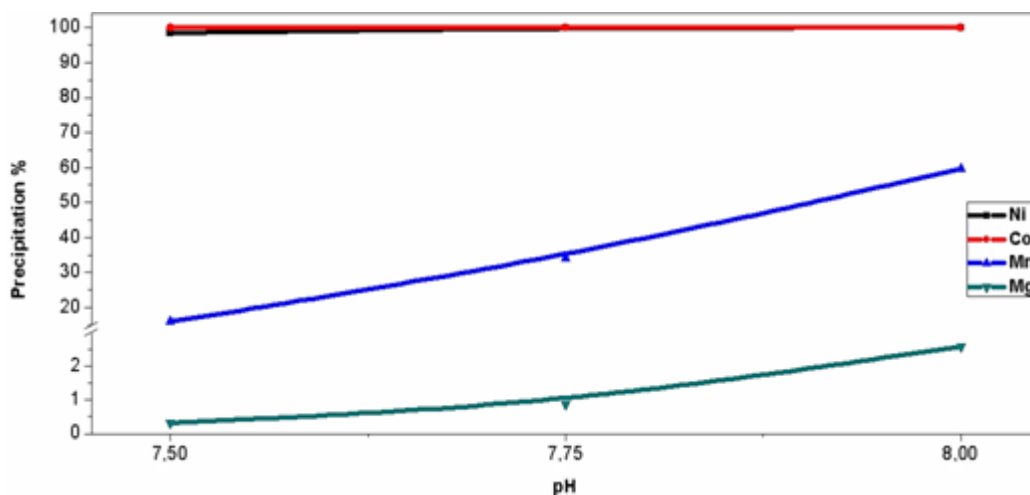


Figure 75 pH effect on several important metal precipitations during MHP 2 step.

As can be seen both nickel and cobalt were completely removed from the solution at all pH levels studied with single exception of 98% precipitation of nickel at the lowest studied pH value. Therefore, all pH values could be a candidate for the optimum pH level since it is desired to deplete the resultant solution by lowering the nickel and cobalt concentrations below 1 ppm for each. On the other hand, manganese precipitation was also increasing with increasing pH level. Since it is not desired to have a high manganese concentration in the precipitate due to the risky manganese accumulation within the process train (as this precipitate will be sent back to recycle leach unit) manganese content of the precipitate should also be considered. Moreover, magnesium contamination within the precipitate can also be problematic for magnesium circulation as in the case for manganese. Hence, it was decided that pH=7.75 was the best suited condition at the so-called fixed conditions. The respective compositional changes are given in Table 43 before and after second mixed hydroxide precipitation. As can be seen from Table 43 that most of the metal concentrations were below the detection limits of ICP hence it was decided to place these limits with less than sign instead of leaving them as blank. The most important point here is to see that nickel and cobalt concentrations were dropped easily below 1 ppm level. However, manganese concentration was rather high that would require an additional step of manganese removal. Hence it is advised to lower the final manganese concentration in PLS to below 10 ppm by applying the manganese removal step if this resultant barren solution is to be used as wash or make-up water. The reagent consumption at the optimum conditions were calculated as follows: 11.6 cc/100 cc PLS or 0.116 g $\text{Ca}(\text{OH})_2$ /100 cc PLS or 4.25 kg $\text{Ca}(\text{OH})_2$ /1 ton of dry ore.

Table 43 Compositional changes before and after MHP 2 step.

Optimum Conditions: pH=7.75, T= 60°C, t=60 minutes		Solution Compositions	
Metals	Precipitation %	Feed Solution (ppm)	Product Solution (ppm)
Ni	100	250	< 0.7
Co	100	17.8	< 0.5
Fe	-	< 0.2	< 0.2
Al	-	1.5	< 0.4
Cr	-	< 0.2	< 0.2
Mg	0.86	3263	2896
Mn	34.1	590	348
Cu	-	< 0.07	< 0.07
Zn	-	< 0.2	< 0.2
ORP (mV)	-	142	120

4.2.4.1. Characterization of Precipitates of Second Mixed Hydroxide Precipitation

As the last characterization step, the precipitate obtained at the optimum conditions were subjected to ICP and XRD analysis only. The precipitates obtained in all experiments of MHP 2 were obviously brownish whereas the precipitates obtained in MHP 1 step were greenish. The chemical composition of precipitate is given in Table 44 whereas its XRD result is given in Figure 76. As can be seen in Table 44, the major elements in MHP 2 were nickel and manganese. Expectedly, the XRD analysis gave somewhat a similar pattern to that of MHP 1.

Table 44 Chemical composition of MHP 2 precipitate obtained at the optimum conditions.

Element	Wt. %	Element	Wt. %
Ni	22.73	Mg	2.56
Co	1.62	Mn	18.3
Al	< 0.0051	Cu	< 0.0014
Cr	< 0.0002	Zn	< 0.0022
S	3.87		

As can be seen in Figure 76, the main peaks were almost exactly at the same 2 theta degrees in XRD result of the previous step. However, as the composition of nickel and manganese were quite close to each other it was hard to decide whether nickel or manganese phases were dominant. Hence, instead of giving the nickel phases once again, it was tried to focus on other possible fitting manganese hydroxide and/or oxyhydroxide phases. As a result of this search, takanelite, groutite and manganese oxide hydrate were found to be present as possible manganese phases. In addition to brucite which was already given as magnesium hydroxide phase, portlandite was also found as unreacted slaked lime phase. As a representative of nickel phase, it was decided to give only nickel hydroxide hydrate phase but it was quite possible that jaborite and theophrastite also existed within the precipitate.

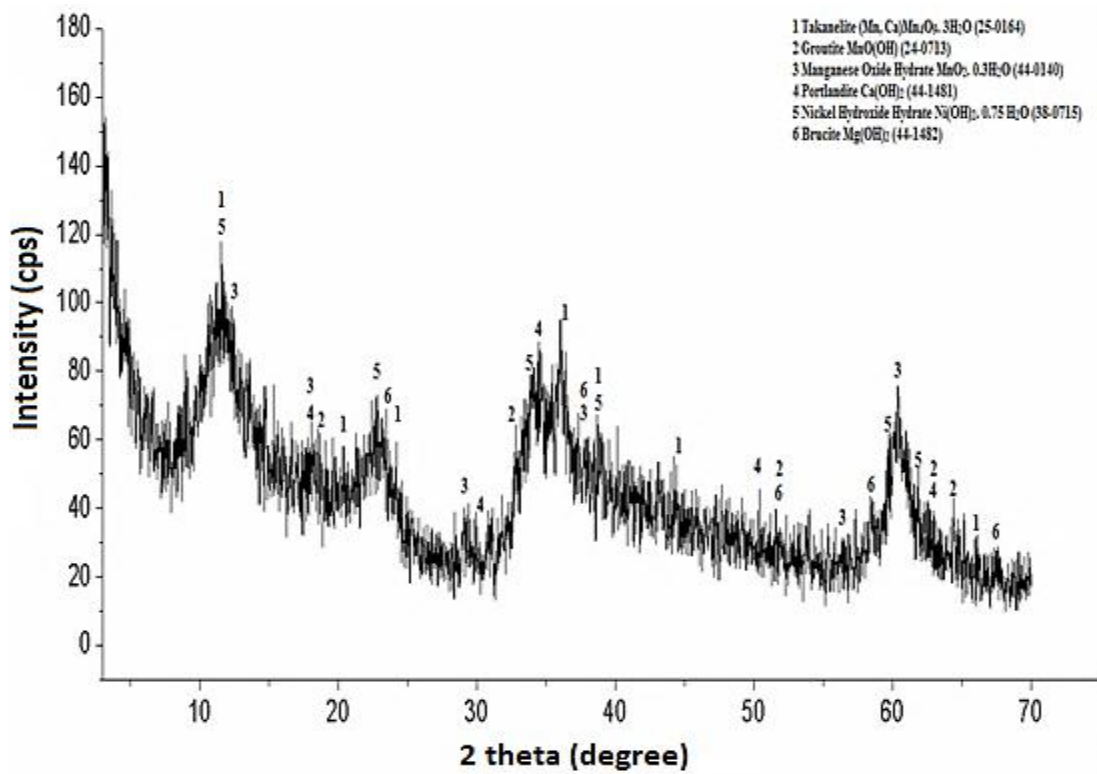


Figure 76 XRD result of MHP 2 precipitate obtained at the optimum conditions.

CHAPTER 5

CONCLUSIONS

The aim of this study was to apply high pressure acid leaching flowsheet on one of the most important nickel reserves of Turkey that is located in Çaldağ, Manisa. The optimum conditions for this flowsheet were determined by studying several parameters including acid load, temperature, duration of leaching and particle size. Once these parameters were decided upon, the processing of obtained pregnant leach solution (PLS) for the mixed hydroxide precipitation by downstream processing was studied. For this purpose, two-step purification-neutralization of solution, two-step nickel-cobalt hydroxide precipitations were conducted for producing a saleable intermediate product called MHP. Results obtained throughout this thesis study are summarized below:

- Chemical characterization of Çaldağ ore sample showed that ore grade was 1.215% nickel and 0.078% cobalt together with 32.7% iron, 1.01% chromium, 1.66% aluminum, 1.62% magnesium and 13.39% silicon.
- Particle size analysis of -0.5, -1 and -1.4 mm ore samples showed that 45-55% of the ore samples were below 38 µm.
- XRD and DTA-TGA examinations of the original run-of-mine ore revealed that the major minerals present were goethite, quartz and hematite and minor minerals were serpentine, smectite, asbolane, calcite, dolomite and other two forms of quartz. SEM-EDX examinations have shown that nickel was found within the minerals asbolane, iron oxide/hydroxides, smectites and serpentines.
- Theoretical acid consumption calculations based on the ore composition showed that at least 300 kg/ton of dry ore was required whereas it was about 1215 kg/ton in case of atmospheric acid leaching.
- The optimum conditions for HPAL step were determined to be 325 kg/ton of dry ore acid load, 250°C temperature, 1 hour leaching duration and 100% -1 mm particle size.
- With respect to these optimum conditions, the extraction efficiencies were 94.1% Ni, 94.0% Co, 1.7% Fe, 51.1% Al, 84.0% Mg and 82.2% Mn whereas heap leaching efficiencies were reported as 79.4% Ni, 82.7% Co, 30.0% Fe, 78.9% Mn and 37.1% Al.
- XRD and SEM-EDX examinations of the HPAL leach residue revealed that all of the goethite, asbolane, serpentine, smectite, calcite and dolomite peaks were completely dissolved and residue contained secondary hematite (might be also in primary form too), quartz (both as amorphous and crystalline) and alunite.
- PLS stock obtained under the stated HPAL conditions contained 4564 ppm Ni, 294 ppm Co, 2231 ppm Fe, 3296 ppm Al, 64.8 ppm Cr and 46200 ppm free acid.
- The optimum conditions for the first iron removal stage were chosen as pH = 3.00, 90°C and 2 hours of residence time.
- At the optimum conditions, the consumption of CaCO₃ slurry was 163.25 kg CaCO₃ per 1 ton of dry ore.
- XRD and SEM-EDX examinations of precipitate from the first iron removal stage indicated the domination of bassanite together with minor phases of goethite, hematite, and bayerite. Calcite was also found which was due to the presence of unreacted limestone particles.

- After the second iron removal experiments, it was decided to choose pH=4.50 as the optimum together with 70°C precipitation temperature and 3 hours residence time.
- Reagent consumption at the optimum conditions was calculated as 21.68 kg CaCO₃ per ton of dry ore.
- XRD and SEM-EDX examinations of the second iron removal precipitate indicated that it was somewhat similar to previous precipitate.
- The optimum conditions for MHP 1 were found to be pH=7.10 at 60°C and 1 hour duration.
- Reagent consumption at these optimum conditions was 8.38 kg MgO per 1 ton of dry ore.
- The composition of MHP 1 product obtained at the optimum conditions was 44.3% Ni, 3.01% Co, 0.08% Fe, 0.09% Al, 2.29% Mg, 3.06% Mn, 0.01% Cu, 0.95% Zn, and 4.01% S.
- Characterization of MHP product was conducted by XRD and SEM. XRD data revealed three nickel phases two of which were nickel hydroxide (theophrastite) and hydrated nickel hydroxide while the other one was complex hydroxide (jamborite). Other phases were brucite due to unreactive magnesia and groutite as manganese oxyhydroxide due to oxidative precipitation of manganese.
- In the second mixed hydroxide precipitation, the optimum conditions were found to be pH=7.75 at 60°C and 1 hour duration.
- The reagent consumption at the optimum conditions were calculated as 4.25 kg Ca(OH)₂ /1 ton of dry ore.
- Resultant MHP 2 precipitate contained 22.73% Ni, 1.62% Co, 18.3% Mn, 2.56% Mg, and 3.87% S.
- Characterization of this precipitate by XRD revealed that it was quite similar to that of MHP 1.

Recommendations for Future Work

Although the HPAL experiments in this thesis were conducted with the addition of sulfuric acid to the slurry at room temperature, it would have been much better to inject the acid at the experimentally planned temperature which was not possible with the available autoclave system at METU.

Instead of fresh water utilization for slurry making, more saline water can be used to test the effect/s of salinity on extraction efficiencies.

The barren solution after the second mixed hydroxide precipitation should be treated by manganese and/or magnesium removal steps if it would be used as wash water in order to prevent accumulation of manganese and magnesium, contamination of MHP 1 product and to save water.

Lastly, a pilot plant testing of HPAL and MHP route for Çaldağ lateritic nickel ore should be carried out and the findings should be compared with the pilot plant heap leaching results. A feasibility study should be done as the final step.

REFERENCES

- [1] R. G. McDonald, B. I. Whittington, *Hydrometallurgy* **2008**, *91*, 35–55.
- [2] International Nickel Study Group, “Production, Usage and Prices,” can be found under <http://www.insg.org/prodnickel.aspx>, **2011**.
- [3] B. I. Whittington, D. Muir, *Mineral Processing and Extractive Metallurgy Review* **2000**, *21*, 527–599.
- [4] European Nickel PLC, *European Nickel Annual Report*, **2009**.
- [5] Ş. Kaya, High Pressure Acid Leaching of Turkish Laterites, Middle East Technical University, Master Thesis, **2011**.
- [6] B. Willis, in *ALTA 2012 Nickel/Cobalt & Copper*, **2012**, pp. 45–76.
- [7] British Geological Survey, *Definition, Mineralogy and Deposits*, **2008**.
- [8] G. M. Mudd, *Ore Geology Reviews* **2010**, *38*, 9–26.
- [9] D. G. E. Kerfoot, in *Ullmann’s Encyclopedia of Industrial Chemistry*, Wiley Interscience, **2005**, pp. 1–63.
- [10] W. Ahmad, *Nickel Laterites*, **2008**.
- [11] J. Joseph R. Boldt, *The Winning of Nickel*, Methuen & Co. Ltd. E.C.4, London, **1967**.
- [12] D. M. Hoatson, S. Jaireth, L. A. Jaques, *Ore Geology Reviews* **2006**, *29*, 177–241.
- [13] A. D. Dalvi, W. G. Bacon, R. C. Osborne, in *PDAC 2004 International Convention, Trade Show & Investors Exchange*, **2004**, pp. 1–27.
- [14] B. V. I. Berger, D. A. Singer, J. D. Bliss, B. C. Moring, *Ni-Co Laterite Deposits of the World — Database and Grade and Tonnage Models*, **2011**.
- [15] E. Marsh, E. Anderson, *Ni-Co Laterites — A Deposit Model*, **2011**.
- [16] J. P. Golightly, in *International Laterite Symposium*, New Orleans, USA, **1979**, p. 22.
- [17] K. Liu, Q. Chen, H. Hu, Z. Yin, B. Wu, *Hydrometallurgy* **2010**, *104*, 32–38.
- [18] M. G. King, *Technology* **2011**, 35–39.
- [19] A. Oxley, N. Sirvanci, S. Purkiss, in *ALTA 2006 Nickel/Cobalt & Copper*, **2006**, pp. 453–472.

- [20] J. Reid, S. Barnett, in *ALTA 2002 Nickel/Cobalt 8.*, Melbourne, Australia, **2002**.
- [21] A. Griffin, G. Johnson, H. Evans, in *ALTA 2002 Nickel/Cobalt 8.*, **2002**.
- [22] M. Valix, F. Usai, R. Malik, *Minerals Engineering* **2001**, *14*, 197–203.
- [23] S. Chander, *Transactions of the Indian Institute of Metals* **1982**, *35*, 366–371.
- [24] C. H. Köse, Hydrometallurgical Processing of Lateritic Nickel Ores, Middle East Technical University, Master Thesis, **2010**.
- [25] E. Büyükakinci, Extraction Of Nickel From Lateritic Ores, Middle East Technical University, Master Thesis, **2008**.
- [26] A. Taylor, M. L. Jansen, in *ALTA Nickel/Cobalt 2000 Proceedings*, Perth, Australia, **2000**.
- [27] R. R. R. Moskalyk, A. M. Alfantazi, *Minerals Engineering* **2002**, *15*, 593–605.
- [28] D. David, in *Metallurgical Plant Design and Operating Strategies*, Perth, Western Australia, **2008**, pp. 223–232.
- [29] R. Mayze, in *ALTA 1999 Nickel/Cobalt & Copper*, **1999**, p. 9.
- [30] E. C. C. Chou, P. B. Qeuneau, R. S. Rickard, P. B. Queneau, *Metallurgical Transactions B* **1976**, *8B*, 547–553.
- [31] T. Norgate, S. Jahanshahi, *Minerals Engineering* **2011**, *24*, 698–707.
- [32] C. J. Arroyo, D. Gillapsie, James, A. Neudorf, David, M. Weenink, Erik, *Method for Leaching Nickeliferous Oxide Ores of High and Low Magnesium Laterites*, **2001**, U.S. Patent WO/2001/032944.
- [33] G. Brock, F. Mccarthy, H. Woerner, in *ALTA 2010 Nickel/Cobalt & Copper*, **2010**, p. 6.
- [34] D. J. Cordier, *Scandium*, **1997**.
- [35] M. Haslam, B. Arnall, in *ALTA 1999 Nickel/Cobalt & Copper*, **1999**, p. 18.
- [36] B. Harris, C. White, in *ALTA 2011 Nickel/Cobalt & Copper*, Perth, Western Australia, **2011**, pp. 1–13.
- [37] B. Creek, *Queensland's Metalliferous and Industrial Minerals: Projects at Feasibility Stage*, **2011**.
- [38] E. Krause, B. C. Blakey, V. G. Papangelakis, in *ALTA 1998 Nickel/Cobalt Pressure Leaching and Hydrometallurgy Forum ALTA Metallurgical Services*, Melbourne, Australia, **1998**.
- [39] S. I. Sobol, *Revista Technologica* **1969**, *7*.
- [40] S. Stopic, B. Friedrich, in *Pressure Hydrometallurgy 34th Annual Hydrometallurgy Meeting*, Alberta, Canada, **2004**, pp. 247–258.
- [41] D. Georgiou, V. G. Papangelakis, *Hydrometallurgy* **1998**, *49*, 23–46.

- [42] G. P. Tindall, D. M. Muir, in *Nickel/Cobalt 97 International Symposium*, Ontario Canada, **1997**.
- [43] F. T. D. Silva, *Minerals Engineering* **1992**, *5*, 1061–1067.
- [44] D. H. Rubisov, J. M. Krowinkel, V. G. Papangelakis, *Hydrometallurgy* **2000**, *58*, 1–11.
- [45] M. Baghalha, V. G. Papangelakis, *Metallurgical and Materials Transactions B* **1998**, *29B*.
- [46] D. H. Rubisov, V. G. Papangelakis, *Hydrometallurgy* **2000**, *58*, 13–26.
- [47] G. P. Tindall, D. M. Muir, in *Second International Symposium on Iron Control in Hydrometallurgy* (Eds.: J.B. Dutrizac, G.B. Harris), Montreal, Canada, **1996**, pp. 249–262.
- [48] D. Georgiou, V. G. Papangelakis, *Minerals Engineering* **2004**, *17*, 461–463.
- [49] V. G. Papangelakis, D. Georgiou, D. H. Rubisov, in *Second International Symposium on Iron Control in Hydrometallurgy*, Montreal, Canada, **1996**, pp. 263–273.
- [50] B. K. Loveday, *Minerals Engineering* **2008**, *21*, 533–538.
- [51] J. H. Kyle, in *ALTA 2003 Nickel/Cobalt & Copper*, **2003**, pp. 2–24.
- [52] J. E. Dutrizac, *Journal of Mining* **1990**, 36–39.
- [53] N. V. Y. Scarlett, I. C. Madsen, B. I. Whittington, *Journal of Applied Crystallography* **2008**, *41*, 572–583.
- [54] K. Liu, Q. Chen, H. Hu, Z. Ding, Z. Yin, *Hydrometallurgy* **2011**, *109*, 131–139.
- [55] D. Marshall, M. Buarzaiga, in *TMS International Laterite Nickel Symposium*, **2004**, pp. 263–271.
- [56] B. I. Whittington, J. A. Johnson, L. P. Quan, R. G. McDonald, D. M. Muir, *Hydrometallurgy* **2003**, *70*, 47–62.
- [57] D. Marshall, M. Buarzaiga, in *Internatinal Laterite Nickel Symposium*, **2004**, pp. 307–316.
- [58] M. E. Chalkley, I. L. Toirac, in *Nickel Cobalt 97, Vol. 1: Hydrometallurgy and Refining*, Montreal, Canada, **1997**, pp. 341–353.
- [59] A. Manceau, A. I. Gorshkov, V. A. Drits, *American Mineralogist* **1992**, *77*, 1144–1157.
- [60] J. Roqué-Rosell, J. F. W. Mosselmans, J. A. Proenza, M. Labrador, S. Galí, K. D. Atkinson, P. D. Quinn, *Chemical Geology* **2010**, *275*, 9–18.
- [61] D. H. Rubisov, V. G. Papangelakis, *Hydrometallurgy* **2000**, *58*, 89–101.
- [62] A. Manceau, M. L. S. Chlegel, M. M. Usso, V. A. S. Ole, C. G. Authier, P. E. P. Etit, F. T. Rolard, *Geochimica et Cosmochimica Acta* **2000**, *64*, 3643–3661.
- [63] D. Georgiou, V. G. Papangelakis, *Hydrometallurgy* **2009**, *100*, 35–40.

- [64] D. M. Muir, B. I. Whittington, R. G. McDonald, in *Second International Symposium on Iron Control in Hydrometallurgy* (Eds.: J.B. Dutrizac, G.B. Harris), Montreal, Canada, **2006**, pp. 611–633.
- [65] B. I. Whittington, R. G. McDonald, J. A. Johnson, D. M. Muir, *Hydrometallurgy* **2003**, *70*, 31–46.
- [66] B. I. Whittington, J. A. Johnson, *Hydrometallurgy* **2005**, *78*, 256–263.
- [67] B. Willis, in *ALTA 2007 Nickel/Cobalt & Copper*, ALTA Metallurgical Services, Perth, Western Australia, **2007**, pp. 222–247.
- [68] M. Mackenzie, M. Virnig, A. Feather, *Minerals Engineering* **2006**, *19*, 1220–1233.
- [69] J. H. Canterford, in *Hydrometallurgy of Nickel and Cobalt 2009, Proceedings of the 39th Annual Hydrometallurgy Meeting* (Eds.: J.J. Budac, R. Fraser, I. Mihaylov, V.G. Papangelakis, D.J. Robinson), Ontario, Canada, **2009**, pp. 511–522.
- [70] B. Willis, in *Alta Nickel/Cobalt Conference*, ALTA Metallurgical Services, Perth, Western Australia, **2008**.
- [71] S. Donegan, *Minerals Engineering* **2006**, *19*, 1234–1245.
- [72] C. Y. Cheng, G. Boddy, W. Zhang, M. Godfrey, D. J. Robinson, Y. Pranolo, Z. Zhu, W. Wang, *Hydrometallurgy* **2010**, *104*, 45–52.
- [73] C. H. Köse, Y. A. Topkaya, *Minerals Engineering* **2011**, *24*, 396–415.
- [74] J. Vaughan, W. Hawker, D. White, in *ALTA 2011 Nickel-Cobalt-Copper, Uranium & Gold Conference*, Perth, Western Australia, **2011**.
- [75] P. Oustadakis, S. Agatzini-Leonardou, P. E. Tsakiridis, *Minerals Engineering* **2006**, *19*, 1204–1211.
- [76] S. Pillay, C. Pawlik, in *ALTA 2012 Nickel/Cobalt & Copper*, **2012**, pp. 37–44.
- [77] C. Sist, G. P. Demopoulos, *JOM Journal of the Minerals, Metals and Materials Society* **2003**, *55*, 42–46.
- [78] P. Oustadakis, S. Agatzini-Leonardou, P. E. Tsakiridis, *Mineral Processing and Extractive Metallurgy* **2007**, *116*.
- [79] H. Wang, J. Zhao, W. Liang, Y. Mei, B. Houdeh, Y. Tian, *International Journal of Minerals, Metallurgy and Materials* **2010**, *17*, 257–261.
- [80] D. T. White, *Selective Precipitation of Nickel and Cobalt*, **2002**, U.S. Patent 6409979 B1.
- [81] S. Agatzini-Leonardou, P. E. Tsakiridis, P. Oustadakis, T. Karidakis, A. Katsiapi, *Minerals Engineering* **2009**, *22*, 1181–1192.
- [82] D. T. White, in *Hydrometallurgy of Nickel and Cobalt 2009, Proceedings of the 39th Annual Hydrometallurgy Meeting, CIM* (Eds.: J.J. Budac, R. Fraser, I. Mihaylov, V.G. Papangelakis, D.J. Robinson), Ontario, Canada, **2009**, pp. 351–367.
- [83] O. Yigit, *Economic Geology* **2009**, *104*, 19–51.

- [84] A. Çağatay, Y. Altun, B. Arman, *Çaldağ (Manisa-Turgutlu) Laterit Demir-Nikel-Kobalt Yatağının Mineralojisi*, **1983**.
- [85] V. Özdemir, Hydrometallurgical Extraction Of Nickel and Cobalt From Çaldağ Lateritic Ore, METU, Master Thesis, **2006**.
- [86] M. Tavlan, R. Thorne, R. J. Herrington, *Journal of the Geological Society, London* **2011**, *168*, 927–940.
- [87] R. Thorne, R. Herrington, S. Roberts, *Mineralium Deposita* **2009**, *44*, 581–595.
- [88] J. C. Ø. Andersen, G. K. Rollinson, B. Snook, R. Herrington, R. J. Fairhurst, *Minerals Engineering* **2009**, *22*, 1119–1129.
- [89] M. Polat, B. Özdemir, Ö. Gökyer, A. Oxley, in *Proceedings of the 11th International Mineral Processing Symposium*, **2008**, pp. 533–539.
- [90] A. Oxley, N. Sırvancı, S. Purkiss, in *Association of Metallurgical Engineers of Serbia AMES*, **2006**.
- [91] A. Oxley, N. Sırvancı, S. Purkiss, in *XXIII. International Mineral Processing Congress*, **2006**.
- [92] F. Arslan, K. T. Perek, G. Önal, in *Sohn International Symposium Advanced Processing Of Metals and Materials Volume 3-Thermo and Physicochemical Principles: Special Materials and Aqueous and Electrochemical Processing*, **2006**, pp. 339–345.
- [93] B. A. Wills, in *Mineral Processing Technology*, **2011**, p. Chapter 3.
- [94] B. Seçen, Pressure Leaching of Sivrihisar-Yunusemre Nickel Laterites, Middle East Technical University, Master Thesis, **2011**.
- [95] R. McDonald, in *Hydrometallurgy of Nickel and Cobalt*, **2009**, pp. 458–499.
- [96] B. Wang, Q. Guo, G. Wei, P. Zhang, J. Qu, T. Qi, *Hydrometallurgy* **2012**, *129-130*, 7–13.
- [97] F. A. López, M. C. Ramirez, J. A. López-Delgado, A. Pons, F. J. Alguacil, *Journal Of Thermal Analysis* **2008**, *94*, 517–522.
- [98] M. Landers, R. J. Gilkes, M. A. Wells, *Clays and Clay Minerals* **2009**, *57*, 751–770.
- [99] M. Földvári, *Handbook of Thermogravimetric System of Minerals and Its Use in Geological Practice*, Occasional Papers Of The Geological Institute Of Hungary, **2011**.
- [100] D. N. Todor, *Thermal Analysis of Minerals*, Abacus Press, **1976**.
- [101] A. Basile, J. Hughes, A. J. McFarlane, S. K. Bhargava, *Minerals Engineering* **2010**, *23*, 407–412.
- [102] J. H. Canterford, in *The Aus. I.M.M. Conference*, North Queensland, **1978**.
- [103] E. Stamboliadis, G. Alevizos, J. Zafiratos, *Minerals Engineering* **2004**, *17*, 245–252.
- [104] Z. Ding and R. L. Frost, *Thermochimica Acta* **2002**, *389(1-2)*, 185–193.

- [105] A. L. Auzende, I. Daniel, B. Reynard, C. Lemaire, *Phys Chem Minerals* **2004**, *31*, 277–282.
- [106] M. Landers, M. Gräfe, R. J. Gilkes, M. Saunders, M. A. Wells, *Australian Journal of Earth Sciences : An International Geoscience Journal of the Geological Society of Australia* **2011**, *58*:7, 745–765.
- [107] J. Xie, A. C. Dunlop, *Journal of Geochemical Exploration* **1998**, *61*, 213–232.
- [108] K. Liu, Q. Chen, H. Hu, *Hydrometallurgy* **2009**, *98*, 281–286.
- [109] M. Alvarez, E. E. Sileo, E. H. Rueda, *American Mineralogist* **2008**, *93*, 584–590.
- [110] E. Eslinger, D. Pevers, *Clay Minerals* **1988**, *19*, 2–1/2–48.
- [111] H. Yamada, H. Nakazawa, K. Yoshioka, T. Fujita, *Clay Minerals* **1991**, *26*, 359–369.
- [112] P. Komadel, *Clay Minerals* **2003**, *38*, 127–138.
- [113] A. C. V. Coelho, G. Poncelet, J. Ladriere, *Applied Clay Science* **2000**, *17*, 163–181.
- [114] B. W. Evans, S. M. Kuehnera, A. Chopelas, *American Mineralogist* **2009**, *94*, 1731–1734.
- [115] N. Verbaan, in *ALTA 2009 Nickel/Cobalt Conference*, Perth, Australia, **2009**.
- [116] X. Guo, W. Shi, D. Li, Q. Tian, *Transactions of Nonferrous Metals Society of China* **2011**, *21*, 191–195.
- [117] E. Krause, A. Singhal, B. C. Blakey, in *Hydrometallurgy and Refining of Nickel and Cobalt*, Ontario Canada, **1997**, p. 441.
- [118] J. Laermans, J. Banker, in *Corrosion Applications Conference*, **2003**.
- [119] G. P. Tindall, D. M. Muir, *Hydrometallurgy* **1998**, *47*, 377–381.
- [120] W. Luo, Q. Feng, L. Ou, G. Zhang, Y. Lu, *Hydrometallurgy* **2009**, *96*, 171–175.
- [121] S. Agatzini-Leonardou, P. Oustadakis, in *IX. Balkan Mineral Processing Congress*, Istanbul, **2001**.
- [122] M. R. C. Ismael, J. M. R. Carvalho, *Minerals Engineering* **2003**, *16*, 31–39.
- [123] T. T. Chen, L. J. Cabri, in *Iron Control in Hydrometallurgy* (Ed.: J.E. Dutrizac), **1986**, pp. 12–54.
- [124] Y. Chang, X. Zhai, B. Li, Y. Fu, *Hydrometallurgy* **2009**, DOI 10.1016/j.hydromet.2009.11.014.
- [125] P. B. Queneau, D. R. Weir, in *Iron Control in Hydrometallurgy* (Ed.: J.E. Dutrizac), **1986**, pp. 77–105.
- [126] Y. Cudennec, A. Lecerf, *Journal of Solid State Chemistry* **2006**, *179*, 716–722.

- [127] J. E. Dutrizac, in *Lead-Zinc-Tin '80s, TMS-AIME World Symposium on Metallurgy and Environment Control* (Eds.: J.M. Cigan, T.S. Mackey, T.J. O'Keefe), Warrendale, PA, **1980**, pp. 532–563.
- [128] K. Wang, J. Li, R. G. McDonald, R. E. Browner, *Hydrometallurgy* **2011**, *109*, 140–152.
- [129] K. Wang, J. Li, R. G. McDonald, R. E. Browner, *Minerals Engineering* **2013**, *40*, 1–11.
- [130] Z. Zhu, Y. Pranolo, W. Zhang, W. Wang, C. Y. Cheng, *Hydrometallurgy* **2010**, *104*, 81–85.
- [131] D. T. White, M. J. Miller, A. C. Napier, in *Proceedings of the 3rd International Mineral Processing Symposium, CIM*, Montreal, Canada, **2006**, pp. 591–609.
- [132] R. Harvey, R. Hannah, J. Vaughan, *Hydrometallurgy* **2011**, *105*, 222–228.
- [133] M. Pourbaix, *Atlas of Electrochemical Equilibria in Aqueous Solutions*, Pergamon Press, **1966**.
- [134] N. Morandi, G. Dalrio, *American Mineralogist* **1973**, *58*, 835–839.
- [135] M. Rajamathi, G. N. Subbannab, P. V. Kamatha, *Journal of Materials Chemistry* **1997**, *7*, 2293–2296.

APPENDIX A

EXAMPLE OF METAL EXTRACTION OR PRECIPITATION CALCULATIONS

The chemical analysis of original limonite sample and leach residues obtained at the end of leaching were performed according to the AAS analysis results of the leach residue done by META Nickel and Cobalt Company. The extractions of nickel and cobalt were found according to Equation A.1 given below:

$$\% \text{Extraction of M} = \left[1 - \frac{\text{Residue Weight (g)} \times \% \text{M in Residue}}{\text{Ore Weight in Batch (g)} \times \% \text{M in Ore Feed}} \right] \times 100 \quad (\text{A.1})$$

Examples of metal extraction calculations for the nickel and cobalt are given in Equations A.2 and A.3, respectively, according to the experimental data given in Table 45.

Table 45 Experimental data for the optimum HPAL conditions for solid based extraction calculations.

Experimental Data	Nickel	Cobalt
% Metal in Leach Residue	0.0820	0.0053
Residue Weight (g)	132.1	132.1
Ore Weight in Batch (g)	150	150
% Metal in Ore Feed	1.215	0.078

$$\% \text{Extraction of Ni} = \left[1 - \frac{132.1 \text{ g} \times 0.082}{150 \text{ g} \times 1.215} \right] \times 100 = 94.1\% \quad (\text{A.2})$$

$$\% \text{Extraction of Co} = \left[1 - \frac{132.1 \text{ g} \times 0.0053}{150 \text{ g} \times 0.078} \right] \times 100 = 94.0\% \quad (\text{A.3})$$

Besides nickel and cobalt, the extraction calculations of the other elements were performed according to the AAS analysis results of the pregnant leach solution done by the Chemical Engineering Department of METU after pressure leaching. The extraction calculations of the other metals were found according to Equation A.4 given below:

$$\% \text{ Extraction of M} = \left[\frac{\text{PLS Volume (cc)} \times \text{M Concentration (ppm OR mg/L)} \times 10^{-4}}{\text{Ore Weight in Batch (g)} \times \% \text{M in Ore Feed}} \right] \times 100 \quad (\text{A.4})$$

Examples of metal extraction calculations for iron and magnesium are given in Equations A.5 and A.6, respectively, according to the experimental data given in Table 46. Metal extraction percentages of the other elements can be found similar to iron and magnesium.

$$\% \text{ Extraction of Fe} = \left[\frac{373.83 \text{ cc} \times 2231 \text{ (ppm OR mg/L)} \times 10^{-4}}{150 \text{ g} \times 32.7} \right] \times 100 = 1.7\% \quad (\text{A.5})$$

$$\% \text{ Extraction of Mg} = \left[\frac{373.83 \text{ cc} \times 5460 \text{ (ppm OR mg/L)} \times 10^{-4}}{150 \text{ g} \times 1.62} \right] \times 100 = 84.0\% \quad (\text{A.6})$$

Table 46 Experimental data at the optimum HPAL conditions for Liquid Based Extraction calculations.

Experimental Data	Iron	Magnesium
Metal Conc. In PLS (ppm)	2231	5460
PLS Volume (cc)	373.83	373.83
Ore Weight in Batch (g)	150	150
% Metal in Ore Feed	32.7	1.62

The precipitation of metals during iron removal and mixed hydroxide precipitation stages were calculated based on the compositional analysis of pregnant leach solution according to the given Equation A.7. Experimental data of mixed hydroxide precipitation performed at pH=7.10, 60°C in 60 min is given in Table 47 to make an illustrative Ni precipitation calculation as in Equation A.8.

$$\% \text{ Precipitation of M} = \left[\frac{((\text{PLS vol. (cc)} \times \text{M in PLS (ppm)}) - (\text{Output PLS vol.} \times \text{M in output PLS (ppm)}))}{(\text{PLS vol. (cc)} \times \text{M in PLS (ppm)})} \right] \times 100 \quad (\text{A.7})$$

Table 47 Experimental data obtained at the optimum MHP 1 conditions for nickel precipitation %.

Experimental Data	Nickel
Metal Conc. In PLS (ppm)	3738
PLS Volume (cc)	100
Output PLS volume (cc)	128.89
Ni in output PLS (ppm)	250

$$\% \text{ Precipitation of Ni} = \left[\frac{((100 \times 3738) - (128.89 \times 250))}{((100 \times 3738))} \right] \times 100 = 91.1\% \quad (\text{A.8})$$

APPENDIX B

POURBAIX DIAGRAMS OF NICKEL AND COBALT

The Pourbaix diagrams of Ni and Co in H₂O system as given in Figures 77 and 78 indicated that Ni²⁺ and Co²⁺ are the stable form of ions throughout the high pressure acid leaching (at low pH). With the increase in pH, the stable forms Ni(OH)₂ and Co(OH)₂ are formed at higher pH values [133].

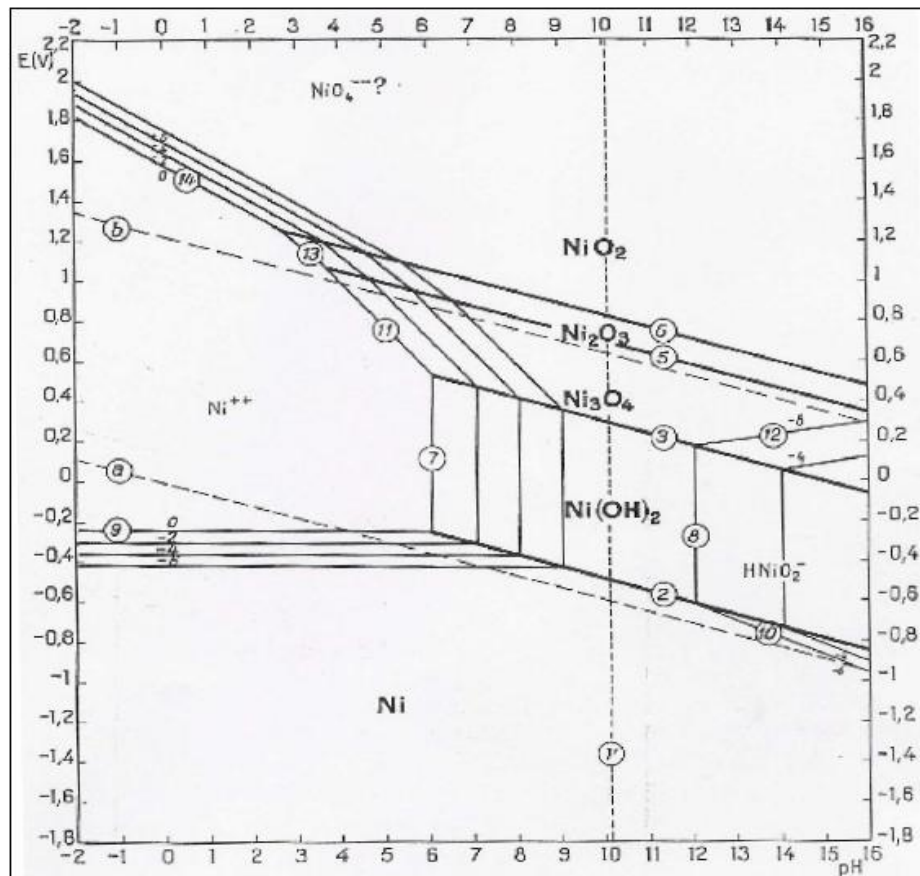


Figure 77 Pourbaix diagram for nickel-water system at 25°C, 10⁻⁶ Molar.

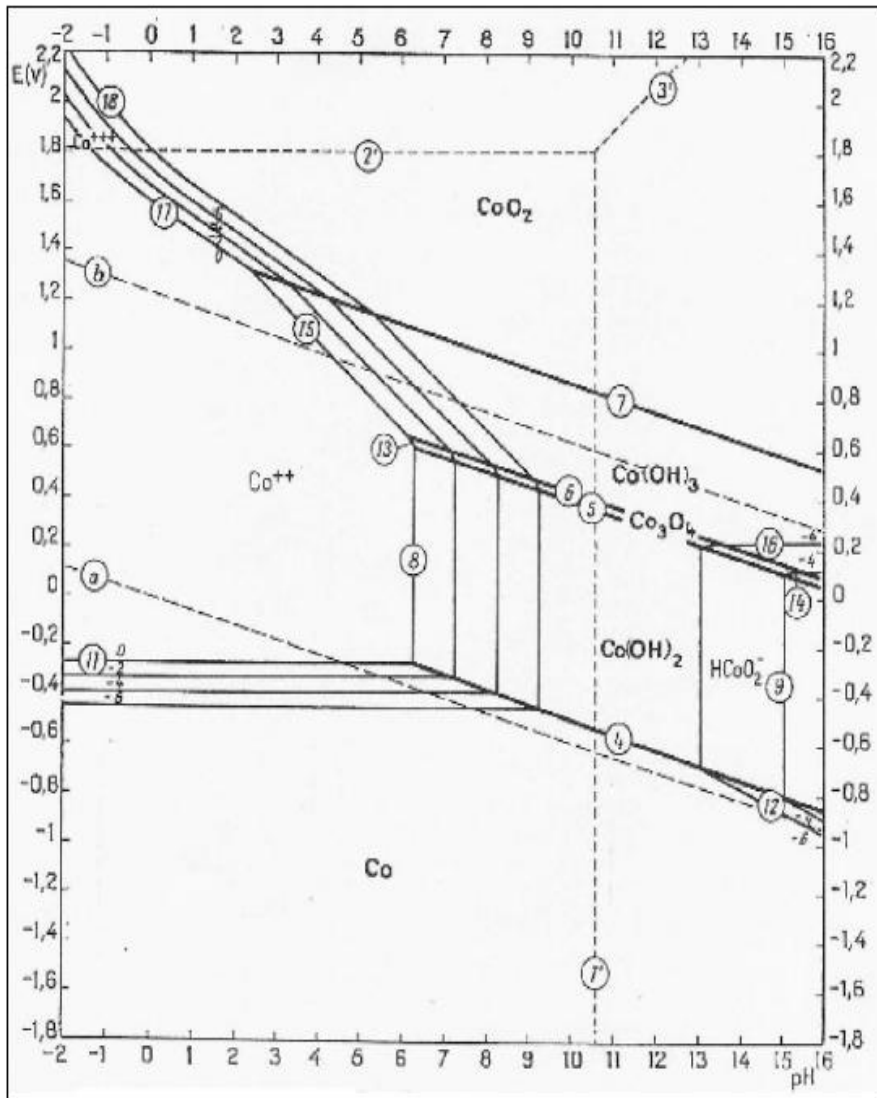


Figure 78 Pourbaix diagram for cobalt-water system at 25°C, 10⁻⁶ Molar.

APPENDIX C

EDX Results of Particles of First Sample Holder

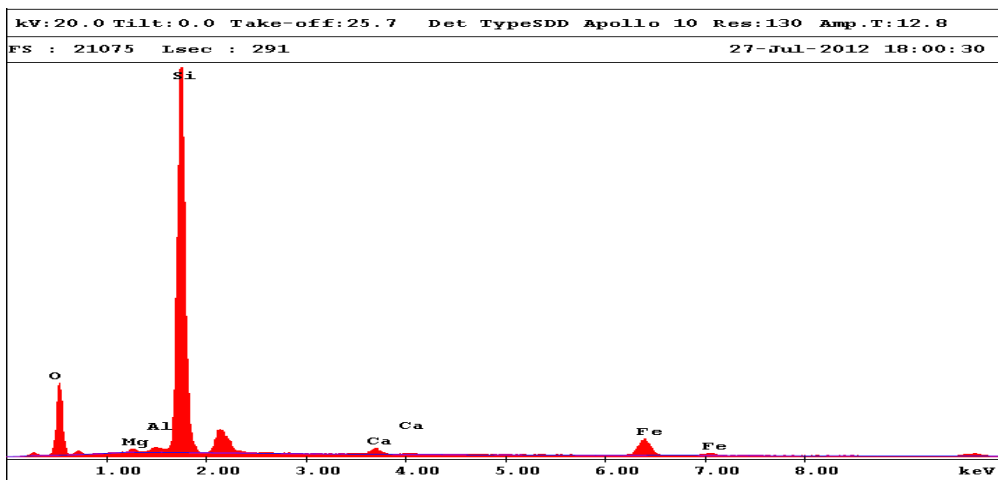


Figure 79 EDX result of particle a (Quartz with iron and calcium inclusions).

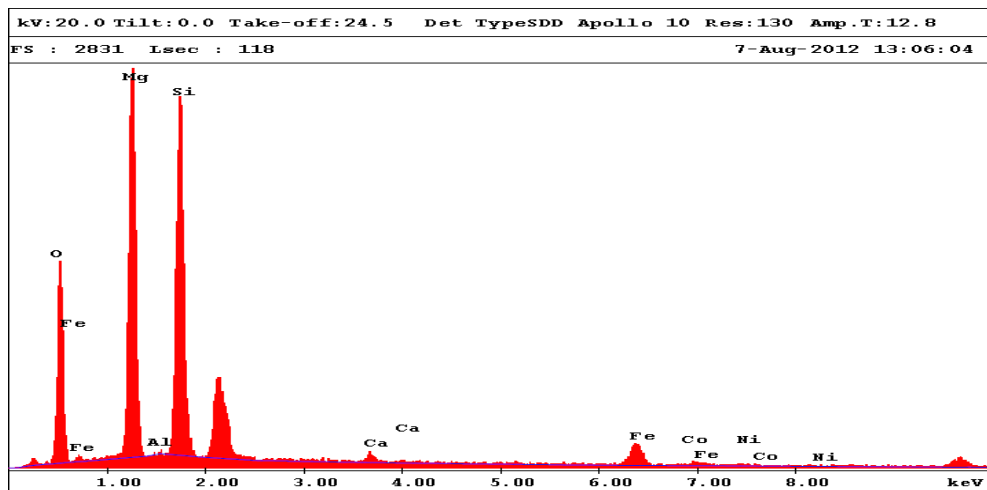


Figure 80 EDX result of particle b (Ferruginous serpentine).

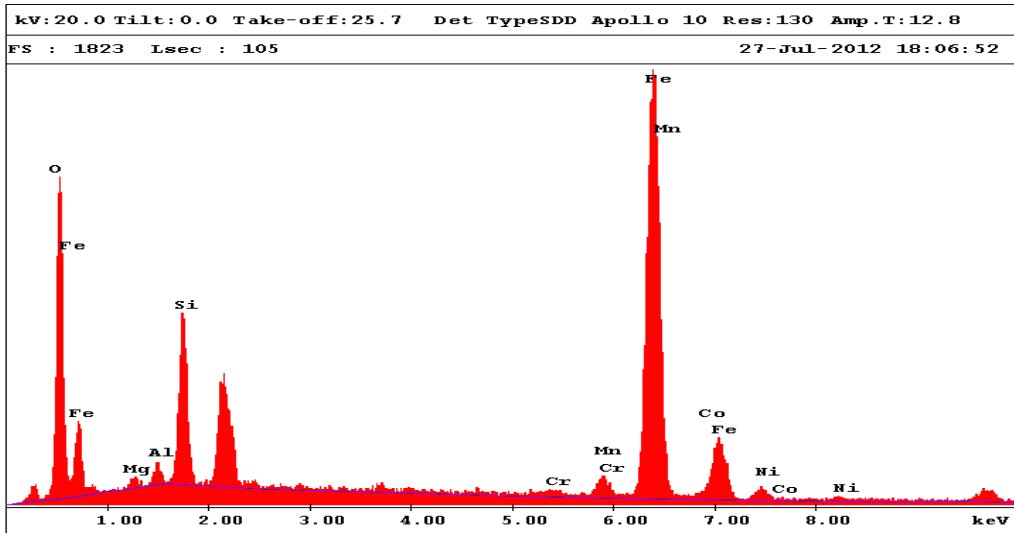


Figure 81 EDX result of particle c (Mn-Iron Oxide).

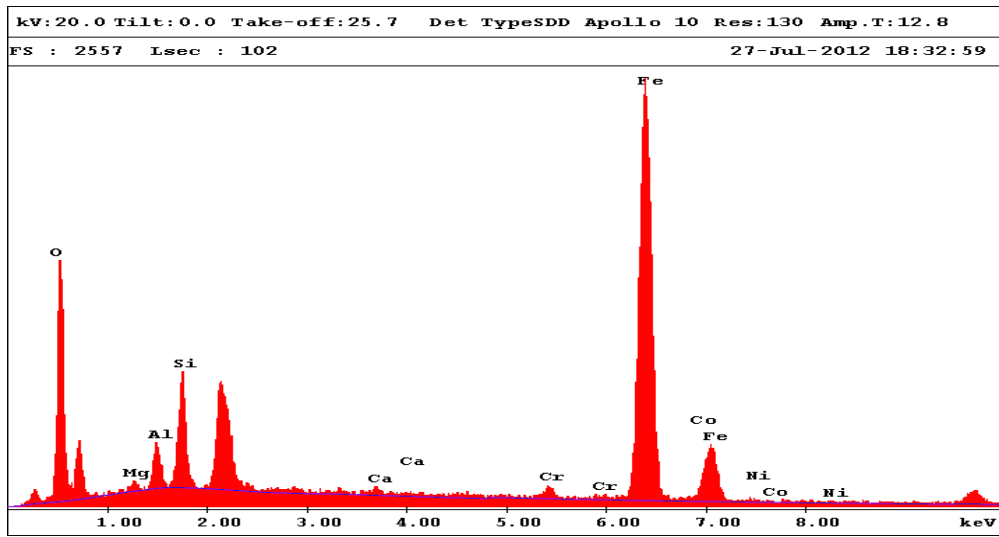


Figure 82 EDX result of particle g (Cr-Hematite).

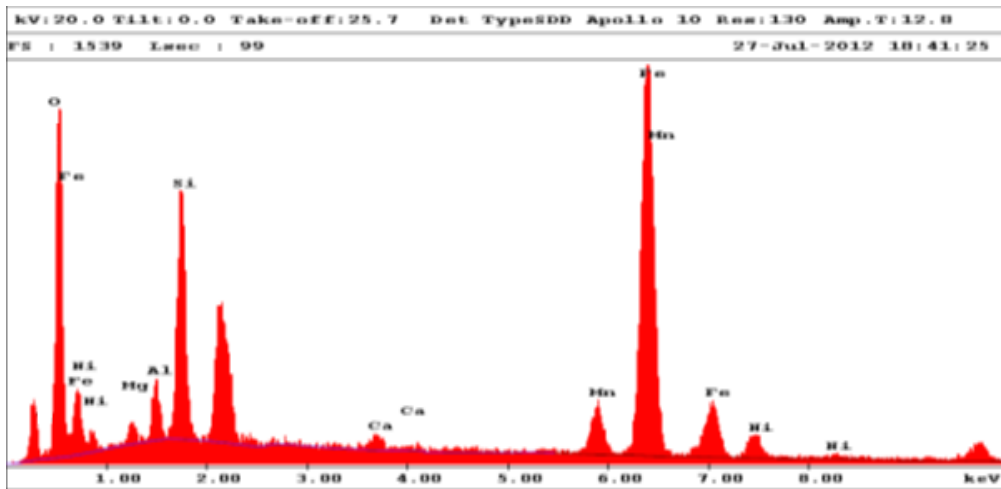
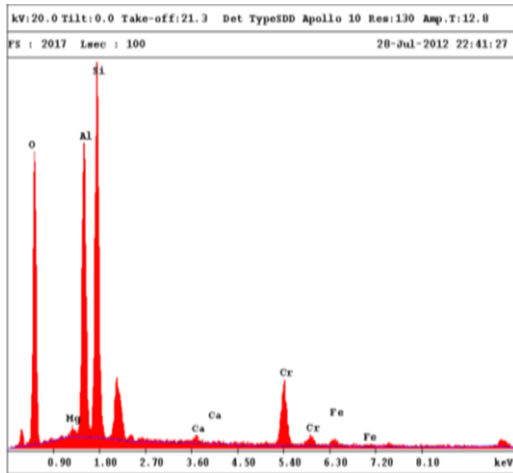
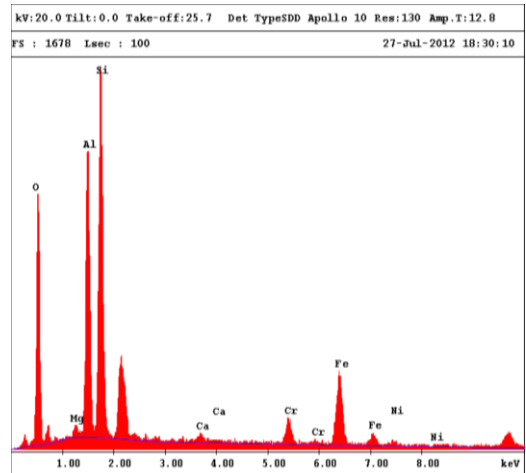


Figure 83 EDX result of particle h (Mn-Iron oxide with ferruginous Ca-smectite (shiny regions)).



Particle e (upper section).



Particle e (lower section).

Figure 84 EDX results from two sections of particle e.

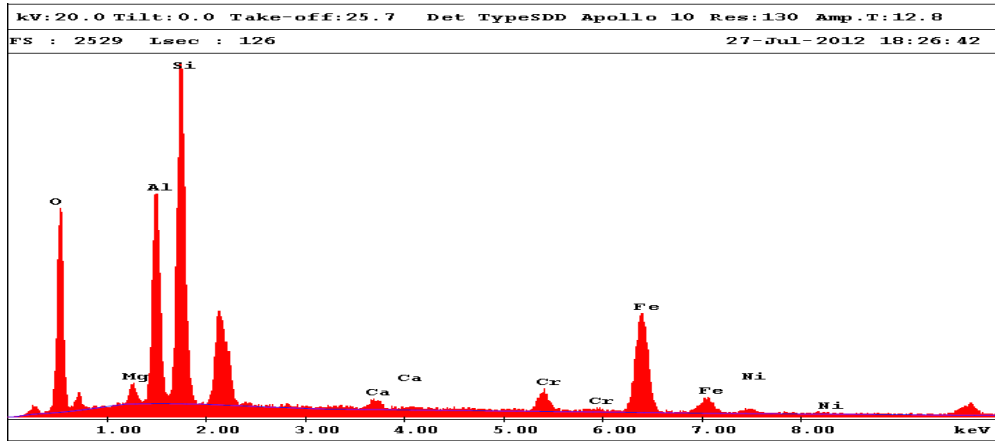
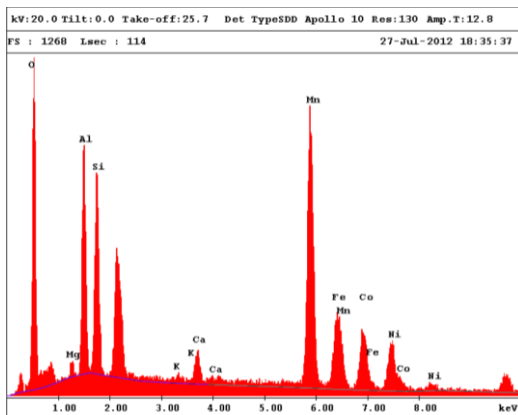
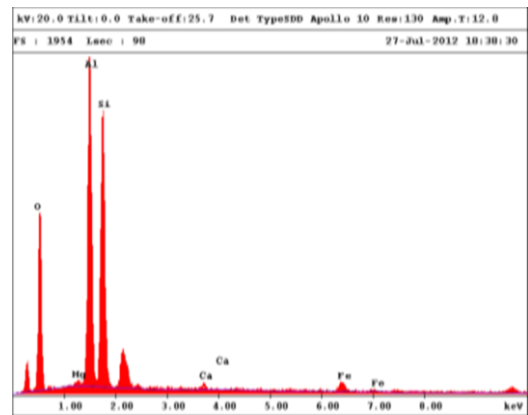


Figure 85 EDX result of particle d (Ferruginous Smectite)



EDX result for particle f.



EDX result for particle f1.

Figure 86 EDX result for two disintegrated particles f and f1.

APPENDIX D

EDX Results of Particles of Second Sample Holder

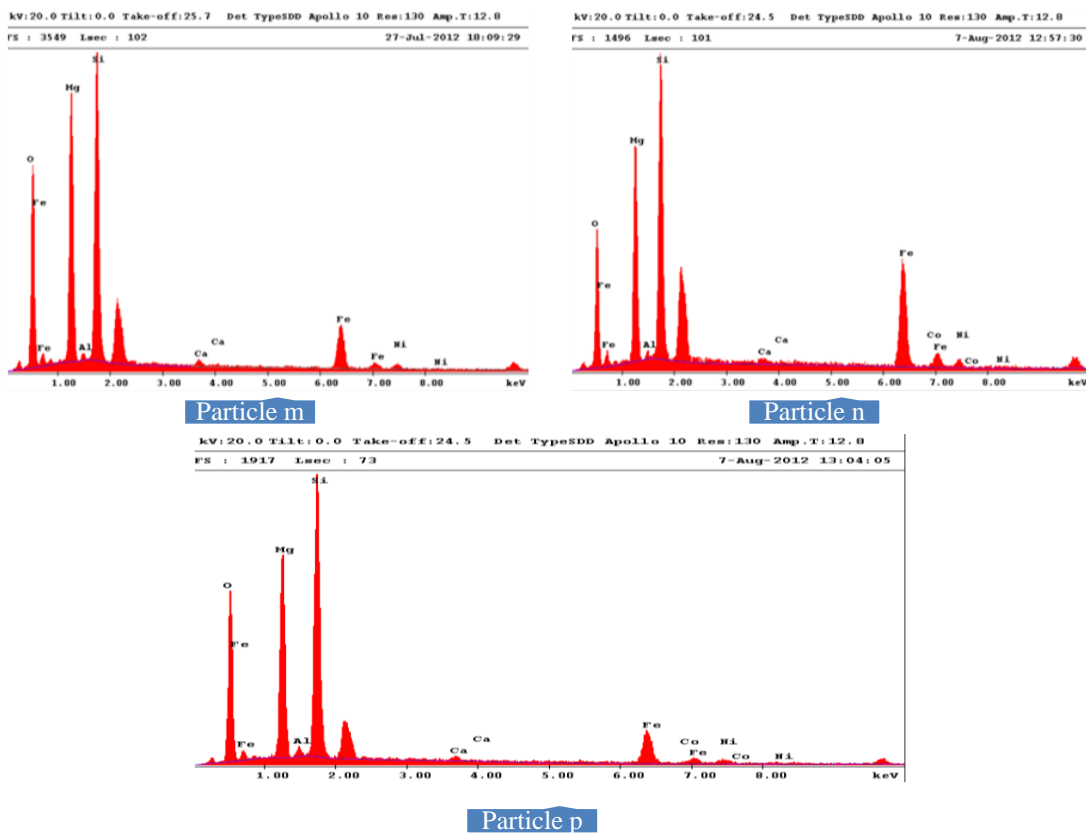
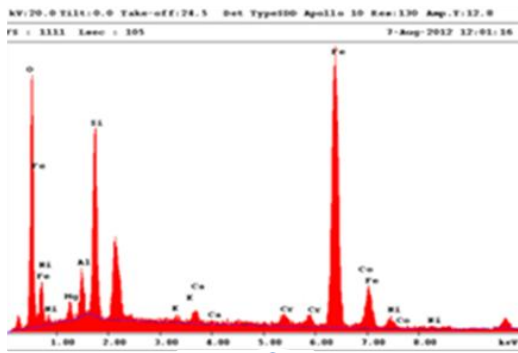
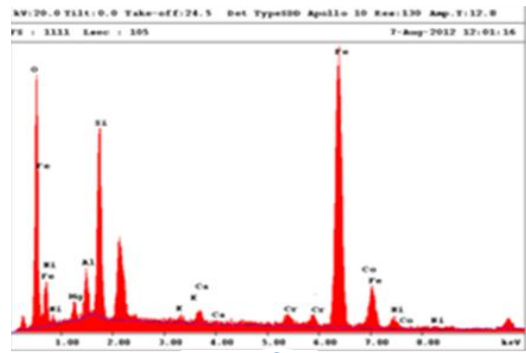


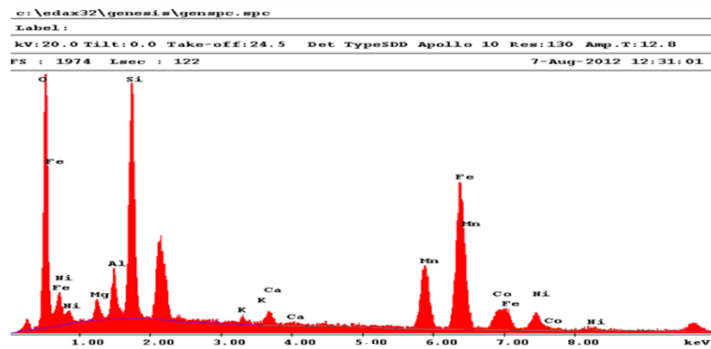
Figure 87 EDX results of particles m, n and p.



Particle q

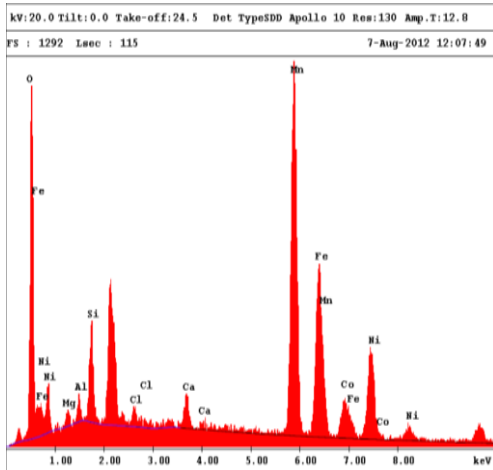


Particle r

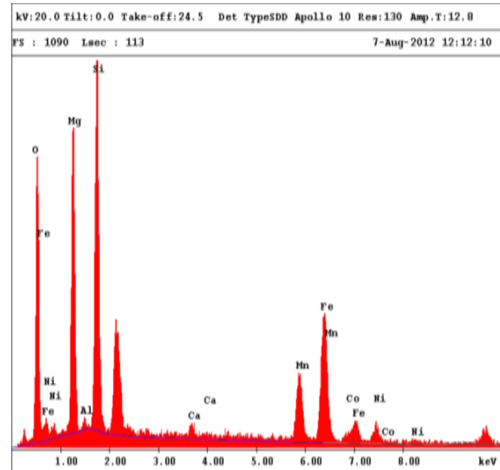


Particle u

Figure 88 EDX results of particles q, r and u.



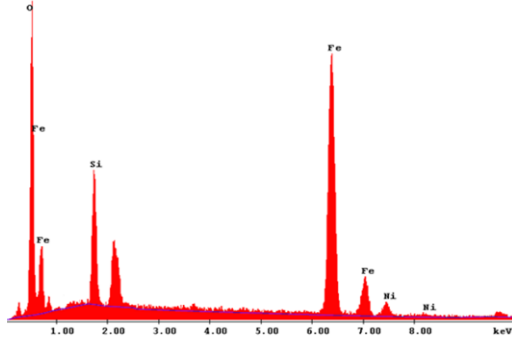
Particle s



Particle t

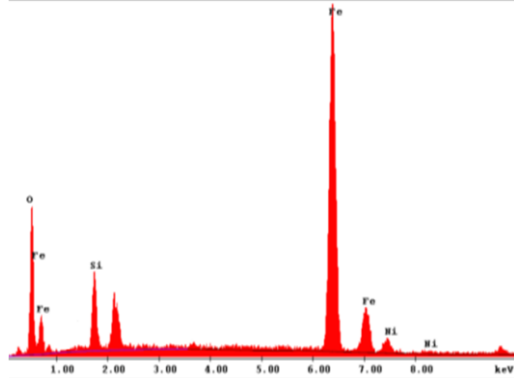
Figure 89 EDX results of particles s and t.

c:\edax32\genesis\genspc.spc
 Label:
 kv:20.0 Tilt:0.0 Take-off:24.5 Det TypeSDD Apollo 10 Res:130 Amp.T:12.0
 FS : 1515 Lsec : 106 7-Aug-2012 13:39:43



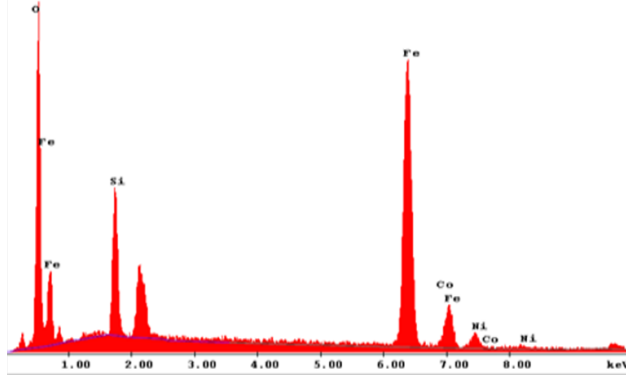
Particle z

kv:20.0 Tilt:0.0 Take-off:24.5 Det TypeSDD Apollo 10 Res:130 Amp.T:12.0
 FS : 1439 Lsec : 105 7-Aug-2012 13:43:25



Particle y

kv:20.0 Tilt:0.0 Take-off:24.5 Det TypeSDD Apollo 10 Res:130 Amp.T:12.0
 FS : 1514 Lsec : 106 7-Aug-2012 13:39:43



Particle w

Figure 90 EDX results for particles y, z and w.